Technische Universität Dresden

Extraction and Detection of Fetal Electrocardiograms from Abdominal Recordings

Fernando Andreotti Lage

von der Fakultät Elektrotechnik und Informationstechnik der Technische Universität Dresden

zur Erlangung des akademischen Grades

Doktoringenieur

(Dr.-Ing.)

genehmigte Dissertation

Vorsitzender:	Prof. Dr. rer. nat. Edmund Koch	
Gutachter:	Prof. Dr.-Ing. habil. Hagen Malberg	
	Prof. Dr. Maarten De Vos	Tag der Einreichung: 07.11.2016
	Prof. Dr. phil. nat. habil. Ronald Tetzlaff	Tag der Verteidigung: 20.01.2017

Abstract

The non-invasive fetal ECG (NIFECG), derived from abdominal surface electrodes, offers novel diagnostic possibilities for prenatal medicine. Despite its straightforward applicability, NIFECG signals are usually corrupted by many interfering sources. Most significantly, by the maternal ECG (MECG), whose amplitude usually exceeds that of the fetal ECG (FECG) by multiple times. The presence of additional noise sources (e.g. muscular/uterine noise, electrode motion, etc.) further affects the signal-to-noise ratio (SNR) of the FECG. These interfering sources, which typically show a strong non-stationary behavior, render the FECG extraction and fetal QRS (FQRS) detection demanding signal processing tasks.

In this thesis, several of the challenges regarding NIFECG signal analysis were addressed. In order to improve NIFECG extraction, the dynamic model of a Kalman filter approach was extended, thus, providing a more adequate representation of the mixture of FECG, MECG, and noise. In addition, aiming at the FECG signal quality assessment, novel metrics were proposed and evaluated. Further, these quality metrics were applied in improving FQRS detection and fetal heart rate estimation based on an innovative evolutionary algorithm and Kalman filtering signal fusion, respectively. The elaborated methods were characterized in depth using both simulated and clinical data, produced throughout this thesis. To stress-test extraction algorithms under ideal circumstances, a comprehensive benchmark protocol was created and contributed to an extensively improved NIFECG simulation toolbox. The developed toolbox and a large simulated dataset were released under an open-source license, allowing researchers to compare results in a reproducible manner. Furthermore, to validate the developed approaches under more realistic and challenging situations, a clinical trial was performed in collaboration with the University Hospital of Leipzig. Aside from serving as a test set for the developed algorithms, the clinical trial enabled an exploratory research. This enables a better understanding about the pathophysiological variables and measurement setup configurations that lead to changes in the abdominal signal's SNR. With such broad scope, this dissertation addresses many of the current aspects of NIFECG analysis and provides future suggestions to establish NIFECG in clinical settings.

Acknowledgments

First, I would like to thank Dr. Sebastian Zaunseder and Prof. Hagen Malberg for the opportunity to be part of the IBMT as well as their supervision and support throughout the process. I'd also like to thank the good men at the IBMT: Alex, Daniel, Felix, Johann and Martin, for making the doctoral experience bearable with our fruitful Fridays 4 p.m. meetings. Likewise, my appreciation to the several friends I made in Dresden, who made this time unforgettable.

I'd also like to thank our clinical partners from the University Hospital of Leipzig Dr. Alexander Jank, Dr. Claudia Schmieder, Sophia Schröder, Susanne Fritze and Prof. Stepan Holger for their helpful insights on the medical aspects of gestation, collecting data, and proving very useful annotations. Also thanks to our colleagues at the Humboldt University of Berlin Dr. Maik Riedl and Dr. Niels Wessel.

Many thanks to Prof. Gari Clifford and Prof. David Clifton for receiving me at the IBME - Oxford. To the several collaborators and friends I made in England, particularly Joachim, Julien, Alistair, Lisa and Tingting, for taking me in and providing me with a greatly productive time in and out of pubs.

This work was sponsored by the Conselho Nacional de Desenvolvimento Tecnologico (CNPq - Brazil) with a doctoral scholarship and by the TU Dresden Graduate Academy as part of the Excellence Initiative of the German Federal and State Governments in the scope of travel and completion grants. Without their financial support, this work would not have been possible.

To Sabrina for her love, understanding and companionship along the years, enduring with me several long work nights. To her family for being my home away from home. I would also like to thank my friends back home for being a constant source of bad decisions and who kept reminding me that being a Ph.D. candidate is not "an actual job". At last but not least, my gratitude goes to my family. To my parents for raising and supporting me, whose hard work and sacrifice has been an example and inspiration for me throughout my whole life. And for my siblings for loving and annoying me, not necessarily in this order.

Contents

Abstract i

Acknowledgment iii

Contents v

List of Figures ix

List of Tables xi

List of Abbreviations xiii

List of Symbols xix

1 Introduction 1
- 1.1 Background and Motivation . . . 1
- 1.2 Aim of this Work . . . 3
- 1.3 Dissertation Outline . . . 3
- 1.4 Collaborators and Conflicts of Interest . . . 4

2 Clinical Background 5
- 2.1 Physiology . . . 5
  - 2.1.1 Changes in the maternal circulatory system . . . 5
  - 2.1.2 Intrauterine structures and feto-maternal connection . . . 6
  - 2.1.3 Fetal growth and presentation . . . 8
  - 2.1.4 Fetal circulatory system . . . 10
  - 2.1.5 Fetal autonomic nervous system . . . 10
  - 2.1.6 Fetal heart activity and underlying factors . . . 11
- 2.2 Pathology . . . 13
  - 2.2.1 Premature rupture of membrane . . . 13
  - 2.2.2 Intrauterine growth restriction . . . 14
  - 2.2.3 Fetal anemia . . . 15
- 2.3 Interpretation of Fetal Heart Activity . . . 15
  - 2.3.1 Summary of clinical studies on FHR/FHRV . . . 15
  - 2.3.2 Summary of studies on heart conduction . . . 17
- 2.4 Chapter Summary . . . 18

3 Technical State of the Art **19**
3.1 Prenatal Diagnostic and Measuring Technique . . . 19
3.1.1 Fetal heart monitoring . . . 19
3.1.2 Related metrics . . . 22
3.2 Non-Invasive Fetal ECG Acquisition . . . 23
3.2.1 Overview . . . 23
3.2.2 Commercial equipment . . . 24
3.2.3 Electrode configurations . . . 26
3.2.4 Available NIFECG databases . . . 27
3.2.5 Validity and usability of the non-invasive fetal ECG . . . 29
3.3 Non-Invasive Fetal ECG Extraction Methods . . . 32
3.3.1 Overview on the non-invasive fetal ECG extraction methods . . . 32
3.3.2 Kalman filtering basics . . . 36
3.3.3 Nonlinear Kalman filtering . . . 46
3.3.4 Extended Kalman filter for FECG estimation . . . 51
3.4 Fetal QRS Detection . . . 59
3.4.1 Merging multichannel fetal QRS detections . . . 60
3.4.2 Detection performance . . . 61
3.5 Fetal Heart Rate Estimation . . . 62
3.5.1 Preprocessing the fetal heart rate . . . 63
3.5.2 Fetal heart rate statistics . . . 63
3.6 Fetal ECG Morphological Analysis . . . 64
3.7 Problem Description . . . 65
3.8 Chapter Summary . . . 66

4 Novel Approaches for Fetal ECG Analysis **67**
4.1 Preliminary Considerations . . . 67
4.2 Fetal ECG Extraction by means of Kalman Filtering . . . 69
4.2.1 Optimized Gaussian approximation . . . 69
4.2.2 Time-varying covariance matrices . . . 74
4.2.3 Extended Kalman filter with unknown inputs . . . 77
4.2.4 Filter calibration . . . 79
4.3 Accurate Fetal QRS and Heart Rate Detection . . . 81
4.3.1 Multichannel evolutionary QRS correction . . . 81
4.3.2 Multichannel fetal heart rate estimation using Kalman filters . . . 84
4.4 Chapter Summary . . . 94

5 Data Material **97**
5.1 Simulated Data . . . 97
5.1.1 The FECG Synthetic Generator (FECGSYN) . . . 97
5.1.2 The FECG Synthetic Database (FECGSYNDB) . . . 100

5.2 Clinical Data . . . 101
5.2.1 Clinical NIFECG recording . . . 101
5.2.2 Scope and limitations of this study . . . 104
5.2.3 Data annotation: signal quality and fetal amplitude . . . 105
5.2.4 Data annotation: fetal QRS annotation . . . 116
5.3 Chapter Summary . . . 118

6 Results for Data Analysis 119
6.1 Simulated Data . . . 119
6.1.1 Fetal QRS detection . . . 119
6.1.2 Morphological analysis . . . 123
6.2 Own Clinical Data . . . 125
6.2.1 FQRS correction using the evolutionary algorithm . . . 125
6.2.2 FHR correction by means of Kalman filtering . . . 127

7 Discussion and Prospective 133
7.1 Data Availability . . . 133
7.1.1 New measurement protocol . . . 134
7.2 Signal Quality . . . 136
7.3 Extraction Methods . . . 139
7.4 FQRS and FHR Correction Algorithms . . . 142

8 Conclusion 145

References 147

A Appendix A - Signal Quality Annotation 175

B Appendix B - Fetal QRS Annotation 177

C Appendix C - Data Recording GUI 179

List of Figures

1.1 Abdominal signal containing FECG signal 3

2.1 Feto-maternal circulatory system. 7
2.2 Exemplary beat demonstrating morphological features 17

3.1 NIFECG recording principle 24
3.2 Predominant sources present in abdominal measurements. 25
3.3 Different electrode configurations present in the literature. 28
3.4 Indirect techniques for FECG extraction and their main characteristics 33
3.5 Representation of Bayesian estimation based on prior observations 38
3.6 Signal processing work-flow for NI-FECG extraction using TS_{ekf}. 52
3.7 Kalman filter ECG modelling algorithm 53
3.8 KF modelling using real recording. 54
3.9 FECG extraction using EKF algorithm 56
3.10 Exemplary fetal heart rate tachogram. 62
3.11 Signal processing steps for morphological analysis. 65

4.1 Low-pass filters for quadratic spline wavelet. 71
4.2 Stationary wavelet transform fitting. 72
4.3 Comparison of best performing fitting methods 74
4.4 State's evolution using the EKF24 75
4.5 Example of covariance matrix adaptation using EKF2 77
4.6 Representation of the xSQI metric 83
4.7 Qualitative example of different sub-functions used for defining the fitness function. 84
4.8 Evolutionary algorithm at different iteration steps 85
4.9 Example of newly proposed SQIs on good and bad quality extracted segments . 89
4.10 Relative frequency of each class the on annotated training set and normalization function used after classification. 92

5.1 Three dipole components and resulting vectorcardiogram. 99
5.2 Side and upper view the of volume conductor 101
5.3 Exemplary simulated signals 102
5.4 Electrode configuration used in this work. 103
5.5 Exemplary signals collected during this work. 104
5.6 Study's population 105
5.7 Collected signals with different quality 107

5.8 Annotated segments for NIFECG signal quality . . . 110
5.9 Channel-by-channel overview of consensus annotations for FECG and SNR . . . 112
5.10 Post-hoc analysis for channel quality . . . 113
5.11 Recording's quality across different gestational weeks . . . 113
5.12 Effect sizes across different gestational weeks . . . 115

6.1 Detailed F_1 results for FQRS detection accuracy . . . 121
6.2 Post hoc analysis for FQRS detection accuracy . . . 122
6.3 Two exemplary segments are portrayed during which BSS_{ica}'s mixing matrix is updated . . . 122
6.4 Differences in measured FQT intervals between extracted channels and reference 124
6.5 Differences in measured FTQRS ratios between extracted channels and reference 124
6.6 Accuracy of FQT and FTQRS extraction for the different methods . . . 125
6.7 Evolutionary QRS correction using three channels . . . 126
6.8 Excerpt of clinical signals extracted using ICA . . . 127
6.9 Segments of data comprising SQI metrics . . . 128
6.10 Bar graph showing the feature importance using RELIEFF . . . 129
6.11 Correlations amongst SQI proposed features . . . 130
6.12 Example multichannel FHR estimation by means of Kalman filtering using three channels . . . 132

7.1 Timeline for new measurement protocol. . . . 134
7.2 Exemplary segment of new measurement protocol . . . 136

A.1 Signal quality annotation interface. . . . 175

B.1 Java GUI used for FQRS annotation . . . 178

C.1 Screenshots of recording GUI. . . . 180
C.2 Chages to the GUI during physiological maneuvers. . . . 181

List of Tables

2.1 Maternal cardiovascular changes during pregnancy 6
2.2 Influencing factors for the fetal heart activity 12

3.1 Available techniques in fetal heart monitoring. 21
3.2 Notation used in this work. 32
3.3 NI-FECG extraction algorithms. 37

4.1 Results for different fitting methods evaluated. 73
4.2 Summary of fetal SQI metrics used in this work. 90
4.3 Fetal QRS detectors evaluated in this work. 91

5.1 Scenarios used for simulating pregnancy's pathophysiological events. 101
5.2 FECGSYN model parameters used within this work 102
5.3 Descriptive statistics on collected data. 106
5.4 Clinical data annotation classes and definitions. 108
5.5 Intra-observer and inter-observer agreement by means of Krippendorff's alpha statistic. 109
5.6 Definition of fetal peak visibility consensus 110
5.7 Measures of dependency and bivariate association used in this study. 114
5.8 Correlation table for clinical data 117

6.1 Case-by-case FQRS results for FECGSYNDB 120
6.2 Results for FQRS detection accuracy and precision using the evolutionary correction algorithm 126
6.3 Resulting confusion matrix for the 10-fold cross validation 128
6.4 Performance comparison using proposed KF technique in terms of FHR accuracy and precision 131

B.1 Fetal QRS annotation markers used in this work 178

List of Abbreviations

abdECG	abdominal electrocardiogram
ACC	accuracy
ADC	analog-digital converter
AHA	American Heart Association
ALS	Autocovariance Least Squares
AM	Adaptive Methods
ANC	Adaptive Noise Canceller
ANFIS	Adaptive Neuro-Fuzzy Interference System
ANOVA	Analysis of Variance
ANS	autonomic nervous system
ANSI	American National Standards Institute
ApEn	approximate entropy
AR	autoregressive
AV	atrioventricular
BBI	beat-to-beat interval
BMI	body mass index
BP	blood pressure
bpm	beats per minute
BSS	Blind Source Separation
BW	baseline wander
cbPPG	camera-based photoplethysmogram
CHD	congenital heart defect
CI	confidence interval

CTG	cardiotocogram
DFA	detrended fluctuation analysis
DORV	double outlet right ventricle
DTW	Dynamic Time Warping
DWT	discrete wavelet transform
EA	evolutionary algorithms
ECG	electrocardiogram
EEG	electroencephalogram
EHG	electrohysterogram
EKF	Extended Kalman Filter
EKS	Extended Kalman Smoother
EM	electrode motion
EMG	electromyogram
EnKF	Ensemble Kalman Filter
eQRS	evolutionary QRS correction algorithm
ESN	Echo State Network
FAMD	Factor Analysis with Mixed Data
FBMs	fetal breathing-like movements
FBS	fetal blood sampling
FDA	U.S. Food and Drug Administration
FECG	fetal electrocardiogram
FECGSYNDB	Fetal ECG Synthetic Database
FECGSYN	Fetal ECG Synthetic Generator
FF	fixed fitting
FFT	fast Fourier transform
FHR	fetal heart rate
FHRV	fetal heart rate variability

FIR	finite impulse response
FMCG	fetal magnetocardiogram
FN	false negative
FP	false positive
FPO	fetal pulse oximetry
FQRS	fetal QRS
FQT	fetal QT
FSE	fetal scalp electrode
FST	fetal ST
FTQRS	fetal T/QRS
FV	fitness value
GBF	Grid-based Filter
GOF	goodness of the fit
GP	Gaussian Processes
GPL	General Public License
GSF	Gaussian Sum Filter
GUI	graphical user interface
HDR	heart rate detection rate
HF	high-frequency
HMM	hidden Markov model
HR	heart rate
HRV	heart rate variability
IBME	Institute of Biomedical Engineering
IBMT	Institut für Biomedizinische Technik
ICA	Independent Component Analysis
IC	independent component
IIR	infinite impulse response

ITAM	Institute of Technical and Medical Equipments
IUGR	Intrauterine growth restriction
IUP	intrauterine pressure
KF	Kalman Filter
LF/HF	low to high-frequency ratio
LF	low-frequency
LMS	Least Mean Squares
MAE	mean average error
MA	muscular artifact
MAP	maximum a posteriori
MECG	maternal electrocardiogram
MHR	maternal heart rate
ML	maximum likelihood
MMSE	minimum mean square error
MQRS	maternal QRS
MSE	mean square error
MVUE	minimum variance unbiased estimator
NIFECG	non-invasive fetal electrocardiogram
NMSE	normalized mean square error
NSSP	Nonlinear State-Space Projection
NSTDB	Normal Stress Test Database
OSET	Open-Source Electrophysological Toolbox
PCA	Principal Component Analysis
PCG	phonocardiogram
PCINC	Physionet/Computing in Cardiology Challenge
PDF	probability density function
πCA	Periodic Component Analysis

PPG	photoplethysmogram
PPV	positive predictive value
PROM	premature rupture of membranes
PVC	premature ventricular contraction
RI	recoding index
RLS	Recursive Least Squares
RMSE	root mean square error
RMSSD	root mean squared differences between adjacent beat-to-beat intervals
ROI	region of interest
RSF	random search fitting
SampEn	sample entropy
SA	sinoatrial
SDNN	standard deviation of all normal beat-to-beat intervals
SE	sensitivity
SGA	small for gestational age
SIS	Sequential Importance Sampling
SNR	signal-to-noise ratio
SOMs	Self-Organizing Maps
SPKF	Sigma-point Kalman filter
SQI	signal quality index
SQUID	superconducting quantum interference device
SQUID	Superconducting Quantum Interference Device
STFT	Short Time Fast Fourier Transform
SVD	Singular Value Decomposition
SWTF	stationary wavelet transform fitting
SWT	Stationary Wavelet Transform

TD	Tensors Decomposition
TP	true positive
TS	Template Subtraction
UF	uniform fitting
UIEKF	Unknown Input Extended Kalman Filter
UKF	Unscented Kalman Filter
VCG	vectocardiogram
VSD	ventricular septal defect
WGN	white Gaussian noise
WOG	weeks of gestation

List of Symbols

Greek Symbols

Symbol	Description	Dimensions	Units
α_i	amplitude normalization factor for i^{th} Gaussian kernel	$\mathbb{R}^{1\times1}$	mV
α_K	Krippendorff's alpha coefficient	$\mathbb{R}^{1\times1}$	–
χ^2	Chi-square statistic	$\mathbb{R}^{1\times1}$	–
δ	sampling period	$\mathbb{R}^{1\times1}$	ms
$\Delta\theta_{i,k}$	phase of the i^{th} Gaussian at time-step k	$\mathbb{R}^{1\times1}$	rad
η	Correlation ratio	$\mathbb{R}^{1\times1}$	–
η_k	random additive noise term	$\mathbb{R}^{1\times1}$	mV
$\eta_{\theta,k}$	Random additive noise to phase state	$\mathbb{R}^{1\times1}$	s
$\eta_{z,k}$	Random additive noise to signal amplitude state	$\mathbb{R}^{1\times1}$	s
κ	Kappa agreement coefficient	$\mathbb{R}^{1\times1}$	–
λ_v	Forgetting factor for weighting measurement noise covariance matrix	$\mathbb{R}^{1\times1}$	s
λ_w	Update coefficient for matrix process noise covariance	$\mathbb{R}^{1\times1}$	s
ω	angular frequency of current beat	$\mathbb{R}^{1\times1}$	rad/s
ϕ_i	position of the i^{th} kernel inside template	$\mathbb{R}^{1\times1}$	rad
ρ	Spearman's ρ correlation coefficient	$\mathbb{R}^{1\times1}$	–
τ_0	Initialization time	$\mathbb{R}^{1\times1}$	s

θ	phase information	$\mathbb{R}^{1\times1}$	rad

Roman Symbols

Symbol	Description	Dimensions	Units
$\widetilde{FQT}$	fetal QT interval error	$\mathbb{R}^{1\times1}$	ms
$\widetilde{FTQRS}$	fetal T/QRS ratio error	$\mathbb{R}^{1\times1}$	–
ACC	fetal QRS accuracy measure	$\mathbb{R}^{1\times1}$	%
$E1/E4$	fetal heart rate scoring statistics	$\mathbb{R}^{1\times1}$	bpm^2
$E2/E5$	root mean squared error between RR intervals	$\mathbb{R}^{1\times1}$	ms
F_1	fetal QRS accuracy measure	$\mathbb{R}^{1\times1}$	%
HDR	heart rate detection rate	$\mathbb{R}^{1\times1}$	%
MAE	mean absolute distance between fetal detections	$\mathbb{R}^{1\times1}$	ms
PPV	positive predictive value	$\mathbb{R}^{1\times1}$	%
s_k	Single diagonal entry from innovation covariance matrix	$\mathbb{R}^{1\times1}$	s
SE	sensitivity	$\mathbb{R}^{1\times1}$	%
$\mathbb{R}_{\geq0}$	non-negative real number	–	–
$\mathbb{Z}_{\geq0}$	non-negative integer number	–	–
$\widetilde{\mathbf{F}}_k$	state transition Jacobian matrix	$\mathbb{R}^{n\times n}$	–
$\widetilde{\mathbf{H}}_k$	observation Jacobian matrix	$\mathbb{R}^{m\times m}$	–
$\widetilde{\mathbf{V}}_k$	measurement noise Jacobian matrix	$\mathbb{R}^{m\times m}$	–
$\widetilde{\mathbf{W}}_k$	process noise Jacobian matrix	$\mathbb{R}^{n\times n}$	–
$\mathbf{D}_k$	unknown input system matrix	$\mathbb{R}^{n\times s}$	–
$\mathbf{E}_k$	unknown input feedthrough matrix	$\mathbb{R}^{m\times s}$	–
$\mathbf{F}_k$	state transition matrix	$\mathbb{R}^{n\times n}$	–
$\mathbf{G}_k$	control input matrix	$\mathbb{R}^{n\times m}$	–

$\mathbf{H}_k$	observation matrix transition	$\mathbb{R}^{m\times n}$	–
$\mathbf{K}_k$	Kalman gain	$\mathbb{R}^{n\times n}$	–
$\mathbf{P}_{k\|k-1}$	a priori state error covariance matrix	$\mathbb{R}^{n\times n}$	–
$\mathbf{P}_{k\|k}$	a posteriori state error covariance matrix	$\mathbb{R}^{n\times n}$	–
$\mathbf{W}$	mixing matrix	$\mathbb{R}^{n\times n}$	–
$\underline{0}$	all zeros column vector	$\mathbb{R}^{n\times 1}$	–
$\underline{d}_k$	unknown input	$\mathbb{R}^{s\times 1}$	–
$\underline{u}_k$	control input	$\mathbb{R}^{n\times 1}$	–
$\underline{v}_k$	measurement noise	$\mathbb{R}^{m\times 1}$	–
$\underline{w}_k$	process noise	$\mathbb{R}^{n\times 1}$	–
$\underline{x}_k$	state variable	$\mathbb{R}^{n\times 1}$	–
$\underline{y}_k$	observation vector	$\mathbb{R}^{m\times 1}$	–
$a_i[n]$	approximation at scale i (wavelet context)	$\mathbb{R}^{1\times 1}$	–
b_i	standard deviation of i^{th} Gaussian kernel	$\mathbb{R}^{1\times 1}$	rad
C_{xy}	spectral coherence between $x(t)$ and $y(t)$	$\mathbb{R}^{1\times 1} \in [0,1]$	–
f_s	sampling frequency	$\mathbb{R}^{1\times 1}$	Hz
$l_i[n]$	low-pass filter at level i (wavelet context)	$\mathbb{R}^{1\times 1}$	–
N_b	number of bins	$\mathbb{Z}_{\geq 0}$	–
N_h	number of harmonics	$\mathbb{N}1\times 1$	–
N_h	number of point for fast Fourier transform	$\mathbb{N}1\times 1$	–
N_k	number of Gaussian kernels	$\mathbb{Z}_{\geq 0}$	–
p_e	percentage of agreement by chance (Kappa statistic)	$\mathbb{R}^{1\times 1}$	–
p_k	Single diagonal entry from state prediction covariance matrix	$\mathbb{R}^{1\times 1}$	s

p_o	percentage of observed total agreement (Kappa statistic)	$\mathbb{R}^{1\times1}$	–
q_k	Single diagonal entry from process noise covariance matrix	$\mathbb{R}^{1\times1}$	s
r	Pearson's r correlation coefficient	$\mathbb{R}^{1\times1}$	–
r_k	Single diagonal entry from measurement noise covariance matrix	$\mathbb{R}^{1\times1}$	s
S_{xy}	cross-spectral density between $x(t)$ and $y(t)$	$\mathbb{R}^{1\times1}$	–
w	Cohen's w coefficient	$\mathbb{R}^{1\times1}$	–
$X(f)$	Fourier transform of signal at frequency f	$\mathbb{R}^{1\times1}$	–

And now for something completely different.

– Monty Python's Flying Circus (1971)

1 Introduction

1.1 Background and Motivation

Prenatal cardiac monitoring is an aspect of utmost importance in early detection of fetal distress. Currently, electronic fetal heart monitoring is used on the majority of pregnancy episodes in the developed world, whereby the analysis of *fetal heart rate (FHR)* is often used to identify risk situations for both mother and fetus [129, 365]. The main reasons for this monitoring is to rule out eventual environmental or congenital conditions that may lead to fetal/newborn morbidity or even death. Every year, about one out of 125 babies are born with some form of *congenital heart defect (CHD)* [13], which is the most common birth defect and the leading cause of birth defect-related deaths. An estimated 2.65 million stillbirths occurred worldwide in 2008, of which 98% occur in countries of low and middle income, with more than 45% during the intrapartum period [49, 242]. These stillbirth rates varied from 2 per 1000 (Finland) to 40 per 1000 (Nigeria and Pakistan) [242]. During 2014 in Germany, the rate of stillbirths was 5.4 per 1000 stillbirths and neonatal (i.e. during the newborn's first week of life) deaths [73]. The early and more effective detection of abnormal fetal health state can help obstetrics and pediatric cardiologists to prescribe proper medications in time, or to consider the necessary precautions during delivery or after birth [362].

Fetal heart monitoring is not only useful for diagnosing and monitoring CHD fetuses, but it also may improve the diagnosis of other heart-related pathologies such as hypoxia, growth restriction and anemia. Such complications can happen prior to or during birth and may have long lasting effects on the newborns health, if exposure is prolonged (e.g. cerebral palsy is related to cerebral hypoxia and birth complications). As mothers progressively decide to postpone their first pregnancy, there is a higher risk for the fetal health [143, 306]. Indeed, increasing the effectiveness and reducing costs of prenatal monitoring on risk pregnancies is a priority for both developed and underdeveloped worlds.

The standard technique for perinatal assessment of the developing heart is the *cardiotocogram (CTG)*. Despite being the most available mean of surveillance, CTG only provides time-averaged mechanical information about the fetal heart. Furthermore, CTG's interpretation is subjective and lacks consensus amongst experts/guidelines on its interpretation. These problems in CTG's usage have lead to high false-positive rates in the detection of pathological patterns [298]. Therefore, instead of producing a decrease in perinatal morbidity/mortality, CTG was made accountable for an increase in unnecessary obstetric interventions (e.g. cesarean delivery) and in instrumental vaginal deliveries [41].

Limitations on the current techniques have instigated the pursuit for alternative fetal monitoring methods over the last few decades. Particularly, because of its potential to furnish prenatal diagnostic information, the so-called *non-invasive fetal electrocardiogram (NIFECG)* (see Fig. 1.1) has become the focus of several studies [51, 92, 310, 333, 365]. Due to its higher temporal, frequency, and spatial resolution, the NIFECG enables the monitoring of *fetal QRS (FQRS)* complexes in a beat-to-beat manner. Therefore, the use of sophisticated FHR/*fetal heart rate variability (FHRV)* techniques is possible. FHRV parameters provide important indices in determining the functional state of the *autonomic nervous system (ANS)* and have been associated with diverse pathological conditions such as hypoxia (i.e. the deprivation of an adequate oxygen supply – see Hutter *et al.* [196] for a complete review) and growth restriction [188]. Beyond FHR and FHRV information, the *fetal electrocardiogram (FECG)* may allow a deeper characterization of the electrophysiological activity (i.e. heart electrical conduction) by means of morphological analysis of FECG's signal waveform. Such a morphological analysis provides additional insights that cannot be obtained through CTG. In contrast to CTG, NIFECG can be measured using regular *electrocardiogram (ECG)* surface electrodes attached to the maternal abdomen. This straightforward recording scheme provides considerable advantages regarding the recording effort, which makes NIFECG a suitable technique for the ubiquitous monitoring of risk pregnancies. Amongst those benefits is the non-requirement of an expert supervision during data collection[1], consequent long-term recording capability of NIFECG technique, and its relative low-cost.

Unfortunately, non-invasively recorded FECG signals are usually corrupted by many interfering noise sources, most significantly by *maternal electrocardiogram (MECG)* whose amplitude is usually much greater than those of the FECG. The generally low *signal-to-noise ratio (SNR)* of the resultant FECG makes the extraction (i.e. methods for separating the FECG from *abdominal electrocardiogram (abdECG)* measurements) and subsequent detection of the FQRS complexes a challenging task. Several contributions in the literature have focused on this canonical source separation problem (see [92, 365]), however slight progress has been made. Moreover, due to the lack of randomized clinical trials available, little is known about the nature of the NIFECG signal and its real diagnostic value. Despite its outstanding potential, the real diagnostic value of current NIFECG approaches have not been demonstrated to date. Consequently, its use in clinical practice is yet restricted.

[1] CTG, on the other hand, often requires medical experts to reposition the ultrasound probe.

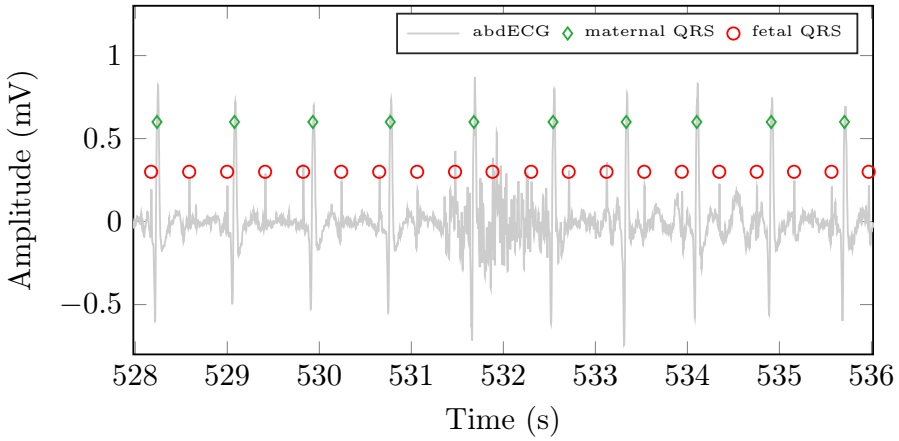

Figure 1.1: Abdominal signal containing FECG signal

1.2 Aim of this Work

The focus of this doctoral work is to tackle the problem of low SNR in NIFECG recordings using suitable signal processing algorithms. The topic is here divided into three main aspects, which are addressed in this dissertation, as follows:

- Several **extraction methods** have been proposed in the literature. Focus of this work is to evaluate these methods. Particular focus is put on improving the existing *Extended Kalman Filter (EKF)* algorithm, suggested by Sameni *et al.* [370]. To that end, the Kalman filter's dynamical model is extended to better characterize the varying signal quality of the NIFECG and better meet the statistical assumptions made on its noise content.
- Fetal **signal quality estimation** is of great importance in order to improve the specificity of FQRS/FHR detection algorithms. For this purpose, state-of-the-art adult signal quality indices are adapted and novel metrics derived. The output of those individual metrics can be then combined using machine learning techniques to classify segments of extracted NIFECG according to their quality.
- Previously suggested **FQRS and FHR detection** methodologies are often based on simple adaptations of adult ECG techniques. In this work, a novel offline algorithm based on evolutionary computing is used to deal with inaccurate FQRS detections. Meanwhile, a Kalman filter approach is used on estimating window-based FHRs online.

1.3 Dissertation Outline

In **Chapter** 2, the clinical background on the NIFECG and factors that may influence the fetal cardiac activity are described. Further in **Chapter** 3, the current technical state-of-the-art on prenatal monitoring is presented. Also in this chapter, an overview on the NIFECG signal processing is provided, including important mathematical concepts of the Kalman filter, relevant for the novel methodologies developed on the following chapter. In **Chapter** 4, novel

and improved methods for treating noisy NIFECG data, following the aspects presented in the previous section, are described in depth. **Chapter 5** summarizes the collected and simulated data materials that are used throughout this work for validating the suggested methodologies. The results of applying the methods from Chapter 4 using the databases provided in Chapter 5 are exhibited in **Chapter 6**. The results are further discussed in **Chapter 7** and last conclusions are drawn for future works in **Chapter 8**.

1.4 Collaborators and Conflicts of Interest

This thesis was written at the *Institut für Biomedizinische Technik (IBMT)* at the TU Dresden. During the development of this work, some collaborators have provided valuable help to the project. This section aims at summarizing the role of each partner. First, our clinical partners from the University Hospital of Leipzig (Prof. Holger Stepan, Dr. Alexander Jank, Dr. Claudia Schmieder, Sophia Schröder, Susanne Fritze and Julia Kage) were responsible for recording abdominal signals (shown in Chapter 5) and helped us define interesting clinical applications and scenarios where the NIFECG could supply valuable information.

In cooperation with Dr. Niels Wessel and Dr. Maik Riedl from the Cardiovascular Physics Department at the Humboldt University of Berlin, the highest score in the *Physionet/Computing in Cardiology Challenge (PCINC)* 2013 was achieved. Due to their expertise in filtering and analyzing *heart rate variability (HRV)* both during the PCINC 2013 and thereafter, a continuous exchange of ideas occurred.

From 2013 onwards, a new cooperation with the University of Oxford (United Kingdom) and the Emory University (United States of America) was established. In this partnership, together with Prof. Gari Clifford, Prof. David Clifton, Dr. Julien Oster and Dr. Joachim Behar, a comprehensive open-source simulation toolbox and large simulated database of NIFECG signals was developed (shown in Chapter 5). In addition, along with Dr. Alistair E. W. Johnson the first place award at the PCINC 2014 was obtained on the topic accurate beat detection from multimodal signals. Lastly, together with Dr. Lisa Stroux and the clinical partners in Leipzig a new recording protocol was implemented, which is currently being carried out (see Chapter 7).

Obstetrician 1*: Get the EEG, the BP monitor, and the AVV.*
Obstetrician 2*: And get the machine that goes "ping!".*
Obstetrician 1*: And get the most expensive machine - in case the administrator comes.*

– Monty Python's The Meaning of Life (1983) - Part I: The Miracle of Birth

2 Clinical Background

During a healthy pregnancy, a series of adaptations occur to both mother and fetus bodies. The aim of fetal monitoring is to evaluate if these changes are related to physiological or pathological conditions during the pregnancy. This chapter provides background information on the current clinical state of fetal monitoring, on which this doctoral work is built. With that in mind, Section 2.1 provides information about the fetal development that are relevant for fetal monitoring. Meanwhile, Section 2.2 describes some complications that may benefit from novel monitoring techniques. Background information on current approaches to interpreting the available information about the fetal heart is presented in Section 2.3.

2.1 Physiology

The duration of a normal human pregnancy spans approximately 280 days (40 weeks), counted from the onset of the last normal menstrual period onwards [361]. In Germany, 90% of births occur between 37 and 42 weeks [72]. During pregnancy, several changes to both fetus and mother's body take place, which are briefly described in the next few sections.

2.1.1 Changes in the maternal circulatory system

The arterial *blood pressure (BP)* of a healthy resting adult is on average around 120/80 mmHg [382, Chap.28], where the first value represents the systolic BP, while the second the diastolic BP. These values vary depending on age, sex, circadian rhythm, posture, respiration and modulation input from the ANS [382]. Changes in BP can occur slowly, e.g. during body changes due to pregnancy, or suddenly with postural changes (e.g., orthostatic maneuvers) [415].

Amongst the various adaptations that take place during physiological pregnancies, in this work focus is given to changes on the cardiovascular system. In this regard, throughout the gestation the maternal cardiovascular system is responsible for providing oxygen to and

Table 2.1: Maternal cardiovascular changes during pregnancy [372, 385, 415]. Upward arrow (↑) indicate an increase, while downward (↓) a decrease.

Parameter	Normal value	Change during pregnancy
Plasma volume	5 – 6 L	↑ 30 – 50 %
Blood pressure	120/80 mmHg	↓ small and temporary
Cardiac output	5 – 7 L/min	↑ 35 – 45 %
Stroke volume	70 – 100 mL	↑ 10 – 20 %
Heart rate	70 – 105 bpm	↑ 20 – 25 %
Vascular resistance	600 – 900 dyn·s·cm^{-5}	↓ 35 – 40 %

removing waste products to/from the unborn baby and, thus, several modifications of this system's parameters and function follow (see Table 2.1 [415]). Already at early stages of pregnancy, a maternal metabolic and endocrine increase occurs due to the growing need for oxygen and nutrients for supplying both fetus and maternal organs. During this period, the maternal blood volume, stroke volume, and heart rate increase [385, Chap.11]. The growth rate of these physiological variables depend on the size and number of fetuses [388]. On early gestational weeks, the vascular resistance around arterioles and veins decrease induced by hormonal changes [385]. Thus, during the first two trimesters, there is a slight decrease in BP (diastolic around −5 to −15 mmHg). The systolic pressure returns to normal values shortly after its decrease, whereas the circadian rhythm for BP remains unchanged during gestation [415].

2.1.2 Intrauterine structures and feto-maternal connection

The placenta (see Figure 2.1) is an organ responsible for connecting mother and fetus. Placental size, shape, and position[1] vary on each individual pregnancy. During the fetal development, this feto-maternal organ adapts itself to the needs of the growing embryo. In early pregnancy, the placenta serves as a barrier between embryo and maternal arterial blood. By the end of the fourth *weeks of gestation (WOG)*, the placenta is fully developed to allow the exchange of substances between mother and fetus [415]. Along the second half of pregnancy, the supply and transport function takes over which are crucial for the fetal development [385, Chap.1]. At this point, oxygen, nutrients, and hormones (endocrine function) are delivered by the umbilical cord to the fetus, whilst waste products such as carbon dioxide return to the maternal blood stream. Additionally, the placenta circulation system works as a barrier that selectively separates the maternal and fetal circulatory systems from one another, where many substances in the maternal blood are passed on to the fetus, but e.g. bacterias are not [289, 415].

Fetal and umbilical BPs are considerably lower than the maternal arterial pressure, with mean aortic pressure around 28 mmHg at 20 weeks and increasing to 45 mmHg towards the

[1] Possible positions are e.g. anterior (between fetus and abdomen), posterior (between fetus and spine), sideways (on either side) or fundal (on top of the maternal cervix). In rare cases, placenta bipartita or placenta praevia positions may occur. The first occurs when the placenta is constricted into occupying two sectors. The second is when the placenta is situated right on top of the internal cervical mouth of the uterus.

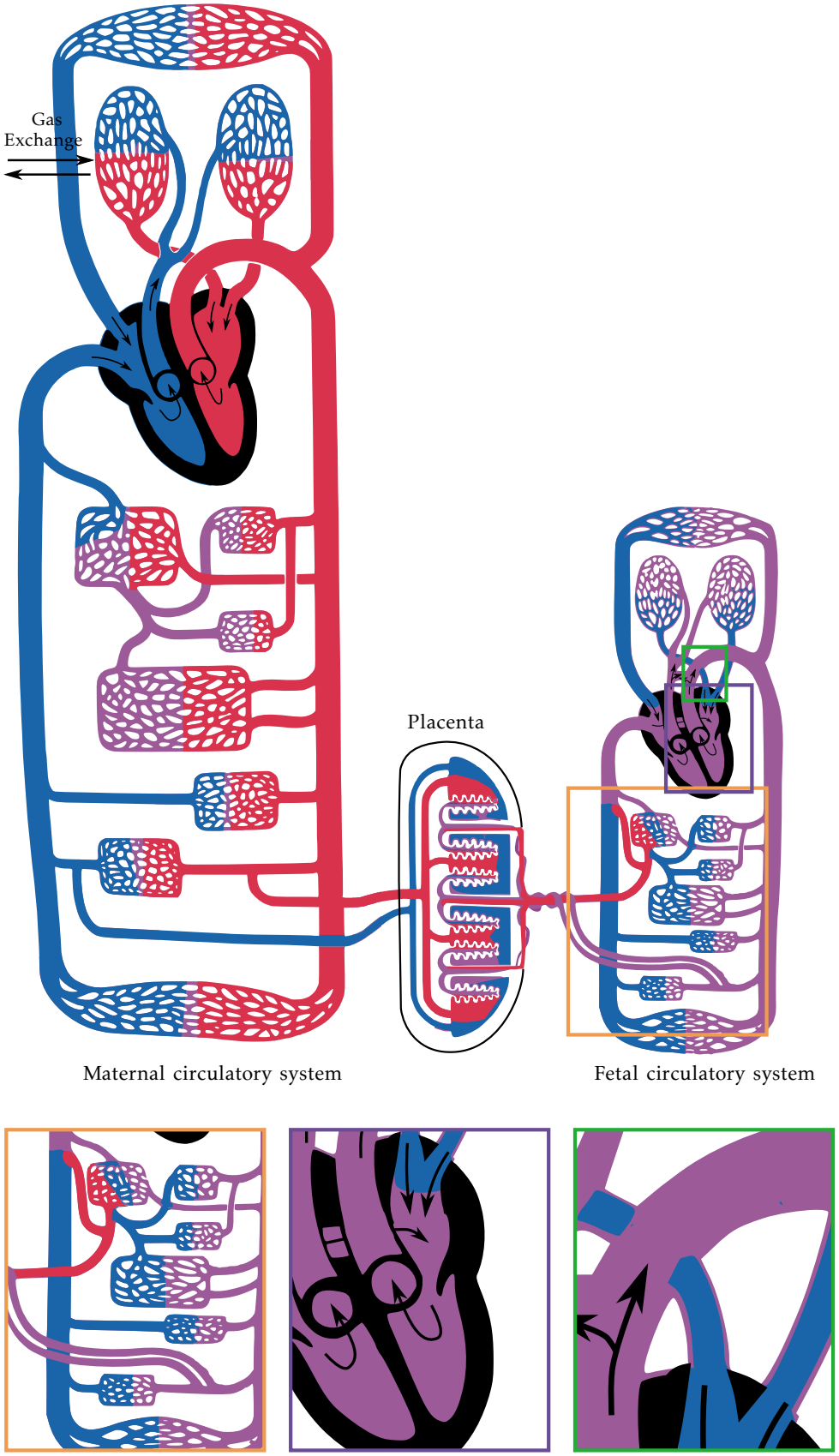

Figure 2.1: Feto-maternal circulatory system. In detail left (umbilical cord and *ductus venosus*), middle (*foramen ovale*) and right (*ductus arteriosus*). Illustration based on [112].

end of gestation [414]. According to Peter and Miller [328, p.83], a major part of the blood pressure fall occurs in the uteroplacental arteries due to its flow resistance. During the course of pregnancy, this resistance decays causing an increase in maternal blood flow. In physiological pregnancies approximately 450-600 mL of maternal blood flows through the placenta (ca. 10% of the total blood volume). As in any other organ, the magnitude of blood flow in the placenta is determined by the driving pressure (maternal BP) and the vascular resistance (uteroplacental). Although intrafetal umbilical vessels are innervated, it is believed that the extrafetal cord and placenta lack innervations. Therefore, neural mechanisms for regulation of placental perfusion are believed to be irrelevant [328, p.179]. On the other hand, increased uterine blood flow is essential to meet metabolic demand from the growing uterus as well as the placenta and fetus [293]. Despite taking part on the body's general vascular regulation, there is no evidence that the uterus itself possesses an auto-regulation mechanism for vasoconstriction. For this reason, minimalistic changes in the maternal BP are expected to have a large and direct effect on the uterine perfusion, therefore on the fetal supply. [385, 415, Chap.11].

The uterine perfusion is influenced by hormonal (e.g. cortisol/catecholamines) changes during pregnancy [365, 385, Chap.11]. For instance, the fetus influences the provision of maternal nutrients via the placental production of hormones that regulate maternal metabolism. Meanwhile, the placenta may respond to the fetal endocrine signals to increase transport of maternal nutrients by growth of the placenta, by activating transport systems and producing placental hormones to influence maternal physiology and even behavior [293].

Several other factors may influence the placental function and play a role in the fetal development, such as maternal drug intake, placental or fetal defects (e.g. genetic disorders). The reader is referred to [293] for a review. A reduction of the uteroplacental circulation may result in fetal hypoxia and growth restriction while severe reductions may result in embryo/fetal death [289]. Some of the pathologies that lead to placental insufficiency are further described in Section 2.2.

2.1.3 Fetal growth and presentation

During the first trimester of pregnancy, the organogenesis takes place. After this period, the underlying structures for larger organs (e.g. brain, eyes, and heart) are present [289, 415]. During the fetal period (from 9^{th} WOG onwards), maturation of tissues and organs, as well as a rapid growth, occur. This growth is characterized by a slowdown in the head growth and increase in body development, where the fetus weight increases from tens of grams to a couple kilograms and the sitting height from approximately 5 to 35 cm. During the fourth and fifth months, the fetus increases in size while most of the weight gain occurs in the last 2.5 months of gestation. During fetal prenatal monitoring, ultrasound assessment of the head, abdominal and femur lengths allow an estimate for the fetal development [361]. This diagnostic is relevant since the deprivation on the supply of nutrients for the fetus through the placenta may lead to a condition called *Intrauterine growth restriction (IUGR)* (see Section 2.2.2). The lungs start developing at the fifth WOG and are complete at late fetal stages. At the end of the 26^{th} WOG, the thin-walled terminal sacs are developed and the lung tissue is vascularized, which means

that ex-utero respiration would be possible. From this point of the gestation onward, premature newborns have a higher chance of survival given that intensive care is provided [289, Chap.10]. A fetus in-utero can obviously not breath. However, as consequence of the ANS development (described in Section 2.1.5) and as part of the lungs' maturation process, *fetal breathing-like movements (FBMs)* can be observed from the 10^{th} WOG onwards [172, 198]. During these intermittent FBMs, lungs contract with amniotic fluid which is essential for the stimulation of lung development [230]. Approximately 30 % of those movements occur during rapid eye movement sleep [289, Chap.10]. According to Blackburn [65, Chap.10], FBMs start rapid and irregular (occurrence around 6 % the time by 19 WOG) and become slower and more regular weeks before delivery (around 30 % to 40 % the time at rates around 30-70 breaths per minute).

During the first and second trimesters of pregnancy, the fetuses can move with relative ease within the uterus and have no specific presentation. This movement can be felt by the mother from the 5^{th} month on. According to Stinstra [409], fetuses move on average on every four minutes between the 8-20^{th} week and on every 5 min between 20-30^{th} WOG. Around the half of the third trimester, the fetus usually settles into a head-down position known as the vertex presentation, which is most appropriate for birth. However, the fetus may also settle in other less probable positions, e.g. breech, shoulder or other variants of the vertex position [16, 362, 409].

The fetus is surrounded by amniotic fluid and the uterus, moving outward the maternal abdomen there are layers of muscle, fat, and skin, respectively. The amniotic fluid is reported to have the best conductivity (at low frequencies and 37 °C) of all feto-maternal tissues, slightly higher than the umbilical cord and placenta [311, 331, 409]. Nevertheless, the abdominal volume conductor is not a steady conductor and its consistency, electrical properties and geometry of its compartments change during pregnancy. A drastic change in the electrical property of the feto-abdominal compartment is the appearance of the *vernix caseosa* in the last trimester [431]. The vernix caseosa is well-documented white-colored waxy layer that covers the fetus almost completely around this period. The vernix has been reported around the eyebrows of fetus at 17 weeks and, as gestation progresses, it coverage of the fetal skin increases until the 32^{nd} WOG, when most of the fetus is covered. From the 32^{nd} WOG onwards the vernix slowly dissolves, covering around 72 % infants' body between 33-37 WOG, 38 % (for 37.1-40.9 WOG) and 12 % (for 41.0-42.3 WOG). Thus some amount of vernix is still present on the skin at birth for virtually all full term infants, humans being the only animal species who present it. Fetal maturation is associated with an increased turbidity of the amniotic fluid, which is believed to be linked to the detachment of the vernix [449]. An important remark for the present work is the fact that the vernix has electrically insulating properties, with conductivity lower (by a factor of approximately 1 million) than the conductivity of other involved tissues e.g. muscles and amniotic fluid [311]. Therefore, it significantly attenuates the electrical potentials transmitted from the fetal heart to the maternal abdomen surface [246], specially between the 28^{th} to 32^{nd} weeks, when the vernix coverage is prevalent [246, 268, 329].

2.1.4 Fetal circulatory system

The heart is the first organ structure to develop and it already carries most of its adult functionalities after the organogenesis [202, 289, 415]. The fetal heart starts to beat in a coordinated manner approximately 21 days after ovulation (at the end of the 5^{th} WOG). Its electrophysiology is believed to be very similar to the one of an adult [289]. Initially, the fetal heart beats at around 80 – 90 bpm and rises up to the end of the 9^{th} week to 150 – 170 bpm, when the heart already attained most of its adult's characteristics [202, 280]. Around the 15^{th} WOG, the average FHR slowly decays reaching 120 – 160 bpm at late gestational age [334, 410]. See [119] for a complete depiction of the average FHR progression. Naturally, these absolute values are modulated along the pregnancy by the developmental stage of the ANS amongst several other external factors, which are further discussed in the following sections of this work.

Still, some mechanical differences between the fetal and adult circulatory systems exist. For instance, in adults the left ventricle pumps blood through the body, while the right ventricle pumps the poorly oxygenated blood into the lungs, where carbon dioxide is replaced by oxygen [403]. In the fetal case, oxygenated blood is supplied by the placenta through the umbilical vein (see Figure 2.1). For enabling the circulation of oxygen-rich blood throughout the body and organs, three different shunts are present, namely the *ductus venosus*, *foramen ovale* and the *ductus arteriosus* [409]. The first diverges ca. 80% [385] of the oxygenated blood that arrives from the umbilical cord into semi-functional liver towards the *vena cava*. The *foramen ovale* is a hole that connects both atria so that most blood bypasses the pulmonary circulation to the left atria, consequently being pumped through the body by the left ventricle. The latter structure, the *ductus arteriosus*, is also used to diverge blood which has reached and is pumped out of the right ventricle from the lungs by connecting the pulmonary artery to the aorta [409]. Despite no gas exchange being performed within the lungs, blood is pumped throughout the whole fetal body (including lungs). After birth, the *foramen ovale* closes with the first seconds/minutes and the *ductus arteriosus* partially closes within 10-15 hours (taking up to 3 weeks for complete closure), and the *ductus venosus* usually closes within the first week. Other minor changes in the physiology of the baby's heart and its circulatory system take place within the first year of life [16, 365].

2.1.5 Fetal autonomic nervous system

Human heart beats are caused by the pseudo-periodical excitation of the myocardium. When physiological, this excitation originates on the *sinoatrial (SA)* node and propagates through different structures of the heart. The nervous system is one of the earliest systems to begin to develop, but it is the last to be completed (after birth). Due to this extensive formation process, prolonged in-utero insults may have consequences to development of the nervous system [178]. The SA node is the primary structure of the electrical conduction system of the heart to manifest, followed approximately 40 days later by a discernible *atrioventricular (AV)* node, the Bundle of His and Purkinje fibers [29, Chap.1]. The electric impulse is usually generated by the SA node that acts as the primary cardiac pacemaker.

The SA node is strongly innervated by ANS's two main functional branches: the parasympathetic (i.e. *nervus vagus*) and sympathetic nervous system (i.e. spinal nerves). Over longer periods of time, this autonomic innervation influences the sinus node and serves as indirect link between the natural pacemaker with regulatory centers in the brain [202, 410]. The sympathetic system is responsible for the physiological changes in the fight-or-flight response in the presence of physical or psychological stress. Meanwhile, the parasympathetic system is responsible for homeostasis, rest, and digest functions. Therefore, an elevated sympathetic activity leads to an accelerated *heart rate (HR)*, while an increase in parasympathetic activity to a deceleration. The balance between these antagonist forces are responsible for the characteristic oscillations of the *beat-to-beat interval (BBI)*s [276], which on the fetal case are responsible for the FHRV. In early pregnancies, the sympathetic activity is predominant, since the nervus vagus (responsible for parasympathetic activity) develops between the 11-20$^{\text{th}}$ WOG [181, 415, 465]. This fact explains the slow decrease on average FHR during the second and third trimesters (as pointed out in the previous section). Moreover, a second form of modulation is provided by the cholinergic and adrenergic nerves of the SA node. The first is already evident at early stages of fetal growth, whereas the second develops much later and is completed only some months after birth [202], so that the FHR further sinks while the FHRV increases. Despite the intense research in the area, the development of the ANS is not yet fully understood [410]. The modulation produced by the ANS is influenced by multiple systems, e.g. respiratory, digestive, metabolic, baroreceptor reflexes and input from higher functions of cerebral centers [181]. Due to this close relationship between FHR/FHRV and the maturation status of the ANS, several researchers focus on estimating the health state and development stage of the fetus through heart rate parameters.

2.1.6 Fetal heart activity and underlying factors

As mentioned in Section 2.1.4, some changes in FHR and FHRV are expected as pregnancy progresses. Meanwhile, in Section 2.1.5, the ANS was shown to modulate these rates distinctly at different stages of development. Indeed, several factors influence the fetal heart activity, such as the stage of pregnancy, environmental conditions to which unborn child and mother are exposed and individual characteristics. In order to evaluate the fetal development and its health state, monitoring its heart activity is crucial (see Section 3.1). In Table 2.2 [276, 385], an overview of the various factors that influence the fetal heart activity is presented. The motivation for such regard to these factors is twofold: i) short-term oscillations of the fetal heart activity can provide usable information about its health state; ii) disregarding some of these factors over longer time periods may have a negative influence on study findings on the fetal development [256]. To elucidate the complexity of the fetal heart activity, some of the aspects presented in Table 2.2 are further explained throughout this section.

For instance, uterine contractions are uterus muscular activities that take place during a large part of the pregnancy and vary in intensity and frequency. Deficiency in the umbilical blood perfusion due to cord compression might happen during a uterine contraction, which in current medicine is associated with a characteristic pattern in FHR (see FHR interpretation guidelines

Table 2.2: Influencing factors for the fetal heart activity [276, 385, Chap.33]

Influencing factors		
endogenous (maternal)	**endogenous (fetal)**	**exogenous**
blood pressure	gestational age	fetal movement
oxygenation	ANS regulation	fetal pathophysiological state
humoral factors (e.g. stress)	acidosis	sleep arousals
body posture	hemodynamics	uterine activity
pharmacological	congenital defects	
drug usage	infection	
body temperature		

[12, 296, 358]). According to these guidelines, in physiological cases, an *early deceleration* occurs when uniform, repetitive and periodic slowing of FHR occurs with early onset in the contraction, and return to baseline at the end of the contraction. *Late decelerations*, on the other hand, are indicators of a pathological state, where the slowing of FHR coincides with the onset mid-end of the contraction and its nadir occurs more than 20 seconds after the peak of the contraction. Changes in the maternal pulmonary pressure or fetal movements may have similar effects leading to a momentary deficiency on the exchange of oxygen and nutrients through the placenta.

Since the normal fetal development entails FBMs, the observation of this activity is an important clinical measure. In adult ECG, respiration has a great importance and reflects on several HRV parameters [421], therefore, the same principle is expected to apply to FHRV.

Based on the presence or absence of fetal movement and patterns of the heart rate, Timor-Tritsch *et al.* [428] and Nijhuis *et al.* [300] described four *fetal behavioral states* (namely, 1F, 2F, 3F, 4F). States are defined as coordinated relationship between different variables, such as gross or fine motor activity, eyes, and FBMs as well as FHR patterns. Behavioral states are reproducible from the 36^{th} onwards [117, 300]. Nevertheless, current studies make often use of simplified versions of the states described by Nijhuis *et al.* [300], particularly the states 3F and 4F rarely occur [335, 438]. As pregnancy progresses the increased occurrence of quiet and active states have been associated with several FHR/FHRV parameters [139, 188, 225, 241, 300, 335, 444].

Analogously to adults, fetal circadian rhythm fluctuations of the basal FHR can be observed on the last trimester [256]. This behavior is however considered as a reaction to the circadian changes in the maternal system. Evidence that supports this hypothesis is the fact that the antenatal circadian rhythm becomes ultradian at birth [281]. Similarly, synchronization periods between maternal and fetal average HR were found by [325, 349, 441, 444]. The latter suggested that this association is due to the maternal respiration. To confirm this hypothesis, Van Leeuwen *et al.* [443] described a higher incidence of such synchronization epochs when mothers exert a higher breathing rate. However, the exact cause for such behavior is still controversial, usually being attributed to heart sounds, since external stimuli such as vibroacoustic stimulation (e.g. music or speech) can affect FHRV [25, 276, 444]. A discussion on this topic is present in [199].

Moreover, it has been shown that psychological factors such as maternal stress [115], anxiety [226, 285], relaxation [116] or emotive state [285] can influence FHR/FHRV [444]. For instance

[285] demonstrated a correlation between maternal anxiety score and basal FHR. In this study, a significant effect for the patient group with low level of anxiety was related to an increase in maternal BP, which could incur in changes in the FHR. Additionally, there was an increase in the breathing rate of both groups, so that not only the acute emotional reaction but also the respiratory influence caused by the distress is plausible.

2.2 Pathology

Many complications during antenatal and intrapartum periods may lead to fetal *hypoxia*. Despite the various fetal compensatory mechanisms that take place, if hypoxia is prolonged, it can lead to acidosis (i.e. an increased acidity in the body fluids). Severe and acute acidosis are associated with significant morbidity (e.g. irreversible neurological damage) and mortality [4, 67, 196]. Hypoxia effectively reduces the energy storage available for repolarization of the myocardial cells, resulting in a changes on the FHR, FHRV and FECG waveforms [11]. Excessive uterine contractions are the leading cause of hypoxia, since they may decrease placental perfusion as well as compress the umbilical cord [38].

In this work, focus is put on three pathological conditions that are related to hypoxia. These conditions are briefly described along the next sections and their relationship with abnormal heart rate/morphological parameters (e.g. FHRV metrics) is hypothesized.

2.2.1 Premature rupture of membrane

Premature rupture of membrane (PROM) refers to rupture of the fetal membranes prior to the onset of labor irrespective of gestational age. According to Caughey *et al.* [77], preterm PROM complicates 2% to 20% of all deliveries and is associated with 18% to 20% of perinatal deaths. There are several factors may promote PROM, such as antepartum vaginal bleeding, direct abdominal trauma, smoking, drug use, low *body mass index (BMI)*, intra-amniotic infection and multiple pregnancy. After the occurrence of PROM, delivery is recommended when the risk of ascending infection is greater than the risk of prematurity [77]. In early preterm PROM patients (< 28 WOG) a lower amount of amniotic fluid (oligohydramnios) is a complicating factor because at these stages of pregnancy it may prevent respiratory breathing movements, therefore retarding the pulmonary growth [230]. Oligohydramnios is also associated with cord compression and, subsequently, with fetal hypoxia [263, 410]. Moreover, there is an increased risk of infection for both mother and fetus during this period, therefore preterm patients are usually admitted to hospitals and closely monitored until birth.

Particularly for patients below the 28^{th} WOG, treatments are generally more conservative and the pregnancy is usually sustained as far as possible [385, Chap. 25]. During this period, intermittent recordings of the FHR, together with the assessment of amniotic fluid volumetry, amniocentesis (to exclude intra-amniotic infection) and administration of antenatal corticosteroids (for accelerating fetal lung maturation [351]) and broad-spectrum antibiotics (for avoiding infections) [77]. From the 32^{nd} week onwards, a more active procedure is adopted, and

induced labor is beneficial for both mother and fetus [385, Chap. 25]. The German guidelines for the treatment of PROM patients are available at [36].

2.2.2 Intrauterine growth restriction

Intrauterine growth restriction (IUGR) describes a decrease in fetal growth rate that prevents an infant from obtaining its complete growth potential (i.e. its genetically predetermined size) [69, 266]. IUGR does not denominate a disease per se, but rather a manifestation of many possible fetal and maternal disorders [347]. Pregnancies affected by IUGR pose a major public health problem affecting from 5% to 7% of all pregnancies [69] since they are also associated with risk of hypoxia increased neonatal morbidity and mortality. In addition, it may increase the risks for the development of hypertension, diabetes, coronary heart disease and stroke in adulthood [347, 435].

In prenatal medicine, the estimated fetal weight is most commonly measured using 2D-ultrasound [435]. However, according to Resnik [347], there is no consensus on what limits should be used to define a *small for gestational age (SGA)* fetus/newborn. The most commonly used definition is a birth weight less than the 10^{th} percentile for a given gestational age [347, 385, 435]. Several standard curves for fetal growth have been suggested in the literature, but it has to be kept in mind that fetal weight depends on several socioeconomic factors. That is, a small fetus/newborn may merely represent the tail of the normal distribution without actually having had any growth restriction. In order to differentiate between SGA fetuses[2] and the pathological state of IUGR, additional tests using Doppler velocimetry are required to examine the umbilical and uterine arteries.

There are two types of IUGR, namely symmetric and asymmetric. Symmetric growth restriction is characterized by fetuses with smaller skeletal and head dimensions as well as abdominal circumference. This variant is considered to be indicative of an early intrinsic impairing condition, e.g.chromosomal abnormalities and congenital malformations. In those cases, growth is symmetrically impaired due to its occurrence during cell division in the first or second trimesters. Symmetric IUGR leads to a underdevelopment of the ANS (described in Section 2.1.5). In contrast, asymmetric IUGR is usually a consequence of exogenous factors, such as inadequacy on the availability of substrates for the fetal metabolism through the placenta. This disorder takes place later in pregnancy when fetal growth occurs primarily by an increase in cell size rather than cell number [69, 347, 410]. There is a strong association between IUGR, chromosomal disorders and congenital malformations. Moreover, intrauterine infections, maternal vascular diseases and maternal under nutrition may favor IUGR [69, 266]. Likewise, chronic hypoxia (high altitudes) associated with placental insufficiency plays a key role in the etiology of IUGR [196]. Nevertheless, the pathophysiological processes that lead to IUGR are not fully understood, and there is a lack of agreement on guidelines for managing this condition [81, 266, 294].

[2] SGA just refers to the fact that the fetus is small, which may be due to genetic reasons such as small parents. When nutrition is not satisfactory and there is an abnormal amount of amniotic fluid, IUGR is likely to be present.

2.2.3 Fetal anemia

Anemia describes a decrease on the density of erythrocytes (i.e. red blood cells) in the peripheral blood system. Erythrocytes' cytoplasm are rich in hemoglobin, an iron-containing molecule which can easily be bound with oxygen [382, Chap.23]. In pregnant women, the plasma volume increase (mentioned in Section 2.1.1) is usually more expressive than the multiplication of red blood cell mass, which results in a "physiological anemia" caused by hemodilution [372, 388]. However, since these quantities widely vary from pregnancy to pregnancy, the distinction between physiological and pathological cases is not straightforward [388].

The most common cause of fetal anemia is a pre-existing iron deficiency or other minerals such as folate or vitamin B12, necessary for the production of hemoglobin [385, Chap. 18]. Another cause is the immunoreaction from the mother to the fetal antigens, known as Rhesus-factor incompatibility. Such incompatibilities generate a high probability of developing fetal anemia (alloimmune-induced hemolytic anemia) of up to 20%-25% the cases [385]. Severe cases of anemia may lead to *hydrops fetalis* [259], a condition characterized by an excess of amniotic fluid (polyhydramnios) and the accumulation of fluids in different fetal compartments [385, Chap. 18]. Moreover, due to the low blood oxygen levels, the fetal heart needs to pump a greater volume of blood, which may cause congested heart failure [259]. Anemia diagnosis is performed through maternal blood sampling, ultrasound (to exclude hydrops or fetal heart failure), amniocentesis (invasive sampling the amniotic fluid) and fetal blood sampling. If the anemia is severe, treatment may include fetal intrauterine blood transfusion [455]. Since the fetal oxygen transport is deficient, anemia may lead to hypoxia. In fact, some FHR sinusoidal patterns are associated with severe anemia and hydrops [44]. For this reason, long-term monitoring of these patients is desirable.

2.3 Interpretation of Fetal Heart Activity

Overall, fetal heart monitoring follows the advances in adult cardiac assessment. As such, it may be divided into the analysis of the FHR and the analysis of morphological features of the FECG signal[3]. For completeness, in this section, a brief summary of those current approaches is presented.

2.3.1 Summary of clinical studies on FHR/FHRV

The FHR is qualitatively evaluated based on the visual inspection of its trace along with measures of *intrauterine pressure (IUP)* in clinical routines. By means of these traces, categorization with respect to baseline heart rate and its variability, accelerations and decelerations as well as sinusoidal patterns are carried out (see [39, 41, 295] for reviews). A number of guidelines for interpretation of these traces have been released and updated e.g. [12, 356, 358]. More precise computerized quantification of heart rate changes were further proposed [105] and

[3] Obviously, morphological analysis of the FECG only applies when electric/magnetic principles are used in data collection.

augmented the evaluation of such traces [39, 446]. However, due to the lack of universally accepted guidelines and poor inter and intra-observer agreements (even in cases where guidelines are accepted amongst clinicians) the effectiveness of current assessment techniques has been strongly criticized [8, 44, 62, 371]. This led researchers to look for alternative automated methods of quantifying those changes in the FHR.

For adults, the heart rate fluctuations (i.e. HRV) has been shown to be a strong, independent predictor of future health problems [391]. Different metrics for adult HRV have been proposed over the past 60 years, which can be divided into temporal (e.g. *standard deviation of all normal beat-to-beat intervals (SDNN)* or *root mean squared differences between adjacent beat-to-beat intervals (RMSSD)*), spectral (e.g. *low-frequency (LF)* or *high-frequency (HF)* content as well as *low to high-frequency ratio (LF/HF)* ratio) and nonlinear techniques (e.g. *approximate entropy (ApEn)*, *sample entropy (SampEn)* and *detrended fluctuation analysis (DFA)*). A rich literature is available on that topic, including a well-known guideline [421]. However, the *U.S. Food and Drug Administration (FDA)* withdrew its support to HRV being used as a clinical parameter in 1993, due to the lack of consensus on its efficacy [93]. Still, HRV is the focus of ongoing research, where novel methods are constantly being proposed. Such studies focus on HRV modulating parameters such as the length of the window around the signal of interest, preprocessing filters used, age and gender of subject, physical and psychological conditions, sleep-awake cycles, respiration and effect of drugs amongst others have been intensively investigated [317]. A historical perspective on HRV is available in [64] and an analysis of signal processing algorithms on [86]. Despite the extensive literature on adult HRV, there is to date no general agreement about how to characterize or interpret the short and long-term oscillations of the HR.

The same discussion is applicable for FHRV parameters, which usually are adaptations of the adult algorithms to consider the higher HR and slightly different spectral content. In this scope, several works are available on the fetal field using several parameters [79, 84, 134, 135, 137, 146, 157, 185, 188, 240, 386, 393, 427]. A review on some of these parameters is provided in [410]. Motivated by the physiological basic assumptions presented in Section 2.1.6, the main focus of FHRV research has been:

- evaluating the fetal ANS maturation or brain age [146, 153, 188, 240, 313, 386, 394, 427, 445, 456]
- distinguishing between IUGR and physiological pregnancies [84, 135, 136, 290]
- correlating FHR/FHRV parameters with fetal acidosis [140, 141, 323, 437, 457]
- synchronization between maternal and fetal heart rates [349, 442–444]
- classification of fetal behavioral states [139, 188, 190, 241, 438]
- effect of maternal physical (e.g. exercise [32, 271]) and psychological (e.g. stress [115] and anxiety [284, 285]) on fetal heart activity

Regardless of how many studies have investigated the FHRV, the vast majority of those works are very limited in terms of number of subjects/patients and pathophysiological conditions.

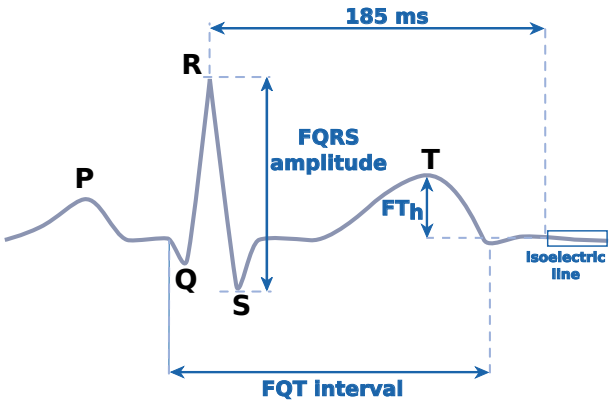

Figure 2.2: Exemplary beat demonstrating FQT interval, fetal T-wave amplitude (FT_h), FQRS amplitude and the defined isoelectric line (starting 185 ms after R-peak)

Another limitation of such studies is the fact that each one utilizes distinct statistical analysis and different recording principles (thus, different temporal and frequency resolutions – see Section 3.1), which makes their comparison and interpretability challenging.

2.3.2 Summary of studies on heart conduction

Similarly to the ECG analysis, the FECG allows for a deeper interpretation of the heart's electrical activity than merely assessing its rhythmic changes. This is realized by performing a morphological analysis over the so-called PQRST complex (see Fig. 2.2). This evaluation suffers from similar limitations as the FHR/FHRV analysis, i.e. the lack of standards. Additionally, FECG analysis is rarely used in clinical practice[4]. Several FECG features have been studied in the context of fetal monitoring (see Symonds *et al.* [418, Chap.6]). Between those features are: width and shape of the QRS complex, R/S ratio (using fetal *vectocardiogram (VCG)*), P wave morphology (inversion, notching, and disappearance), PR interval, QT interval and ST-segment. The reader is referred to Behar *et al.* [51] for an overview on available morphological features. In this work, focus was on the following metrics that have initially shown promising results [51]:

***Fetal QT (FQT)* segment:** in adults changes in the QT-interval are associated with myocardial ischemia [292], infarct [380], cardiomyopathy [59], sudden cardiac death [332] amongst several other conditions (see the position statement in [46]). Thus, the FQT interval is of much interest in the monitoring of fetal hypoxia. In a study by Oudijk *et al.* [316], a significant shortening of the FQT interval has been shown to be associated with intrapartum hypoxia resulting in metabolic acidosis, whereas in normal labor none of such changes do occur. In Behar [49], Behar *et al.* [56] the authors showed the possibility to automatically recover the FQT from NIFECG recordings. Three clinicians manually annotated the FQT from invasive and non-invasive recordings from 22 laboring women. The annotations

[4] As further presented in Section 3.1, there is one exception that invasively monitors the FECG during labor. However, the technique has recently been target of unfavorable criticism about its clinical value, see [57, 63, 297, 360].

were fused, and the errors between reference and automated detection were found to be in a similar range to adult QT-analysis.

***Fetal ST (FST)* segment:** it is believed that an elevation of the FST segment and T wave identifies hormone-induced fetal heart muscle responding to hypoxia, where a deviation from the baseline indicates a pathological response [11]. For this reason, fetal monitoring could greatly benefit from FST analysis. However, the ST segment delineation involves the detection of the end of the T-wave and J-point, which even in adult ECG is a challenging task. Due to the considerably lower amplitudes and surrounding noise, the FST is hardly attainable. An alternative is to use the *fetal T/QRS (FTQRS)* ratio (as follows) as a proxy for the FST elevation.

***Fetal T/QRS (FTQRS)* ratio :** FTQRS was demonstrated to be a proxy for the ST segment using animal models by Greene *et al.* [165], where the authors examined 10 chronically instrumented fetal lambs at 115 days to term. The study showed that the normal FTQRS ratio was lower than 0.30, whereas it was in the range of 0.17 to 0.59 for eight of the lambs after inducing hypoxia and reverted to normal with normoxia. However, studies [57, 63, 297, 360] suggest that the FTQRS as proxy for the FST level is either not accurate enough, or that it does not provide meaningful information for fetal monitoring (see Section 3.1).

Regarding the difficult task of segmenting the largely unexplored FECG beats, the duration of such intervals highly depend on the gestational age and projection of the fetal heart (i.e. electrode configuration), and should be taken into consideration. Since no standard is available for morphological analysis, clinical considerations from the current studies have to be analyzed with caution. Symonds *et al.* [418] concluded in 2001 that "The issue of the value of current use of the FECG morphological characteristics and time intervals for the prediction of fetal compromise remains promising but unresolved". As Behar *et al.* [51] pointed out: 15 years later the problem remains unresolved.

2.4 Chapter Summary

In this chapter, an overview on the main pathophysiological influencing factors to the fetal heart activity were presented on Sections 2.1 and 2.2). In Section 2.3, the current antepartum clinical standards for interpreting the cardiac activity of the fetus were introduced. In the following chapter, the state-of-the-art on techniques for prenatal diagnostic (i.e. data acquisition) are presented. Particular focus is put on the NIFECG technique's signal acquisition and processing methods to enable its analysis.

All sorts of computer errors are now turning up. You'd be surprised to know the number of doctors who claim they are treating pregnant men.

– Isaac Asimov, quoted in Des MacHale, "Wit" (2003)

3 Technical State of the Art

In the previous chapter, clinical background information on the fetal development and cardiac activity was presented. The current chapter is mainly divided into two part, namely signal acquisition and processing. The first, comprises diagnostic techniques for prenatal monitoring devices available (Section 3.1) and NIFECG signal acquisition (Section 3.2). The latter, i.e. NIFECG signal processing, is the focus of this work and is investigated in depth within this chapter. MECG suppression / FECG extraction is presented throughout Section 3.3, where the method of choice (i.e. the Kalman filter) is discussed extensively in Sections 3.3.2 to 3.3.4. Further in Sections 3.4 to 3.6, techniques to perform and evaluate FQRS detection, FHR estimation, and FECG morphological analysis are showed. Lastly, in Section 3.7, the major signal processing challenges in fetal electrocardiography are summarized.

3.1 Prenatal Diagnostic and Measuring Technique

3.1.1 Fetal heart monitoring

Monitoring methods for the fetal heart activity may be divided into invasive (i.e. used during labor) and non-invasive (i.e. antepartum/intrapartum periods). Table 3.1 shows an overview of the available methods, which are further described throughout this section. The first works in fetal heart rate monitoring emerged during the 19^{th} century and dealt with the *auscultation of the fetal heart sounds*. By using the wooden stethoscope introduced in 1816 by René Laennec, Pinard suggested the intermittent auscultation of the FHR in prenatal care in 1895 [408]. Early works associated a slow return of the FHR to its baseline after a deceleration with "fetal sufferance" and that head compression produced bradycardia [418, Chap.2]. This rudimentary 120 years-old technique, was still the most often used method until the 1960's [385, Chap.33] and is still in use in developing countries and in resource-poor settings.

Recording the heart sounds using electronic amplification (i.e. collected using a microphone),

the so-called *phonocardiogram (PCG)*, was first suggested at the end of the 19$^{\text{th}}$ century. However, the presence of several noise sources (e.g. intestines and veins sounds, external noise, and fetal movements) have rendered the method impracticable [385, Chap.33]. Nevertheless, the technique substituted auscultation using stethoscopes until the 1960s, when its sensitivity began to be questioned [224]. Still, equipment based on PCG technology continue to be released, such as the Sensa monitor (Nuvo Group, Tel Aviv, Israel).

In the 1960s electronic monitoring of the FHR by means of *Doppler ultrasound* became available and its use rapidly disseminated. This recording of the FHR combined with the recording of uterine activity by an external pressure transducer (i.e., the IUP), constitutes the modern CTG [385, Chap.33]. As mentioned in Section 2.3.1, visual inspection of the FHR is subjective and has lead to high false-positive rates in the detection of pathological patterns [298]. Moreover, recent studies found no decrease in perinatal mortality or cerebral palsy associated with the use of CTG, aside from a potential reduction in neonatal seizures. On the contrary, CTG was associated with an increase in unnecessary obstetric interventions such as cesarean delivery (63% increase) and in instrumental vaginal deliveries (15% increase) [8, 39, 41, 358]. Furthermore, the side effect of long-term ultrasound exposure on the fetus is not completely understood, and there is a risk of provoking the heating of fetal tissues [45, 92, 411]. For this reason, the non-invasiveness of the CTG technique should be contested. These limited benefits provided by CTG have instigated further research on alternative techniques for fetal monitoring.

For instance, *hand-held Doppler ultrasounds* have recently gained researchers' interest as a low-cost method for under-developed countries [270, 413]. However, due to considerable susceptibility to noise and the need for directing the ultrasound probe towards the fetal heart at all times, it is usually used as an intermittent auscultation method such as the Pinard stethoscope and PCG (see [244] for a review of these methods and guidelines). Overall, acoustic signals such as PCG and Doppler methods have the benefit of providing means for obtaining cardiac valves opening and closure times, which is under current research in adult [406] (using low-cost PCG) and fetal monitoring [270] (using hand-held Doppler).

During late stages of labor, a simple pulse oximeter can be attached to the fetal cheek (i.e. invasively). Theoretically, the so-called *fetal pulse oximetry (FPO)* provides benefits over other techniques since in addition to fetal pulse rate, it may also serve as a proxy for oxygen saturation and tissue perfusion [114]. Despite initial reports about its usefulness [114, 261], a Cochrane study [122] analyzing four trials rapidly criticized the technique for not reducing cesarean rates when assisting CTG or increasing fetal and maternal outcomes.

Another non-invasive method for assessing the fetal cardiac activity is the *fetal magneto-cardiogram (FMCG)*. The FMCG measures the magnetic flux density which emanates from the heart to the surroundings of the maternal abdomen. Due to the low magnitude of these magnetic fields ($B_{FECG} \approx 10^{-12}\ T$, i.e. several of orders of magnitude weaker than earth's magnetic field) and necessity for substantial noise reduction, highly sensitive *Superconducting Quantum Interference Device (SQUID)* sensors are required. For this reason, the FMCG is usually measured by a large equipment (i.e. short-term only) within a magnetically shielded room and using several channels (ranging up to a couple hundred channels). The FMCG is well-suited

Table 3.1: Available techniques in fetal heart monitoring [51, 92, 329]. Approaches based on magnetic and electric principles may provide information on the cardiac conduction, while acoustic ones on valve opening/closing times. Abbreviations stand for: Stand. = standardized analysis; Invas. = invasive method; Intrap. = intrapartum; CTG = cardiotocogram; FCMG = fetal magnetocardiogram; FPO = fetal pulse oximetry; FSE = fetal scalp electrode.

Method	Principle	Stand.	Invas.	Antepartum	Intrap.	FHR	Cost[†]	Long-term	Other characteristics
CTG	mechanic/ acoustic	Yes	✗[‡]	✓ (≥ 20 WOG)	✓	✓	$$[§]	✗	– trained expert required during recording – only short-time capable – FHR available on window averages – active method (ultrasound irradiation) – prone to maternal/fetal HR confusion – sensible to fetal/maternal movement
FMCG	magnetic	No	✗	✓ (≥ 20 WOG)	✗	✓	$$$	✗	– multichannel (≫ 20 channels) – high SNR for FECG – expert personnel required during recording – only short-term capable
FPO	optic	No	✓	✗	✓	✓	$	✗	– single channel only – application possible after rupture of membranes – estimate for fetal oxygen saturation available – usability often questioned
FSE	electric	No	✓	✗	✓	✓	$$	✗	– single channel only – application possible after rupture of membranes
NIFECG	electric	No	✗	✓ (≥ 20 WOG)[¶]	✓	✓	$	✓	– low SNR for FECG – presence of vernix caseosa severely reduces SNR – no skilled personnel required during recording
PCG	mechanic/ acoustic	No	✗	✓ (≥ 28 WOG)	✗	✓	$	✗	– lowest SNR of all methods – requires expert to locate fetus – sensitive to surrounding and gastrointestinal noises

[†] Cost displayed as $ = hundreds of dollars; $$ = thousands of dollars; $$$ = tens of thousands of dollars. Estimated values based on author's best of knowledge.

[‡] The aspect of safety and invasiveness on CTG recordings is still controversial and it has not been demonstrated that ultrasound irradiation exposure was completely safe for the fetus [92]. See Duck [120] for a detailed overview on the topic.

[§] Hand-held Doppler are a low-cost 1-D variant of the clinically used ultrasound, whose prices on the tens of dollars range.

[¶] As mentioned in Section 2.1.3, between the 28^{th}-32^{nd} WOG, the vernix caseosa completely involves the fetus. This layer is highly insulating and severely reduces the fetal SNR. From the 32^{nd} week onwards the layer slowly dissolves from the fetal skin into the amniotic fluid [409], around the 37^{th} WOG about 60% of the fetal body is free of the layer [449]

for clinical measurement, generally producing fetal cardiac waveforms of good quality, which are used for diagnosing fetal cardiac conduction disorders. Despite being already available on the mid-1970s, its popularity only increased at the beginning of the 1990s. Due to the expensive equipment and necessity of skilled personnel to carry out measurement, its use has been hampered [329, 330, 410]. Nevertheless, owing to its high temporal/spatial resolution and good SNR for the fetal signal, several published works investigate FHRV metrics using FMCG recordings, e.g. [157, 189, 190, 386, 427, 440, 443].

The FECG is the electrical equivalent of the FMCG [246] and presents a viable alternative that can be recorded invasively or non-invasively. Invasive FECG technology, the so-called *fetal scalp electrode (FSE)*, uses an electrode attached to the presenting part of the fetal scalp. This electrode is fixated to the fetal skin using either a needle-like spiral electrode that penetrates (screws into) the skin surface, or using a spring-loaded clip to skew a piece of skin. In any case, one electrode (positive electrode) is attached to the fetus, while other is used to make contact with the vaginal vault and cervix (negative electrode) and a third is used as common mode e.g. on the maternal thigh [418, Chap.4]. Three major drawbacks discourage the use of the FSE: i) its restricted usability (i.e. it can only be used during labor stages, after the rupture of membranes); ii) its associated risk of infection, due to its invasiveness; and iii) the reduced number of available leads (which prevents a three-dimensional analysis of the myocardium electrical activity [52]) [18]. To date, the only FSE commercial equipment available is the STAN® monitor (Neoventa Medical, Mölndal, Sweden), which performs both heart rate and morphological analysis of the FECG in clinical environments [92]. For this purpose, STAN provides FHR readings, a proxy measure for the FST segment deviation (the FTQRS ratio, mentioned in Section 2.3.2) and evaluates whether biphasic FST segments are present or not [18, 466]. Despite being readily available, a recent Cochrane study [297] reviewed six randomized trials that compared the effect of analyzing FECG waveforms during labor with alternative fetal monitoring methods. The trials used different versions of the STAN and included a total of 26,446 women, but showed no significant difference in primary birth outcome achieved using the FST proxy when compared to FHR monitoring alone. More recently, another study including 11,108 women has revealed that ST-segment analysis, as an adjunct to conventional intrapartum electronic fetal heart-rate monitoring, did not improve perinatal outcomes and did not decrease operative-delivery rates either [57]. Therefore the FSE premise is under current debate, see [47, 63, 66, 297, 360, 469].

The latter non-invasive FECG technique, namely NIFECG, is the focus of this work and is described separately in Section 3.2.

3.1.2 Related metrics

In addition to the several challenges in the fetal heart monitoring, the definition for fetal outcome is largely discussed in the medical society about their efficacy in predicting neonatal morbidity. Some of the metrics for assessing the fetal state hypothesize about the relationship between hypoxia and fetal metabolic acidosis. The most established one is the Apgar score [28], which is a summary metric developed on the 1950s that infer the health state of newborns

based on five criteria (Appearance, Pulse, Grimace, Activity, and Respiration - which forms the acronym Apgar). The scores range from 0 to 10 and are usually performed 1 and 5 minutes after birth. Despite being largely used to date, the score has been criticized about its value in asphyxia assessment for over 30 years [417].

During labor, *fetal blood sampling (FBS)* may be applied in evaluating parameters such as pH and base deficit/excess and lactate changes. Some studies [48, 212] attribute a decrease in the number of interventions to this technique. Nevertheless, reports in literature are contradictory [8, 80] about the efficacy of such adjunctive methods. Correlation of FBS values and perinatal outcome depends on the time interval between sampling and birth. Moreover, fetal capillary blood is likely to be affected by the redistribution of circulation during fetal hypoxemia, thus not being a well-representing factor for the central circulation [450]. The analogous to FBS after birth is the umbilical cord blood sampling (from artery or vein), which suffer from similar drawbacks in terms of interpretation since fetuses usually tolerate acidosis through compensatory mechanisms until it is very severe [30].

3.2 Non-Invasive Fetal ECG Acquisition

3.2.1 Overview

In 1906, only 3 years after the first suggestion of ECG by Einthoven, Cremer [99] proposed the use of FECG. Cremer along with following works on the beginning of the 20$^{\text{th}}$ century suggested the use of abdomino-vaginal or abdomino-rectal electrodes [418, Chap.2], while the use of non-invasive abdominal leads was suggested in the mid-1900s by [183, 184]. A detailed history of the developments that lead to NIFECG technique is available in [418].

As earlier discussed, there are several advantages of using the NIFECG technique. For instance, it makes use of convenient surface electrodes which can be spatially distributed onto the maternal abdomen (see Figure 3.1), usually being applicable from 20th week of gestation onwards. As in adult ECG, the premise is to detect the summation of the stage-wise electrical events that occur within myocardial cells, seen from the body surface projection. These electrical potential changes relate to fluctuations in biochemical action potentials in the myocardium over time and result in the PQRST complex [11] (see Fig. 2.2). Early works on extracting morphological information from NIFECG recordings have been published by [53, 85, 344]. As regards to the FHR estimation, due to its high temporal resolution, NIFECG allows a beat-to-beat determination of the RR-intervals, while the CTG usually averages its estimates in 2-5 s blocks due to the poor quality of ultrasound recordings [15, 40, 107]. Another advantage is NIFECG's availability for multiple channels, that may provide information about the heart in three-dimensional projection, using e.g. the VCG representation of the myocardial activity. The VCG may help on predict ventricular arrhythmia [426] and assess QT dispersion [235]. Lastly, long-term continuous monitoring can be achieved by NIFECG when using Holter-like equipment. This feature is particularly relevant to evaluate the fetal circadian heart activity, behavioral states and periods of breathing movements (described in Section 2.1).

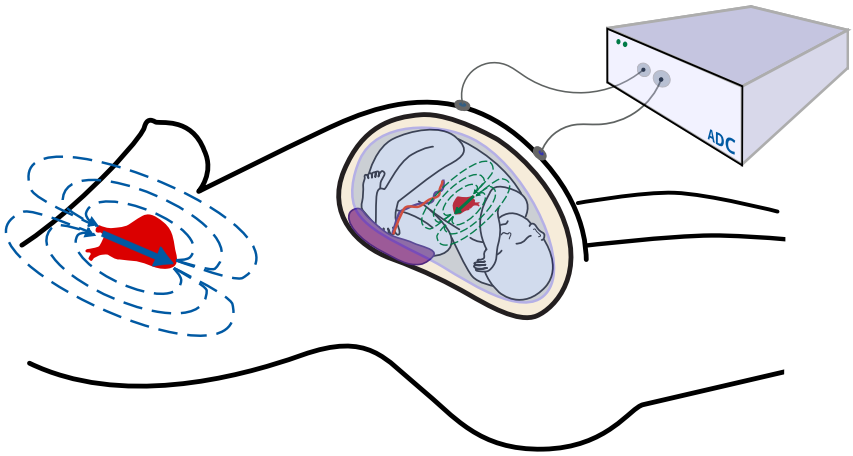

Figure 3.1: NIFECG recording principle

NIFECG's undemanding recording setup comes at the cost of a generally lower SNR for the FECG signal [144, 173]. Several noise sources are responsible for the relatively low SNR (summarized in Figure 3.2), where the MECG is the main interference overlapping the FECG both in time and frequency domains. This makes the task of extracting the fetal signal from the abdominal mixture arduous and, in fact, has hindered NIFECG's further usage in the clinical practice [18, 92]. Looking at the "bright side", one of the noise sources presented in Fig. 3.2, namely the uterine activity i.e. *electrohysterogram (EHG)*, presents yet another benefit of NIFECG technique. This because EHG can be used as a surrogate for IUP [354], therefore as in the CTG one could interpret the fetal heart response to uterus contractions. On the following subsections, further specifics about this technique's current state are provided.

3.2.2 Commercial equipment

Taking into account the various advantages of NIFECG technique, the recent advances in electronics and signal processing and the lacking proof of current standard techniques' efficacy, the commercial interest for NIFECG technology has re-emerged along the last few decades. At first glance, these commercial devices should be very similar to a Holter ECG with some few peculiarities [51]:

- sufficiently high *analog-digital converter (ADC)* resolution, to capture low amplitude FECG signals while avoiding that baseline changes (e.g. during movement or postural changes) saturate the ADC. Current studies on the literature use 16 to 24 bit ADC resolution [16];
- sampling frequency of 1 kHz is desirable to accurately define MECG and FECG peaks, moreover, low sampling frequencies can affect the accuracy of morphological measurements such as the FQT interval [46];
- number of channels should be around 3-10 channels, depending on the trade-off between capturing the multidimensional nature of both the fetal and maternal ECG and mother comfort (see Section 3.2.3 for a deeper discussion on the topic);

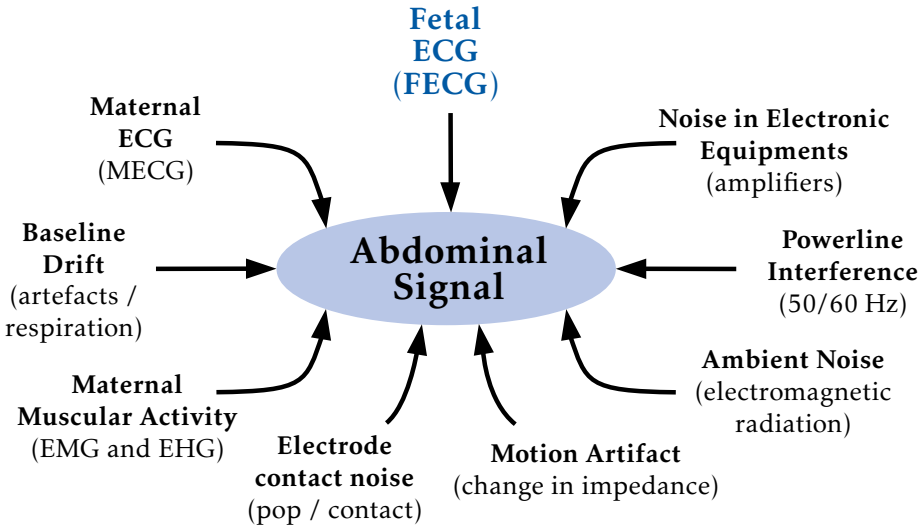

Figure 3.2: Predominant sources present in abdECG measurements. Interferences with biological origins (on the left), noises originated on interfaces between mother and equipment (below and in the middle), and equipment noise (on the right). Maternal ECG is the most significant disturbance. Modified from [16].

- battery life should be able to cover 24-48 h of recordings so that the feto-maternal circadian rhythm and fetal behavioral states (presented in Section 2.1.6) can be observed.

Currently, only two commercial NIFECG monitoring equipment are available, both having obtained FDA 510(k) clearance for intrapartum period (WOG > 36 weeks), namely AN24/Novii from Monica Healthcare (Nottingham, UK) and M100/M1000 monitors from MindChild Medical (North Andover/MA, USA).

Monica's AN24 was the first available apparatus which has been commercialized in Europe (CE approval) for nearly 10 years. Despite being recommended for WOG≥36 weeks, in Europe, its use is allowed for earlier WOGs (≥20 weeks). Monica provides the FHR, *maternal heart rate (MHR)* and uterine activity (EHG) in real-time with information on three leads and has shown some initial fair results. However, studies using the AN24 are still limited in population size and heterogeneity. Besides, Monica depends on the patient's abdomen receiving thorough skin preparation with a special abrading solution and gentle scrub of the skin for a better signal quality, which may be an inconvenience [16, 466].

Meridian monitors use a 32 lead system [51] where no skin preparation is required [466], however, its use is still restricted, and little information is available about its design and characteristics. Furthermore, very few studies are available since it has obtained FDA(k) for intrapartum monitoring on 2012.

Aside from the described commercial equipment, a handful of other companies, such as Nemo Healthcare (Eindhoven, Netherlands), PregSense from Nuvo Group (Tel Aviv, Israel) and KOMPOREL from the *Institute of Technical and Medical Equipments (ITAM)* (Zabrze, Poland),

have shown their intention of releasing novel NIFECG monitors in the near future. However, when applying commercial instruments in research there is the disadvantage of not knowing exactly what is inside the architecture and how the signal extraction is precisely performed. These cons can lead to unwitting mistakes and do not permit a full analysis of the data. All in all, commercial applications of NIFECG monitoring are in their early days, and there is a growing interest in improving their performance, aiming to reach a point where they provide actionable information to clinicians.

3.2.3 Electrode configurations

Aside from the ADC used, when attempting to collect NIFECG data careful consideration has to be given to the electrode configuration applied. To date, there is no available standard for the positioning of abdominal electrodes in NIFECG recordings. Similarly to adult electrocardiography, the morphology of the cardiac signal strongly depends on the lead configuration employed. In the abdECG case, although the lead system may be chosen and kept relatively constant (depending of course on the maternal and girth's size), the fetal position is time-varying, individual-dependent and cannot be easily identified prior to electrode placement. A general-purpose optimal electrode placement is impracticable for this reason [4].

Before proceeding, the terminology used in this work is defined based on the recommendations of the *American Heart Association (AHA)* [231]. Bioamplifiers usually make use of differential amplifiers, thus there are two main electrical potential inputs (V_{in}^{+} and V_{in}^{-}). As input to the amplifier, one generally has two active electrode, one connected to the positive terminal (V_{in}^{+}, henceforth graphically shown as ⊕) and another on the negative terminal (V_{in}^{-}, depicted as ⊖). In addition, a reference electrode (here termed as ground electrode – "GND") is used to improve common mode (unwanted noise) rejection. Take for instance Einthoven's lead II, the positive, negative, and ground electrodes are located on the left leg, right arm, and right leg, respectively. The negative electrode can physically exist (as in Einthoven's lead II) or be calculated as the average of some (or all) leads, as in Wilson's central terminal. When this electrode physically exists, the derivation is often referred to as "bipolar", when otherwise it is referred as "unipolar". However, the use of this historical nomenclature (i.e. "bipolar" and "unipolar") is discouraged by the AHA since all leads are effectively bipolar, thus, the term "unipolar" is described as lacking precision [231].

Numerous configurations have been proposed in the literature in an attempt to standardize the recording procedure. Several of those configurations are presented in Figure 3.3. From Fig. 3.3 it is evident that some authors rely on the most common fetal presentation (i.e. vertex, breech or shoulder), in order to reduce the number of leads used by aiming at usual positions for fetal head/thorax and, consequently, minimizing the application's complexity. Meanwhile, other authors aim at covering most of the abdomen to maximize the chances of obtaining FECG signal [4]. The inter-electrode distance also plays an important role in the signal SNR, FECG and MECG power. The closer the electrodes are from one another in a differential scheme, the more local similar information is collected on both electrodes. As a consequence, the MECG

power is generally smaller, while FECG, and *electromyogram (EMG)* noise (muscle crosstalk) have a higher power.

Despite the various electrode configurations proposed, to date very few studies have compared the different options that exist. Rooijakkers *et al.* [354] is one exception, in which both negative and ground electrodes placed on the patient's right side (as depicted in Fig. 3.3 d). Rooijakkers *et al.* [354] evaluated the effect of increasing the distance between electrodes, considering the SNRs of maternal and fetal ECGs as well as EHG as goodness criteria. The authors suggested two differential lead schemes, one with 5 electrodes for intrapartum recordings (inter-electrode distance of 16 cm - similar to figure 3.3a with an additional central electrode) and a 6 electrodes scheme for preterm recordings (distance 20 cm - similar to Figure 3.3d). Such configurations should optimally record the MECG, FECG, and uterine activity. Despite the interesting analysis, this clinical study was limited to 5 patients, each recording having 20 min in duration and performed at high gestational weeks (> 39 weeks). Moreover, the proposed lead configuration was very restrictive with a single triangular configuration and negative electrode kept in the same position. Another study, which considered signal quality throughout different channels was performed by Clifford *et al.* [85, 89]. The authors described an "over-complete" set of electrodes (see Fig. 3.3 j) and mentioned that some channels, at a particular time instant, contributed most to the quality of the FECG signals. However, the authors noted that the signal quality varies across patients (and time), thus an automatic selection of channels based on signal quality measures is necessary [51]. Lastly, the optimal number of electrodes may depend on the extraction method used. For instance, extraction routines may require from one to several abdominal leads, meanwhile, other methods need one (or more) MECG chest leads. Further details about these signal processing requirements are discussed in Section 3.3.1.

While designing electrode configurations for portable equipment, it should be kept in mind that an increasing number of electrodes is responsible for higher power consumption and decrease in patient comfort. The same applies for MECG leads, which despite being convenient for distinguishing between maternal from fetal ECG signals, they increase the hardware requirements and add extra leads outside the abdominal area that may be less comfortable. Another consideration is the location of the negative and common ground electrodes. For NIFECG applications, a ground electrode is recommended, since it reduces the common mode interference while enhancing the relative contribution of the signals of interest [164, 268, 354].

3.2.4 Available NIFECG databases

The increasing interest in the NIFECG created the need for data platforms where researchers could compare their extraction/detection results. Few freely available databases emerged over the last two decades, which are summarized below [49, 51, 365]:

DAISY database [109, 288] consists of a single 10 seconds recording using eight ECG channels (5 abdominal and 3 thoracic leads) sampled at 250 Hz. The study was performed by the Department of Electrical Engineering of the Katholieke Universiteit Leuven (Belgium). The dataset is available at `http://homes.esat.kuleuven.be/~smc/daisy/`.

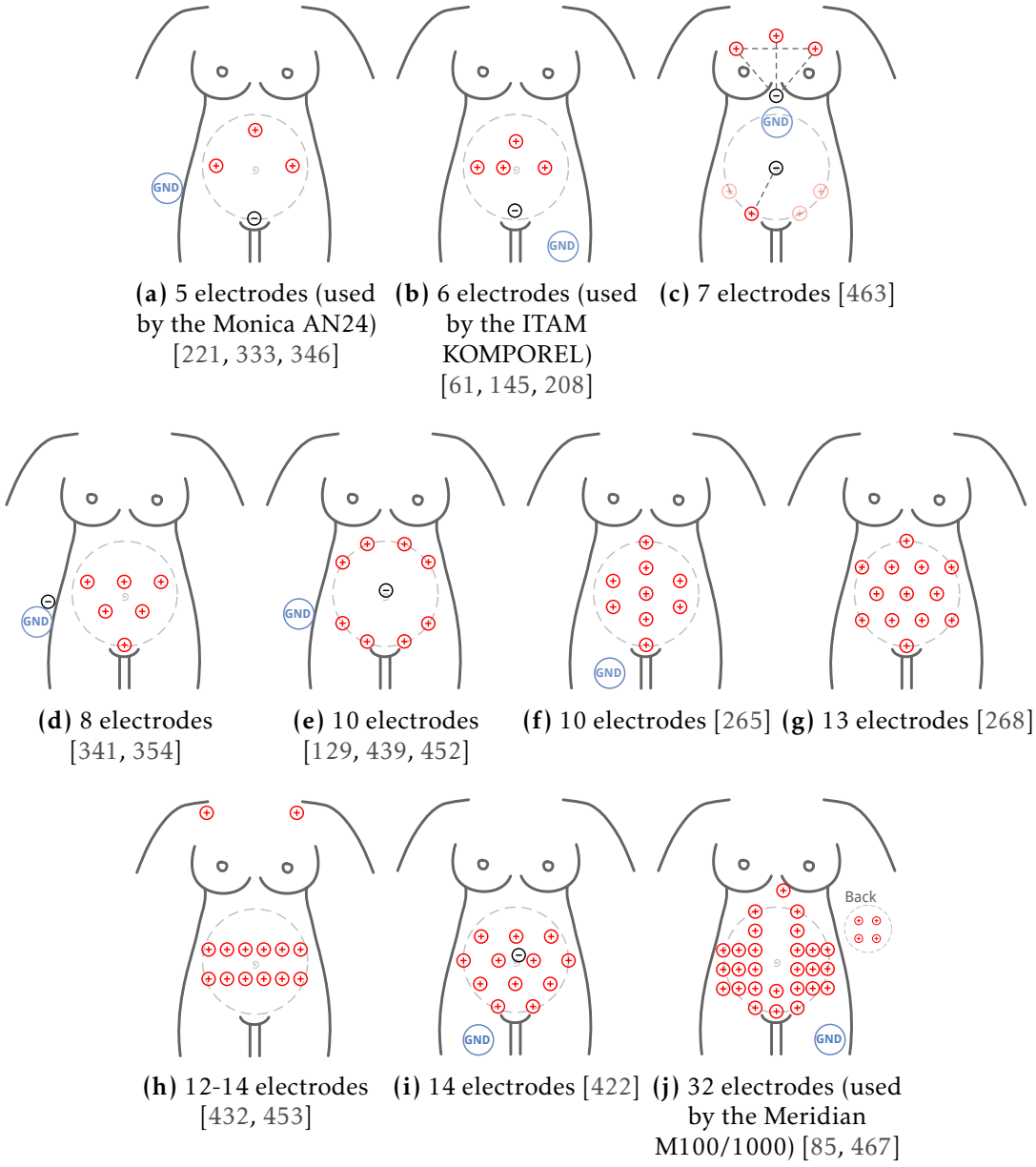

(a) 5 electrodes (used by the Monica AN24) [221, 333, 346]

(b) 6 electrodes (used by the ITAM KOMPOREL) [61, 145, 208]

(c) 7 electrodes [463]

(d) 8 electrodes [341, 354]

(e) 10 electrodes [129, 439, 452]

(f) 10 electrodes [265]

(g) 13 electrodes [268]

(h) 12-14 electrodes [432, 453]

(i) 14 electrodes [422]

(j) 32 electrodes (used by the Meridian M100/1000) [85, 467]

Figure 3.3: Different electrode configurations present in the literature. Similar comparisons are presented in Agostinelli *et al.* [4], Andreotti [16]. As detailed in the text, the symbols ⊕, ⊖ and "GND" represent the positive, negative, and ground electrodes, respectively. Some general remarks: (b) Bergveld and Meijer [61] made use of suction electrodes with the common electrode on the patient's back; (c) Widrow *et al.* [463] only made use of one abdominal lead, however different configurations were suggested (depicted with lighter color); (e) Fanelli [129] did not specify his common ground electrode; (h) Ungureanu *et al.* [432] did not make use of MECG leads (i.e. merely 12 leads); (g) Martens *et al.* [268] presented two variations of the depicted scheme including a differential lead system.

Non-Invasive Fetal Electrocardiogram Database [161] comprises 55 multichannel (2 thoracic and 3-4 abdominal leads) recordings taken from a single woman between the 21st and 40th WOG. Recordings were performed using a g.BSamp Biosignal Amplifier (GTech GmbH, Austria) at 1 kHz, with 16-bit resolution, bandpass filtered around 0.01-100 Hz and using a notch filter at 50 Hz. Recordings widely vary in duration ranging from less than 2 min segments up to 46 min, however, no reference annotation was provided. The data has been prepared by the Digital Signal Processing Group of the Electronics Engineering Department at the University of Valencia (Spain) and is available on Physionet [161] (`https://physionet.org/physiobank/database/nifecgdb/`).

Abdominal and Direct Fetal Electrocardiogram Database [208] consists of five, 5-minute, multichannel (4 abdominal and one scalp ECG channels) recordings of women in labor (38th to 41st WOG). The electrode configuration consisted of four electrodes placed around the navel, a reference electrode placed above the pubic symphysis and a common mode electrode placed on the left leg. Recording were performed using the KOMPOREL (mentioned in Section 3.2.2) that has 16-bit resolution, 1 kHz sampling rate, bandwidth 1-150 Hz and digital filters for removing baseline and power-line interference. Reference FQRS annotation was derived from the FSE recording. The recordings were acquired in the Department of Obstetrics at the Medical University of Silesia (Poland) and are available on Physionet [161] (`https://physionet.org/physiobank/database/adfecgdb/`).

Physionet/Computing in Cardiology Challenge 2013 Database [92, 395] is a compilation from five different databases [54, 395]: the two previous datasets, Scalp FECG Database (private), Ukraine Non-Invasive FECG (private) and simulated data (further described). The database includes 447 min of data, with up to 4 channels, resampled at 1 kHz. This is the largest publicly available FECG dataset to date, available on Physionet [161] (`http://www.physionet.org/challenge/2013/`). The database was used as training set for the PCINC 2013.

However, the present databases are still very limited in: i) number and duration of the recordings; ii) variety of WOG; iii) information on the subject's pathophysiological background; iv) expert's annotations of the FQRS locations v) events such as fetal movement and presence of ectopic beats; vi) silver-standard for FECG morphology. Hence, there is a demand for a more complete database, which may allow FHR, FHRV and morphological analysis of the FECG. Some further specifics on such idealistic database are described in [49, 51, 54].

3.2.5 Validity and usability of the non-invasive fetal ECG

As previously shown, NIFECG can be used for two major types of analysis, namely FHR/FHRV and the morphological analysis of the extracted FECG waveform. Regarding gold-standards for the afore mentioned metrics, FHR/FHR can be compared with CTG (antepartum/intrapartum,

less accurate) and FSE (intrapartum, accurate), while for FECG morphology requires either FMCG (antepartum[1]) or FSE (intrapartum) as reference.

Although the Monica AN24 has not yet gained a significant foothold in the monitoring market, several studies and commercial NI-FECG equipment claim to obtain accurate FHR tracings [51, 466]. For instance, Reinhard *et al.* [346] has found that the NIFECG and CTG characterize FHR trace in a similar manner with regards to acceleration count, decelerations count and coincidence, variability and baseline for $n = 27$ subjects. Moreover, the author found an overall strong correlation (Pearson's $r = 0.91$) between the techniques' FHR traces. Similar results were obtained by a more recent study by [228], on which moderate to high correlations ($r = 0.57 - 0.97$) were found $n = 39$ recordings of 20 min duration including 2 min of auditory stimulus. Another important aspect addressed by [407] was the lower rate of confusion between maternal HR and FHR achieved by NIFECG, when compared with CTG. High accuracy has also been reported in the literature when comparing FSE and NIFECG specially when using the open-source databases that counted with FSE for FQRS gold-standard.

With regards to the morphology of the signal, in Clifford *et al.* [85], the authors recorded the NIFECG on $n = 32$ term laboring women who had FSE placed after clinical indication. They evaluated the accuracy of the FST segment extracted on the NIFECG (by an automated algorithm) against the reference FST segment extracted from the FSE (using the same automated algorithm). The root mean square error between the FST calculated by both modalities averaged over all processed segments was 3.2%, indicating that accurate extraction of the FST segment from the NIFECG may be feasible. Similarly, [344] investigated the feasibility of NIFECG FST analysis by comparing the AN24 and STAN on $n = 6$ pregnant women during birth. Non-invasive FST was possible in 50 % the cases due to absence of fetal T-wave. Furthermore, McDonnell *et al.* [274] has found a very low difference between T/R ratios obtained by STAN and the Meridian monitor for $n = 27$ term laboring women. Lastly, in Behar *et al.* [56] the authors showed the possibility to recover the FQT from the NIFECG from $n = 22$ term women. The study made use of manually annotated FQT on both NIFECG and FSE, which were fused prior to comparison. The errors found between NIFECG and FSE FQT were in the range of QT annotations performed on adult ECGs [51]. All these studies are very encouraging, nevertheless a careful reader should have concerns about the reference being provided by a single cephalic lead and how the effect of the electrode positioning may affect the final results for NIFECG technique. Since the current studies are fairly limited in number, such conclusions should be considered with caution.

Considering the quality of such recordings, as early as 1995 Crowe *et al.* [100] have qualitatively shown the benefits and challenges in long-term NIFECG monitoring, due to the lower SNR of the fetal signal. Taylor *et al.* [423] reported being able to visually inspect FECG signal (including P, QRS and T waves) in 80 % for this study's population (15 pregnant women, 24-41 WOG, half of which with $\geq$ 39 weeks) using 15 min recordings. Pieri *et al.* [333] made use of 400 short-term recordings (5-10 min) at different stages and pregnancy, using a FHR obtainal success rate the authors produced trends for signal quality throughout pregnancy.

[1] Please note that there is a fundamental complication in using both NIFECG and FMCG simultaneously, due to the electromagnetic interference that the techniques have on each other.

Although little information on the subjects pathophysiological states is revealed, it is clear that around the 28^{th} WOG NIFECG's quality is expressively reduced. Fuchs *et al.* [145], who used the KOMPOREL, investigated pregnant women ranging between 28 and 42 WOG and have found no correlation between the percentage of signal loss and gestational age, nor between signal loss and BMI. A more comprehensive study using the AN24 by Graatsma *et al.* [163] evaluated long-term 15 h recordings of 150 preterm pregnant and 1-hour recordings of 22 laboring women, who had FSE simultaneously applied. Regarding the quality of recordings, the authors have found that 82 % the long-term recordings were of good quality (i.e. where on 60 % of the time FECG signal was present – as defined by the authors). The study also suggests that during the night period signal quality increased. According to the authors, a strong and significant correlation between FSE and NIFECG's FHR ($r = 0.99$) and FHRV short-term variability [106] ($r = 0.79$) were found during labor. Analogously, Reinhard *et al.* [345] assessed the signal quality of the FHR estimated from $n = 144$ NIFECG and CTG recordings during the first and second stages of labor. The study showed significant better results for NIFECG during the first stage, while no difference in signal loss was found during the second stage. Associated to these results, both Graatsma *et al.* [163], Van Laar *et al.* [439] have found no significant effect of BMI on NIFECG recording quality, however Van Leeuwen *et al.* [446] showed an increase in signal loss due to obesity.

Aside from the few publications herein listed and a handful of others provided by the current NIFECG commercial equipment, there is not much evidence on the ability of these devices to extract and detect fetal signals. For instance, neither Monica's nor Meridian have published any large randomized trial to compare NIFECG recordings with other gold-standards such as CTG and FSE. Nor have they demonstrated NIFECG's ability to improve neonatal outcome. Moreover, little is known about the quality of NIFECG recordings, particularly on earlier WOG (i.e. $WOG < 28$). This latter analysis is important to figure out what factors aside from the vernix caseosa can influence the quality of NIFECG recordings, which would enable the technique to be used in a broader number of patients. Moreover, as previously describe, a study on FHRV is only complete if additional information about the fetal behavioral state, time of day and activity (i.e. fetal movement) is available. Similarly, to be able to analyze the FECG morphology, information about the observed projection (i.e. electrode positioning) is required. Such information could be partially obtained by obtaining a VCG representation of fetal heart, as suggested by [452].

In any manner, the fetal signal component in the NIFECG should be reliably extracted and detected before any further clinical analysis take place. Due to the more fundamental data collection and signal processing problems that are involved in NIFECG technique, the clinical analysis of the parameters that could be obtained through these recordings (i.e. FHR, FHRV and morphological analysis) are out of the scope of this thesis.

3.3 Non-Invasive Fetal ECG Extraction Methods

Before proceeding, the mathematical notation adopted in the following sections (common in estimation theory) is summarized in Table 3.2. When looking for any other variable, please refer to the List of Symbols.

Table 3.2: Notation used in this work.

Notation	Represents	Font characteristics
x	regular font	scalar
x_k, $x[n]$	subscripted index/ square brackets	discrete-time variable x at time k/n
$x(t)$	parenthesis	signal at continuous time t
$\underline{x}$	underlined	vector
$\mathbf{A}$	capitalized, boldfaced	matrix
$\bar{x}$	overlined	mean
$\hat{x}$	hat	estimate for variable x
$\tilde{x}$	tilde	estimation error for x, i.e. $x - \hat{x}$
$\tilde{\mathbf{A}}$	capitalized, tilde	linearized/approximate matrix
$\hat{\underline{x}}_{k\|k-1}$	subscripted index†	a *priori* estimate of $\underline{x}_k$ conditioned to all prior measurements except at time k
$\hat{\underline{x}}_{k\|k}$	subscripted index‡	a *posteriori* estimate of $\underline{x}_k$ conditioned to all measurements up to time k

† Also often described in literature as $\hat{x}_k^-$. The notation in this work is adopted from Sayed [379].
‡ Also often described in literature as $\hat{x}_k^+$.

3.3.1 Overview on the non-invasive fetal ECG extraction methods

One of the major challenges in FECG analysis is separating the fetal signal from its surrounding noise. This section gives an overview on the current solutions to the problem. Particular focus is given to the *Kalman Filter (KF)* algorithm, due to its versatile and mathematically sound framework. For further information on these signal processing techniques, the reader is referred to the following reviews [51, 92, 173, 365, 418].

Extraction techniques aim at estimating the fetal signal either directly from abdominal signals or indirectly by first estimating the MECG and then treating the signal residuals as FECG and noise. The first (i.e. direct FECG estimation) is usually unfeasible due to various noise signals involved which makes the source separation problem more complex. Therefore, most approaches available in the literature are indirect. In the following sections, a brief description of the most important algorithms is presented (see Fig. 3.4). These methods can be categorized in: Adaptive Methods, Template Subtraction, Blind Source Separation or combination of those (i.e. Hybrid Methods). Since the *Physionet/Computing in Cardiology Challenge (PCINC)* 2013 [92, 395] enabled a direct benchmark between some of these methods, exemplary applications are mentioned while describing each category.

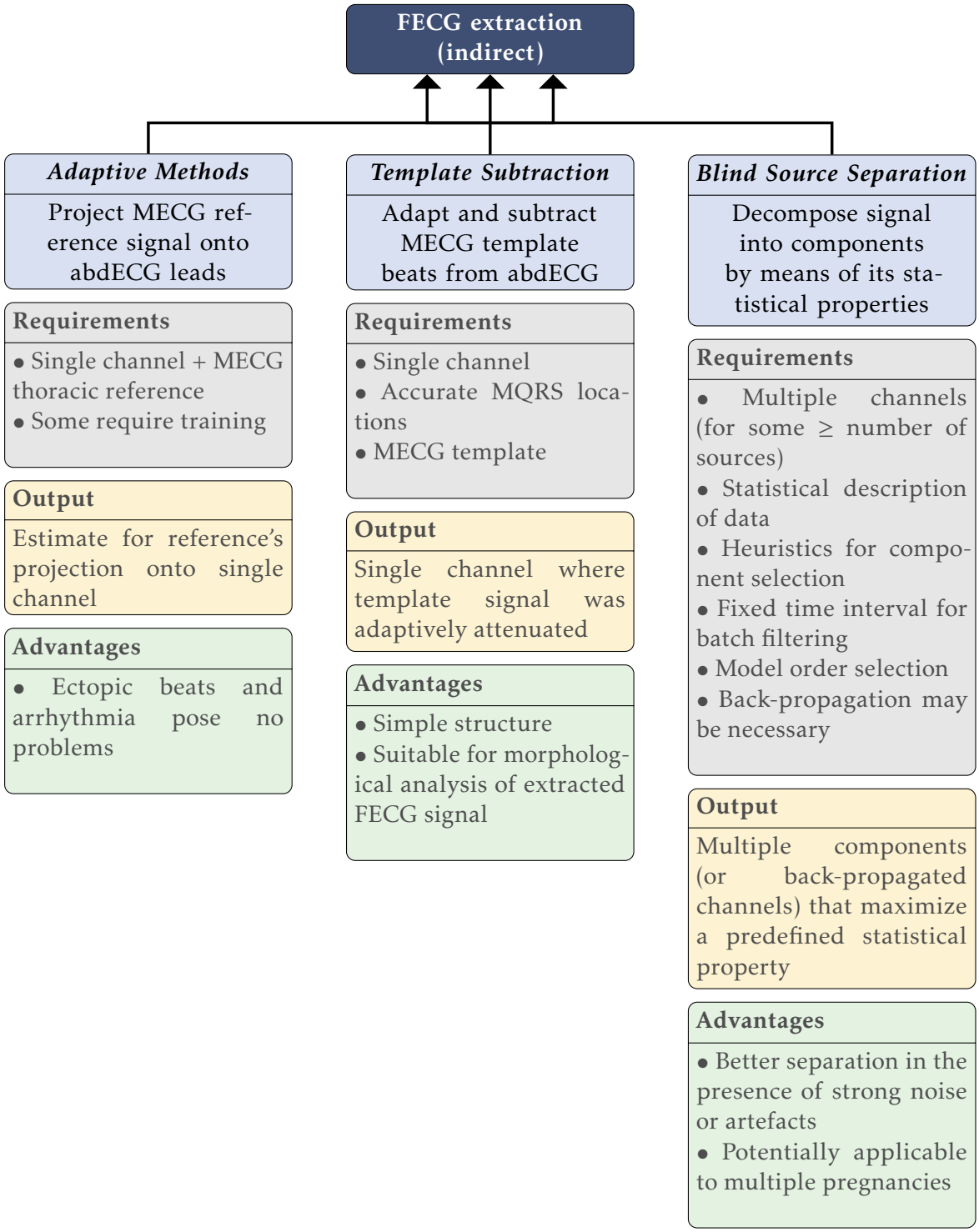

Figure 3.4: Indirect techniques for FECG extraction and their main characteristics. Aside from those shown in this figure, "Hybrid Methods", i.e. combination of these methods, have also been described in the literature.

Adaptive methods

As the FECG overlaps in time and frequency with its surrounding noise, especially with the MECG, simple linear filters with fixed coefficients (i.e. constant transfer function) are not able of separating the FECG from NI-FECG recordings [173]. *Adaptive Methods (AM)* are more sophisticated approaches that attempt to project one (or more) MECG reference lead(s) onto each abdominal lead, hence estimating the projection of the maternal signal on the abdECG channels. This is obtained by continuously adapting AM's filter coefficients while following the MECG reference. In the literature, some authors refer to such structure as *Adaptive Noise Canceller (ANC)* [463]. Exemplary AM methods are the *Least Mean Squares (LMS)* [463], *Recursive Least Squares (RLS)* and *Echo State Network (ESN)* [200]. According to Behar *et al.* [52], the LMS attempts to minimize the *mean square error (MSE)* between reference MECG and abdominal signal, regarding solely the information on the current and previous samples. Similarly, the RLS minimizes the sum of squared errors using all available samples of the measured signal. For this filter, a forgetting factor is required for weighting down the past error's influence while calculating the current filter weight. Both LMS and RLS assume linear propagation of the MECG signal throughout the body. Unlike the previously described methods, the ESN is capable of nonlinear projecting the MECG onto abdominal channels, achieving better FECG estimates [18, 52]. However, ESN entails a neural network approach that comes at cost of a much higher computational load. A more extensive review on AM for FECG can be found in Behar *et al.* [52]. Several alternative methods, both linear and nonlinear, have been proposed for the purpose of extracting the FECG, e.g. using Wiener filtering [352, 387] or adaptive *finite impulse response (FIR)* schemes e.g. [34, 35, 76, 257, 390, 412]. Due to the lack of MECG reference leads, AM were not preferred during the PCINC 2013, one exception was Rodrigues [352], who obtained poor results by making use of the Wiener filter to follow 3 out of the 4 available abdominal leads. Some of the drawbacks from AM are: i) the stringent necessity of a reference lead, which adds complexity and potential discomfort to recording system, and ii) the fact that some of those methods e.g. ESN and *Adaptive Neuro-Fuzzy Interference System (ANFIS)* [35] are based on neural networks, therefore require a training phase which can increase computational/time cost.

Template subtraction methods

Template Subtraction (TS) methods make use of the maternal signal pseudo-periodicity in obtaining a mean MECG cycle (so-called "template"), i.e. coherent averaging [353] maternal beats [267]. This procedure heavily depends on accurate *maternal QRS (MQRS)* detections. Next, the template is adapted onto the abdECG on a beat-to-beat basis, therefore estimating the MECG on each channel. Last, the estimated MECG signal is subtracted from the abdECG channel, leaving behind FECG signal and noise as residuals. In order to account for varying morphologies of the MECG, this average template is usually built on every couple seconds/minutes or updated online. TS algorithms impose the fewest number of restrictions on the recording system and can be applied on a single lead. A variety of TS techniques have been described in the literature

[20, 54, 78, 113, 254, 268, 430, 433, 454, 477]. For instance, the TS_c [78, 111, 434] simply adapts each beat using a single scalar gain [54]. This approach was used in early works at the IBMT in the field of FECG [16, 477]. Analogous procedures were applied during the PCINC 2013 by [54, 337]. More elaborate techniques such as the TS_m [268] make use of different scalar gains for each P-QRS-T waveform. Template adaptation (TS_a) [20, 179] enables width and height adaption of the template on a sample-basis, using concepts of *Self-Organizing Maps (SOMs)*. Ungureanu *et al.* [433], Vullings *et al.* [454] suggested the use of linear prediction for individually weighting previous maternal cycles, here called TS_{lp}. Sameni *et al.* [368, 369, 370] proposed the use of a TS technique based on the EKF, namely TS_{ekf}. Differently from the previously described methods, TS_{ekf} performs a continuous and adaptive sample-by-sample estimation of the MECG and, consequently, the FECG and noise contained in the residual. As compared with the other approaches, TS_{ekf} framework is more adaptive, theoretically allowing better estimation of the MECG in highly non-stationary scenarios [18]. TS are usually straightforward techniques, that imply the least distortions on the estimated FECG as shown in [18].

Blind source separation

Differently from AM and TS, *Blind Source Separation (BSS)* methods strive to decompose the multichannel abdominal mixture into different components without *a priori* knowledge about the signal itself. In fact, BSS attempts to separate the sources present in the abdECG (i.e. FECG, MECG and noise/artefacts) according to their statistical properties, e.g. correlation or independence. Exemplary BSS algorithms are the *Principal Component Analysis (PCA)* [42, 308], *Independent Component Analysis (ICA)* [109, 447, 474, 475], *Singular Value Decomposition (SVD)* [75, 219], *Gaussian Processes (GP)* [301, 350], *Tensors Decomposition (TD)* [301–303] and *Nonlinear State-Space Projection (NSSP)* [236, 348, 387]. In case additional information is provided (e.g. MQRS locations) methods are referred to as semi-BSS, e.g. the *Periodic Component Analysis (πCA)* [366]. For consistency, BSS extraction techniques using ICA, PCA and etc. are further referred to as BSS_{ica}, BSS_{pca}, etc., respectively.

Some early works on BSS techniques for solving the NIFECG problem have been published [42, 109, 474] and revisited during the PCINC 2013 [54, 447]. BSS techniques generally process segments of signal, within this segment the mixture between sources is assumed to be stationary, i.e. the statistical properties of the signal do not vary over time. This assumption was shown in Andreotti *et al.* [18] to be a dangerous assumption. Moreover, these algorithms usually[2] require multiple abdominal (and/or thoracic) leads, BSS_{ica} in particular, requires as input at least the same number of leads as sources [221]. Additionally, some BSS methods suffer from scaling (e.g. BSS_{pca}) and permutation indeterminacy[3] (e.g. BSS_{ica}). Furthermore, the

[2] Some works have described SVD-based approaches for single-lead applications [37, 219, 304]

[3] Component selection constitutes the major challenge concerning BSS techniques [18]. Selecting one or more components that well represent the MECG is as-is difficult, making a distinction between MECG and FECG and correctly selecting the FECG signal (for a direct approach) is nearly impossible. Particularly for ICA, permutation indeterminacy is a well know problem, where the positioning of *independent component (IC)*s inside ICA's output is a priori unknown. This problem makes the already cumbersome task of automatic selection of the IC(s) of interest (i.e. MECG/FECG) more complex [20, 83, 459].

issue of determining the optimal number of underlying sources, referred to as model order selection problem [201, 327], should be addressed. The problem states that an inappropriate choice/estimation of the number of components may lead to unsatisfactory source separation. In order to partially overcome this difficulty, a PCA dimension reduction step is usually applied [197]. Lastly, the length of the evaluated signal segment has to be considered. The longer the segment, the more critical the assumption of stationarity becomes. For lengthy segments, BSS techniques are expected to underperform; meanwhile, if this segment is too short, there may not be sufficient statistical information to represent MECG/FECG's features (e.g. non-Gaussianity), therefore also preventing a satisfactory source separation. Nevertheless, if those technique's assumptions are respected and parameters/heuristics well-designed, accurate FQRS results can be achieved. Regarding morphological analysis, Andreotti *et al.* [18] has shown that it should be performed in the observational domain, rather than source domain. Unlike AM and TS, BSS techniques are usually applied in batches[4] of signal.

Hybrid extraction methods

Aside from the aforementioned techniques, extraction routines may also be composed by combining methods from different subgroups (shown in Fig. 3.4). One example is the deflation procedure introduced by Sameni *et al.* [367]. This general procedure transforms multichannel abdominal signals into the source-domain (by means of any BSS method); next the MECG interference is removed from the source-domain components by means of TS techniques; and, at last, the denoised sources are back-propagated to the observational domain. This procedure is repeated a number of times until the output signals satisfy some predefined measure of signal separability [367]. Sameni *et al.* [367] themselves applied the framework in NI-FECG extraction using $BSS_{\pi CA}$ [366] and TS_{ekf} combination, as did [170] during the PCINC 2013, while [303] combined TD and BSS techniques. Another example of hybrid method is the TS_{pca} [18, 54, 219] which, in essence, is a TS method that decomposes stacked maternal cycles using PCA. TS_{pca} selects a couple first principal components, next a back-propagation step takes place on a beat-to-beat basis, producing MECG estimates for every maternal cycle. TS_{pca} was applied during the PCINC 2013 by [54, 254]. Table 3.3 summarizes the different extraction methods mentioned throughout the present section as in [51].

3.3.2 Kalman filtering basics

In the previous section, the strengths and weaknesses of three different classes of extraction methods were delineated. When contemplating real world applications, a reduced number of electrodes is desirable for improving subject's comfort and allowing its use in an ambulatory environment. As mentioned in Sections 3.2.3 and 3.3.1, selecting applicable extraction methods is highly dependent on the available electrode configuration. TS techniques impose the fewest

[4] Please notice that every category of method requires some initialization procedure, after this period TS and AM can run only e.g. TS initializes its templates and can adapt it on-the-go. BSS techniques, on the other hand, require a chunk of data which should be long (e.g. 1 min long) and spatially complete (e.g. 8 channels) to enable the extraction of the desired components.

Category	Examples
AM	AM_{lms} [463], AM_{rls} and AM_{esn} [52]
TS	TS_c [78], TS_m [268], TS_{lp} [433], TS_a [20], TS_{ekf} [369]
BSS	BSS_{ica} [474], BSS_{pca} [42], BSS_{svd} [75], BSS_{GP} [350], BSS_{TD} [302], $BSS_{\pi ca}$ [366]
Hybrid methods	deflation procedure [366], TS_{pca} [219]

Table 3.3: NI-FECG extraction algorithms [51].

restrictions on the recordings system and are capable of performing NIFECG extraction on single leads. Moreover, due to their simple structure, TS methods usually implicate few distortions on estimated FECG, thus enabling the acquisition of morphological information. For these reasons, TS approaches have been favored since IBMT's earliest works [16].

Past contributions by this author have applied the TS_c [16, 476, 477], TS_a [20, 21] and TS_{ekf} [16–18, 20, 21, 23, 24, 476, 477]. Moreover, a complete benchmark using various methods is presented in [18]. In this work, focus is given to TS_{ekf}, since the KF approach provides a versatile, modular, but yet mathematical framework for FECG extraction, which allows diverse extensions. In the following sections a brief review on Kalman filtering is provided and its use in NIFECG extraction explained.

Background

The history of optimal filtering began with the *Wiener-Kolmogorov filter* [233, 464], where for linear systems the optimal Bayesian solution to the estimation problem (with *minimum mean square error (MMSE)* loss) coincides with the least squares solution [373] (for a detailed description on Bayesian estimators, the reader may refer to [222, Chap.10-13]). On his seminal work on *Kalman Filter (KF)* written in 1960 [217, 218], Rudolph E. Kalman elegantly applied the concept of state-space models to the Wiener-Kolmogorov filter. Through this change of perspective on the KF's formulation, the filter yields a more general form than the Wiener-Kolmogorov filter, which does not require its system to possess deterministic dynamics nor the random process to have stationary property [166, 379]. Indeed, the KF provides the optimal solution to estimation problems for linear non-stationary stochastic processes, if some explicit conditions are met (further discussed in this section) [272, 399]. Such performance is attainable since KF makes use of all provided information by processing each available measurement, regardless of its precision, to estimate the current value of the variables of interest [272]. Aside from its wide usability, assimilating capacity and optimality, KF is a powerful tool that can be efficiently implemented in digital processors through fairly simple matrix operations using a two-step data assimilation algorithm[5] (denoted as prediction and update steps, further explained in detail). One of KF's first and most remarkable real-world applications was the guided descent of the Apollo 11 lunar module [383, 424], which resulted in the first man landing on the moon in 1969 [399]. For this reason, the filter is considered one of the greatest

[5] This two-step algorithm is by many described as 'recursive', however from an engineering point of view, the algorithm is rather iterative than recursive.

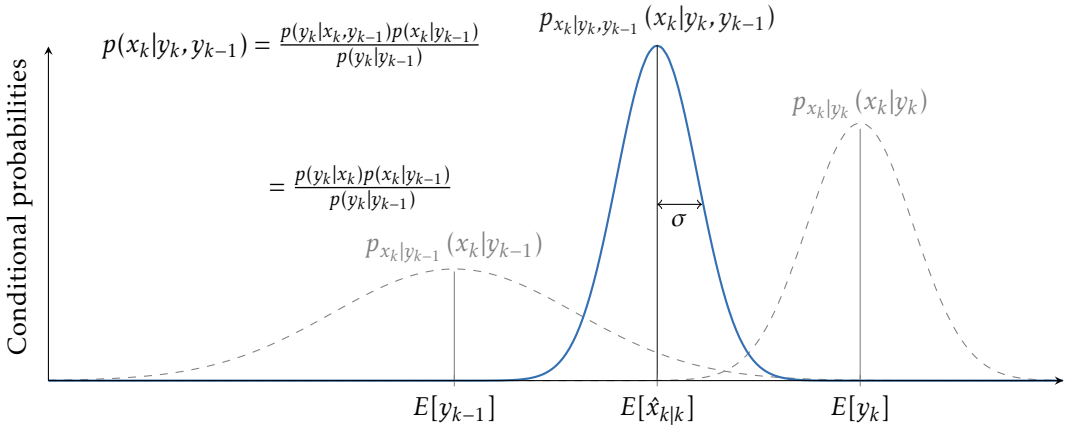

Figure 3.5: Illustrative representation of Bayesian estimation based on prior observations [272]. Bayes' rule used by KF is explicitly presented for clarity as in [82], with low-case $p(A|B)$ describing the conditional probability density function of A given B. This figure demonstrates how the Kalman filter estimates the a posteriori PDF given the current and prior observations y_k and y_{k-1}.

discoveries in the history of estimation theory and possibly one of the greatest discoveries of the 20$^{\text{th}}$ century [166]. A more complete historic perspective on KF as well as tools that enabled its development is presented in [166, Chap.1].

Bayesian approaches for linear state estimation attempt to construct the posterior *probability density function (PDF)* of the state ($\underline{x}_k$– assumed to be a random variable) based on prior knowledge about its PDF and the observed measurements [33, 166, 222]. This step is referred to as prediction step. Using Gaussian PDFs is, hence, convenient because all information present in the conditional probability density can be represented by the first and second order statistical moments (only moments necessary for describing Gaussian distributions). Therefore, the KF only needs to propagate these moments from one step to the next [272]. During its update step, KF makes use of the latest measurement in correcting its state prediction PDF (shown in Fig. 3.5). This is possible using *Bayes theorem*[6], which breaks down a conditional probability function into three densities of easier evaluation [33, 272]. Such prior knowledge about the hidden state lead to a more accurate estimator [222], i.e. a sharper PDF as shown in Fig. 3.5.

Several variants of the KF have been developed, including for continuous-time systems (so called Kalman-Bucy filter [71, 218, 359]). Kalman filters may be classified by their systems (e.g. linear/nonlinear or discrete/continuous), by its data assimilation algorithm (optimal/suboptimal) or by its noise (colored/white or additive/non-additive). An overall classification presenting the different algorithms is infeasible due to the number of variable criteria involved. Moreover, there are several analogies between KF and different algorithms such as GPs

[6] The well-known Bayes theorem describes the fundamental probability law governing the process of logical inference [82], which refers to calculating the probability of a given event, based on conditions that may be related to another event. This powerful theorem is formulated as $P(A|B) = \frac{P(B|A)P(A)}{P(B)}$, where P(A) is the probability that event A occurs, which can be inferred by calculating the remaining conditional probabilities and vice-versa. From an estimation point of view, one is interested in estimating a random variable $\underline{x}_k$ based on noise-corrupted measurements related to this variable $\underline{y}_k$ and $\underline{y}_{k-1}$, i.e. $P(x_k|y_k, y_{k-1})$ [272] (see Fig. 3.5).

[82, 342, 357], *hidden Markov model (HMM)* [147] and Particle Filters [33]. This work focuses on the digital implementation of the KF algorithm, therefore its discrete form is used. A brief derivation is presented based on [70, 222, 245, 272, 362, 379, 399, 424, 461]. Basic concepts in linear algebra, system theory and probability theory, necessary for the understanding of this derivation, are explained in [399, Chap.1-3].

A discrete-time linear system can be represented in the state-space form as follows, also known as canonical representation of the KF model [218]:

$$\underline{x}_k = \mathbf{F}_{k-1}\underline{x}_{k-1} + \mathbf{G}_{k-1}\underline{u}_{k-1} + \underline{w}_{k-1}\,, \tag{3.1}$$

$$\underline{y}_k = \mathbf{H}_k\underline{x}_k + \underline{v}_k\,, \tag{3.2}$$

where $k \in \mathbb{Z}_{\geq 0}$ represents the discrete-time index. $\underline{x}_k$ is the hidden state variable, which we attempt to estimate from our observations $\underline{y}_k$ (sensor data). The matrices $\mathbf{F}_k$, $\mathbf{G}_k$ and $\mathbf{H}_k$ are considered known matrices. The state transition matrix $\mathbf{F}_k$ is responsible for describing the dynamics of our state, the control input matrix ($\mathbf{G}_k$) determines how a known control input ($\underline{u}_k$) influences the system, while the observational matrix ($\mathbf{H}_k$) explains how these states are observed. The process ($\underline{w}_k$) and measurement noises ($\underline{v}_k$) are often considered uncorrelated *white Gaussian noise (WGN)*, whose PDF can be described as follows [272]:

$$\underline{w}_k \sim \mathcal{N}(0, \mathbf{Q}_k) \quad \text{and} \quad \underline{v}_k \sim \mathcal{N}(0, \mathbf{R}_k)$$

with

$$E\left[\underline{v}_k \cdot \underline{v}_k^T\right] = \mathbf{R}_k \cdot \delta_{i-j}$$
$$E\left[\underline{w}_k \cdot \underline{w}_k^T\right] = \mathbf{Q}_k \cdot \delta_{i-j}$$
$$E\left[\underline{v}_i \cdot \underline{w}_j^T\right] = 0 \quad \forall i, j \in k$$

where '$\sim$' stands for "distributed as", $\mathcal{N}(\mu, \mathbf{C})$ symbolizes a Gaussian distribution with mean μ and covariance $\mathbf{C}$ and δ_{i-j} is the Kronecker delta, which is unitary for $i = j$ and zero for $i \neq j$. In our case $\mathbf{Q}_k$ and $\mathbf{R}_k$ being, respectively, the process and measurement noise covariance matrices. KF assumes that both $\mathbf{Q}_k$ and $\mathbf{R}_k$ are known matrices well representing the system.

The first equation in the Kalman model (Eq. 3.1) is known as "process equation", which is a differential equation describing the dynamics of the unobserved state as simple first-order Markov process[7]. On top of that, since $\underline{w}_k$ is assumed Gaussian and additive, the state $\underline{x}_k$ happens to be a first-order Gauss-Markov random process [222, 357]. Additionally, the dynamic of the filter presented in Equation 3.1 may be regarded as a first-order *autoregressive (AR)* process ($AR(1)$) [222, Chap.13]. The latter equation (Eq. 3.2) is called "measurement equation" and describes how the hidden state is observed throughout physical sensors. Similar to the system equation, $\underline{y}_k$ and $\underline{x}_k$ are jointly Gaussian but $\underline{y}_k$ is not a Markov process since the past observations $\underline{y}_{k-2}$ and $\underline{y}_{k-1}$ may convey more joint information about $\underline{y}_k$ than $\underline{y}_{k-1}$ alone [14].

As described by Kay [222, Chap.12], there are three main problems that can be treated using

[7] Markov processes are based on the Markov property that a state at time $k+1$ can be entirely determined/predicted by its present state at k, i.e. past observations bring no additional information. The assumption is usually formulated using conditional probabilities [150].

the KF framework, namely *filtering*, *smoothing* or *prediction* problems. Filtering aims at estimating $\underline{x}_k$ based on the observations $\underline{y}_1 \dots \underline{y}_k$, i.e. using present and past data only; as k increases the effect of the estimation is causal. Smoothing attempts to estimate $\underline{x}_k$ using all data available $\underline{y}_1 \dots \underline{y}_{N-1}$, therefore it requires the estimation to be performed offline. Lastly, prediction aims at estimating $\underline{x}_{k-1+l}$, with the lag l being a positive integer, based on measurements $\underline{y}_1 \dots \underline{y}_{k-1}$. This study focuses on the problem of estimating the FECG from noisy NIFECG recordings, unless stated otherwise, the reader should consider that these techniques are being used for filtering purposes. Smoothing may be later applied to improve filtering results.

Kalman filter assumptions and optimality

As previously mentioned, the classical KF is based on some basic assumptions[8]. These assumptions are listed and properly justified below [218, 272]:

i) the system equations (i.e. Eqs 3.1 and 3.2) must be linear, possibly time-variant and well-representing of the real system;

ii) present noises $\underline{w}_k$ and $\underline{v}_k$ are additive, zero-mean, white and Gaussian distributed (i.e. WGN);

iii) the initial state variable has a known mean ($\underline{x}_0$) and covariance matrix ($\mathbf{P}_0$).

The linearity assumption is suitable since linear systems and linear differential equations can be better manipulated by engineering tools. Indeed this assumption may not hold for a large class of problems [272], however, for this end there are KF extensions (further described in this work). The restriction of unbiased noise (zero-mean) does not impose any loss of generality, since a mean value for noise could be modelled within the remaining parameters of the system [357]. White noise implies that the noise values are uncorrelated from time step to time step. Despite this being a concept that does not apply for real-world problems, one could interpret the definition of white noise as a wide band noise, which is present in a system that has an intrinsic low pass effect on its output (as all real systems do). This consideration makes the mathematics involved in the filter tangible. Similar to nonlinear cases, colored or even correlated noise may also be treated by the KF if a shaping filter is applied [272, 399]. Whereas whiteness refers to time/frequency relationships of a noise source, Gaussianity reflects its amplitude values. In the literature, the Gaussianity assumption is weakly motivated by the central limit theorem[9]. Nonetheless, a stronger and more practical argument is that using Gaussian densities improves the analytical tractability of the filter's mathematics [272, 357]. That is, by having Gaussian

[8] In fact, Kalman's original derivation of the Kalman filter [217] did not require the underlying system equations to be linear or have Gaussian probability densities. The only assumption made were i) the estimator was linear, ii) that predictions of the state and of the system observations can be calculated, and iii) that consistent estimates of the system random variables could be obtained by simply propagating their first and second-order moments (means and covariances) [278, Chap.1].

[9] That is, physically justified by the fact that the system and measurement noise are usually caused by several small sources. The central limit theorem shows mathematically that when a number of independent random variables are added together, the summed effect can be described very closely by a Gaussian probability density, regardless of the shape of the individual densities [272].

noise one ensures that all variables stay Gaussian and, therefore, the mean and covariance fully characterize the system dynamics.

Under those conditions mentioned above, KF produces the optimal estimate for $\underline{x}_k$, in terms of virtually any available criterion [272, 399]. There are several criteria for optimality, some examples are MMSE, *maximum a posteriori (MAP)*, *maximum likelihood (ML)* or Minimax (for complete reviews on the topic refer to [82, 222]). Cost functions of the general quadratic form, i.e. $J_k = E[(\underline{x}_k - \underline{\hat{x}}_{k|k})^T \mathbf{M}_k (\underline{x}_k - \underline{\hat{x}}_{k|k})]$ with $\mathbf{M}_k$ being a symmetric positive definite matrix [166, 222, 245, 272, 399], are usually preferred due to their mathematical tractability [222]. In fact any cost function which is symmetric and convex could be used [245]. In [222, Chap.11] alternative cost functions are presented, such as the absolute error and hit-or-miss error. For quadratic functions the MMSE estimator is usually the mean of the posterior PDF, for proportional cost functions the median and for hit-or-miss functions the mode. For $M = I$, the definition of MMSE is obtained:

$$E\left[\left\|\underline{x}_k - \underline{\hat{x}}_{k|k}\right\|\right] = E\left[\left(\underline{x}_k - \underline{\hat{x}}_{k|k}\right)^T \left(\underline{x}_k - \underline{\hat{x}}_{k|k}\right)\right] \tag{3.3}$$

The MMSE is often used in the literature, but for any reasonable choice for optimality criterion, the Bayes estimate obtains the same estimate e.g. mean, median or mode coincide [272, 404]. The proof for KF's optimality for the MMSE is available in [222] and using MAP in [82]. Even if the Gaussianity criterion is relaxed, KF is still the optimal "linear" filter, meaning that there might exist a nonlinear filter that is more accurate [399]. In the next section the algorithm for the discrete KF approach is presented in detail. The MMSE is further used as motivation for its optimization problem.

Derivation of the discrete Kalman filter

In the literature, there are several ways of writing and deriving the KF equations where most of those are mathematically equivalent [399]. In this section, the time and measurement-update form is presented, since it clearly demonstrates the filter philosophy in a simple iterative algorithm. Alternative formulations presented in [399, Chap.6] aim at improving KF's computational performance or filter's precision.

At this point, it is convenient to define the hat notation $\left(\underline{\hat{x}}_{k|k-1}\right)$ as being the estimate for the state variable $\underline{x}_k$. The sub-index $k|k-1$ makes explicit that it is an "a priori" estimate, which refers to the fact that the present observation (at time k) is not taken into consideration. Otherwise, it would be "a posteriori" state estimate $\underline{\hat{x}}_{k|k}$ or simply $\underline{\hat{x}}_k$. It is important to remark that both $\underline{\hat{x}}_{k|k-1}$ and $\underline{\hat{x}}_{k|k}$ are estimates for $\underline{x}_k$ before and after the measurement $\underline{y}_k$ is taken into consideration [399]. The "a priori" and "a posteriori" estimate error covariance matrices for $\underline{x}_k$ are given in Eqs. 3.4–3.5 [399]. The main goal of the KF algorithm, as for any estimation problem, is to find $\underline{\hat{x}}_k$ that minimize the "a posterior" state estimate error covariance matrix $\mathbf{P}_{k|k}$. The a priori and posteriori state covariance matrices are defined in Eqs. 3.4 and 3.5.

$$\mathbf{P}_{k|k-1} = E\left[(\underline{x}_k - \underline{\hat{x}}_{k|k-1})(\underline{x}_k - \underline{\hat{x}}_{k|k-1})^T\right]\Big|_{\underline{y}_1 \cdots \underline{y}_{k-1}} \tag{3.4}$$

$$\mathbf{P}_{k|k} = E\left[(\underline{x}_k - \underline{\hat{x}}_{k|k})(\underline{x}_k - \underline{\hat{x}}_{k|k})^T\right]\Big|_{\underline{y}_1 \cdots \underline{y}_k} . \tag{3.5}$$

According to the previous section, KF's algorithm requires initial values for its state and estimation error covariance matrix. Since no measurement is available at $k = 0$ to estimate $\underline{x}_0$, it is reasonable to use the expected value of the initial state $\underline{x}_0$, such as $\underline{\hat{x}}_{0|0} = E[\underline{x}_0]$. Similarly, $\mathbf{P}_{0|0}$ is usually initialized with $\mathbf{P}_{0|0} = E\left[(\underline{x}_0 - E[\underline{x}_0])(\underline{x}_0 - E[\underline{x}_0])^T\right]$ [272, 399]. An alternative is to initialize the state covariance by choosing a constant α and setting $P_0 = \alpha^2 \cdot Q_0$, where typically $\alpha = 10$ is a reasonable estimate. Nevertheless, in general, the effect of these initial estimates diminishes with time and they do not affect the steady state performance of the KF [121].

From Eq. 3.1 and the assumption of unbiased noise, the propagated state is obtained as in Eq. 3.6.

$$\begin{aligned} \underline{\hat{x}}_{k|k-1} &= E\left[\underline{x}_k\right]\Big|_{\underline{y}_1 \cdots \underline{y}_{k-1}} \\ &= E\left[\mathbf{F}_{k-1}\underline{x}_{k-1} + \mathbf{G}_{k-1}\underline{u}_{k-1} + \underline{w}_{k-1}\right]\Big|_{\underline{y}_1 \cdots \underline{y}_{k-1}} \\ &= \mathbf{F}_{k-1}\underline{\hat{x}}_{k-1|k-1} + \mathbf{G}_{k-1}\underline{u}_{k-1} \end{aligned} \tag{3.6}$$

From Eq. 3.4 and assuming that $\underline{w}_{k-1}$ and $\underline{\hat{x}}_{k-1|k-1}$ are uncorrelated, the a priori propagated state error covariance matrix is shown in Eq. 3.7 (also known as Lyapunov equation) [272, 343].

$$\begin{aligned} \mathbf{P}_{k|k-1} &= E\left[(\underline{x}_k - \underline{\hat{x}}_{k|k-1})(\underline{x}_k - \underline{\hat{x}}_{k|k-1})^T\right] \\ &= E\Bigg\{\Big[\overbrace{\left(\mathbf{F}_{k-1}\underline{x}_{k-1} + \mathbf{G}_{k-1}\underline{u}_{k-1} + \underline{w}_{k-1}\right)}^{\text{(from Eq. 3.1)}} - \overbrace{\left(\mathbf{F}_{k-1}\underline{\hat{x}}_{k-1|k-1} + \mathbf{G}_{k-1}\underline{u}_{k-1}\right)}^{\text{(from Eq. 3.6)}}\Big]\Big[\cdots\Big]^T\Bigg\} \\ &= E\left\{\left[\left(\mathbf{F}_{k-1}\underline{x}_{k-1} + \underline{w}_{k-1}\right) - \left(\mathbf{F}_{k-1}\underline{\hat{x}}_{k-1|k-1}\right)\right]\left[\cdots\right]^T\right\} \\ &= \mathbf{F}_{k-1}E\left[(\underline{x}_{k-1} - \underline{\hat{x}}_{k-1|k-1})(\underline{x}_{k-1} - \underline{\hat{x}}_{k-1|k-1})^T\right]\mathbf{F}_{k-1}^T + E\left[\underline{w}_{k-1}\underline{w}_{k-1}^T\right] \\ &= \mathbf{F}_{k-1}\mathbf{P}_{k-1|k-1}\mathbf{F}_{k-1}^T + \mathbf{Q}_{k-1} . \end{aligned} \tag{3.7}$$

So far, the KF's time update equations were derived for $\underline{\hat{x}}$ and $\mathbf{P}$, next focus is put on the measurement update step i.e. attempting to improve our estimates regarding the current measurement $\underline{y}_k$ [70, 399]. In order to do so, let us define the innovation process ($\underline{\nu}_k$ - also known as measurement residual) and derive its covariance matrix $\mathbf{S}_k$ (based on Eq. 3.2 and uncorrelation assumption for observational noise) [343, 399]:

$$\underline{\nu}_k \triangleq \underline{y}_k - \mathbf{H}_k\underline{\hat{x}}_{k|k-1} \tag{3.8}$$

$$\begin{aligned} \mathbf{S}_k &= E\left[\underline{\nu}_k\underline{\nu}_k^T\right] \\ &= E\left[(\underline{y}_k - \mathbf{H}_k\underline{\hat{x}}_{k|k-1})(\underline{y}_k - \mathbf{H}_k\underline{\hat{x}}_{k|k-1})^T\right] \\ &= E\left\{\left[(\mathbf{H}_k\underline{x}_k + \underline{v}_k) - \mathbf{H}_k\underline{\hat{x}}_{k|k-1}\right]\left[(\mathbf{H}_k\underline{x}_k + \underline{v}_k) - \mathbf{H}_k\underline{\hat{x}}_{k|k-1}\right]^T\right\} \\ &= \mathbf{H}_k\mathbf{P}_{k|k-1}\mathbf{H}_k^T + \mathbf{R}_k . \end{aligned} \tag{3.9}$$

The innovation represents the new information about the state made available at k by the observation $\underline{y}_k$. The innovation sequence is a zero-mean and white noise random process. Theoretically, if $\underline{\hat{x}}_k$ is an optimal estimate, there is no information left in $\underline{\nu}_k$ [151]. Thus, a good way of verifying KF's performance is to monitor its residual. In case its state estimate or state covariance error are not as expected, there might be incorrect assumptions on the model or noise statistics [175, 245, 343, 399]. Moreover, the innovation process is uncorrelated and orthogonal, yet statistically equivalent [216, 277] to the observations $\underline{y}_k$. For this reason KF is considered as a whitening filter [14, 245, 343].

From the estimation theory [222], it is known that the MMSE estimator with a linear Bayesian model yields the same form as the *minimum variance unbiased estimator (MVUE)* for classical linear models. Moreover, the estimation can be done in a sequential manner (rather than processing the whole data offline as a batch), similarly to the recursive least squares estimator [222, Chap.4]. Therefore, as $\underline{y}_k$ becomes available, the a posteriori estimate for our state can be described as in Eq. 3.10.

$$\begin{aligned} \underline{\hat{x}}_{k|k} &= \underline{\hat{x}}_{k|k-1} + \mathbf{K}_k(\underline{y}_k - \mathbf{H}_k\underline{\hat{x}}_{k|k-1}) \\ &= \underline{\hat{x}}_{k|k-1} + \mathbf{K}_k\underline{\nu}_k \end{aligned} \tag{3.10}$$

This equation blends noisy measurements and prior estimate by computing the "a posteriori" state estimate by means of a weighted difference between the new measurement $\underline{y}_k$ and the measurement prediction $\mathbf{H}_k\underline{\hat{x}}_{k|k-1}$. $\mathbf{K}_k$ is a blending factor which is yet to be determined [70, 461]. Substituting Eq. 3.10 into Eq. 3.5 and assuming that the cross-product between the explicit expression for the updated error covariance matrix $\mathbf{P}_{k|k}$ is obtained [272, 343]:

$$\begin{aligned} \mathbf{P}_{k|k} &= E\left[\left(\underline{x}_k - \underline{\hat{x}}_{k|k}\right)\left(\underline{x}_k - \underline{\hat{x}}_{k|k}\right)^T\right] \\ &\qquad\qquad \overbrace{\qquad\qquad\qquad\qquad}^{\text{(from Eq. 3.10)}} \\ &= E\left\{\left[\underline{x}_k - \underline{\hat{x}}_{k|k-1} - \mathbf{K}_k\left(\underline{y}_k - \mathbf{H}_k\underline{\hat{x}}_{k|k-1}\right)\right]\left[\cdots\right]^T\right\} \\ &\quad \underbrace{\qquad\qquad}_{\substack{\text{(a priori state} \\ \text{estimation error)}}} \qquad \overbrace{\qquad\qquad}^{\text{(from Eq. 3.2)}} \\ &= E\left\{\left[\underbrace{(\underline{x}_k - \underline{\hat{x}}_{k|k-1})}\ -\mathbf{K}_k(\overbrace{\mathbf{H}_k\underline{x}_k + \underline{v}_k}\ -\mathbf{H}_k\underline{\hat{x}}_{k|k-1})\right]\left[\cdots\right]^T\right\} \\ &= E\left\{\left[(\mathbf{I}-\mathbf{K}_k\mathbf{H}_k)(\underline{x}_k - \underline{\hat{x}}_{k|k-1}) - \mathbf{K}_k\underline{v}_k\right]\left[(\mathbf{I}-\mathbf{K}_k\mathbf{H}_k)(\underline{x}_k - \underline{\hat{x}}_{k|k-1}) - \mathbf{K}_k\underline{v}_k\right]^T\right\} \\ &= (\mathbf{I}-\mathbf{K}_k\mathbf{H}_k)\,E\left[(\underline{x}_k - \underline{\hat{x}}_{k|k-1})(\underline{x}_k - \underline{\hat{x}}_{k|k-1})^T\right](\mathbf{I}-\mathbf{K}_k\mathbf{H}_k)^T + \mathbf{K}_k E\left[\underline{v}_k\underline{v}_k^T\right]\mathbf{K}_k^T \\ &= (\mathbf{I}-\mathbf{K}_k\mathbf{H}_k)\mathbf{P}_{k|k-1}(\mathbf{I}-\mathbf{K}_k\mathbf{H}_k)^T + \mathbf{K}_k\mathbf{R}_k\mathbf{K}_k^T. \end{aligned} \tag{3.11}$$

Although Eq. 3.11 can be further simplified for easing computational cost, the presented form is more stable and robust. This form, so-called the Joseph stabilized version of $\mathbf{P}_{k|k}$, assures that $\mathbf{P}_{k|k}$ is symmetric positive definite as long as $\mathbf{P}_{k|k-1}$ is symmetric positive definite [71, 399].

Returning to our optimization problem, the aim of the filter is to find a linear function of the measurements $\underline{y}_k$, which minimizes any quadratic cost function, for example the MSE shown in Eq. 3.3. It can be noticed that the error criterion shown in Eq. 3.3 is similar to the definition of a posteriori state estimate error covariance matrix (see Eq. 3.5). In fact, those

functions are equivalent [82, 245] and according to the Gauss-Markov theorem produce the MMSE. That being said, the KF attempts to minimize the trace of the posterior estimation error covariance matrix $Tr(\mathbf{P}_{k|k})$ by selecting a suitable blending factor $\mathbf{K}_k$. Several derivations of this optimization are available in the literature. Brown and Hwang [70, Chap.5] presents a detailed derivation considering the least squares criterion and squares completion based on previous works from [404]. For the sake of brevity, this deduction is here omitted. Instead, it is here derived as in [151, Chap.4] as follows:

$$\begin{aligned} J_k &= Tr(\mathbf{P}_{k|k}) \\ \frac{\partial J_k}{\partial \mathbf{K}_k} = 0 \quad &\Longrightarrow \quad \frac{\partial Tr(\mathbf{P}_{k|k})}{\partial \mathbf{K}_k} = -2\left(\mathbf{H}_k \mathbf{P}_{k|k-1}\right)^T + 2\mathbf{K}_k \mathbf{S}_k = 0 \\ \therefore \quad \mathbf{K}_k &= \mathbf{P}_{k|k-1}\mathbf{H}_k^T \mathbf{S}_k^{-1}. \end{aligned} \tag{3.12}$$

This blending factor is referred to as "Kalman gain" matrix, which is optimal in the MMSE sense if KF's assumptions are met. By evaluating its Hessian, it can be shown that $\mathbf{K}_k$ indeed minimizes $Tr(\mathbf{P}_{k|k})$ [151]. By evaluating Eq. 3.9, 3.10 and Eq. 3.12, an intuition on the basic working principle of the Kalman filter is attained [461]:

$$\lim_{R_k \to 0} K_k = H^{-1} \tag{3.13}$$

$$\lim_{P_{k|k-1} \to 0} K_k = 0. \tag{3.14}$$

That is, if the observation error covariance matrix $\mathbf{R}_k$ is small, the current measurement is deemed trustworthy and the predicted value for the state estimate ($\mathbf{H}_k \underline{\hat{x}}_{k|k-1}$ is trusted less. On the contrary, if the a priori state error covariance matrix approaches zero, the measurement $\underline{y}_k$ is trusted less and the filter output consists basically of the a priori state estimate. Moreover, it is imporant to notice from Eq. 3.7 that $\mathbf{P}_{k|k-1}$ depends not only on the a posteriori error covariance matrix from the previous filter iteration, but also on the previous value for the model error covariance matrix $\mathbf{Q}_{k-1}$. That causes the Kalman gain to depend on a non-trivial counterbalance between $\mathbf{R}_k$ and $\mathbf{Q}_{k-1}$. The complete recursive discrete Kalman filter algorithm is summarized in Algorithm 1. Furthermore, Eq. 3.13 it is clear that the filter requires matrix $\mathbf{H}$ to be invertible. This fact may be interpreted as the necessity of the filter having a complete set of observations (i.e. matrix $\mathbf{H}$ is full-rank) that links the hidden state with the latent state vector.

Kalman filter's performance

Despite its theoretical optimality, real-world applications of the KF may face some implementational issues. Two of these main difficulties are finite arithmetic precision and modelling errors. Digital implementations of the KF are unavoidably bounded to finite precision, which may cause divergence or instability in the filter. For example, although the filter does not formally require a non-singular covariance matrix, in practice a singular covariance increases the possibility of numerical problems [401]. Some algorithmic strategies may increase the robustness of the filter, as suggested by Simon [399]. Meanwhile, modelling errors can be improved by better designing Kalman's model. Particularly, it is assumed that $\mathbf{F}_k$, $\mathbf{G}_k$, $\mathbf{H}_k$, $\mathbf{Q}_k$

Algorithm 1 Pseudo-code summarizing the KF algorithm (time and measurement-update form)

Require: models for $\mathbf{F}_k$,$\mathbf{H}_k$, $\mathbf{Q}_k$, $\mathbf{R}_k$
Initialize: $\underline{x}_0$, $\mathbf{P}_0$
for $k = 1$ *to* $N_{samples}$ **do**
  // Prediction step
  $\underline{\hat{x}}_{k|k-1} = \mathbf{F}_{k-1}\underline{\hat{x}}_{k-1|k-1} + \mathbf{G}_{k-1}\underline{u}_{k-1}$; // a priori state estimate
  $\mathbf{P}_{k|k-1} = \mathbf{F}_{k-1}\mathbf{P}_{k-1|k-1}\mathbf{F}_{k-1}^T + \mathbf{Q}_{k-1}$; // a priori covariance estimate
  // Update step
  $\underline{\nu}_k = \underline{y}_k - \mathbf{H}_k\underline{\hat{x}}_{k|k-1}$; // innovation signal
  $\mathbf{S}_k = \mathbf{H}_k\mathbf{P}_{k|k-1}\mathbf{H}_k^T + \mathbf{R}_k$; // innovation covariance
  $\mathbf{K}_k = \mathbf{P}_{k|k-1}\mathbf{H}_k^T\mathbf{S}_k^{-1}$; // obtain Kalman gain
  $\underline{\hat{x}}_{k|k} = \underline{\hat{x}}_{k|k-1} + \mathbf{K}_k\underline{\nu}_k$; // a posteriori state estimate
  $\mathbf{P}_{k|k} = (\mathbf{I} - \mathbf{K}_k\mathbf{H}_k)\mathbf{P}_{k|k-1}(\mathbf{I} - \mathbf{K}_k\mathbf{H}_k)^T + \mathbf{K}_k\mathbf{R}_k\mathbf{K}_k^T$; // a posteriori error covariance
end

and $\mathbf{R}_k$ are known and that the noise processes respect the assumptions described previously in this section. If the model does not reflect well the real process, the filter may not work [399].

With regards to modelling errors, as previously described, $\mathbf{Q}_k$ and $\mathbf{R}_k$ play an important role in the determination of the Kalman gain. For example, $\mathbf{Q}_k$ interferes on the asymptotic performance of the estimate $\underline{\hat{x}}_{k|k}$ [175], since the larger its value the bigger is the assimilation of the measurements into the estimated state [424]. However, these matrices are usually not simple to obtain and their tuning is non trivial. If some training data with the true values of the estimated parameters is available (e.g. when using simulated data), *consistency* [121] or simple distance measures (e.g. MSE) between estimate and true state can be calculated. Unfortunately, in any real application the true values are not available (otherwise one would not have an estimation problem), therefore, other measures are necessary. Shyam Mohan *et al.* [392, Chap. 3] provides an overview on the different practical approaches for tuning the noise covariance matrices and categorizes the main approaches into four classes: Bayesian, Maximum Likelihood, Covariance Matching and Correlation Techniques. For example, the last approach takes into consideration the fact that the innovation sequence should be a zero-mean, white and Gaussian process. Some authors [277] suggest the use of autocorrelation for verifying if the implemented Kalman gain produces statistically acceptable white noise sequences. Odelson *et al.* [307] have shown that the process and measurement matrices are not sufficient nor necessary (as described by Mehra), additionally Odelson *et al.* [307] proposed an improved method namely *Autocovariance Least Squares (ALS)*, which should produce much smaller variances and better estimates [392].

Another modelling consideration is how the state variable $\underline{x}_0$ and state covariance $\mathbf{P}_0$ are initialized. As previously denoted, $\underline{x}_0$ and $\mathbf{P}_0$ are generally initialized with rough estimates of their expected values, but the initialization effect vanishes with time. That is, given that the

filter is properly tuned and well-represents our system, $Tr(\mathbf{P}_{k|k}) \to 0$ and the estimates $\underline{\hat{x}}_k$ tends to the true value of $\underline{x}_k$. Thus, an important test is to monitor the filter's performance is to check if $Tr(\mathbf{P}_{k|k})$ converges to zero.

3.3.3 Nonlinear Kalman filtering

The classical discrete KF assumes that the system is linear, however such systems do not exist in practice [399, Chap.13]. In fact, real-world systems may be described as[10]:

$$\underline{x}_k = f_{k-1}(\underline{x}_{k-1}, \underline{u}_{k-1}, \underline{w}_{k-1}) \tag{3.15}$$

$$\underline{y}_k = h_k(\underline{x}_k, \underline{v}_k) \tag{3.16}$$

where the system equation $f(\cdot)$ and measurement equation $h(\cdot)$ are nonlinear functions. It is known that the optimal solution to nonlinear filtering problems demands a complete description of the conditional PDF. However, this exact description requires a potentially unbounded number of parameters [214]. Thus, several sub-optimal solutions for nonlinear Bayesian estimation have been developed. Based on [33, 166, 278, 399, 424] these practical approaches can be grouped into the following categories:

Linearized Kalman filters make use of partial derivatives to linearize the nonlinear model. This is performed by expanding the system and measurement nonlinear functions using Taylor series around a nominal control u_0, nominal state x_0, nominal output y_0 and nominal noises w_0, v_0 point. This method assumes very small perturbations on the nominal state trajectory. Unfortunately, the nominal trajectory is not always easy to be found [399].

Gaussian approximate methods are nonlinear extensions of the KF, whose estimator merely propagates the first and second-order moments of the random variables involved [424]. Four exemplary methods within this group are [424] the *Extended Kalman Filter (EKF)* [206, 384], the *Sigma-point Kalman filter (SPKF)* [214, 279], *Ensemble Kalman Filter (EnKF)* [126, 127, 159] and the *Gaussian Sum Filter (GSF)* [10, 405].

The EKF was the first and is undoubtedly the most widely used nonlinear variant of the KF [278, 399]. Proposed by Stanley F. Schmidt[11] [383, 384], EKF aims at linearizing the KF system around its estimate (i.e. $x_0 = \hat{x}$), which in turn is estimated based on the linearized system (as in the Linearized KF). This bootstrap philosophy allows the filter to estimate the nominal state trajectory, overcoming the difficulties presented on the Linearize KF method. Unfortunately, due to the linearization procedure, EKF happens to be a sub-optimal implementation of the KF [278]. This is caused by the linearization approach which, while calculating the means and covariances of the random variables

[10] An attentive reader should notice that in Eqs. 3.15-3.16 the process and measurement noises are not regarded as additive. This formulation taken over from [399, Chap.13] is more general than the additive case (i.e. $\underline{x}_k = f_{k-1}(\underline{x}_{k-1}, \underline{u}_{k-1}) + \underline{w}_{k-1}$ / $\underline{y}_k = h_k(\underline{x}_k) + \underline{v}_k$), which can be easily derived from the derivation here presented.

[11] According to Grewal *et al.* [166], Schmidt was an early adopter and successful advocate of the KF. After Kalman has visited Schmidt at NASA in the fall of 1960, Schmidt began working on the probably the first full implementation of the KF algorithm, soon discovering what is now called EKF.

involved, disregards the fact that the PDF of these variables are no longer normal after undergoing their respective nonlinear transformations [436, 461]. This failure to account for the "probabilistic spread" of the state variables can seriously affect the accuracy of the posterior estimates [278]. Furthermore, EKF's shortcomings include its sensitive and complex initialization/tuning procedure and the fact that for strong nonlinear systems the linearization procedure may heavily affect the estimation accuracy or even lead to divergence [215, 279, 424].

In an attempt to minimize the linearization errors from EKF, a subgroup of approaches termed as SPKF [279] has been proposed. SPKF schemes are derivative-free state estimators that in order to estimate the state information focus on approximating the probability distribution directly, rather than approximating the nonlinear function at an operating point as EKF does [82]. This is performed by deterministic sampling approaches that propagate the Gaussian statistics [278], i.e. the sigma points are transformed and combined in a special way so that an estimate of the state and an estimate of the covariance of the state estimation error are obtained [400]. For some problems SPKF approaches can better approximate state estimate nonlinearities than a standard EKF, because EKF's estimates are always approximately Gaussian [33]. A well-known SPKF algorithm is the *Unscented Kalman Filter (UKF)* [214, 215], which makes use of the scaled unscented transformation in the calculation of the optimal terms for the Gaussian approximate Bayesian update. The sigma-point weights used in the unscented transform are combined to provide unbiased estimates for the output mean and covariance. The unscented transform is advantageous due to its computational efficiency [166]. Furthermore, the UKF estimates the mean and covariance of the state to third-order accuracy, compared to EKF's first-order approximation [82, 400]. However, in practice UKF often encounters ill-conditioned covariance matrix (not positive semi-definite), which can be alleviated by using regularization through square-root UKF [82].

Similarly to SPKF, the EnKF [74, 125] uses a reduced number of ensembles to propagate the mean and covariance of random vectors undergoing nonlinear transformations. EnKF was developed for high-dimensional systems, whose state covariance matrix evolution has an elevated computational cost. Instead of calculating the propagation integral, EnKF uses a Monte Carlo method to represent the distribution of the state using a random sample (so-called ensemble) and replace the covariance matrix by the sample covariance computed from the ensemble [264]. EnKF uses individual ensembles for each data assimilation step, considering as mean the current measurement and the variance of the current ensemble as measurement error [126–128, 159, 424]. Therefore both prediction and update steps are stochastic analyses [128]. In contrast to SPKF the number of ensembles is heuristically chosen [424], the greater this number the more accurate are the estimates [128, 187, 282]. Still, it is an approximate solution since EnKF does not treat the Bayesian update for non-Gaussian PDFs, but linearly combines the a priori non-Gaussian ensembles in its update. Therefore, some non-Gaussian properties will be inherited, notwithstanding it is

a sub-optimal scheme [128].

The last group, GSF [10, 405], aims at approximating non-Gaussian posterior PDFs using finite weighted sum of Gaussian densities [82, 279, 399]. Each Gaussian component is propagated in using paralell Kalman filters, the results are then combined into obtaining an approximate estimate. The idea of using sums of Gaussians distributions is similar to performing a piecewise linearization, thus GSF and EKF are similar [399]. In fact, GSF still requires EKF algorithm to propagate each Gaussian distribution, therefore it also suffers from the same drawbacks. Similar to EnKF, the number of filters incurs in a trade-off between approximation accuracy and computational effort [399].

Grid-based filters approximate the value of the posterior PDF (Bayesian integrals) with a large but finite sum over a uniform N-dimensional grid around the state-space region of interest. In *Grid-based Filter (GBF)*, PDF of the state is approximated, stored, propagated, and updated at discrete points in state-space [399]. As the dimensionality of the state-space increases, the computational cost of the approach increases drastically, which hinders its further usage [33, 278, 279]. Both optimal and approximate solutions for this filter exist [33].

Particle filters are much less restrictive approaches, since no assumption on the shape of the posterior distribution densities is made. Rather than merely propagating the first and second-order moments of PDFs, Particle filters aim at approximating the N-dimensional Bayesian integrals using Monte Carlo sampling [424]. More specifically, by representing the posterior PDF by a set of random samples ("particles") with associated weight [324]. The estimate mean and covariance are then computed based on these particles and weights using the *Sequential Importance Sampling (SIS)* algorithm. SIS resample or continuously importance samples data at each time-step to obtain sharper statistical estimates. Next, those particles are individually propagated by simulating the known nonlinear dynamics of the system. By assimilating the newest measurement, the a posteriori covariance is calculated, which is then used to comput the Kalman gain [166]. Due to the application of Monte Carlo and SIS algorithms, Particle filters are also referred to as Sequential Monte Carlo.

Both UKF and EnKF could be understood as a particle filtering methods [424] and, in fact, Particle filters can be considered as a generalization of those [400]. In comparison with UKF, Particle filters also make use of dynamic simulation of samples (i.e. "particles"), which are carried forward in time by nonlinear dynamics and used to reconstruct the propagated mean and covariance matrix. Meanwhile, UKF's time update is deterministic. Moreover, the number of sigma-points in UKF are commonly chosen to be slightly larger than the system's state dimension (usually $n+1$, $2n$ or $2n+1$), while Particle filters have no upper bound but usually increase exponentially with the state [166, 400]. The a priori estimation step is performed similar to EnKF's but with varying weights. Differently from EnKF, the Gaussian approximation in the update step is avoided. Particle filters are also

comparable with GBF, except that in Particle filtering one chooses the particles to be distributed in state-space according to the state's PDF, whereas GBF does not. Hence the computational requirements for GBF increase exponentially with the dimension of the state, being considerably more expensive than Particle filters. For this reason, Particle filtering could be regarded as an "intelligent" GBF [399].

Particle filters can be applied to general nonlinear and non-Gaussian problems, however they are computationally more expensive than most Gaussian approximation methods [278]. The PDF estimates converges to the true PDF as the number of particles approaches infinity [400]. Nevertheless, dimensionality is this filter's main drawback, since the computational complexity grows exponentially with the dimension of the state vector. Therefore, an online implementation of Particle filters may not be feasible [424]. With larger sample sizes, particle filters have the potential to obtain better estimates of the means and covariances than the UKF [166]. Another common problem with the Particle filter is the sample degeneracy phenomenon, where after a few iterations, all but one particle will have negligible weight [33, 142]. In order to solve this problem a large computational effort is made to avoid the propagation of particles with negligible importance [324].

Due to its wide acceptance, lower complexity and computational expense [399] and based on the previous works in FECG from Sameni [362], EKF is used throughout this work. Thus, in the following Section, EKF algorithm is presented in detail.

The extended Kalman filter

As previously mentioned, EKF attempts to linearize the nonlinear functions described in Eqs. 3.15 and 3.16 around the estimated state $\underline{\hat{x}}_k$. This linearization can be numerically or analytically performed, here a demonstration of the analytical procedure is shown. Given Eq. 3.15, that $\underline{u}_k$ is known $\forall k \in \mathbb{Z}_{\geq 0}$, regarding the point x_0 as the a posteriori state estimate at time $k-1$ ($\underline{\hat{x}}_{k|k-1}$) and assuming the unknown noise value to be $\underline{w}_{k-1} = \underline{0} \in \mathbb{R}^{n\times 1}$, $\underline{x}_k$ is approximated using the first-order Taylor expansion series as follows [399]:

$$\begin{aligned}\underline{x}_k &\approx f_{k-1}\left(\underline{\hat{x}}_{k-1|k-1}, \underline{u}_{k-1}, \underline{w}_{k-1}\right)\Big|_{w_{k-1}=\underline{0}} \\ &+ \underbrace{\frac{\partial f_{k-1}}{\partial \underline{x}_{k-1}}\bigg|_{\substack{\underline{x}_{k-1}=\underline{\hat{x}}_{k-1|k-1} \\ \underline{w}_{k-1}=\underline{0}}}}_{\widetilde{\mathbf{F}}_{k-1}} (\underline{x}_{k-1} - \underline{\hat{x}}_{k-1|k-1}) + \underbrace{\frac{\partial f_{k-1}}{\partial \underline{w}}\bigg|_{\substack{\underline{x}_{k-1}=\underline{\hat{x}}_{k-1|k-1} \\ \underline{w}_{k-1}=\underline{0}}}}_{\widetilde{\mathbf{W}}_{k-1}} \underline{w}_{k-1} \\ &\approx \widetilde{\mathbf{F}}_{k-1}\underline{x}_{k-1} + \underbrace{\left[f_{k-1}\left(\underline{\hat{x}}_{k-1|k-1}, \underline{u}_{k-1}, \underline{0}\right) - \widetilde{\mathbf{F}}_{k-1}\underline{\hat{x}}_{k-1|k-1}\right]}_{\text{(known signal } \quad \widetilde{\underline{u}}_{k-1})} + \widetilde{\mathbf{W}}_{k-1}\underline{w}_{k-1}\end{aligned} \tag{3.17}$$

where $\widetilde{\mathbf{F}}_{k-1}$ and $\widetilde{\mathbf{W}}_{k-1}$ are known matrices. Similarly to Eq. 3.17, the measurement equation (Eq. 3.16) is linearized around the a priori state estimate $\underline{\hat{x}}_{k|k-1}$ [399]:

$$\begin{aligned}\underline{y}_k &\approx h_k\left(\hat{\underline{x}}_{k|k-1}, \underline{v}_k\right)\Big|_{v_k=\underline{0}} + \overbrace{\left.\frac{\partial h_k}{\partial \underline{x}_k}\right|_{\substack{\underline{x}_k=\hat{\underline{x}}_{k|k-1}\\ \underline{v}_k=\underline{0}}}}^{\widetilde{\mathbf{H}}_k}(\underline{x}_k - \hat{\underline{x}}_{k|k-1}) + \overbrace{\left.\frac{\partial h_k}{\partial \underline{v}}\right|_{\substack{\underline{x}_k=\hat{\underline{x}}_{k|k-1}\\ \underline{v}_k=\underline{0}}}}^{\widetilde{\mathbf{V}}_k}\underline{v}_k \\ &\approx \widetilde{\mathbf{H}}_k\underline{x}_k + \left[h_k\left(\hat{\underline{x}}_{k|k-1}, 0\right) - \widetilde{\mathbf{H}}_k\hat{\underline{x}}_{k|k-1}\right] + \widetilde{\mathbf{V}}_k\underline{v}_k \quad .\end{aligned} \tag{3.18}$$

One can redefine the a priori and a posteriori state estimate as [399]:

$$\hat{\underline{x}}_{k|k-1} = f_{k-1}(\hat{\underline{x}}_{k-1|k-1}, \underline{u}_{k-1}, \underline{0}) \tag{3.19}$$

$$\hat{\underline{x}}_{k|k} = \hat{\underline{x}}_{k|k-1} + \mathbf{K}_k\left[\underline{y}_k - h(\hat{\underline{x}}_{k|k}, 0)\right] \tag{3.20}$$

Next, based on Eqs. 3.17, 3.19, and 3.20, the nonlinear a priori and a posteriori estimation error is defined as:

$$\underline{x}_k - \hat{\underline{x}}_{k|k-1} \approx \widetilde{\mathbf{F}}_{k-1}(\underline{x}_{k-1} - \hat{\underline{x}}_{k|k-1}) + f_{k-1}\left(\hat{\underline{x}}_{k-1|k-1}, \underline{u}_{k-1}, 0\right) - f_{k-1}(\hat{\underline{x}}_{k-1|k-1}, \underline{u}_{k-1}, \underline{0}) + \widetilde{\mathbf{W}}_{k-1}\underline{w}_{k-1} \tag{3.21}$$

$$\begin{aligned}&\approx \widetilde{\mathbf{F}}_{k-1}(\underline{x}_{k-1} - \hat{\underline{x}}_{k|k-1}) + \widetilde{\mathbf{W}}_{k-1}\underline{w}_{k-1} \\ \underline{x}_k - \hat{\underline{x}}_{k|k} &\approx \underline{x}_k - \hat{\underline{x}}_{k|k-1} - \mathbf{K}_k\left[\underline{y}_k - h(\hat{\underline{x}}_{k|k}, 0)\right] \\ &\approx \underline{x}_k - \hat{\underline{x}}_{k|k-1} - \mathbf{K}_k\left[\widetilde{\mathbf{H}}_k(\underline{x}_k - \hat{\underline{x}}_{k|k-1}) + \widetilde{\mathbf{V}}_k\underline{v}_k\right]\end{aligned} \tag{3.22}$$

Given Eqs. 3.21 and 3.22 a priori and a posteriori state estimation error covariance as well as Kalman gain matrices, can be calculated analogously to Eqs. 3.7, 3.11 and 3.12, respectively. This derivation (here omitted) results into the following matrices:

$$\mathbf{P}_{k|k-1} = \widetilde{\mathbf{F}}_{k-1}\mathbf{P}_{k-1|k-1}\widetilde{\mathbf{F}}_{k-1}^T + \widetilde{\mathbf{W}}_{k-1}\mathbf{Q}_{k-1}\widetilde{\mathbf{W}}_{k-1}^T \tag{3.23}$$

$$\mathbf{P}_{k|k} = (\mathbf{I} - \mathbf{K}_k\mathbf{H}_k)\,\mathbf{P}_{k|k-1}\,(\mathbf{I} - \mathbf{K}_k\mathbf{H}_k)^T + \mathbf{K}_k\widetilde{\mathbf{V}}_k\mathbf{R}_k\widetilde{\mathbf{V}}_k^T\mathbf{K}_k^T \tag{3.24}$$

$$\mathbf{K}_k = \mathbf{P}_{k|k-1}\mathbf{H}_k^T\left(\mathbf{H}_k\mathbf{P}_{k|k-1}\mathbf{H}_k^T + \widetilde{\mathbf{V}}_k\mathbf{R}_k\widetilde{\mathbf{V}}_k^T\right)^{-1}. \tag{3.25}$$

Algorithm 2 shows a summary of the EKF algorithm. This formulation enables the state estimation by means of KF for nonlinear systems. If the functions involved are approximately linear around their mean, good results can be achieved. As mentioned in the previous section, due to the linearization approach that disregards the nonlinear transformation performed over the state variables' PDF, EKF algorithm is sub-optimal. Moreover, the first-order Taylor series approximation causes estimation errors, which are propagated through the means and covariance matrices used by the EKF algorithm (thoroughly demonstrated in [399, Chap.13]). If the functions $f(\cdot)$ and $h(\cdot)$ are non-differentiable, those errors are large and the EKF may diverge [399].

Some approaches attempt to minimize those linearization errors within EKF framework, two examples are the Iterated EKF and the Second-order EKF. The first, makes use of the more accurate a posteriori state estimate provided by EKF algorithm to iteratively re-estimate the a posteriori state at each time-step k. The latter method improves the linearization procedure by using the second-order Taylor expansion instead of the first. These improvements can promote

some minor improvement, however for highly nonlinear systems other methods (presented in the previous Section) should performed better.

Algorithm 2 Pseudo-code summarizing the Extended Kalman Filter algorithm (time and measurement-update form)

Require: models for $f_{k-1}(\cdot)$,$h_k(\cdot)$, $\mathbf{Q}_k$ and $\mathbf{R}_k$
Initialize: $\mathbf{x}_0$, $\mathbf{P}_0$
for $k = 1$ *to* $N_{samples}$ **do**
  // Prediction step
  $\widetilde{\mathbf{F}}_{k-1} \approx \frac{\partial f_{k-1}}{\partial \underline{x}_{k-1}}\Big|_{\substack{\underline{x}_{k-1}=\underline{\hat{x}}_{k-1|k-1} \\ \underline{w}_{k-1}=\underline{0}}}$ and $\widetilde{\mathbf{W}}_{k-1} \approx \frac{\partial f_{k-1}}{\partial \underline{w}}\Big|_{\substack{\underline{x}_{k-1}=\underline{\hat{x}}_{k-1|k-1} \\ \underline{w}_{k-1}=\underline{0}}}$; // linearization
  $\underline{\hat{x}}_{k|k-1} = f(\underline{\hat{x}}_{k-1|k-1}, \underline{u}_{k-1}, 0)$; // *a priori* state estimate
  $\mathbf{P}_{k|k-1} = \widetilde{\mathbf{F}}_{k-1}\mathbf{P}_{k-1|k-1}\widetilde{\mathbf{F}}_{k-1}^T + \widetilde{\mathbf{W}}_{k-1}\mathbf{Q}_{k-1}\widetilde{\mathbf{W}}_k^T$; // *a priori* covariance estimate
  // Update step
  $\widetilde{\mathbf{H}}_k \approx \frac{\partial h_k}{\partial \underline{x}_k}\Big|_{\substack{\underline{x}_k=\underline{\hat{x}}_{k|k-1} \\ \underline{v}_k=\underline{0}}}$ and $\widetilde{\mathbf{V}}_{k-1} \approx \frac{\partial h_k}{\partial \underline{v}}\Big|_{\substack{\underline{x}_k=\underline{\hat{x}}_{k|k-1} \\ \underline{v}_k=\underline{0}}}$; // linearization
  $\underline{\nu}_k = \underline{y}_k - \underline{h}_k(\underline{\hat{x}}_{k|k-1}, 0)$; // innovation signal
  $\mathbf{S}_k = \widetilde{\mathbf{H}}_k\mathbf{P}_{k|k-1}\widetilde{\mathbf{H}}_k^T + \widetilde{\mathbf{V}}_k\mathbf{R}_k\widetilde{\mathbf{V}}_k^T$; // innovation covariance
  $\mathbf{K}_k = \mathbf{P}_{k|k-1}\widetilde{\mathbf{H}}_k^T\mathbf{S}_k^{-1}$; // obtain Kalman gain
  $\underline{\hat{x}}_{k|k} = \underline{\hat{x}}_{k|k-1} + \mathbf{K}_k\underline{\nu}_k$; // a posteriori state estimate
  $\mathbf{P}_{k|k} = (I - \mathbf{K}_k\widetilde{\mathbf{H}}_k)\mathbf{P}_{k|k-1}(I - \mathbf{K}_k\widetilde{\mathbf{H}}_k)^T + \mathbf{K}_k\widetilde{\mathbf{V}}_k\mathbf{R}_k\widetilde{\mathbf{V}}_k^T\mathbf{K}_k^T$; // a posteriori error covariance
end

3.3.4 Extended Kalman filter for FECG estimation

The KF is a versatile framework that has been used in various biomedical engineering applications. For example in filtering (ECGs [369], *electroencephalogram (EEG)* [309], heart [251] and breathing rates [299, 419]), for feature extraction (e.g. intracranial pressure [193], EEG spectra [31, 204]) and in classification (e.g. of arrhythmias in ECG [314, 378, 402]). Moreno and Pigazo [291, Chap.7] provide a good overview of biomedical applications of the filter. In the scope of NIFECG extraction, EKF was first suggested by Sameni *et al.* [368, 369, 370]. A complete description is present in his doctoral thesis [362] and a MATLAB® (The MathWorks, Inc., Natick, USA) implementation of his code is available is freely available in the *Open-Source Electrophysiological Toolbox (OSET)* [363]. Since its first suggestion in 2005, the TS_{ekf} has rapidly obtained wide acceptance amongst researchers and featured in several publications e.g. Andreotti *et al.* [20], Behar *et al.* [54], Li *et al.* [248], Niknazar *et al.* [304], Panigrahy *et al.* [322], Roonizi and Sassi [355], Sayadi *et al.* [377], and Zaunseder *et al.* [477].

As TS technique, the EKF method aims at estimating the MECG signal on a single lead, which is subsequently subtracted from the original signal. In fact, the EKF was first proposed for adult ECG filtering [369, 370] and its application to FECG emerged shortly after [362]. Figure 3.6 demonstrates a general work-flow for FECG extraction and detection by means of the TS_{ekf}. In the present section, specifics on the MECG estimation (i.e. "Fetal Extraction" block)

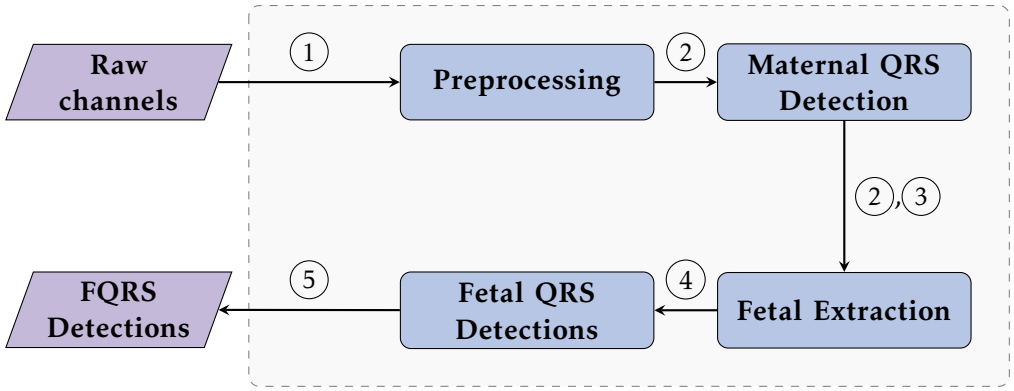

Figure 3.6: Signal processing work-flow for NI-FECG extraction using TS_{ekf}. (1), (2), (3), (4) and (5) represent the raw channel, preprocessed channel, MQRS detection, fetal channel (preprocessed - maternal channel) and FQRS detection, respectively.

follow. Pre-requisites for this step are the preprocessed abdECG channels[12] and reliable MQRS detections.

While applying the TS_{ekf} to abdECG, the first step is to obtain a coherent/ensemble averaged [353] MECG beat (henceforth called "template"). To build this template, an initialization period τ_0 (e.g. $\tau_0 = 60$ s)[13] is required, on which multiple maternal cycles are available. A wrapping approach then takes place, stretching (or compressing) beats with different lengths into a pre-determined number of bins (N_b) before the average is taken (shown in Figure 3.7a). Additionally, the wrapping approach enables the calculation of the inter-beat standard deviation, which is further used in the filter modelling (see Figure 3.7b).

Next, as detailed in the previous sections, the EKF requires an accurate mathematical description of its system model (i.e. MECG template). In order to obtain such model, Sameni *et al.* [369] made use of the ECG model proposed by McSharry *et al.* [275], which approximates ECG waveforms by a sum of N_k Gaussian kernels. EKF's system model, described by Eq. 3.26, requires information about two parameters: a phase information (θ_k) and an amplitude signal (z_k), as follows [180, 362]:

$$\begin{cases} \theta_k &= (\theta_{k-1} + \omega\delta) \bmod 2\pi \\ z_k &= z_{k-1} - \sum_{i=1}^{N_k} \delta \frac{\alpha_i \omega}{b_i^2} \Delta\theta_{i,k-1} exp\left(-\frac{\Delta\theta_{i,k-1}^2}{2b_i^2}\right) + \eta_{k-1}, \end{cases} \tag{3.26}$$

θ_k is produced by linearly assigning values between $[-\pi, \pi]$ for each beat (e.g. where $-\pi/3$ marks the maternal R-peak), thus resulting in a sawtooth-shaped signal. z_k is the actual MECG amplitude at time-step k. Regarding the first equation, ω represents a constant angular

[12] Simple bandpass and notch filters (for 50/60 Hz powerline interference) are usually applied. The cutoff bands for the bandpass are usually application dependent, e.g. if focus is on FQRS detections (a narrower band) or FECG morphology (broader band). This topic is closer addressed in the following Chapter, see [18, 51] for more information.

[13] This initialization period is the only restriction to the online application of the EKF filter

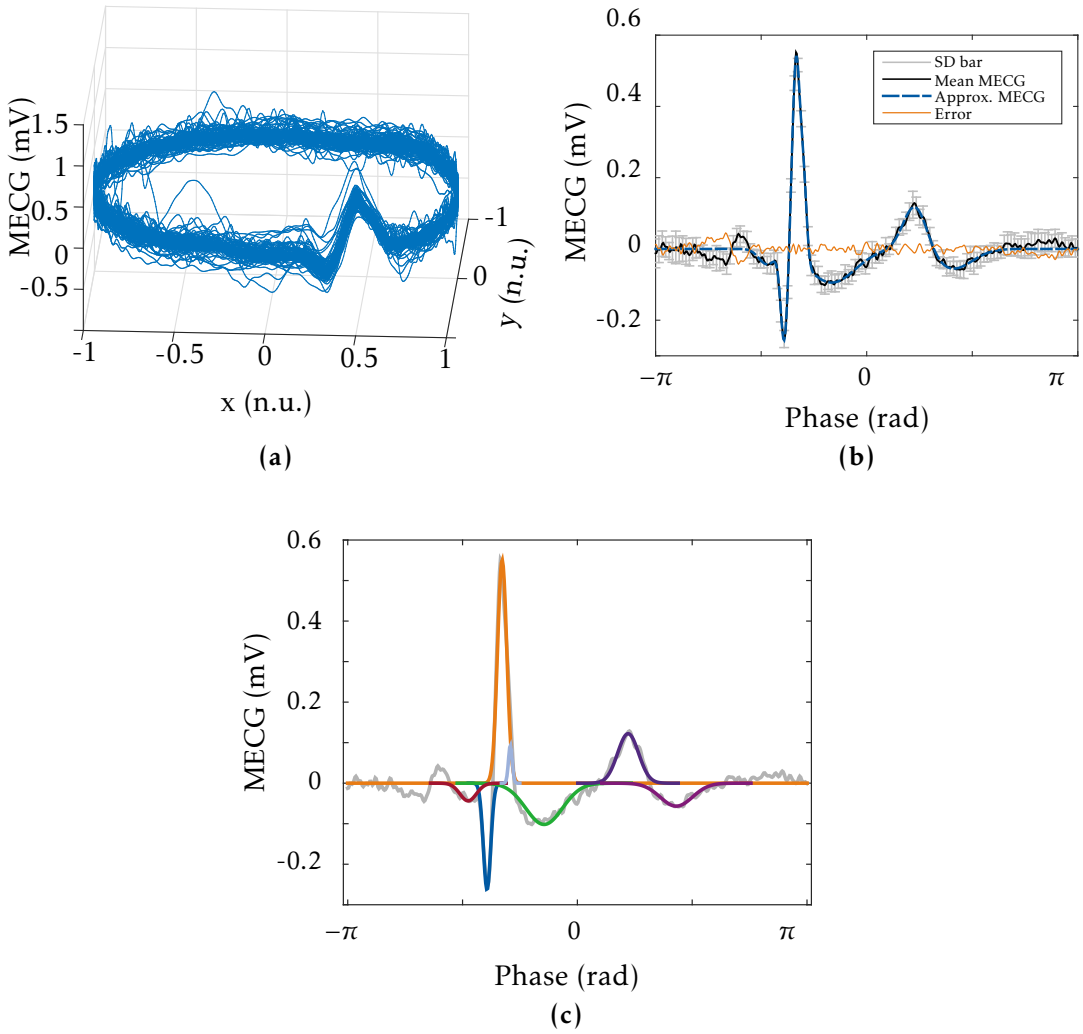

Figure 3.7: Kalman filter ECG modelling algorithm for a real recording. In (a) the phase wrapping used in stretching/compressing MECG beats is shown; (b) depicts an average MECG beat with respective standard deviation (σ_b) for each bin (N_b); and (c) demonstrates the approximation to the averaged MECG beat using $N_k = 7$ Gaussian kernels. Illustration based on [362, 363].

frequency (i.e. maternal heart rate, or approximate pace for the maternal heart cycle - in rad/s), δ is the small sampling period (i.e. $1/f_s$, in s). The angular frequency ω was originally set to $\omega = 2\pi/T$, where T is an average RR-interval period for the MECG cycle. The second equation is the analogous time-discrete form of Eq. 5.2, η_k is a random additive noise term to include e.g. baseline wander. The procedure of adapting N_k Gaussian kernels into the averaged template results in a nonlinear optimization problem. In order to solve this problem, Clifford [87], Clifford and McSharry [90] and Sameni [362] used a nonlinear least-squares optimization approach in providing the best estimate in the MMSE sense. In MATLAB® the problem can be solved using the *lsqnonlin* function [362], see Figure 3.7 (c) for an exemplary fitting for $N_k = 7$.

Figure 3.8 demonstrates an abdECG channel and typical models obtained for θ_k and z_k. The model described can be applied into the KF framework by regarding θ_k and z_k as the states

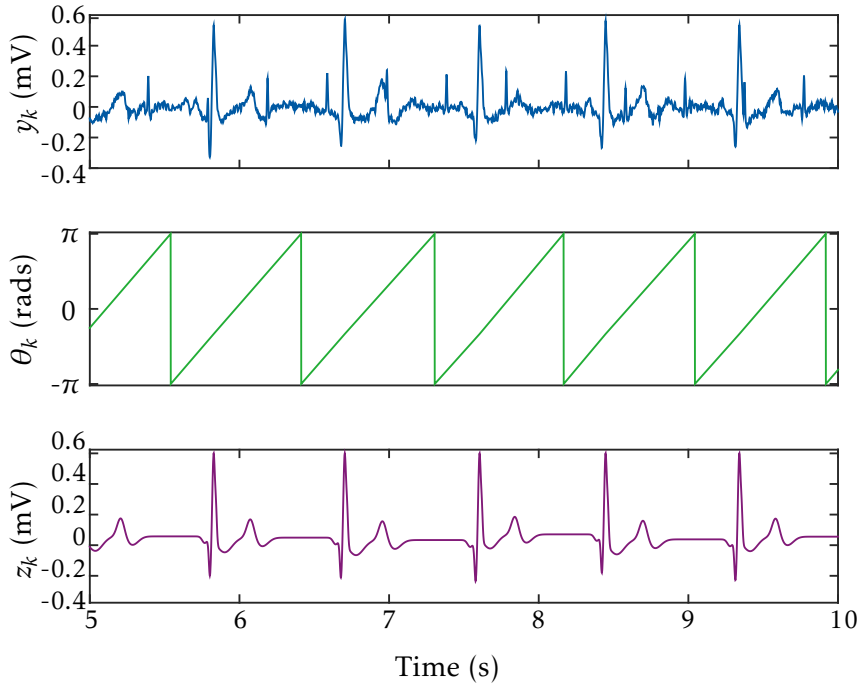

Figure 3.8: KF modelling using real recording (channel 5 - see Figure 5.4). On the top the preprocessed abdominal signal, in the middle the phase information and at the bottom is KF's system model (previous to adaptation).

variables, whilst $\alpha_i, b_i, \phi_i, \omega, \eta_k$ are Gaussian[14] random variables considered to be process noises, so that:

$$\underline{x}_k = [\theta_k, z_k]^T,$$
$$\underline{w}_k = \left[\alpha_1, \cdots, \alpha_{N_k}, b_1, \cdots, b_{N_k}, \phi_1, \cdots, \phi_{N_k}, \omega, \eta_k\right]^T.$$

Therefore, based on Eqs. 3.15 and 3.16, the EKF model can be described as [49, 362]:

$$\begin{aligned} \underline{x}_k &= \begin{bmatrix} f_0(\theta_{k-1}, \omega) \\ f_1(\theta_{k-1}, z_{k-1}, \omega, \{\alpha_{i,k-1}\}, \{b_{i,k-1}\}, \{\phi_{i,k-1}\}, \eta_{k-1}) \end{bmatrix}, \quad \text{for} \quad i \in [1, N_k] \\ \underline{y}_k &= \begin{bmatrix} 1 & 0 \\ 0 & 1 \end{bmatrix} \underline{x}_k + \underline{v}_k. \end{aligned} \tag{3.27}$$

As the reader may notice, the k index from the nonlinear functions $f(\cdot)$ were dropped since the proposed system model by Sameni [362] is time-invariant. Instead the set of functions $f_0(\cdot)$ and $f_1(\cdot)$ is used to represent the nonlinear function applied to each state. Since the system model is nonlinear, its process equation has to be linearized prior to applying the EKF algorithm. As results from the Eqs. 3.17 and 3.18 [362]:

[14] As discussed by Sameni [362], the assumption of Gaussianity is described as a "working assumption" that in theory may not hold for some of the parameters.

$$
\begin{aligned}
\widetilde{\mathbf{F}}_{k-1} &\approx \left.\frac{\partial f}{\partial \underline{x}_{k-1}}\right|_{\substack{\underline{x}_{k-1}=\underline{\hat{x}}_{k-1|k-1} \\ \underline{w}_{k-1}=\underline{0}}} \\
&\frac{\partial f_0}{\partial \theta_{k-1}} = \frac{\partial f_1}{\partial z_{k-1}} = 1, \qquad \frac{\partial f_0}{\partial z_{k-1}} = 0 \\
&\frac{\partial f_1}{\partial \theta_{k-1}} = -\sum_{i=1}^{N_k} \delta \frac{\alpha_i \omega}{b_i^2}\left(1 - \frac{\Delta\theta_{i,k-1}^2}{b_i^2}\right) exp\left(-\frac{\Delta\theta_{i,k-1}^2}{2b_i^2}\right), \\
\widetilde{\mathbf{W}}_{k-1} &\approx \left.\frac{\partial f}{\partial \underline{w}}\right|_{\substack{\underline{x}_{k-1}=\underline{\hat{x}}_{k-1|k-1} \\ \underline{w}_{k-1}=\underline{0}}} \\
&\frac{\partial f_0}{\partial \alpha_i} = \frac{\partial f_0}{\partial b_i} = \frac{\partial f_0}{\partial \phi_i} = \frac{\partial f_0}{\partial \eta_{k-1}} = 0, \qquad \frac{\partial f_1}{\partial \eta_{k-1}} = 1, \qquad \frac{\partial f_0}{\partial \omega} = \delta \\
&\frac{\partial f_1}{\partial \alpha_i} = -\delta \frac{\omega \Delta\theta_{i,k-1}}{b_i^2} exp\left(-\frac{\Delta\theta_{i,k-1}^2}{2b_i^2}\right), \\
&\frac{\partial f_1}{\partial b_i} = 2\delta \frac{\alpha_i \omega \Delta\theta_{i,k-1}}{b_i^3}\left(1 - \frac{\Delta\theta_{i,k-1}^2}{2b_i^2}\right) exp\left(-\frac{\Delta\theta_{i,k-1}^2}{2b_i^2}\right), \\
&\frac{\partial f_1}{\partial \phi_i} = \delta \frac{\alpha_i \omega}{b_i^2}\left(1 - \frac{\Delta\theta_{i,k-1}^2}{b_i^2}\right) exp\left(-\frac{\Delta\theta_{i,k-1}^2}{2b_i^2}\right), \\
&\frac{\partial f_1}{\partial \omega} = -\sum_{i=1} \delta \frac{\alpha_i \Delta\theta_{i,k-1}^2}{b_i^2} exp\left(-\frac{\Delta\theta_{i,k-1}^2}{2b_i^2}\right) \quad \forall i \in [1, N_k].
\end{aligned}
\tag{3.28}
$$

So far, the nonlinear system model and its linearization procedure for applying the EKF on abdominal signals were described. As explained in Section 3.3.2, the initialization of the algorithm's covariance matrices plays an important role in the performance of the EKF. Based on [49, 362, 363] the following initial parameters for the state and the filter's covariance matrices can be defined:

$$
\begin{aligned}
\mathbf{Q}_k = \mathbf{Q}_0 &= diag\left(\left[\sigma^2_{\alpha_1..\alpha_{Nk}}, \sigma^2_{b_1..b_{Nk}}, \sigma^2_{\phi_1..\phi_{Nk}}, \sigma^2_{\omega}, \overline{\sigma}^2_{fit}\right]\right) \\
\mathbf{R}_k = \mathbf{R}_0 &= \begin{bmatrix} (\omega\delta)^2 & 0 \\ 0 & \overline{\sigma}^2_{fit} \end{bmatrix} \\
P_0 &= \begin{bmatrix} (2\pi)^2 & 0 \\ 0 & 10 * max(|y_{1:\tau_0}|^2) \end{bmatrix}
\end{aligned}
\tag{3.29}
$$

where $diag(\cdot)$ is a function which diagonalizes its argument, σ_x^2 with $x = \{\alpha_i, b_i, \phi_i, \omega\}$ represents the manually defined variance for each Gaussian parameter and angular frequency, $\overline{\sigma}^2_{fit} = 1/N_b \sum_b \sigma^2_{fit}(b)$ is the mean standard deviation obtained during the template fitting for all bins (see Figure 3.7-(b)) and $max(\cdot)$ returns the maximum value of its argument. On its simplest form, Sameni [362] defined Q_k and R_k as time-invariant, thus Q_0 and R_0. As explained in Section 3.3.2, KF's performance depends on its model and the tunning of its covariance matrices. Therefore, the parameters described in Equation 3.29 should be exhaustively calibrated depending on the application (e.g. electrode configuration). Considering that this tunning is satisfactory,

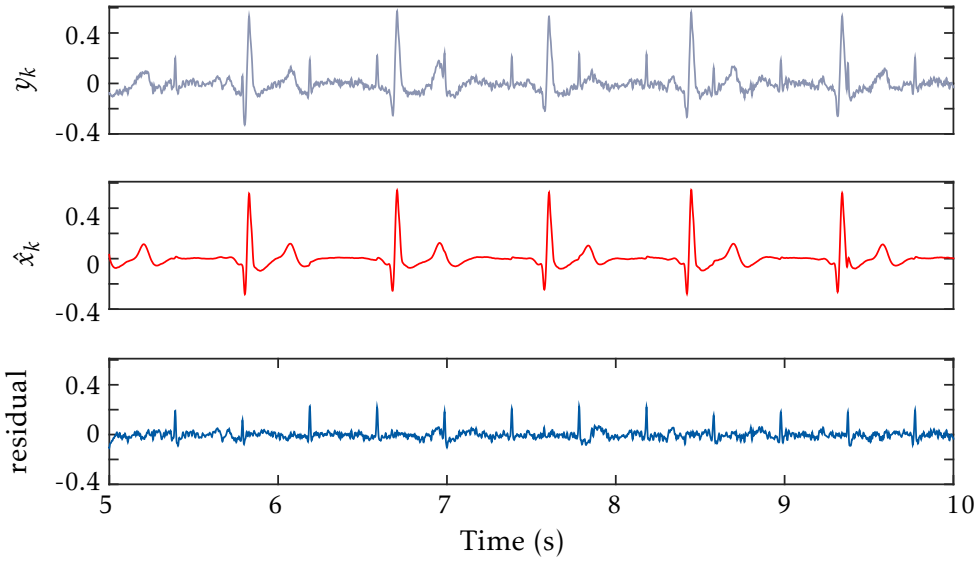

Figure 3.9: FECG extraction using EKF algorithm using clinical recording (channel 5 - see Figure 3.8). On the top the preprocessed abdominal signal, in the middle the estimated MECG signal and at the bottom the residual signal (FECG + noise). Amplitude in millivolts.

P_0 should rapidly converge. If one has a trustworthy system model, the EKF algorithm (see Algorithm 2) may be iteratively applied in obtaining estimates for the MECG at every time-step k. In Figure 3.9 an application example using EKF for FECG extraction output is presented.

Improvements on the extended Kalman model

During the last decade, several improvements to the EKF's model were proposed in the literature. In the previous section the initialization procedure for EKF was demonstrated. Independent of how well this initialization is performed, the average MECG template was originally not designed to evolve through time. It is clear that for long-term recordings such consideration would lead to an undesired lack of trust on the model by the Kalman algorithm. Moreover, the filter's MECG estimates could greatly benefit on a beat-to-beat basis from a time-varying Kalman model, on which small P-QRS-T wave variations are foreseen. For this purpose, instead of considering each Gaussian kernel parameter (i.e. $\underline{\alpha}_{i,k}, \underline{b}_{i,k}, \underline{\phi}_{i,k}$) as a noise processes (described in Section 3.3.4), Sayadi and Shamsollahi [375] suggested to consider them as hidden states following a random walk, increasing the number of states by $3{\times}N_k$. An almost identical approach was adopted by Akhbari *et al.* [6], Lin *et al.* [253], who suggested[15] the modelling of angular frequency ω as an additional state (i.e. ω_k). This improvement is relevant, since

[15] On a side note, similar to the works by Akhbari *et al.* [7], Niknazar *et al.* [305] suggested the use of *Dynamic Time Warping (DTW)* for allowing nonlinear phase adaptation. Both methods are indeed relevant, however, they were validated in filtering adult ECG using Physionet's MIT-BIH Arrhythmia Database [161, 286], which contains patients suffering from a variety of heart conditions, including *premature ventricular contraction (PVC)*. Their approach, therefore, attempted to adapt the phase of the model to represent those morphologically different heartbeats. To better cope with those cases of cardiac ectopy, a more suitable extension of the model is the switching Kalman filter proposed by Oster *et al.* [314], which changes its ECG model based on the innovation of the signal.

on the original filter equation (see Eq. 3.26) no additive noise was associated with the phase information. Lastly, as proposed by [305], a random additive noise ($\eta_{\theta,k}$) was added to the phase state equation so that the phase is no longer "strictly" linear, but fluctuations around its modelled values are allowed. Therefore, the resulting model with $3{\times}N_k + 1$ [6, 305, 375] additional state variables is summarized as follows:

$$\begin{cases} f_0: & \theta_{k+1} = (\theta_k + \omega_k \delta) \bmod 2\pi + \eta_{\theta,k} \\ f_1: & z_{k+1} = z_{k-1} - \sum_{i=1}^{N_k} \delta \frac{\alpha_i w}{b_i^2} \Delta\theta_{i,k-1} exp(-\frac{\Delta\theta_{i,k-1}^2}{2b_i^2}) + \eta_{z,k-1} \\ f_2: & \omega_k = \omega_{k-1} + \varepsilon_{1,k-1} \\ f_3: & \alpha_{1,k} = \alpha_{1,k-1} + \varepsilon_{2,k-1} \\ \vdots & \\ f_{N_k+2}: & \alpha_{N_k,k} = \alpha_{N_k,k-1} + \varepsilon_{(N_k+1),k-1} \\ f_{N_k+3}: & b_{1,k} = b_{1,k-1} + \varepsilon_{(N_k+2),k-1} \\ \vdots & \\ f_{2\cdot N_k+2}: & b_{N_k,k} = b_{N_k,k-1} + \varepsilon_{(2\cdot N_k+1),k-1} \\ f_{2\cdot N_k+3}: & \phi_{1,k} = \phi_{1,k-1} + \varepsilon_{(2\cdot N_k+2),k-1} \\ \vdots & \\ f_{3\cdot N_k+2}: & \phi_{N_k,k} = \phi_{N_k,k-1} + \varepsilon_{(3\cdot N_k+1),k-1} \end{cases} \tag{3.30}$$

so that the state $\underline{x}_k$ and noise process $\underline{w}_k$ become:

$$\begin{aligned} \underline{x}_k &= \left[\theta_k, z_k, \omega_k, \{\alpha_{1:N_k,k}\}, \{b_{1:N_k,k}\}, \{\phi_{1:N_k,k}\}\right]^T \\ w_k &= \left[\eta_{\theta,k}, \eta_{z,k}\{\varepsilon_{1:3\cdot Nk+1,k}\}\right]^T. \end{aligned} \tag{3.31}$$

The new state equations may be linearized as in Eq. 3.28 [49, 180, 375]:

$$\widetilde{\mathbf{F}}_{k-1} \approx \left.\frac{\partial f}{\partial \underline{x}_{k-1}}\right|_{\substack{\underline{x}_{k-1}=\underline{\hat{x}}_{k-1|k-1} \\ \underline{w}_{k-1}=\underline{0}}}$$

$$\begin{aligned} &\frac{\partial f_0}{\partial \theta_{k-1}} = \frac{\partial f_1}{\partial z_{k-1}} = 1, \quad \frac{\partial f_0}{\partial \omega_{k-1}} = \delta, \\ &\frac{\partial f_0}{\partial z_{k-1}} = \frac{\partial f_0}{\partial \alpha_{i,k-1}} = \frac{\partial f_0}{\partial b_{i,k-1}} = \frac{\partial f_0}{\partial \phi_{i,k-1}} = 0, \\ &\frac{\partial f_1}{\partial \theta_{k-1}} = -\sum_i \delta \frac{\alpha_{i,k-1}\omega}{b_{i,k-1}^2}\left(1 - \frac{\Delta\theta_{i,k-1}^2}{b_{i,k-1}^2}\right) exp\left(-\frac{\Delta\theta_{i,k-1}^2}{2b_{i,k-1}^2}\right), \\ &\frac{\partial f_1}{\partial \omega_{k-1}} = -\sum_{i=1} \delta \frac{\alpha_i \Delta\theta_{i,k-1}^2}{b_i^2} exp\left(-\frac{\Delta\theta_{i,k-1}^2}{2b_i^2}\right), \\ &\frac{\partial f_1}{\partial \alpha_{i,k-1}} = -\delta \frac{\omega \Delta\theta_{i,k-1}}{b_{i,k-1}^2} exp\left(-\frac{\Delta\theta_{i,k-1}^2}{2b_{i,k-1}^2}\right), \end{aligned} \tag{3.32}$$

$$\frac{\partial f_1}{\partial b_{i,k-1}} = 2\delta\frac{\alpha_i\omega\Delta\theta_{i,k-1}}{b^3_{i,k-1}}\left(1-\frac{\Delta\theta^2_{i,k-1}}{2b^2_{i,k-1}}\right)exp\left(-\frac{\Delta\theta^2_{i,k-1}}{2b^2_{i,k-1}}\right), \tag{3.32 cont.}$$

$$\frac{\partial f_1}{\partial \phi_{i,k-1}} = \delta\frac{\alpha_i\omega}{b^2_{i,k-1}}\left(1-\frac{\Delta\theta^2_{i,k-1}}{b^2_{i,k-1}}\right)exp\left(-\frac{\Delta\theta^2_{i,k-1}}{2b^2_{i,k-1}}\right),$$

$$\frac{\partial f_i}{\partial x^{j+1}_{k-1}}\begin{cases}\text{being} & x^j_{k-1}\text{is the } j^{\text{th}}\text{ variable in state vector } \underline{x}\\ 1, & \text{if } \forall\{i=j|i=2,3,\cdots,3\cdot N_k+2\}\\ 0, & \text{otherwise}\end{cases}$$

$$\widetilde{\mathbf{W}}_{k-1} = \left.\frac{\partial f}{\partial \underline{w}}\right|_{\substack{\underline{x}_{k-1}=\underline{\hat{x}}_{k-1|k-1}\\ \underline{w}_{k-1}=\underline{0}}} \approx \mathbf{I}^{(3\cdot N_k+3)\times(3\cdot N_k+3)} \tag{3.33}$$

Another improvement proposed by Sameni *et al.* [370], Tarvainen *et al.* [420] was adapting the covariance matrix $\mathbf{R}_k$ by using a normalized innovation for state z_k such that:

$$c_i = \frac{1}{N}\sum_{k=i-N+1}^{i}\frac{(\nu_k)^2}{s_k} \tag{3.34}$$

where ν_k is the second entry of the innovation vector $\underline{\nu}_k$ presented in Eq. 3.8 that refers to the MECG amplitude state z_k. Similarly, s_k is the second diagonal entry of filter-calculated innovation matrix $\mathbf{S}_k$ (see Eq. 3.9). The factor c_i then normalizes the estimated innovation for z_k over its estimated variance s_k using a moving average window of length N. Such approach, also present in [166, Sec. 8.11], is termed as information-weighted square innovation. According to [370], ideally is $c_i \approx 1$, if it has values greater than unit the innovation signal variance is being underestimated, while values close to zeros indicate it is being overestimated. The authors then adaptively updated the matrix $\mathbf{R}_k$ by using a AR moving average window of length M:

$$s^2_k = \lambda_v s^2_{k-1} + (1-\lambda_v)\frac{1}{M}\sum_{j=k-M}^{k-1}\left(s_j\right)^2 \tag{3.35}$$

where $0 < \lambda_v < 1$ is a forgetting factor, set to $\lambda_v = 0.95$ in [420]. If $M > 1$, the adaptation represents a moving average filter with the ω changing the slope of the filter's response, otherwise it is a first order AR model as in [420]. For updating the second entry q^2_k of the model noise covariance $\mathbf{Q}_k$, Tarvainen *et al.* [420] proposes the following correction factor:

$$q^2_k = \lambda_w\frac{s^2_k}{p^2_k} \tag{3.36}$$

where p^2_k is the second diagonal entry of matrix $\mathbf{P}_{k|k}$ and λ_w is the update coefficient, empirically defined. The observation variance (s^2_k) is included in order to remove the influence of signal amplitude of the estimate.

Further extensions

In Section 3.3.3 several extensions of the linear Kalman filter were presented. Aside from the EKF, the UKF [370] and Particle Filters [253] have also been applied in the scope of adult ECG denoising, which could be simply applied to NIFECG signals. In [365], the use of Particle filters is suggested as future work, however, to date there are no studies known to the author who applied McSharry's ECG model using such filters.

Additionally, if a delay in our filter or offline processing is allowed, smoothing may be used. There are 3 types of smoothing filters: *fixed-point*, *fixed-lag* and *fixed-interval*. In fixed-point smoothing, the point one intends to estimate is fixed, but the number of measurements continually changes. Fixed-lag smoothers allow a constant lag of some samples between the newest measurement and the current estimated sample. The last, and in our case most relevant, type is fixed-interval smoothing. Fixed-interval smoothers process in batches a fixed interval of measurements, using all available samples [399, Chap.9], i.e. offline processing. The *Extended Kalman Smoother (EKS)* is another extension of the EKF which enables the use of future information into improving the current estimate. The EKS algorithm consists of a forward EKF stage followed by a backward recursive smoothing stage. Due to its non-causal nature, the EKS is expected outperform the EKF [377].

In [370] a comparison between the EKF, EKS and UKF is presented. According to the authors, EKS demonstrated the smoothest results, while UKF performed better than EKF. Moreover, the authors affirmed that the most remarkable differences in estimation occur around sharp turning points of the signal (e.g. QRS complexes), where derivative-free methods such as UKF are better suited for strong non-linearities [370]. Based on the presented state-of-the-art on the EKF model, novel improvements are proposed further in Chapter 4.

3.4 Fetal QRS Detection

Analogous to the analysis of adult electrocardiography, the FQRS complexes obtained from FECG signals provide a first interesting feature, which can be directly linked to clinical diagnostic information. The current state-of-the-art for FQRS detectors are discussed in this section, meanwhile multi-channel merging considerations are presented in Section 3.4.1 and statistical metrics for evaluating these detector's accuracy and precision are described in Section 3.4.2. From FQRS detections, one can almost directly derive the FHR (described in Section 3.5) and obtain FHRV parameters (Section 2.3.1). However, the importance of accurate FQRS is not limited to FHR and FHRV analysis. In fact, reliable detection of fetal peak locations is pre-requirement for further analysis of FECG's morphology, since FQRS locations are crucial for segmentation of the FECG cycle.

Several algorithms have been proposed in the literature for QRS detection in adult ECG. A comprehensive overview on those methods can be found in Köhler *et al.* [232]. For the sake of example, methods may be based on adaptive thresholding [171, 320], filter-banks [3], matched-filters [123, 220], slope-detection [5, 416] or in representations such as the Hilbert [58]

or Wavelet transforms [154, 247].

Fetal QRS detectors present in the literature are usually adaptations of adult QRS detectors to cope with the higher FHR. During the PCINC 2013 several participants made use of this strategy, including some open-source entries available at Physionet e.g. Behar *et al.* [54] proposed an adapted implementation of the Pan and Tompkins [320] algorithm. Another relevant source of FQRS detection methods is the OSET [363], which includes a maxima search algorithm. Other examples of this strategy are matched filters [169, 254], slope-detection [337], supervised machine learning using the ESN algorithm [255], Wavelet transform [9, 155, 269]. Aside from the PCINC 2013, there is to date no study evaluating the performance of those FQRS detectors against each other known to the author. Some authors separate the FQRS procedure performed after FECG extraction (see Figure 3.6) into a "FECG enhancement" and "FQRS detection" step. In this work, however, the preprocessing performed to enhance the fetal peaks (i.e. feature extraction) is regarded as part of the FQRS algorithm.

3.4.1 Merging multichannel fetal QRS detections

Most FQRS detectors available in the literature make use of a single extracted FECG channel. However, real applications usually make use of multi-lead systems (as discussed in Section 3.2.3). In order to cope profit from this higher data dimensionality, one can either select/merge the available FECG channels (i.e. prior to FQRS detection), or select/merge the different FQRS detections available. In any case, some sort of metric for fetal signal quality (i.e. *signal quality index (SQI)*) has to be applied for determining which lead(s) to use. Typical measures take in consideration: 1) the morphology of the FECG signal, such as a kurtosis as "peakedness" measure; or 2) the pseudo-peridicity of the FQRS detections, i.e. a RR interval regularity. Therefore, performing the selection/merge after the FQRS detection occurs is advantageous since a regularity metric for each FECG channel is then available.

While the selection of one single FQRS source to represent the whole measurement may work in short datasets (e.g. PCINC 2013[16]) , it is sub-optimal for long-term recordings due to the varying nature of the fetal signal's SNR. Therefore, adaptively fusion of the information contained in multiple FQRS detections is a more attractive solution. One solution is to adaptively (e.g. on every few seconds) choose the lead with the best SQI, the so-called *lead switching* approach. An exemplary application of such method was proposed by Johnson *et al.* [209, 211], who made use of several SQI measures and lead switching to multi-modal adult beat detection in obtaining the best scores on the PCINC 2014. Another option is to use weighted or majority voting to obtain a consensus detections. Such approaches have been often for merging the results of different QRS detectors/classifiers [205, 283] and for producing consensus from annotations provided by different experts [170, 429, 479].

[16] Behar *et al.* [54] obtain top-scoring results in the PCINC 2013 by making use of a regularity SQI in selecting the most periodic FQRS detection source. The method proposed by the author not only used every lead, but also extracted channels using different extraction methods.

3.4.2 Detection performance

In order to report FQRS detection statistics different measures were proposed in the literature. The main goal of these metrics is to assess the accuracy and precision of the obtained FQRS detections. In an attempt to standardize this assessment, challenge organisers at PCINC 2013 suggested the use of the *root mean square error (RMSE)* of corresponding RR intervals as scoring measure for its events 2 and 5 ($E2/E5$ - in ms) [20, 395]:

$$E2/E5 = \sqrt{\frac{1}{N_p}\sum_{n=1}^{N_p'}\left(RR_n^t - RR_n^r\right)^2} \quad \text{(in ms)} \tag{3.37}$$

being n the detection index, N_p the number of existent reference FQRS anotations, N_p' the number of FQRS detections available, RR_n^t each detected RR interval (t = test) and RR_n^r the nearest reference (r) RR interval available. However, the measure mixes both precision and accuracy in one score, which is not optimal for the interpretation of the results.

In order to more clearly present the accuracy of FQRS detections, measures presented in the *American National Standards Institute (ANSI)* [26] can be used. Particularly, the number of *true positive (TP)* denotes correctly detected peaks, *false negative (FN)* being existing peaks which were not detected and *false positive (FP)* nonexistent peaks that were falsely detected can be reported. Differing from the adult norm [26] of 150 ms acceptance interval between detection and reference annotation, to account for the higher FHR a window of 50 ms is usually applied [20, 52, 477]. Based on from these absolute numbers, the following summary metrics can be used:

$$SE = 100 \cdot \frac{TP}{TP+FN} \quad \text{(in \%)} \qquad PPV = 100 \cdot \frac{TP}{TP+FP} \quad \text{(in \%)} \tag{3.38}$$

where *sensitivity (SE)* measures the percentage of actual FQRS complexes that were correctly identified and *positive predictive value (PPV)* defines the proportion of detected peaks that indeed correspond to FQRS peaks. Once again, these measures can be condesed into two FQRS detection accuracy measures, namely *accuracy (ACC)* [221] and the F_1 score [52, 374]:

$$ACC = 100 \cdot \frac{TP}{TP+FN+FP} \quad [\%] \tag{3.39}$$

$$F_1 = 100 \cdot 2 \cdot \frac{PPV \cdot SE}{PPV + SE} = 100 \cdot \frac{2 \cdot TP}{2 \cdot TP + FN + FP} \quad \text{(in \%)} \tag{3.40}$$

ACC is simply the percentage of the correctly detected peaks, over all detected and un-detected peaks, while F_1 provides the harmonic mean between SE and PPV, therefore summarizing those measures in one score. Despite some criticism [339, 340], the latter measure is particularly suitable for situations when the average of rates is desired [51, 374].

Beyond the presented metrics for evaluating FQRS's window-based accuracy (i.e. SE, PPV and F_1), a distance measure is necessary to discriminate between precise and imprecise detections, e.g. if any jitter occurs, information which is not captured by window-based metrics. Andreotti *et al.* [18] suggest the used of the *mean average error (MAE)*. MAE consists of the absolute time difference between the reference annotation time-stamp (QRS_n^r) and detected

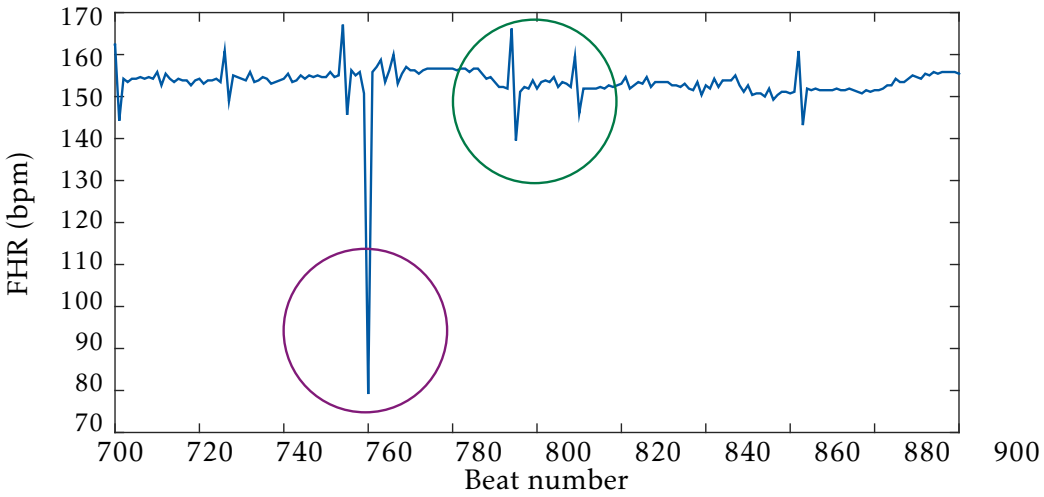

Figure 3.10: Exemplary fetal HR tachogram from own clinical data. Highlighted around the beat number 760 there is a clear example of missing beat, on which the FHR is assumed to be the half as its baseline value. The consequence of detection jitter on the FQRS is also highlighted (around beat number 800) and is characterized by a shorter FHR estimate followed by a longer, or vice-versa.

annotation (QRS_n^d). In order to make this distance criterion independent from the detection accuracy, Andreotti *et al.* [18] only made use of TP detection peaks in the MAE calculation. Therefore, MAE is expressed as in Equation 3.41:

$$MAE = \frac{1}{TP} \cdot \sum_{i=n}^{TP} |QRS_i^r - QRS_i^d| \quad \text{(in ms)}. \tag{3.41}$$

Aside from the mean detection jitter (i.e. MAE), the standard deviation of the detection jitter, which measures the spread of the FQRS detections, has also been referred to in the literature [148, 176]. In order to perform a proper benchmark of the FQRS detector's capabilities, results should always be presented for both accuracy and distance (or spread) [18]. For further information on FQRS metrics, the reader is referred to [51].

3.5 Fetal Heart Rate Estimation

As presented in Section 2.3.1, the FHR is the most often used parameter in clinical routine to evaluate the fetal health state. This parameters is usually obtained through the Doppler ultrasound (averaged using a ca. 3.75 s window interval) or using the STAN monitor during the intrapartum period. Since the accurate FQRS are a pre-requirement but are generally faulty (e.g. missing detections), the attained FQRS need to be preprocessed before further analysis (presented in Section 3.5.1). Considering that accurate FHRs are available, the analysis shown in Section 2.3.1 may be applied.

3.5.1 Preprocessing the fetal heart rate

Despite one's best effort on obtaining accurate detections, FQRS are usually imperfectly identified. These inaccuracies may have physiological, pathological or technical origins [326]. For instance, according to Clifford *et al.* [88], the fiducial markers should always be set on the onset of the P-wave rather than on the R-peaks, since this is a more accurate marker of the sinoatrial node stimuli. However, the R-peaks are considerably simpler to detect, particularly in the NIFECG case. Aside from this technical difficulty, several other aspects should be considered. Peltola [326] presents an overview on available methods for preprocessing HR tachograms, while Clifford [86] provide a more in-depth analysis of available methods.

The RR series obtained from ECG recordings are usually functions of the number of heartbeats instead of time (usually in *beats per minute (bpm)*) [249]. Figure 3.10 exhibits an exemplary fetal RR series tachogram, obtained by taking the first derivative of the FQRS timestamps (in s) and dividing its inverse. As Figure 3.10 hints, some of the common difficulties encountered when analyzing FHRV. These may have a technical (e.g. detection jitter, missing detections or uneven sampling) or a pathophysiological origin (e.g. ectopic beats). Different preprocessing methods are available in the literature to treat each of these events. Despite being an interesting research topic, such techniques to process heart rate series exceed the scope of this work. As previously explained, this work focuses on more fundamental problems in the signal processing of FHR rather than clinically interpreting those results. For this reason, in this work 5 seconds moving median windows with 1 second overlap were applied when calculating FHR estimates. This approach is specifically applied in Section 4.3.2, where a multichannel approach to improve FHR estimates is proposed.

3.5.2 Fetal heart rate statistics

Similarly to the F_1 accuracy metric presented for FQRS detections, the *heart rate detection rate (HDR)* has been often applied in adult HR detection. HDR assesses the percentage of the HR values within ±5 bpm tolerance [27] of the reference HR annotations (regarded as TP estimates) [51, 52]. On the fetal case, this tolerance was modified to ±10 bpm to reflect the higher FHR (accelerations and decelerations of the FHR are usually defined by changes greater than 15 bpm [12]). HDR results (in percent) are given by dividing the number of TP by the total number of measured FHR estimates [22], i.e. similar to Eq. 3.39, as follows:

$$HDR = 100 \cdot \frac{TP}{TP + FN + FP} \quad \text{(in \%)} \tag{3.42}$$

As for precision metric, the distance between the produced FHR and the reference values were also often used in the literature. Its use is particularly relevant when some averaging window is applied in producing the RR estimates (e.g. CTG's 3.75 s averaged FHR values). During the PCINC 2013, the mean square error between matched reference and test FHR measurements (i.e. FHR^r and FHR^t, respectively) at 12 instances for each recording (on every 5 s) [20, 51, 395].

The scoring statistic was used for the Events 1 and 4 ($E1/4$ - in bpm^2):

$$E1/E4 = \frac{1}{12}\sum_{i=1}^{12}\left(FHR_n^t - FHR_n^r\right)^2 \quad (\text{in bpm}^2) \tag{3.43}$$

As before, the Challenge scoring is hardly interpretable and depends on pre-defined Physionet WFDB functions (see [161, 398]). In this work, a more straightforward measure is used, namely the RMSE between reference and test FHR, described as:

$$RMSE = \sqrt{\frac{1}{N_p}\sum_{n=1}^{N_p'}\left(FHR_n^t - FHR_n^r\right)^2} \quad (\text{in bpm}) \tag{3.44}$$

3.6 Fetal ECG Morphological Analysis

In Section 2.3.2 the three major parameters used in fetal morphological analysis were clarified, namely the FQT, FST and the FTQRS. Due to the lack of standards for FECG morphological analysis, there are several aspects of this evaluation that require further investigation. In this section, focus is put on the signal processing tools that enable the derivation of these morphological features. Further on, metrics on how to evaluate the accuracy of such estimated measures are proposed.

The first aspect to be regarded is the bandwidth used while extracting the NIFECG signal, since it can deform the fetal signal, e.g. the T-wave. Throughout this work the signal bandwidth was configured as recommended by the American Heart Society for adult electrocardiography [231] (as further described in Section 4.1). Similarly, the extraction method used (see Section 3.3.1) is expected to have an impact on those parameter estimates and are evaluated in Chapter 6.

Another important consideration is whether the morphological features should be obtained on a beat-to-beat basis or on an averaged FECG template. The first option is obviously more attractive, however due to the usually low SNR of the fetal signal it is impracticable, making the use of averaged FECG beats imperative[17]. As an example, even though direct FSE recordings comprise a much higher FECG SNR, commercial equipments such as STAN, still makes use of this averaging procedure. For this reason, this work is restricted to the analysis of FECG template beats. A general signal processing scheme for obtaining the aforementioned features is presented in Figure 3.11.

Template generation plays an important role in this analysis, important details are the number of average beats, which central tendency measure is used (e.g. mean, median), and if low correlating or ectopic beats are excluded from final template. In preliminary works [18] the template construction method proposed by Oster *et al.* [314] has provided better results than similar methods, therefore it is used in this thesis.

The template generation step is followed by beat segmentation, which aims at finding the

[17] On a side note, in fact, even for adult ECG analysis there are no current standards and signal-averaging is not a consensus among researchers, despite its wide usage in the literature (e.g. [85, 132, 162, 473])

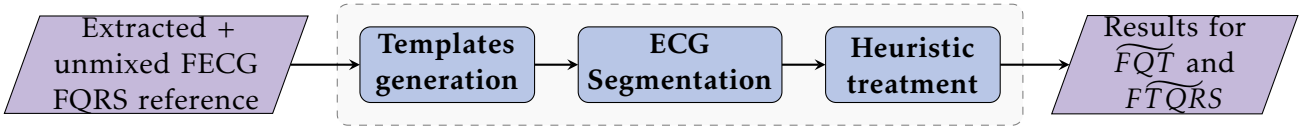

Figure 3.11: Signal processing steps for morphological analysis, regarding morphological features shown in Figure 2.2.

necessary fiducial points, i.e. locations for Q-onset, T-offset as well as T-peak. Several ECG segmentation algorithms have been proposed in the literature [203, 269, 376, 381, 451], however current algorithms are mainly designed and trained using adult ECG databases and are likely to be sub-optimal for FECG analysis. To the authors best knowledge, the only FECG segmentation algorithm present in the literature is an adaptation by Hurezeanu *et al.* [195] of the Wavelet delineation algorithm from Martinez *et al.* [269]. Additionally, despite the large number of adult segmentation algorithms available, only a very few of those have been made open-source such as: the *ecgpuwave* [203], as part of the WFDB toolbox [161, 398][18], and very recently the Wavelet delineation script [269], made available under the *ecg-kit*[19]. As demonstrated in Figure 3.11, the last step is an heuristic treatment of the obtained fiducial locations. This simple step is necessary for making sure that the fiducial annotations are valid, e.g. from the physiology not too short/long.

At last, one can define the FQT and FTQRS errors as [18]:

$$\widetilde{FQT} = \frac{1}{N}\sum_{i=1}^{N}\left|FQT_{abdm} - FQT_{ref}\right| \quad \text{(in ms)} \tag{3.45}$$

$$\widetilde{FTQRS} = \frac{100}{N}\cdot\sum_{i=1}^{N}\left|\frac{FT_{h,abdm}}{FQRS_{abdm}} - \frac{FT_{h,ref}}{FQRS_{ref}}\right| \quad \text{(in \%)} \tag{3.46}$$

Alternatively, if simulated data is used, distance measures such as the MSE or SNR between the fetal reference and an extracted signals could be applied Behar *et al.* [51].

3.7 Problem Description

Despite the rich and growing literature that focus on NIFECG extraction and FQRS detection, few of those works are actually reproducible. This is mainly due to the lack of common dataset and open-source software. Due to its versatile framework, many authors make use of the EKF approaches (described in Section 3.3.4). However, EKF heavily depends on a well-representative model and is sensitive to its initialization/calibration. The non-observance of these aspects leads to the undesired suppression of fetal peaks, either when MECG temporal overlap occurs (lack of trust in model) or partial suppression of the FECG due to (noise overestimation – remember that the FECG is treated as noise). In this work, those topics were further explored, particularly regarding the MECG/FECG modelling. Therefore, three aspects are further explored: i) the

[18] Available at: `https://www.physionet.org`
[19] Available at: `https://github.com/marianux/ecg-kit`

creation of the MECG template/model, ii) the varying presence of measurement noise, and iii) the ill-conditioned assumption that the FECG can be represented as WGN. A systematic calibration procedure is carried out to guarantee the general validity of the designed filters.

Regarding FQRS detection and FHR estimation (presented in Section 3.4-3.5), as can be seen on the PCINC 2013-related papers, current techniques are often faulty. This problem is addressed in this work by using two different multichannel FQRS/FHR correction methods, which take into consideration different signal quality metrics that weight down unreliable detections. One of those techniques is considered as responsible for the author's first-place award and top-scores on PCINC 2013 competition [20, 21], as further clarified.

3.8 Chapter Summary

In this chapter, current prenatal diagnostic techniques were presented and the benefits from NIFECG clearly stated. Further, an overview on NIFECG extraction algorithms was provided. Further in this section, the discrete-time KF and EKF algorithms were briefly derived. In Section 3.3.4 the current state-of-the-art on EKF for FECG extraction was presented. Particularly two models were presented, the 2-state EKF algorithm [370] (henceforth named $EKF2$), extended states EKF [6, 375] (henceforth called $EKF24$ - i.e. $3{\cdot}N_k + 3$ states, considering $N_k = 7$ as discussed in the next chapter of this work). In Sections 3.4-3.6 the metrics to assess FQRS, FHR and FECG morphology parameters were presented. In Section 3.7, the current challenges on NIFECG signal processing that were addressed in the remaining of this work were clarified. In the next chapter, novel methods are proposed to deal with the limitation of current techniques.

All models are wrong, but some are useful.

– George E.P. Box (1978)

4

Novel Approaches for Fetal ECG Analysis

In this chapter, newly developed approaches for NIFECG analysis are presented. These methods are divided into NIFECG extraction (Section 4.2) and FQRS/FHR correction methods (Section 4.3). Before proceeding with the proposed improvements on FECG signal extraction and FQRS detection/correction performed throughout this thesis, some preliminary issues about the available signals are presented in the following section.

4.1 Preliminary Considerations

Regarding NIFECG's signal processing chain (see Fig. 3.6), preprocessing is an important step, on which FQRS detection results or morphological analysis strongly depend. For this reason, before proceeding, some definitions on the following aspects shall be considered:

- bandpass filtering range;
- MQRS reference and re-alignment;
- initialization window allowed and online/offline execution strategy;
- channel selection.

The pre-filtering bands are a crucial aspect of NIFECG research on which depending on the application the final results may be heavily influenced. For instance, if the aim is to detect FQRS complexes, a narrower band is required than when the focus is on FECG morphological analysis. While dealing with FQRS detection accuracy, Behar *et al.* [54] evaluated different high-pass cut-off frequencies using several extraction methods. For most approaches by raising the higher cut-off frequencies to 10 Hz, an improvement of up to 3% in the F_1 (see Section 3.4.2) occurred. On the order hand, for morphological analysis a higher cut-off will lead to P and T-wave distortion and suppression (see Kligfield *et al.* [231] guideline for adult electrocardiography).

In this work, two passing bands (henceforth called narrow and wide bands), were defined as in Andreotti *et al.* [18]. Both bands made use of a low-pass cutoff frequency at 100 Hz and used Butterworth zero-phase filters. The narrow band consists of a 3^{rd} order low-pass and 5^{th} order high-pass filter with cutoff at 3 Hz. Meanwhile the wide band made use of a 7^{th} order low-pass filter and 8^{th} high-pass filter with cutoff at 0.5 Hz, in order to preserve most of the fetal T-wave. Both filters were designed to match a 20 dB attenuation at the stop-band and 0.1 dB gain at the pass-band) [18]. Additionally, an *infinite impulse response (IIR)* notch filter was included for suppressing the powerline interference suppression at 50 or 60 Hz (±1 %).

With regards to MQRS locations, as mentioned in Section 3.3.4 EKF extraction strongly depends on a reliable MQRS reference annotation. As discussed in Section 3.2.3, NIFECG analysis can greatly benefit from the presence of a MECG reference lead with little additional computational effort and increase in hardware complexity. Therefore, in this work it is assumed that a MQRS reference is available. From the author's own experience on collecting this study's clinical data, a MECG channel is not a too restrictive assumption and the benefits are valuable. In order to align this maternal reference to each abdominal channel's peak a re-alignment was performed. During EKF's initialization, the absolute maxima around each maternal references peak with a window of ±100 ms was sought. The average lag between reference and maxima location was then regarded as re-alignment factor and every MQRS annotation is shifted by this factor before the extraction takes place.

A common strategy for signal processing algorithms running on biomedical devices is to allow a short initialization period, after which algorithms should be able to run online. Aiming at producing online methods for NIFECG, throughout this work an initialization window of 60 seconds is used for every extraction method. Moreover, for the same reason no offline smoothing filter was applied. In the scope of NIFECG such initialization window is interesting since it allows a reproducible comparison between TS, AM and BSS extraction methods, by allowing that each technique:

- TS: generation of initial template;
- AM: initialization of adaptive filter coefficients or training period;
- BSS: mixing matrix calculation;

Channel selection is another topic to be considered when dealing with multichannel recordings of abdECG signals. Indeed the information obtained from bad quality channels should be weighted down (or discarded). However, to date there is no consensus for assessing the signal quality in NIFECG recordings. Moreover, adult SQI metrics are prone to confound between FQRS and MQRS complexes. For this reason, in this work, no channel selection on the preprocessing step is performed. Instead, the extraction algorithms (developed in Section 4.2) were applied on every available channel and, by using specifically designed fetal SQI metrics in association with novel FQRS detectors (further shown in Section 4.3), the information from multiple channels is fused.

4.2 Fetal ECG Extraction by means of Kalman Filtering

In Section 3.3.2 it is noticeable that the "art" of Kalman filtering consists of optimizing its model. In Section 3.3.4, two state-of-the-art variants of the EKF model for NIFECG analysis were presented, namely the 2-state model $EKF2$ and the extended state model $EKF24$ (with $3{\cdot}N_k + 3$ states, considering $N_k = 7$ further defined in Section 4.2.1). These models serve as basis for this work's developments, which were implemented in MATLAB®environment as described in Section 3.3.4. Regarding $EKF24$'s implementation, the extended states (see Eq. 3.31) do not strictly require the same update rate as the first two states (i.e. phase and amplitude of the MECG signal), since these processes are expected to have a slower rate of change. For avoiding unnecessary computation, an update frequency was empirically set to 10% the sampling frequency of the NIFECG signal ($f_u = f_s/10$). In the following subsections, novel improvements on the Kalman model are proposed, which are benchmark using both $EKF2$ and $EKF24$ as reference in the following chapter.

4.2.1 Optimized Gaussian approximation

As described in Section 3.3.4 and illustrated in Fig. 3.7, EKF's dynamic model is obtained by wrapping and coherent averaging MECG beats to generate the so-called MECG template. The maternal template is henceforth denoted using the simple time-discrete notation $t_m[n]$, since the template is converted from polar notation $t_m(\theta_k)$, where $\{\theta_k\} \in [-\pi, \pi]$ the phase into bins with $k \in \{1, ..., 300\}$ bins. As explained in the aforementioned section, $t_m[n]$ is approximated using a number N_k of Gaussian kernels, whose parameters α_i (amplitude), b_i (width/standard deviation) and ϕ_i (position) with $i \in \{1, ..., N_k\}$ are optimized to fit the template (see Fig. 3.7-c). This optimization procedure was solved as proposed by Clifford [87], Clifford *et al.* [91] using the nonlinear least-squares approach, e.g. using the *lsqnonlin* function from MATLAB® [362]. Initial values for each kernel parameters were defined by the local template amplitude (i.e. $\alpha_i = t_m(\phi_i)$) and the fixed width $b_i = 0.04$ rad. Although Clifford [87] allowed these positions to vary, Sameni *et al.* [370] fixed the initial positions (ϕ_i) for these kernels for simplicity and stability, this latter procedure is denoted as *fixed fitting (FF)* in this work. The widely varying abdominal projections may hinder such a generalization of initial parameters. Moreover, due to the discontinuities present in the MECG waveform (e.g. the QRS complex) the pursuit for global minima is not straightforward and the optimization function may return a position of local minimum.

Based on the limitations of the existent approaches, in this work an improved approached for performing this optimization procedure was suggested in Andreotti *et al.* [17]. Based on the hypothesis that the approximation of $t_m(\phi_i)$ can be improved by introducing an intelligent initialization procedure, relying on an iterative approach that exploits the effects of random initialization and on the *Stationary Wavelet Transform (SWT)* technique. In the following section the suggested SWT approach as well as alternative techniques suggested in the literature are explained.

Gaussian fitting strategies

In the FF initialization, the pre-determined kernel positions were obtained from publications that followed the works from McSharry *et al.* [275]. Specifically, for $N_k = 5$ [275], $N_k = 6$ [91], $N_k = 7$ [87, 91] and for $N_k = 9$ to 11 [364]. Additionally, a model for $N_k = 15$ was extrapolated from the model using 11 kernels by inserting 4 new kernels between the existing ones. A similar approach for the FF can be achieved by simply distributing these N_k kernels uniformly within the interval $[-\pi, \pi]$, which is here denoted *uniform fitting (UF)*. For both FF and UF, the optimization procedure was performed considering as lower/upper bounds ±2 its initial values for each parameter α_i, b_i and ϕ_i, regardless of their units (i.e. mV or radians). The number of steps permitted for the optimization procedure was limited to $100 \times N_k$.

Another method suggested in the literature is a brute-force search method based on the FF/UF approaches. However, the method has the remarkable distinction of being stochastic. The so-called *random search fitting (RSF)* [52] initializes the Gaussian kernel parameters at random positions and repeats the optimization procedure several times. The best results, defined as the minimal *normalized mean square error (NMSE)* fitting the Gaussian to the MECG template, are kept and further used. This exhaustive search approach was previously used in the NIFECG context by Behar *et al.* [53, 54]. As in the previous approaches, the Gaussian kernels' parameters were searched using $100 \times N_k$ steps[1] of the optimization procedure, the best results were then selected.

An alternative deterministic algorithm for initializing the Gaussian kernel positions based on the cross-correlation between the MECG template and pre-defined Gaussian functions with varying standard deviations was proposed in [87]. As mentioned by the authors, the use of wavelet scaling functions is an alternative to the cross-correlation procedure. Aiming at improving the computational efficiency of this optimization procedure, this author (see Andreotti *et al.* [17]) proposed an approach using the SWT framework. The SWT is a discrete version of the Wavelet transform, which provides translation invariant output. The computational efficient calculation is performed by using the *algorithme à trous* [182], which upsamples and zero-pads the filter coefficients instead of performing downsampling (therefore, the approach is also called the undecimated wavelet transform). This property makes the SWT a redundant scheme computationally more complex than the *discrete wavelet transform (DWT)*. Aside from the Wavelet algorithm used, the choice for wavelet is very important. In this work, the quadratic spline wavelet [262] was applied, due to its qualitatively resemblance to Gaussian kernels (see Fig. 4.1).

Note that the approach does not rely on the wavelet coefficients themselves, instead it exploits a side effect of the iterative scheme to calculate the transform, namely the low-pass filters. In this work, the first six dyadic scales were used i.e. $2^j, j \in \{1, ..., 6\}$. Since the low-pass filters (scaling functions) have different number of samples at different levels, their signal power vary. In order to normalize this power, the SWT was calculated and further divided by the standard deviation

[1] Despite having used a fixed number of iterations, the author acknowledges that to reduce the total iterations in more practical scenarios may required the inclusion of a tolerance threshold. That is, when the model reaches an acceptable fitting error the optimization procedure should be terminated.

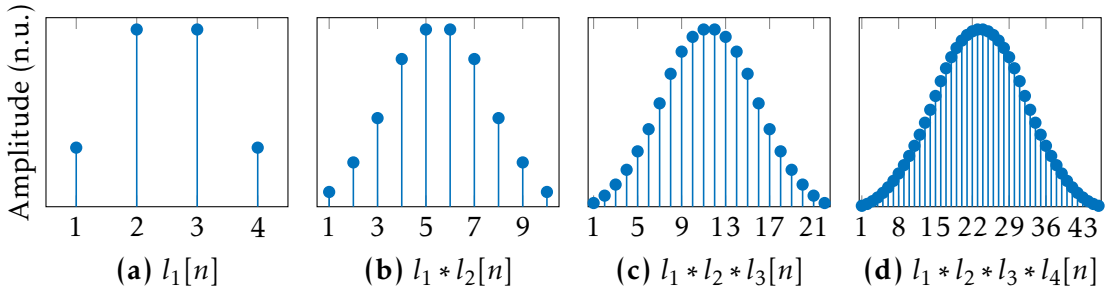

Figure 4.1: First four low-pass convoluted filters for quadratic spline wavelet (from (a)-(d)). Being l_i for $i \in [1,4]$ the low-pass filters at each level, when regarding the filter-bank scheme for the SWT. These filters are used in locating optimal positions for fitting Gaussians (at various scales / widths) into a MECG template.

of the low-pass filter and template, i.e. using the cross-correlation coefficient, described in the following Equation 4.2:

$$a_i[n] = t_m[n] * \underbrace{(l_1 * l_2 \cdots * l_i)[n]}_{l_{1..i}[n]} \tag{4.1}$$

$$a_i[n] = \frac{(t_m \star l_{1..i})[n]}{\sigma_{t_m}\sigma_{l_{1..i}}} \quad \text{for } i \in [1,6] \tag{4.2}$$

where a_i (not to be confounded with Gaussian amplitude α_i) is the approximation at scale i and $\star$ represents the cross-covariance operation. The initial position for each kernel is iteratively defined as the absolute maxima of the approximation (i.e. $|a_i[n]|$ with $i \in [1,6]$). For each kernel, the nonlinear least squares optimization procedure was employed with a maximal number of 100 steps for fitting α_i, b_i and ϕ_i parameters, as in the previous approaches. Three variants of this iterative approach, here denoted *stationary wavelet transform fitting (SWTF)*, were evaluated as follows:

- implementation as previously explained, henceforth denoted as "SWTF1";
- inclusion of constraints to the optimization procedure, variant here denoted as "SWTF2":
  - direction constraint to each α_i based on current unnormalized scale amplitude value to avoid kernels from changing sign;
  - each b_i was initialized with the current scale's standard deviation to dynamically give it a realistic starting value;
  - for each ϕ_i fitting, a shift of $\pm\pi/10$ was allowed to avoid that kernels adapt themselves to other waves;
- after applying the SWTF2, the selected Gaussian parameters were used as input for a last optimization round, i.e. performing the fine-tuning all N_k kernels at once. This latter method is here named "SWTF3".

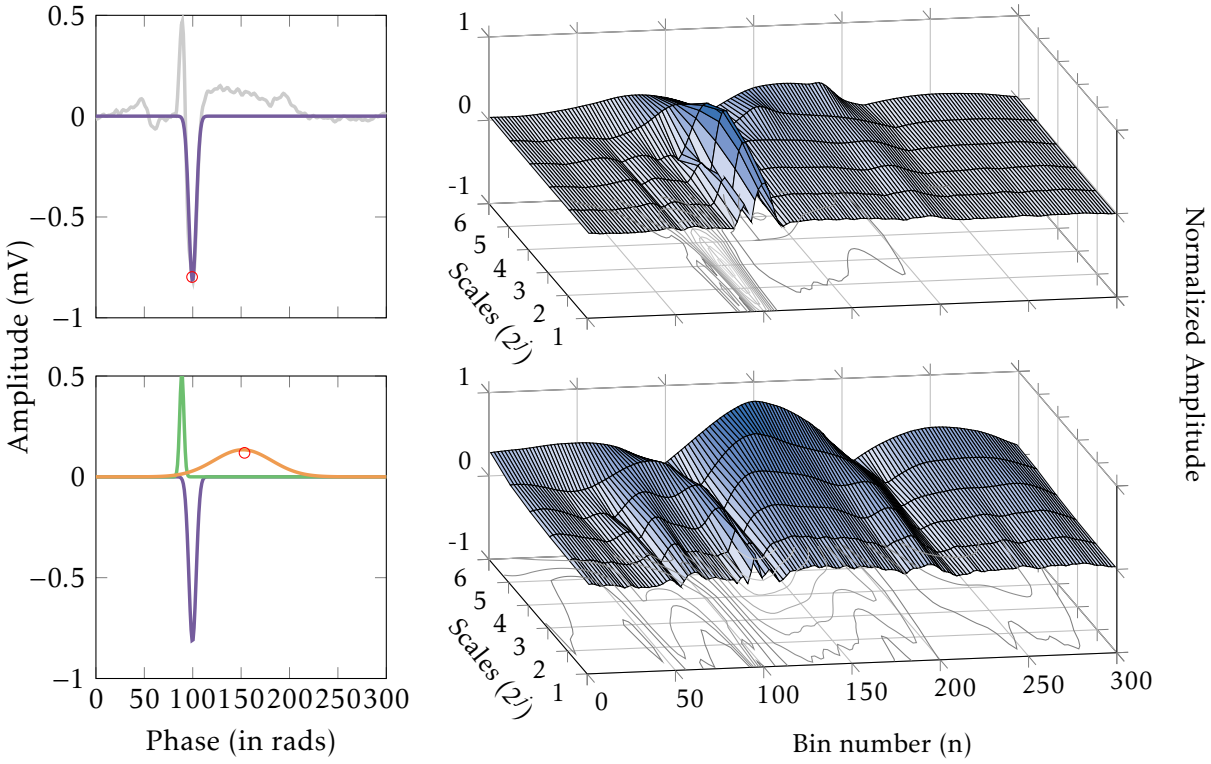

(a) Fitted Gaussians

(b) View of different scales

Figure 4.2: Stationary wavelet transform fitting. Inclusion of first (top) and third (bottom) Gaussian kernels.

Database and Validation

In order to evaluate which of the proposed methodologies can most accurately approximate t_m, the clinical dataset collected during this work and further described in Section 5.2 was used. Template generation was performed once for each abdominal channel in each recording during the initialization period, totalizing 168 templates. The *goodness of the fit (GOF)* was selected as performance measure, which is based on the NMSE as follows:

$$GOF = 1 - \underbrace{\left\| \frac{t_m[n] - \widehat{t}_m[n]}{t_m[n] - \bar{t}_m[n])} \right\|}_{\text{NMSE}}, \qquad (4.3)$$

$$\widehat{t}_m[n] = interp\left(\sum_{i=1}^{N} \alpha_i \cdot exp\left(-\frac{(\theta_k - \phi_i)^2}{2 \cdot b_i^2} \right) \right),$$

where $GOF = 1$ represents a perfect fit, $\|.\|$ is the Euclidean norm operator, and $interp()$ is the interpolation function to convert templates from a polar notation to the predefined number of bins (N_b).

Since the ECG modelling procedure is a fundamental part of the EKF's initialization and common for all Kalman variants presented along this chapter, it is here treated as preliminary work. Therefore the results and discussion are exceptionally shown within the next sub-

Table 4.1: Results for different fitting methods evaluated (shown as median ± (interquartile range - IQR). Methods used include fixed (FF), uniform (UF), random search (RSF), and variants of the SWT fitting approach (SWTF). The best results are highlighted for each number of kernel (N_k).

(a) Results for GOF (n.u.)

N_k / Method	5	6	7	9	10	11	15
FF	0.95 (0.09)	0.19 (0.26)	0.18 (0.22)	0.99 (0.03)	0.98 (0.06)	0.99 (0.03)	0.99 (0.05)
UF	0.19 (0.19)	0.21 (0.21)	0.97 (0.07)	0.32 (0.59)	0.99 (0.02)	0.94 (0.73)	0.99 (0.57)
RSF	0.98 (0.03)	0.99 (0.02)	0.99 (0.02)	1.00 (0.01)	1.00 (0.01)	1.00 (0.01)	1.00 (0.00)
SWTF1	0.96 (0.04)	0.97 (0.03)	0.98 (0.02)	0.99 (0.01)	0.99 (0.01)	0.99 (0.01)	1.00 (0.01)
SWTF2	0.96 (0.04)	0.97 (0.03)	0.98 (0.02)	0.99 (0.01)	0.99 (0.01)	0.99 (0.01)	1.00 (0.01)
SWTF3	0.97 (0.02)	0.98 (0.02)	0.99 (0.01)	0.99 (0.01)	1.00 (0.01)	1.00 (0.01)	1.00 (0.01)

(b) Computational time (in seconds)

N_k / Method	5	6	7	9	10	11	15
FF	0.11 (0.07)	0.27 (0.33)	0.26 (0.44)	0.23 (0.17)	0.32 (0.20)	0.35 (0.24)	0.47 (0.36)
UF	0.15 (0.15)	0.24 (0.32)	0.14 (0.08)	0.37 (0.45)	0.28 (0.14)	0.49 (0.44)	0.58 (0.77)
RSF	19.7 (12.7)	26.3 (15.3)	33.7 (18.0)	50.2 (25.3)	59.2 (26.7)	68.2 (31.0)	102.3 (45.7)
SWTF1	0.10 (0.03)	0.11 (0.03)	0.13 (0.03)	0.15 (0.03)	0.17 (0.04)	0.18 (0.04)	0.24 (0.05)
SWTF2	0.09 (0.02)	0.10 (0.03)	0.11 (0.03)	0.14 (0.03)	0.15 (0.03)	0.17 (0.04)	0.22 (0.04)
SWTF3	0.14 (0.04)	0.16 (0.06)	0.20 (0.08)	0.28 (0.12)	0.32 (0.13)	0.35 (0.18)	0.55 (0.23)

section. Further developments presented in this chapter are evaluated in Chapter 6 (*Results*) and discussed in Chapter 7 (*Discussion*).

Preliminary results and discussion

Table 4.1 shows median results for GOF and computational time using a Dell Optiplex 760 desktop computer with Intel® Core™2 Duo E8400 3.00 GHz processor with 16 GB of RAM. Meanwhile, Figure 4.3 provides a graphical glimpse on the results.

Table 4.1a and Fig. 4.3 show that both SWTF and RSF methodologies were able to provide better fits for the average MECG beat than the fixed model in the NMSE sense. Moreover, the generally poor and highly varying performance obtained by UF highlights how sensible the nonlinear least-squares optimization procedure is to its initialization, which advocate for the use of non-parametric techniques as SWTF and RSF. Results for SWTF3 demonstrate that if the many initial parameters are well adjusted, the optimization routine is able to produce even better results than iteratively positioning each kernels (as in SWTF1 and SWTF2) [17]. Meanwhile, from investigating Table 4.1-(b) it becomes clear that SWTF approaches are computationally efficient particularly for larger number of kernels.

When compared with RSF, SWTF3 is 140 to 180 times faster with very little distinction in the GOF (see Table 4.1). Based on the superior results, from this point onwards $N_k = 7$ kernels are used and fitted during EKF's initialization by means of the SWTF3 approach.

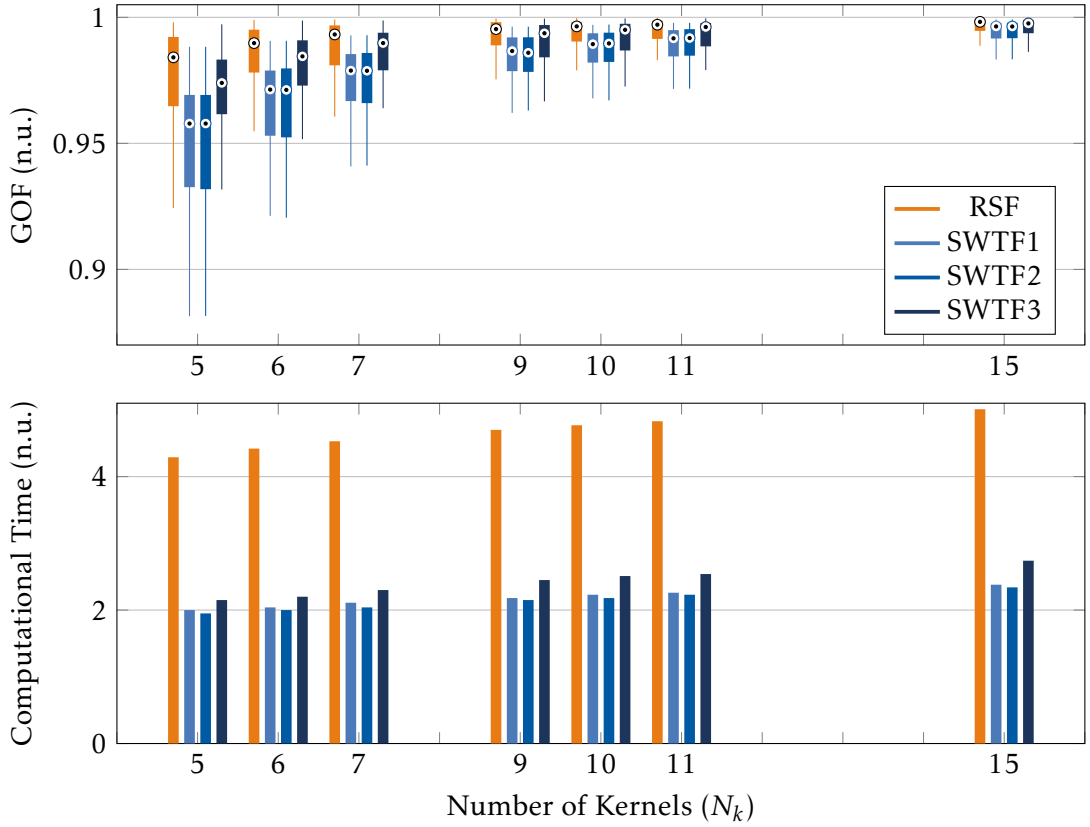

Figure 4.3: Comparison of best performing fitting methods. Fixed and uniform fittings are omitted for visibility purposes, since their results are occasionally much lower than that of RSF and SWT approaches (see Table 4.1. Missing variants are due to the lack of models described in the literature. Goodness of fit is shown (on the top) and the semi-log bar graph of median computational time (at the bottom), with input computational time in milliseconds.

4.2.2 Time-varying covariance matrices

When comparing the $EKF24$ model with the simpler $EKF2$, by modelling the angular velocity ω_k and Gaussian parameters as time-varying AR models the system becomes considerably more dynamic. That means, it can theoretically better track the non-stationary characteristics of the MECG such as HRV changes (with ω_k) and morphological features (with Gaussian parameters) such as T-wave amplitude changes over time. Figure 4.4 illustrates this adaptability. Since this evolving characteristics for the model are implemented, there is no explicit need for updating the model noise covariance $\mathbf{Q}_k$. On the other hand, these modifications do not provide information on the current level of confidence that one has on the measurements (i.e. covariance matrix $\mathbf{R}_k$). Based on the works of [370, 420] (mentioned in the Section 3.3.4), the idea of a time-variant $\mathbf{R}_k$ is further evaluated throughout this section.

Independent from the EKF variant used, the premise is that the uncorrelated WGN processes are well-represented by their respective noise covariance matrices. In real applications, however, these conditions vary with time. For instance, the measurement noise SNR of each abdominal lead is expected to change through time, as the fetus moves, muscular and ambient artefacts

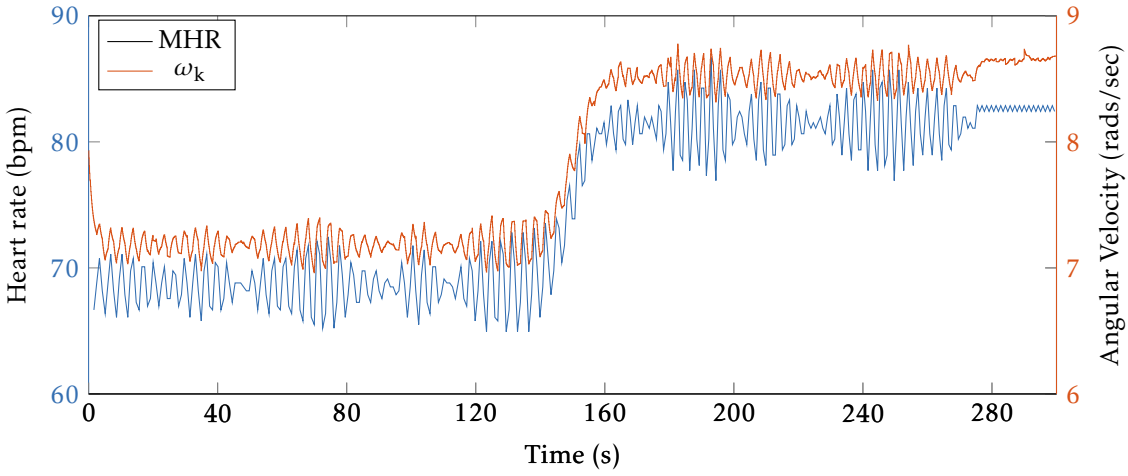

(a) Evolution of state ω_k

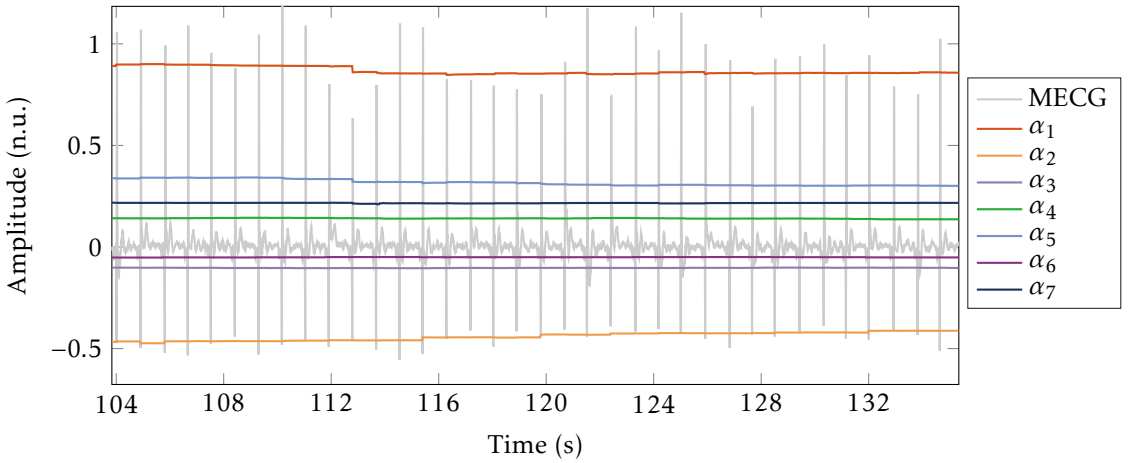

(b) Evolution of $\alpha_{i,k}$ states

Figure 4.4: Evolution for ω_k (a) and $\alpha_{i,k}$ (b) states using the *EKF*24. In this example a Case 2 (see Table 5.1) is portrayed, where there is a clear change in maternal HR. As it can be seen, ω_k is capable of reliably follow those changes. Some slow evolution of $\alpha_{i,k}$ is also visible.

occur (see Fig. 3.2). For this reason, the filter could benefit from an adaptive measurement noise covariance $\mathbf{R}_k$. The observed phase θ_k noise (i.e. $v_k(1)$) depends on the robustness of the MQRS and quantization errors (i.e. jitter) due to the signal sampling frequency. The initial variance $R_0(1,1) = (\omega\delta)^2$ (see Eq. 3.29) is a conservative error estimate for the quantization. However, since accurate MQRS detections are assumed to be a pre-condition (see Section 4.1), the adaption of the first observed state covariance is not performed. The noise in amplitude information z_k (i.e. $v_k(2)$), on the other hand, is initialized with the average signal variance $\overline{\sigma}^2_{fit}$. As the recording progresses, artefacts should have a direct impact on the reliability of such estimate. For this purpose, as described in [166, 370], it is convenient to monitor the innovation covariance matrix ($\mathbf{S}_k$ - see Eq. 3.8 and 3.9) throughout the EKF filtering procedure [180]. Monitoring these variables provides means of rejecting anomalous measurement data and monitoring the fidelity of the filter and updating the values for the measurement noise covariance matrix. In this work, differently from the constant correction factor proposed by

Sameni *et al.* [370], a correction is applied only in cases when the innovation covariance exceeds a given confidence interval as further shown.

As explained in Section 3.3.2, on the linear case the innovation is a random, zero-mean and Gaussian distributed variable, which should be independent and white as long as the KF properly works [277] (for EKF this is only marginally true). If that is the case, $\mathbf{S}_k$ (from Eq. 3.9 should match the true innovation covariance matrix, i.e. $\sigma^2_{S,k} = \mathrm{E}[\nu_k(2)\cdot\nu_k(2)^T]$. If this is not true, considering Eq. 3.9 it can be concluded that either $\mathbf{P}_{k|k-1}$, $\mathbf{H}$ or $\mathbf{R}_k$ does not represent the system anymore. Since several improvements to the EKF model took place as demonstrated on the previous chapter, it can be assumed that $\mathbf{R}_k$ (i.e. $\mathbf{R}_0$ for the invariant case) is the cause for such mismatch. An online adaptation for r_k (i.e. noise relative to z_k, following the notation from Section 3.3.4) is attained from Eq. 3.9 as [180, 277]:

$$r_k = \sigma^2_{S,k} - \underline{h}\cdot p_{k|k-1}\cdot\underline{h}^T, \tag{4.4}$$

where $\underline{h}$ represents the second row of the observational matrix H and $p_{k|k-1}$ is the second element on the main diagonal of $P_{k|k-1}$. Assuming that the innovation $\nu_k \sim \mathcal{N}(0, \mathbf{S}_k)$, one can empirically estimate the true innovation variance as the sample variance S^2 [180, 277, 307]:

$$\hat{S}^2 = \frac{1}{L-1}\sum_{i=k}^{k-L}(\nu_i(2) - E[\nu_i(2)])^2 = \frac{1}{L-1}\sum_{i=k-L}^{k-1}\nu_i^2(2), \tag{4.5}$$

where the L is the number of samples that should be averaged. $\hat{S}^2$ is a random variable, whose sampling distribution follows a Chi-square distribution ($^{S^2(L-1)}/_{\mathbf{S_k}(2,2)} \sim \chi^2_{L-1}$). Therefore, while updating r_k (in Eq. 4.4), it is important to make sure that the empirical value $\hat{S}^2$ has values outside a given *confidence interval (CI)*, i.e. it is very probable that $\mathrm{E}\left[S^2\right] \neq \underline{h}\cdot p_{k|k-1}\cdot\underline{h}^T$. In this work a 99% CI is used, in case the empirical variance exceeds these limits r_k shall be updated. The CI for the χ^2 distribution with L degrees of freedom, is given by [180]:

$$CI = \left[\frac{L\cdot S^2}{\chi^2_{1-\frac{\alpha}{2},L}},\ \frac{L\cdot S^2}{\chi^2_{\frac{\alpha}{2},L}}\right]. \tag{4.6}$$

The specified χ^2 quantiles are obtained based on [180] as:

$$\chi^2_{1-\frac{\alpha}{2};L} = 0.5(\sqrt{2L-1} + 2.58)^2, \tag{4.7}$$

$$\chi^2_{\frac{\alpha}{2};L} = 0.5(\sqrt{2L-1} - 2.58)^2. \tag{4.8}$$

An implementation detail is the definition for the value L. This window length should make sure that it represents actual SNR changes and not physiological changes on the MECG signal amplitude, e.g. due to shift of the cardiac vector during respiration. For this reason, in this work L was empirically set to comprise 10 MECG cycles [180], i.e. $L = 10\cdot(^{2\pi\cdot f_s}/_{\omega_k})$. Moreover, the changes in the r_k process are expected to be slower than the EKF filter. For avoiding unnecessary computational effort, r_k is updated with a frequency that equals 10% the signal's sampling frequency, similarly to the extended state update in $EKF24$ variant previously mentioned. In

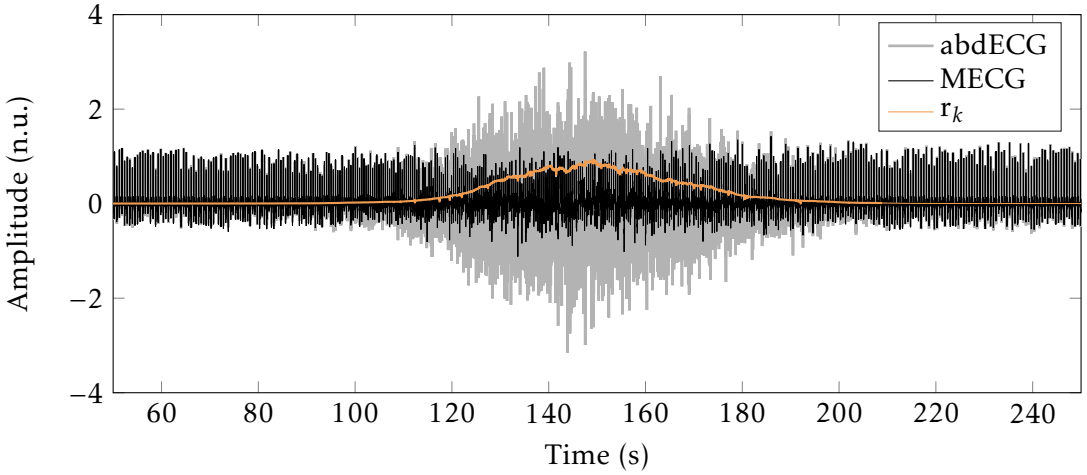

Figure 4.5: Example of covariance matrix adaptation using EKF2. In this example a Case 3 is portrayed (i.e. muscular artefact - see Table 5.1), where a large change in SNR due to a simulated uterine contraction is presented. As it can be seen, r_k is able to reproduce those changes in signal quality.

Fig. 4.5, this adaptive concept put to test using a dataset simulating a large muscular artefact due to uterine contraction. As it can be seen from this figure, the noise covariance matrix is able to reflect those changes in signal quality. This proposed adaptive variant is henceforth named $vEKF2$ and $vEKF24$ for the $EKF2$ and $EKF24$ filters, respectively.

4.2.3 Extended Kalman filter with unknown inputs

Despite its practical success in the literature, up to date most[2] of the proposed models using the EKF framework attempt to estimate the MECG while considering the FECG signal as part of the signals noise process. This assumption, however, is not always appropriate since one considers that the FECG signal is a zero-mean, white and Gaussian random process (as described in Section 3.3.2) [156]. In practice, due to the FECG signal's actual nature (and of course, depending on the filters initialization) implementations of the EKF tend to estimate part of FQRS peaks as MECG estimation, leading to attenuated fetal peaks on the estimation residuals. This is particularly visible when MQRS and FQRS complexes are overlapped in time, as described by [304]. The fact that this exogenous input (i.e. the FECG) is present transforms the NIFECG estimation problem into an state estimation and identification problem. An attractive theoretical solution to such problems containing highly non-Gaussian signals as input is the inclusion of an "unknown input" vector $\underline{d}_k$ on the filter equations. In such systems, it is assumed that no prior information on $\underline{d}_k$ is available regarding its dynamics or statistics [425]. In this section this novel formulation, applied to our EKF models, is further explored.

Some of the pioneer works in treating linear systems with exogenous unknown inputs are

[2] Two exceptions are Dual EKF models proposed by [53, 304], which take into consideration both FECG and MECG for its model. This is performed by including additional states for the fetal phase θ_k^f and amplitude z_k^f to the state-space model (see Eq. 3.26). However, these approaches require the FQRS locations as well as information on the dynamics of the signal (on those works, also approximated using a sum of Gaussian kernels).

[103, 186, 191, 223, 229]. These methods usually modify the filter's equations (described in Eqs. 3.15 and 3.16) and are separated into methods with or without direct feedthrough. Systems with direct feedthrough [102, 131, 160, 186, 425, 471] model the exogenous unknown input in both process and measurement equations of the filter. On the other hand, systems without feedthrough describe this unknown input either in the process (e.g. [103, 158, 191, 229, 319, 425]) or in the measurement equation (e.g. [319, 425]). The decision of which of these approaches to take depends on the way the system is modelled, but does not imply limitations to the filter.

The inclusion of an unknown input in the EKF system generates concerns about the system's unbiasedness, minimal variance, rank deficiency (i.e. in case the direct feedthrough matrix from the unknown input to system measurement is not full rank), and stability. Several approaches have been proposed in the literature to cope with these model inadequacies. For instance, Darouach *et al.* [103], Kitanidis [229] have proposed MVUE filters without feedthrough, which served as base for further optimal implementations with direct feedthrough by [102, 186]. However, these methods did not enable the estimation of the unknown input itself. For this purpose, Gillijns and De Moor [158], Hsieh [191] developed simultaneous input and state filters that were also MVUE for systems without direct feedthrough. While some approaches e.g. [131] require the feedthrough matrix to have full rank, others [192] focus on treating rank deficiency at cost of a biased input estimate [471]. Yong *et al.* [471] have recently proposed a filter that simultaneously estimates the state and unknown input, producing MVUE estimates with no restriction to the direct feedthrough matrix.

Most approaches available in the literature assume linear KF models, which are optimal and hold assumptions on the signals, e.g. the whiteness of the innovation. Indeed the presence of unknown inputs could severely restrict the performance of nonlinear filters, since a high bias may be introduced in the state estimation due to the uncertainties from the unknown inputs [156]. Moreover, this approach for nonlinear systems is more challenging, since the unknown inputs make it unnecessary to linearize the system equations where both state and input may be coupled [130]. Amongst the few studies in the literature that have applied these concepts making use of nonlinear models and the EKF are e.g. [130, 156, 321, 470]. The *Unknown Input Extended Kalman Filter (UIEKF)* model obtained from Eqs 3.15 and 3.16 is described setting the known-input $\underline{u}_k = \underline{0}$, $\forall k$, assuming additive noise as well as unknown input models, and linear observation equations (specific for the model presented in Section 3.3.4) as:

$$\begin{aligned}\underline{x}_k &= f_{k-1}(\underline{x}_{k-1}, \underline{d}_{k-1}, \underline{w}_{k-1}) \\ &= f_{k-1}(\underline{x}_{k-1}) + \mathbf{D}_{k-1}\underline{d}_{k-1} + \underline{w}_{k-1} \qquad (4.9)\\ \underline{y}_k &= h_k(\underline{x}_k, \underline{d}_k, \underline{v}_k) \\ &= \mathbf{H}_k\underline{x}_k + \mathbf{E}_k\underline{d}_k + \underline{v}_k \qquad (4.10)\end{aligned}$$

where $\underline{d}_k \in \mathbb{R}^{s\times 1}$ is the unknown input with covariance $S_{d,k} \in \mathbb{R}^{s\times s} = E\left[\left(\underline{d}_k - \hat{\underline{d}}_k\right)\left(\underline{d}_k - \hat{\underline{d}}_k\right)^T\right]$, $\mathbf{D}_{k-1} \in \mathbb{R}^{n\times s}$ and $\mathbf{E}_k \in \mathbb{R}^{m\times s}$ are known matrices. In this particular work, the following assump-

tion $\mathbf{E}_k = \underline{0} \forall k$ is made. As mentioned, this assumption is not limiting and merely a design choice. The derivation however is only valid if the number of measurements m is larger than the number of unknown inputs s [156]. An implementational detail is the fact that the unknown input estimation is delayed by one time-step, since the novel information contained in the observation is available at the end of the Kalman filter recursion. The assumption of linear additive unknown input and noises simplify the linearization procedure, which can be simply derived from applying Eqs. 3.17-3.18 into Eqs. 4.9-4.10. The $EKF2$ model presented in Section 3.3.4 is therefore expanded as follows, with $D_k = [0, 1]^T \forall k$:

$$\begin{cases} \theta_k &= (\theta_{k-1} + \omega\delta) \bmod 2\pi \\ z_k &= z_{k-1} - \sum_{i=1}^{N_k} \delta \frac{\alpha_i \omega}{b_i^2} \Delta\theta_{i,k-1} exp\left(-\frac{\Delta\theta_{i,k-1}^2}{2b_i^2}\right) + \underbrace{d_{k-1}}_{\text{unknown input}} + \eta_{k-1}, \end{cases} \tag{4.11}$$

As explained in [156, 425], the joint estimation of both state $\underline{\hat{x}}_k$ and unknown input $\underline{\hat{d}}_k$ for a nonlinear stochastic system can be regarded as a constrained optimization problem, where the state unbiasedness is the constraint, but the joint global optimization of state and unknown input cannot be guaranteed. The estimates for $\underline{\hat{x}}_{k|k-1}$ and $\underline{\hat{d}}_{k|k-1}$ can be determined by minimizing the objective function $J_k(\mathbf{K}_k)$ representing the sum of square errors between true and predicted values for the state variable $\underline{x}$ [156, 321, 425]:

$$J_k(\mathbf{K}_k) = \sum_{i=1}^{k} \Delta_i^T \mathbf{R}_{i,i}^{-1} \Delta_i = \underline{\Delta}_i^T \mathbf{R}_{i,i}^{-1} \underline{\Delta}_i \tag{4.12}$$

with $\Delta_i = y_i - h(y_i, d_i, v_i)$ and $\mathbf{R}_{i,i}$ is the i^{th} diagonal element of the measurement noise covariance matrix. This objective function is subjected to the unbiasedness constraint $(I - \mathbf{K}_k \mathbf{D}_k) = \underline{0}$ (see [425]). The derivation of this filter can be found in [156, 321, 425] and is omitted in this work. Instead, the recursive UIEKF filter equations are summarized in Algorithm 3. To test this novel methodology, the UIEKF was evaluated regarding the $EKF2$ model. Its expansion to the $EKF24$ model is possible, yet it requires a more complex calculation due to the non-observable states that lead to rank-deficiency for the matrix $\mathbf{E}_k$, thus, it remains for further studies.

4.2.4 Filter calibration

As presented in Section 3.3.4, several parameters were empirically defined in order to model the covariance matrices $\mathbf{P}_0$, $\mathbf{R}_0$ and $\mathbf{Q}_0$. In order to fine-tune these parameters, a multiplying factor was added to each diagonal element of those covariances. This number of parameters make the EKF initialization a highly dimensional optimization problem, which is known to severely affect the filter's performance. While the linear KF may rely on properties such as the whiteness of the innovation, most these concepts do not necessarily apply for the nonlinear variant used in this work. For this reason, the filter calibration is an exhaustive and empirical process. Each proposed EKF approach (i.e. $EKF2$, $EKF24$ and etc) was calibrated individually. For this purpose, a subset of 15 randomly chosen simulated recordings from the *Fetal ECG*

Algorithm 3 Pseudo-code summarizing the Unknown Input Extended Kalman Filter algorithm (time and measurement-update form)

Require: models for $\mathbf{A}_k$,$\mathbf{H}_k$, $\mathbf{Q}_k$, $\mathbf{R}_k$
Initialize: $\mathbf{x}_0$, $\mathbf{P}_0$
for $k = 1$ *to* $N_{samples}$ **do**
// Prediction step
$\widetilde{\mathbf{F}}_{k-1} \approx \frac{\partial f_{k-1}}{\partial \underline{x}_{k-1}}\Big|_{\substack{\underline{x}_{k-1}=\underline{\hat{x}}_{k-1|k-1} \\ \underline{w}_{k-1}=\underline{0}}}$ and $\widetilde{\mathbf{W}}_{k-1} \approx \frac{\partial f_{k-1}}{\partial \underline{w}}\Big|_{\substack{\underline{x}_{k-1}=\underline{\hat{x}}_{k-1|k-1} \\ \underline{w}_{k-1}=\underline{0}}}$; // linearization
$\underline{\hat{x}}_{k|k-1} = \widetilde{\mathbf{F}}_{k-1}\underline{x}_{k-1|k-1} + \mathbf{D}_{k-1}\underline{d}_{k-1|k-2}$; // *a priori* state estimate
$\mathbf{P}_{k|k-1} = \widetilde{\mathbf{F}}_{k-1}\mathbf{P}_{k-1|k-1}\widetilde{\mathbf{F}}_{k-1}^T + \widetilde{\mathbf{W}}_{k-1}\mathbf{Q}_{k-1}\widetilde{\mathbf{W}}_k^T$; // *a priori* covariance estimate
// Update step
$\underline{\nu}_k = \underline{y}_k - \underline{h}_k(\underline{\hat{x}}_{k|k-1}, 0)$; // innovation signal
$\mathbf{S}_k = \mathbf{H}_k\mathbf{P}_{k|k-1}\mathbf{H}_k^T + \mathbf{R}_k$; // innovation covariance
$\mathbf{S}_{d,k} = \left[\mathbf{D}_k\mathbf{H}_k\mathbf{R}_k^{-1}\left(\mathbf{I} - \mathbf{H}_k^T\mathbf{K}_k\right)\mathbf{H}_k\mathbf{D}_k\right]^{-1}$; // unknown input covariance
$\mathbf{K}_k = \mathbf{P}_{k|k-1}\mathbf{H}_k^T\mathbf{S}_k^{-1}$; // obtain Kalman gain
$\underline{\hat{x}}_{k|k} = \underline{\hat{x}}_{k|k-1} + \mathbf{K}_k\underline{\nu}_k$; // a posteriori state estimate
$\underline{\hat{d}}_{k-1|k} = \mathbf{S}_{d,k}\mathbf{D}_k^T\mathbf{H}_k^T\mathbf{R}_k^{-1}\left[\left(\mathbf{I} - \mathbf{H}_k^T\mathbf{K}_k\right)\left(\underline{\nu}_k + \mathbf{H}_k^T\mathbf{D}_{k-1}\underline{d}_{k-2|k-1}\right)\right]$; // unknown input estimate
$\mathbf{P}_{k|k} = (I - \mathbf{K}_k\mathbf{H}_k)\left[\mathbf{P}_{k|k-1} + \mathbf{D}_{k-1}\mathbf{S}_k\mathbf{D}_{k-1}^T\left(I - \mathbf{K}_k\mathbf{H}_k\right)^T\right]$
end

Synthetic Database (FECGSYNDB) was used. A random search[3] was carried out in attempting to minimize a multiobjective cost function comprising the following three subfunctions:

This fitting problem is similar to the problem presented in Section 4.2.1, for this reason the GOF was also used.

MECG residuals: effectively, the EKF attempts to estimate the maternal ECG signal. In order to assess the quality of EKF's MECG estimation, the NMSE between estimated and true maternal signal (available for simulated data) was evaluated. The NMSE was calculated only within a ±50 ms window around each MQRS complex, excluding segments were FQRS and MQRS overlaps occurred.

FECG estimation: analogously to the previous metric, while estimating the MECG, the FECG should not be confounded with the MECG, i.e. the filter should not completely trust the observed signal. For this purpose, the NMSE difference between the estimation residual (or unknown input in the *uiEKF2* case) and the true fetal signal (available in simulated data) was evaluated around a ±25 ms of each FQRS complex.

FQRS detection accuracy: this last metric is what one in fact aims to improve, namely the accuracy of the FQRS detections. This was done by using a simple maxima search FQRS detector [363] and the F_1 metric (see Section 3.4.2) over each extracted signal.

The global cost function consisted of a weighted average of these aforementioned subfunctions by using weights from 1 to 3 to MECG residuals, FECG estimation and FQRS detection accuracy,

[3] The EKF extraction is a computationally expensive operation. Random search algorithms enable the search for hyper-parameters in an efficient manner, compared to grid search algorithms. [60]

respectively. These weights were arbitrarily chosen to reflect the importance of each subfunction on the extraction result. The set of parameters which at last delivered more often the best results was used.

4.3 Accurate Fetal QRS and Heart Rate Detection

The increasing interest in NIFECG analysis culminated on PCINCC 2013 [92], which dealt with the accuracy of FQRS detections and FHR estimates. Indeed, reliable FQRS/FHR estimates are crucial for the further clinical analysis of NIFECG (e.g. FHR variability or morphological analysis signal). During the PCINC 2013, various approaches for improving fetal heart rate detection were presented e.g. [20, 54, 447]. While most available FQRS detection methods are simple re-parametrized single-channel adult QRS detectors (as described in Section 3.4), FHR estimates are often based on heuristic rules for how a smooth FHR tracing should appear. The lack of a general framework impede the understanding and hamper these method's further use. Aiming at improving the accuracy of FQRS detections obtain from those simple detection algorithms, two multichannel correction frameworks are proposed in this work. For this purpose, the following input signals are assumed to be available:

(i) at least one maternal chest lead;

(ii) reliable MQRS detection/annotation;

(iii) multiple channels of abdominal signals;

(iv) extracted FECG signals from (*iii*);

(v) initial FQRS detections for each channel.

The two correction methods have substantially distinct characteristics and aim at different applications. Nonetheless, both algorithms are based on the common idea of applying novel SQI measures in FECG analysis. In Section 4.3.1, an offline, stochastic approach is presented, which exhaustively searches for a global solution to the detection problem. The method considers multiple SQIs as cost functions, requiring a SQI value for each individual FQRS candidate. The second approach (shown in Section 4.3.2), focuses on real-time applications and is an online, deterministic and window-based method. For this method a large variety of SQI metrics are proposed and accordingly evaluated.

4.3.1 Multichannel evolutionary QRS correction

The multichannel method presented in this section was developed at the IBMT by this author [20, 21] and obtained the highest FQRS detection accuracy scores at the PCINC 2013, regarding the scoring metrics $E1/E4$ and $E2/E5$, amongst all participants. The method was developed in the scope of a side project in the student research from Himmelsbach [179]. The identification of fetal peaks on extracted signals is challenging, due to the low SNR of the FECG as well as the

presence of MECG residuals (mainly MQRS complexes), which can easily be confounded with the FQRS. In order to cope with such demanding task, this novel method makes use of basic concepts from *evolutionary algorithms (EA)*[4]. Due to its origins in evolutionary computing, the algorithm is henceforth named *evolutionary QRS correction algorithm (eQRS)*.

In EAs artificial *individuals* are used to populate the search space, through *selection*, *mutation* and *recombination* the population evolves towards optimal regions of the search space. The recombination mechanism allows the mixing of parental characteristics to be passed to their descendants and mutation introduces innovation into the population [43]. In our application, FQRS detections were treated as individuals, where on each iteration FQRS candidates were allowed to originate, change location or cease existence. That is, although the proposed approach inherits characteristics from EA that involve randomness, it does not perform a whole-circuit optimization. Particularly, recombination and mutation are not present due to the lack of suitable interpretation for such concepts in our application. Although EA's population is often arbitrarily initialized [43], for the purpose of faster convergence the start our method with initial FQRS detections provided by a simple QRS algorithm applied to each channel.

According to Bäck and Schwefel [43], the *environment* delivers the quality information (i.e. *fitness value (FV)* – denoted as $FV_{t,i}$, being fitness value for individual i at iteration time-step t) about the search points. The selection process then favors those individuals with higher fitness to reproduce more often than those of lower fitness. On our FECG application, FVs describe how well a certain FQRS suits the extracted fetal signal (environment). In order to evaluate FV values for each individual, particularly designed fetal SQIs are proposed. This global SQI metric was composed by multiple real-valued objective functions, which can be divided into two groups based on their features: the FQRS pseudo-periodicity and FECG beat morphology. These sub-functions can be thought of as different SQI metrics that exploit the morphological characteristics or regularity of the candidate fetal peaks. The first group of the fitness function, i.e. morphological features, can not be described by one single feature signal due to the presence multiple noise sources (e.g. MECG and muscular noises). In order to assess FECG morphology, two sub-functions were used, namely conformity ($cSQI$) and extravagance ($xSQI$). The latter group of SQI functions is described by a single function that involves the plausibility of the FHR trace (henceforth called $gSQI$). A summary on those newly developed SQIs follows:

cSQI measures how conform the FECG complexes are in relation to an coherent averaged FECG template. This FECG template is created based on the current FQRS location candidates. By simply taking the correlation coefficient between the averaged template and each cycle i (centered at the FQRS occurrences), a value in the interval $[0,1]$ is obtained for each individual. In other words, conformity portraits how similar each individual is to a

[4] Evolutionary algorithms are a class of approaches based on biological evolution, as Charles Darwin [104] described the "survival of the fittest". Generic algorithms and EA have various similarities and were proposed by the groups of John Holland and Hans-Paul Schwefel, respectively [462]. The reader is referred to [43, 462] for general overviews. In contrast to traditional algorithms for optimization, EAs are working with probabilistic rules thereby enabling parallel solutions. EAs have become a popular heuristic near-optimal solution for problems with large search spaces [462]. Due to the lack of boundaries in creating the global cost function, EAs can be applied in an easy and flexible way [338].

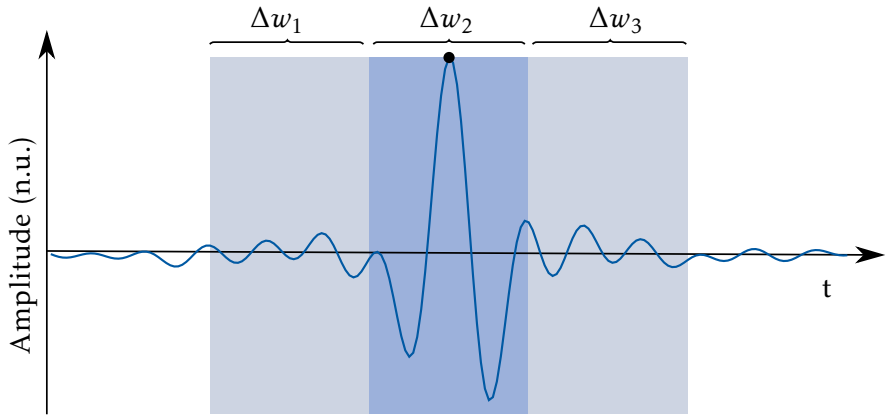

Figure 4.6: Representation of the xSQI metric, modified from [177]. The metric builds the ratio between the power of the abdominal signal in Δw_2 over the total power in $\Delta w_{1\ldots3}$ for each detection. In this work $\Delta w_1 = \Delta w_2 = \Delta w_3 = 50$ ms.

relatively clean template.

xSQI is a measure of contrast between the detected FQRS peak and the embedded noise. By using a window of ±25 ms length around location of each individual FQRS, the FECG peak amplitude is compared against the power of the signal within three times that window length. Therefore, **xSQI** obtains a measure between $[0, 1]$ representing how powerful is the current FQRS compared its surrounding noise. A graphical depiction of $xSQI$ is available in Figure 4.6.

gSQI is a function that places around each individual i six Gaussian kernels (three on each side) on probable locations for neighboring detections. To obtain an average distance were the nearby detections can occur, the local value of a smoothed FHR trace was obtained. The amplitude of such kernels depends on two factors: i) local value of FV (amplitude increase with rising $FV_{t,i}$) and ii) distance from actual individual, i.e. $\{1 \cdot FV_{t,i\pm1}, 0.9 \cdot FV_{t,i\pm2}, 0.8 \cdot FV_{t,i\pm3}\}$, i.e. decaying amplitude with increasing distance. Gaussians' standard deviation was defined as 20% the recording's shortest smoothed RR-interval. The sum of the individually generated curves resulted on the FHR plausibility curve presented in Figure 4.7. Additionally to providing a rough measure for certainty on FQRS positions, $gSQI$ generates a competitive behavior between neighboring individuals. Differently from morphological features, for implementation purposes $gSQI$ assumes values for each sample of the original abdominal signal, not only one for each detection.

A global fitness value ($SQI(global)$ in Figure 4.7) is then calculated for each individual by combining the different sub-functions. During the PCINC 2013, a linear combination of these function was used, where optimal weights were empirically determined.

Based on the initial detections, the eQRS iteratively improves these detections by attempting to maximize a the global fitness function. As the number of iterations increased, $gSQI$ kernels are expected to interfere constructively with one another and generate a more skewed values (see Figure 4.8). After selection of most fit individuals, the fitness values are re-evaluated at

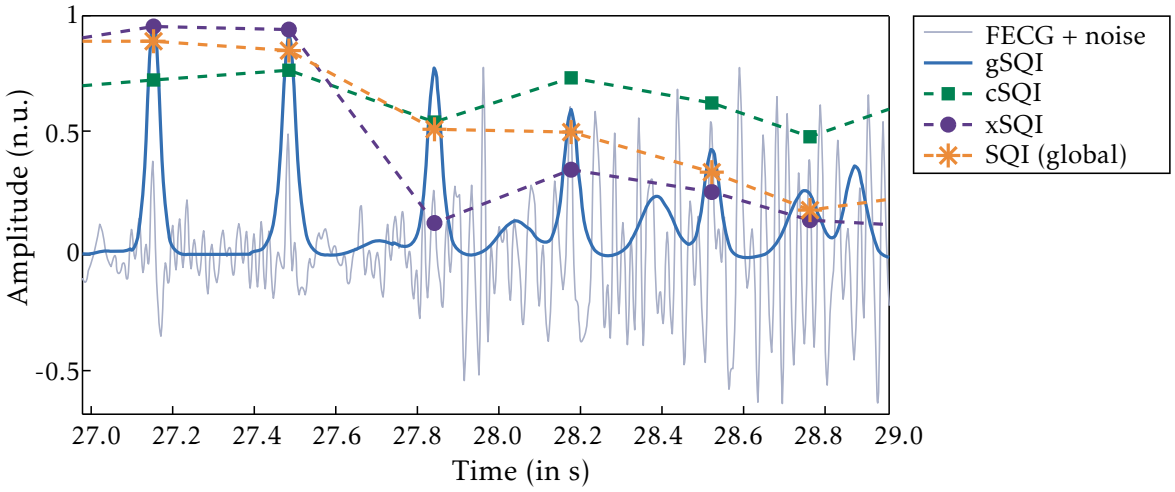

Figure 4.7: Qualitative example of different sub-functions used for defining the fitness function.

the beginning of each iteration. Following the idea of Simulated Annealing [227], the amount of changes (i.e. number of detections to originate/move/vanish) was reduced after every cycle. This procedure was firstly performed on each individual channel, until the convergence criteria is achieved, i.e. the majority of the detections settled (did not move), or the maximum number of iterations was achieved ($i = 1000$). After providing viable FQRS within each lead, the detector uses the channels which were considered to be most trustworthy (largest overall FV) to generate a set of multichannel detections. This is done by using the mean SQI values across the channels and exhaustively including and removing channels until the optimal solution is encountered. Since this procedure is stochastic, the optimization algorithm may get stuck in local optima or not converge producing random differences on its results. Nevertheless, the computationally expensive and redundant iterative re-calculation of the fitness function leads to satisfactory results. Further developments of the evolutionary detector at the IBMT [177, 472] have focused on applying it to other biosignals (e.g. capacitive ECG recordings) and including ectopic beats detection. The latter can be done by modifying the morphological SQI functions (using multiple templates on $cSQI$ for instance) and weighting down the confidence in the signal's pseudo-periodicity i.e. $gSQI$.

4.3.2 Multichannel fetal heart rate estimation using Kalman filters

Despite the promising results obtained using the eQRS method presented in the previous section, the method is restricted to offline applications and its computational cost is high. In this section, the focus is to obtain an online method for improving window-based FHR estimates (see Section 3.5), which similarly to the previous method is based on SQI metrics (e.g. the $cSQI$ and $xSQI$). Based on the approach by Li *et al.* [251], the use of Kalman filters for improving the FHR estimates using the information from multiple channels is proposed. The novelty of this work is the design of a number of SQI specific for NIFECG application as well as adaptation of existing ECG metrics for its use with fetal signals. Additionally, a careful characterization and construction of a combined SQI metric is presented.

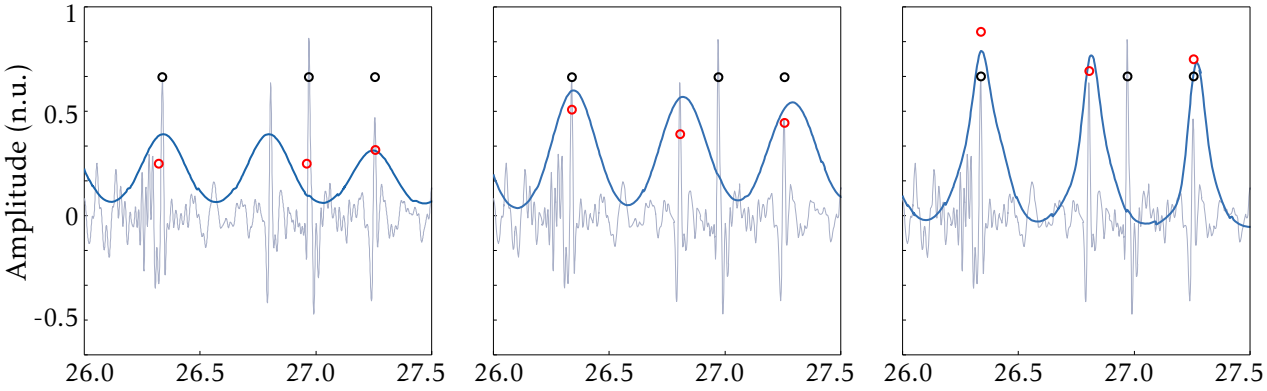

(a) $t = 119$ **(b)** $i = 126$ **(c)** $i = 742$

Figure 4.8: Evolutionary algorithm at different iteration numbers (i) using record "a01" from PCINC 2013. The continuous line depicts $gSQI$ curve (from Figure 4.7). The FV are represented by the height of the actual detection at each iteration with (○). Initial detections (i.e. $i = 1$) are depicted by (○) [20].

Fetal signal quality indices

As discussed in Section 3.2, several noise sources (e.g. muscular/uterine noise, electrode motion and etc. – see Fig. 3.2) are present in the abdECG. The presence/absence of such signals affects the SNR of the fetal signal. These interfering sources, which typically show a strongly non-stationary behavior, make the detection of the FQRS complexes a challenging signal-processing task where erroneous detections are unavoidable. This situation raises two issues: 1) how can segments with high rate of miss detections be identified? 2) how can the occurrence of erroneous detections in cases of low fetal SNR be avoided?

The first point is closely related to the usage of SQIs, as addressed by many works on adult ECG monitoring (e.g. [55, 89]). With such SQI, an increase in specificity of built-in signal processing techniques is aimed [315]. The importance of this topic is confirmed by the recent Physionet challenges that dealt with the determination of ECG's clinical acceptability (i.e. PCINC 2011 [397]) and robust peak detection in multimodal data (i.e. PCINC 2014 [396]). Both these competitions have in common that top-scoring entries ([89, 211]) made use of SQIs to improve the specificity of their results. SQI metrics, in their current form, were firstly proposed by Li *et al.* [251], who suggested various SQIs for both ECG and BP signals. Since then, SQI metrics have been successfully applied in adult ECG [55, 89, 101, 211, 336], BP [211, 252, 336], *photoplethysmogram (PPG)* signals [22, 250, 312]. A review on such methods is provided in [149]. Despite the abundance of works in adult ECG analysis, the concept of SQIs has not been properly conveyed to the context of NIFECG. This application of SQIs is particularly interesting since the NIFECG suffers from low/varying SNR, moreover, it contains an additional pseudo-periodic signal, i.e. the MECG, whose residuals can mimic high quality signals. Concerning the second question, given that suitable NIFECG SQIs are available, it should be possible to transfer approaches from adult ECG to the NIFECG. Particularly, those that incorporate the information about the signal quality into the heart rate detection [19].

In this work, as specified in Section 4.3, it is assumed that both raw and extracted abdominal signals are available as well as MQRS reference locations and at least one MECG chest lead. These input signals should not impose any restriction to the method since they should be readily available after the FECG extraction is performed. As discussed in Section 4.3.1, the eQRS attributed SQI values to each FQRS complex ($cSQI$ and $xSQI$) or continuously throughout the abdominal signal ($gSQI$). Differently from the eQRS approach, Li *et al.* [251] made use of a window-based approach for calculating HR estimates segment-wise. In this work, the SQI metrics were evaluated on 5-second windows with 1 s overlap (as described in Section 3.5).Although some SQI algorithms may benefit from longer segments, e.g. for building FECG templates or estimating spectral content, the 5 s interval was deemed as appropriate for the trade-off between window length and online capability of the FHR correction algorithm. Moreover, this interval is consistent with the one used in the signal quality annotations (see Section 5.2.3) here used as gold-standard for assessing the performance of the developed SQI metrics.

Table 4.2 summarizes the SQI metrics used in this work. Amongst those metrics are adaptations of the SQI algorithms for adult ECG (derived from the literature) and two of the three indices[5] proposed in the previous section (i.e. $cSQI$ and $xSQI$). Additionally, the use of four novel indices that are particularly applicable to our signal of interest (FECG) is suggested, namely $mxSQI$, $mpSQI$, $mcSQI$ and $miSQI$. These indices attempt to make use of all available information in estimating how well the MECG suppression performed. The available SQI methods were divided into four classes of algorithms: time, frequency, detection-based, and FECG-specific approaches. *Time-based methods* refer to calculus of simple statistics of the extracted FECG signal (e.g. kurtosis - $kSQI$ and skewness - $sSQI$). *Frequency metrics* attempt to identify the spectral power of QRS complexes ($pSQI$) or baseline noise[6] ($basSQI$) normalized at a wider spectral band. *Detection-based methods* may be subdivided into two types, namely those that evaluate the regularity of FQRS detections and those that based on the fetal peak locations aim at assessing the morphology of the FECG signal. In the first sub-category are methods that apply compare multiple detectors applied to a single channel ($bSQI$), same detector used on multiple channels ($iSQI$) and the $rSQI$, which counts the number of FHR changes that exceed a pre-defined physiological threshold (set to 30 bpm as in [54]). For both $bSQI$ and $iSQI$ a 50 ms acceptance interval (±25 ms) was used, as specified in Section 3.4.2. On the latter sub-category of detection-based approaches are the FECG morphology metrics presented in the previous section (i.e. $xSQI$ and $cSQI$). As previously mentioned, *FECG-specific approaches* are specifically designed to regard the presence (and potential confusion) of the MECG component in extraction residuals. These latter metrics are throughly explained as follows:

mxSQI is the analogous of $xSQI$ with focus on the maternal extravagance on residuals of extraction procedure. This metric uses the extracted abdominal signal and MQRS reference locations to estimate the strength of MECG residuals on the estimated FECG signal. To

[5] $gSQI$ was excluded from this analysis, since it delivers continuous values for probable FQRS locations, rather than a quality metric itself. In a window-based SQI metric such values are hardly applicable.

[6] Please notice that pre-filtered abdominal signals using the narrow band for FQRS detection (explained in Section 4.1) are expected to have less power at lower frequencies due to the elevated high-pass cutoff frequency.

account for the broader maternal complexes, an interval of 100 ms around the MQRS was used. The metric is obtained as:

$$mxSQI = 1 - xSQI\big|_{MQRS,FECG}. \tag{4.13}$$

mpSQI makes use the magnitude-squared of the FECG's Fourier transform and the median reference MHR for each segment. Similarly to the approach by de Haan and Jeanne [108], the aim is evaluate the relative power of MHR and its harmonics on the frequency-domain, which should be an index for left-over maternal residuals. In order to do so, the MQRS fundamental frequency and its N_h first harmonics (within an empirically defined ±0.3 Hz band) were compared with the power of the [0.5, 10] Hz band (based on the expected frequency range for MHR), so that:

$$mpSQI = 1 - \frac{\sum_{f_i=f_0}^{N_h \cdot f_0} \left(\int_{f_i-0.3\text{ Hz}}^{f_i+0.3\text{ Hz}} |X(f)|^2 df \right)}{\int_{0.5\text{ Hz}}^{10\text{ Hz}} |X(f)|^2 df} \quad . \tag{4.14}$$

where $X(f)$ represents the *fast Fourier transform (FFT)* spectrum of the FECG signal, f_0 represents the fundamental frequency of the MHR. A graphical representation of the involved signals is presented in Figure 4.9 and $mpSQI$ is illustrated in Figure 4.9 (c). From this figure it is clear that the metric depends on the MHR, i.e. a higher maternal fundamental frequency leads to a lower number of harmonics (N_h) in the interval [0.5, 10] Hz. Thus, two approaches were evaluated in order to deal with this problem. The first (**mpSQI$_\mathbf{a}$**) fixated $N_h = 5$ and only regarded the frequencies up until the fifth harmonic of the MHR for calculating the SQI as in Eq. 4.14 (i.e. using $5 \cdot N_h + 0.3$ Hz instead of 10 Hz as integration limit). The second approach (**mpSQI$_\mathbf{b}$**) makes use of the whole spectral band between [0.5, 10] Hz and sets N_h to the total number of harmonics that occur on this interval. To deal with the aforementioned MHR dependency, it corrects the fraction presented in Eq. 4.14 using an empirically defined function with a $factor = log(8/N_h) + 1$, where 8 is the expected number of harmonics (i.e. $MHR \approx 75$ bpm). This function, therefore, increases the weight of segments with higher MHR and weights down segments with lower MHR. The $mpSQI_2$ function is then truncated to deliver values between [0,1].

mcSQI spectral coherence (or magnitude-squared coherence) is a measure of cross-correlation between frequency spectra with values between [0, 1], described as:

$$C_{xy}(f) = \frac{|S_{xy}(f)|^2}{S_{xx}(f) \cdot S_{yy}(f)} \tag{4.15}$$

being $S_{xy}(f)$ the cross-spectral density between $x(t)$ and $y(t)$. In this work, focus is put on applying the coherence to measure the extraction performance by using the involved signals (i.e. raw data, extracted abdECG and MECG chest lead). For this purpose, the function *mschohere*() from MATLAB® was used, with default parameters aside from a pre-defined FFT length of $N_f = 1024$ samples, which leads to values of $C_{xy}(f)$ being calculated for $(N_f/2) + 1$ values of $f = 0, \frac{f_s}{N_f}, \frac{2 \cdot f_s}{N_f}, \cdots, \frac{f_s}{2}$ Hz. In Figure 4.9 (d) an example of

successful and unsuccessful extraction are presented. Following this idea, two metrics were developed, namely **mcSQI$_a$** and **mcSQI$_b$**. The first measures the similarity between the MECG chest (i.e. $x(t)$) lead and extracted FECG ($y(t)$) on the [0,100] Hz band as:

$$mcSQI_a = 1 - \frac{1}{N_{f'}} \cdot \sum_{f'} C_{xy}(f) df \quad , \tag{4.16}$$

with $f' \Leftarrow f \leq 100$ Hz and $N_{f'}$ being the number of frequencies in f that match the desired band. The second metric, focuses on evaluating if the extraction method has included artifacts on higher frequent spectrum of the extracted signal. This could occur, e.g. when using the EKF algorithm Gaussian kernels do not perfectly fit a MQRS complex in a couple samples, leaving behind some artifacts with high-frequency content (see Figure 4.9 (d) - on the right). This was done by evaluating the coherence between the preprocessed abdECG ($x(t)$) and extracted FECG ($y(t)$) on the band [60,100] Hz as follows:

$$mcSQI_b = \frac{1}{N_{f'}} \cdot \sum_{f'} C_{xy}(f) df \quad , \text{ for } 60 \text{ Hz} \leq f' \leq 100 \text{ Hz}. \tag{4.17}$$

miSQI metric based on the $iSQI$ and on the premise that in cases where the FECG extraction performs poorly, the MQRS residuals have larger amplitudes then the FQRSs themselves. As a consequence, the sub-optimal extraction leads to MQRS peaks being detected (instead of FQRS), which could be assessed by using the $iSQI$-like algorithm to compare the detected extracted abdominal signal and MQRS reference. Therefore, the metric is calculated using a 50 ms acceptance interval as:

$$miSQI = 1 - iSQI\big|_{MQRS,FQRS}. \tag{4.18}$$

Since both detection-based SQIs and $miSQI$ metrics (see Table 4.2) make use of FQRS detectors, their outcomes are dependent on the FQRS detectors' performance. In this work, five publicly available FQRS detectors were evaluated as presented in Table 4.3. For further reference, the indices listed in this table are used to describe variants of SQI metrics to which they are pertained, e.g. $bSQI_{12}$ represents the $bSQI$ evaluated using the maxsearch algorithm [363] and $jqrs$ [54] detectors.

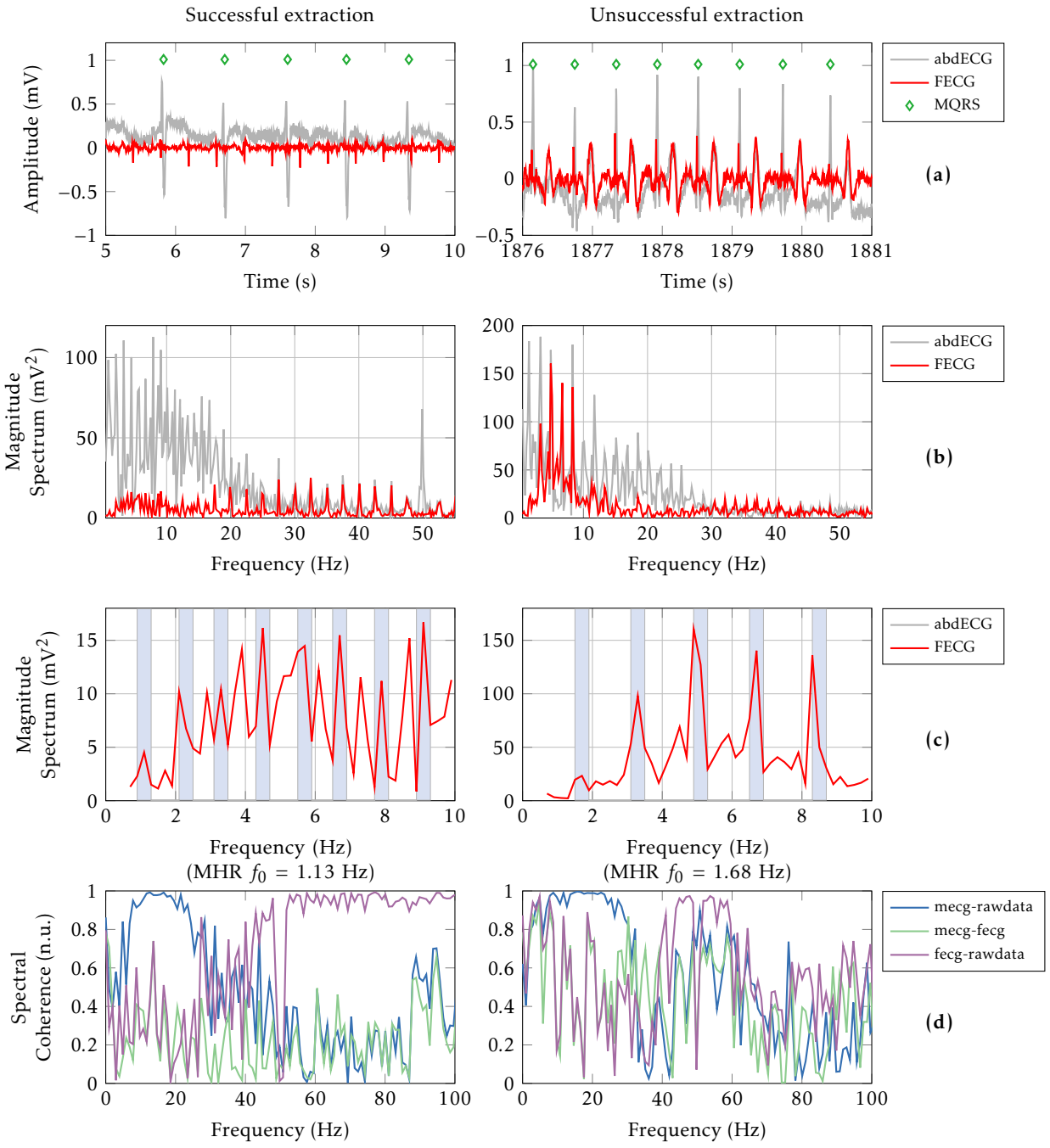

Figure 4.9: Example of newly proposed SQIs on good (left column) and bad quality (right column) extracted segments. (a) Demonstrates the signals in time domain; (b) presents the magnitude spectrum from the segments in (a) in the interval [0,55] Hz; (c) shows an excerpt from (b) that is used to calculate the $mpSQI_b$ based on the maternal fundamental frequency (MHR f_0) and its harmonics; (d) presents the spectral coherences between available signals that are used in assessing the $mcSQI$ indices.

Table 4.2: Summary of fetal SQI metrics used in this work. "Cat." refers to category and "Mult." to the method requiring multiple channels or not (including MECG chest lead). Except for the time domain metrics, all other output belong to $\mathbb{R} \in [0,1]$.

Cat.	SQI	Mult.	Description	Range	Reference
Time	$stdSQI$	✗	standard deviation of signal, i.e. $stdSQI = std(x(t)) = \sqrt{E\left[(x(t)-\bar{x}(t))^2\right]}$	$\mathbb{R}_{\geq 0}$	[89, 251] (other moment)
	$sSQI$	✗	third moment (skewness) of signal, i.e. $sSQI = \frac{E\left[(x(t)-\bar{x}(t))^3\right]}{std(x(t))^3}$	$\mathbb{R}$	[89, 251]
	$kSQI$	✗	fourth moment (kurtosis) of signal: $kSQI = \frac{E\left[(x(t)-\bar{x}(t))^4\right]}{std(x(t))^4}$	$\mathbb{R}_{\geq 0}$	[89, 251]
Frequency	$pSQI$	✗	relative power in the FQRS complex: $pSQI = 1 - \int_{5\ Hz}^{15\ Hz} \lvert X(f)\rvert^2 df / \int_{5\ Hz}^{45\ Hz} \lvert X(f)\rvert^2 df$, where $X(f) = \mathcal{F}(x(t))$ is the Fourier transform of $x(t)$. Differently from Li et al., the inverse of the power was applied to represent MQRS suppression.	$[0,1]$	[89, 251] (inversed)
	$basSQI$	✗	relative power of baseline (bandwidth modified to $[0,3]$ Hz to include most of the EHG), i.e. $basSQI = 1 \int_{0\ Hz}^{3\ Hz} \lvert X(f)\rvert^2 df / \int_{0\ Hz}^{100} \lvert X(f)\rvert^2 df$	$[0,1]$	[89, 251] (modified band)
Detection-based	$bSQI$	✗	percentage of beats commonly detected by two different QRS detectors. This metric is nothing more than an accuracy measure between those detectors (as described in Section 3.4.2). In this work F_1 metric is used.	$[0,1]$	[89, 251]
	$iSQI$	✓	percentage of beats detected on current lead that were detected on all other leads.	$[0,1]$	[89, 251]
	$rSQI$	✗	regularity of obtained FQRS intervals $rSQI = 1 - N_{out}/N_d$, where N_{out} is the number of outliers ($FHRV > 30$ bpm) and N_d the total number of detections in the segment	$[0,1]$	[54, 211]
	$cSQI$	✗	morphology conformity measure for FQRS similarity as presented in Section 4.3.1. Negative correlations were set to zero.	$[0,1]$	this work, based on [20]
	$xSQI$	✗	extravagance of FQRS peaks compared to its surroundings, explained in Section 4.3.1 (see Fig. 4.6).	$[0,1]$	this work, based on [20]
FECG-specific	$mxSQI$	✓	analogous to $1 - xSQI$ considering the amplitude of MECG complexes residuals (100 ms window around MQRS reference annotations of ±50 ms) in comparison with surrounding extracted abdominal signals.	$[0,1]$	this work
	$mpSQI$	✓	relative spectral power of the first five harmonics of the MHR ($mpSQI_a$) or all harmonics in the interval [0.5,10] Hz ($mpSQI_b$).	$[0,1]$	this work, based on [108]
	$mcSQI$	✓	spectral coherence calculated between available signals. Two variants applied: $mcSQI_a$ uses MECG and FECG (0-100 Hz) and $mcSQI_b$ abdECG and FECG (60-100 Hz) as previously explained.	$[0,1]$	this work, based on [210]
	$miSQI$	✓	similar to $iSQI$ between current FQRS detection and MQRS reference: $miSQI = 1 - iSQI_{MQRS,FQRS}$, aims at exposing falsely detected MQRS residuals.	$[0,1]$	this work, based on [152]

Table 4.3: Fetal QRS detectors evaluated in this work.

Index	Name	Description	Reference
1	maximal search	Simple algorithm that search for an absolute maximum within a pre-defined window.	[363]
2	*jqrs*	Implementation of the Pan and Tompkins [320] peak energy detector. The algorithm is based on filtering, adaptive thresholding as well as forward and backward search.	[54, 320]
3	P&T algorithm	Alternative implementation of the Pan-Tompkins algorithm.	[320, 458]
4	*gqrs*	QRS matched filter with a custom- built set of heuristics (such as search back). It has been designed by George Moody, and is freely available on Physionet	[161, 398]
5	*wqrs*	Detector based on low-pass filtering, a nonlinear curve length transformation and adaptive thresholding.	[398, 480]

Classification using a Bayesian probabilistic classifier

With the aforementioned fetal SQIs at hand, one aim to evaluate if some combination of those features can be indeed used in classifying good/bad quality FECG signals. This is performed by using the annotated clinical data presented in Section 5.2.3 and visibility index from Table 5.6. Several machine learning techniques are available to solve the classification problem at stake. For the purpose of classification, a Naive Bayes classifier was employed using prior probability and attribute probability densities given each class to model its posterior probability. During classification, the class with the maximum posterior probability is usually selected [118]. However, in this work, the posterior probabilities were used to transform the classified values into continuous valued outputs for further processing, as described in the following section [19].

In order to assess the expected classification performance of the trained Naive Bayes model, i.e. the efficiency in assigning the signal quality based on the used SQIs to appropriate class, a 10-fold cross validation was performed. Here, all 9,065 observations in the dataset (only abdominal channels) were used to generate training and test sets, respectively. The final Naive Bayes classification model was trained using all available observations as training set. To avoid the trained classifier to be bounded by the training data's class imbalance (as reported in Section 5.2.3 and Fig. 4.10), the prior class probabilities were assumed to be equal for all classes during performance assessment and when training the final classifier [19]. For completeness, results are presented using both ordinal (Krippendorf's α_K) and nominal (Cohen's κ) agreement measures, presented in Section 5.2.3.

Kalman filter approach to multichannel consensus

As described by Oster and Clifford [315], several methods have been proposed for fusing multichannel HR estimates using SQI-like metrics. Amongst those are simplistic weighted averages and computationally demanding machine learning approaches. This consensus, there are generally two types of possible combinations, namely channel selection or fusion. In channel

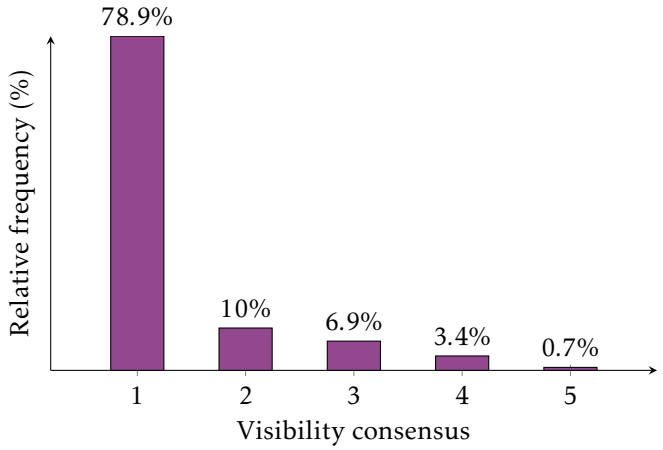

Figure 4.10: Relative frequency of each class the on annotated training set (on the left) and sigmoid function for normalization applied after classification (on the right).

selection, the lead with the best quality is selected. For example, Johnson *et al.* [211] applied SQI metrics on 10 s segments of the PCINC 2014 multimodal data, selecting the channel with highest SQI to produce a consensus of adult HR. In channel fusion, HR estimates from different channels are merged, e.g. by simple majority voting or weighted averaging based on a quality metric. A more sophisticated framework proposed for this end is the KF. The use of KF is motivated by its well-defined paradigm, which has the advantage of incorporating knowledge of the FHR dynamics as well as the amount of uncertainty in its measurement and intrinsic model. Through their innovation, KF methods can identify trends and abrupt changes in the underlying features not requiring an intensive training period [315]. The use of KFs in improving heart/respiratory rate measures was firstly suggested by [251, 419]. The algorithm can be divided into two stages, namely single-channel HR estimation (using the unfiltered FHR estimates and the classified fetal SQI as input) and multichannel data fusion (using Kalman filtered single-channel estimates, fetal SQI and the innovation signal as byproduct of the KF algorithm).

On the single-channel stage, with both information at hand (i.e. FHR rough estimates and combined SQI), the linear Kalman filter algorithm is applied, which was explained in detail in Section 3.3.2 and summarized in Algorithm 1. Differently from its previous application in FECG extraction, the state variable x_k is now defined as the FHR estimates. For the purpose of modelling the dynamics of this system (i.e. HRV), AR models were often applied in the literature [251, 419]. Moreover, AR processes are convenient since they can be easily implemented into KF's framework using its Markovian representation (as the reader may recall from Section 3.3.2). For completeness, this model is generalized as a p^{th} order AR process, which allows the system to have memory. However in this work the first-order model (i.e. $p = 1$) is applied [19]. A univariate p^{th} order AR process is described as [22, 31]:

$$\begin{aligned} a_{k+1} &= \sum_{i=1}^{p} \left(\varphi_{i,k} \cdot a_{k-i+1} + w_k\right), \\ \underline{a}_{k+1} &= \underline{\varphi}_k^T \cdot a_k + w_k, \end{aligned} \tag{4.19}$$

where $i \in [1, p]$ is the index, x_k denotes the order, $\varphi_{i,k}$ are the time-dependent AR coefficients and w_k is an additive zero-mean white Gaussian noise process. By applying this modelling into a KF framework, one aims to obtain a linear regression of the p previous FHR measures $(FHR_{k-1} \cdots FHR_{k-p})$ to estimate the current FHR_k, represented in Eq. 4.20:

$$\widehat{\mathrm{FHR}}(n) = [FHR(n-1) \cdot \varphi_1 + FHR(n-2) \cdot \varphi_2 + ... + FHR(n-p) \cdot \varphi_p] \tag{4.20}$$

Equations 4.19-4.20 can be modelled into KF's space-state representation as Eqs. 3.1 and 3.2. The state variable $\underline{x}_k \in \mathbb{R}^{p \times 1}$ is defined as the signal of interest (i.e. the FHR p previous estimates), the state vector $\underline{y}_k \in \mathbb{R}^{q \times 1}$ contains the observations (rough FHR values), $\underline{w}_k$ is the process noise and $\underline{v}_k$ the observational noise. The filter noise covariance matrices are defined by $w \sim \mathcal{N}(0, \mathbf{Q}_k)$ and $v \sim \mathcal{N}(0, \mathbf{R}_k)$. The state transition matrix $\mathbf{A}$ is the $p \times p$ matrix, describing the expected dynamics of our state (see Eq. 4.21), while the observational matrix $\mathbf{H}$ is a $1 \times q$ null vector, except for its first element which is unitary.

$$\underline{x}_k = \left[FHR_k, FHR_{k-1}, \cdots, FHR_{k-p+1}\right]^T$$

$$\text{and} \qquad \mathbf{F} = \begin{bmatrix} \varphi_1 & \varphi_2 & \cdots & \varphi_{p-1} & \varphi_p \\ 1 & 0 & \dots & 0 & 0 \\ 0 & 1 & \dots & 0 & 0 \\ \vdots & & \ddots & & \vdots \\ 0 & 0 & \dots & 1 & 0 \end{bmatrix} \tag{4.21}$$

he KF's gain is mostly influenced by its defined process and observational noise covariance matrices ($\mathbf{Q}_k$ and $\mathbf{R}_k$). In order to integrate the information on the signal quality, Li *et al.* [251] proposed modulating the KF's measurement covariance matrix as described in Eq. 4.22.

$$\mathbf{R}_k \equiv \mathbf{R}_0 \cdot exp(1/SQI_k^2 - 1) \tag{4.22}$$

where SQI_k (with $SQI \in [0, 1]$) denotes the time dependent combined signal quality and $\mathbf{R}_0$ is the initial value of measurement covariance matrix, which is signal dependent. The employed nonlinear weighting function leads to $\mathbf{R}_k \to \mathbf{R}_0$ (if $SQI_k \to 1$) and $\mathbf{R}_k \to \infty$ (if $SQI_k \to 0$). The adaptive covariance matrix enhances the influence of cleaner estimates on the filter's outcome, providing the filter with a more rapid response to sudden changes in the signal quality [315].

n this work, to obtain continuous SQI values, the use of posterior probabilities $P(i, k)$ from the previously depicted classifier is proposed. Thus, the continuous valued SQI output is generated by $SQI_k = \sum_{\{i=A,B,...,E\}} P(i, k) * v_{i,k}$. The initial values for the measurement and process covariance matrices, were empirically determined using a grid-search algorithm (as in [22]) on the first minute of each annotated dataset, for avoiding over-training. The calibration procedure resulted

on $R_0 = 10^{-3}$ and $Q_0 = 1$.

After obtaining a Kalman filtered FHR estimate for each available channel, the second stage (i.e. sensor data fusion) step takes place. This multichannel consensus is obtained by using both KF innovation (ν_k) and consensus SQI signal such that:

$$\underline{x}'_k = \sum_{s}^{N_c} \left(\frac{\prod_{i=1, i\neq s}^{N_c} \sigma_{k,i}^2}{\sum_{i=1}^{N_c} \left(\prod_{j=1, j\neq i}^{N_c} \sigma_{k,j}^2 \right)} \cdot x_{k,s} \right) \tag{4.23}$$

where x'_k represents the final FHR estimate, $x_{k,s}$ is the current FHR estimate for each available channel s at time-step k and $\sigma_{k,s}^2 \equiv (\nu_{k,s}/SQI_{k,s})^2$. This approach was likewise proposed by [251].

The accuracy of our estimated FHR was evaluated based on two measures, as described in Section 3.5.2, namely the HDR and RMSE. In order to generate the FHR reference, FQRS complexes were manually annotated as described in Section 5.2.4. The reference FHR was then obtained by calculating the mean of the annotated RR intervals in windows of 5 seconds with 1-second overlap.

Applicability to other biosignals

As a side note, in a preliminary work [22] this author made use of a similar strategy for obtaining more accurate HR estimates from *camera-based photoplethysmogram (cbPPG)* recordings by means of SQI measures for video images. cbPPG is a contactless measuring technique, which based on the slight variations of skin color during a heart cycle, allows the acquisition of cardio-respiratory signals using conventional cameras [194]. As usually occurs, the ease with which it is recorded is counterbalanced by subject's movements and light changes that generally lead to a signal of interest with low SNR. At the IBMT several works have been performed on this topic [243, 459, 460, 478]. In order to cope with the low SNR of the cbPPG signal, the green channel is often preferred. Next, one or more *region of interest (ROI)*s are usually selected from the output of a face detection algorithm. The resulting cbPPG signal is obtained by averaging the intensity signal within these ROIs. Notwithstanding, even after some bandpass filtering, the pulsatile signal obtained is often buried into noise.

In Andreotti *et al.* [22], 10 s segments were processed using the *Short Time Fast Fourier Transform (STFT)*, whose main frequency was assumed to represent the HR. The KF approach, presented in the previous section, was then used for improving HR detection. For this purpose, two SQI metrics were applied, namely frequency-based ($mpSQI_a$, as previously described in this section) and a novel image velocity-based ($vSQI$) index. This latter measure aims at detecting motion artefacts, which usually influences the reliability of the cbPPG measurement and respective HR estimate.

4.4 Chapter Summary

In this chapter, several improvements in NIFECG extraction, detection and heart rate estimation were proposed. In Section 4.2, two major improvements in the $EKF2/EKF24$ models were

proposed, namely the time-varying covariance matrices ($vEKF2/vEKF24$) and the unknown input addition to its model (i.e. $uiEKF2$), to better represent the non-Gaussian nature of fetal peaks. In Section 4.3, methods to improve the detection of FQRS complexes (i.e. location accuracy for individual peaks) or their time-average (i.e. FHR) were proposed. Both those methods had in common the necessity of metrics to improve their specificity. For this reason, several novel fetal SQI metrics were suggested (see Section 4.3.2). Fetal QRS locations was improved with the eQRS method, which exhaustively attempts to optimize a global objective function based on each individual peak's SQI values. Fetal HR estimation was improved using a KF approach, whose noise covariance matrix $\mathbf{R}_k$ was adapted using a Naive Bayes classifier and several novel SQI metrics. In the next chapter, the data material produced during this work is presented.

In God we trust, all others (must) bring data

– controversially attributed to W. Edwards Deming

5 Data Material

Data is a crucial part of training and testing of signal processing algorithms. In the previous chapters, novel methods for NIFECG were proposed, however due to the lack of publicly available NIFECG databases, as mentioned in Section 3.2.4, the clinical usage of NIFECG has been hindered. Therefore, in this work alternative sources of data were sought. For this purpose, a simulator and large database of simulated data was created in cooperation with the Institute of Biomedical Engineering at the University of Oxford, which is presented in Section 5.1. Concomitantly, to validate the performance of signal processing algorithms in a real-world scenario, clinical recordings were performed at the University Hospital of Leipzig (see Section 5.2).

5.1 Simulated Data

Simulated data provides means for training NIFECG processing algorithms with gold-standard information on the accurate location of FQRS, MQRS and FECG signal waveform. In the following sections, the toolbox and simulated database developed during this work are described.

5.1.1 The FECG Synthetic Generator (FECGSYN)

A straightforward manner of representing the myocardial electrical activity is to use a three-dimensional time-varying vector, whose origin is modelled as a punctual source at the center of the heart. This heart dipole vector can be written as $\underline{d}(t) = v_1(t)\hat{\underline{i}} + v_2(t)\hat{\underline{j}} + v_3(t)\hat{\underline{k}}$, where $\hat{i}$, $\hat{j}$, $\hat{k}$ are unit vectors for the three-dimensional body axes and $v_n(t)$ with $n \in [1,3]$ depicts three orthogonal signals, which constitute the VCG, and are used to represent the heart cycle. The potential difference $\phi(\underline{r},t) - \phi_0(\underline{r},t)$ measured at a point on the torso (i.e. volume conductor)

and a reference potential (negative electrode, as explained in Section 3.2.3) is represented in Equation 5.1 [49, 50]:

$$\phi(\underline{r},t)-\phi_0(\underline{r}_0,t)=\frac{\underline{d}(t)}{4\pi\varepsilon_0}\left(\frac{\underline{r}(t)}{|\underline{r}(t)|^3}-\frac{\underline{r}_0(t)}{|\underline{r}_0(t)|^3}\right), \tag{5.1}$$

where $\underline{r}(t)$ is the vector from the dipole center to observational point, ε_0 is the permittivity of the volume conductor (here regarded as isotropic[1] and unitary). As the heart dipole $\underline{d}(t)$ changes with time (i.e. during a heart cycle, i.e. time-point on the VCG waveform) or its position $\underline{r}(t)$ (e.g. with respiration), the potential difference is expected to vary [50].

Based on this simplified representation of the cardiac electrical activity by McSharry *et al.* [275] and Sameni *et al.* [364] proposed a model for generating realistic ECG waveforms. The model is built on the premise that a set of N_k Gaussian kernel functions can be used to approximate VCG cycles. By modelling all three dimensions of VCG signals (see Fig. 5.1), available for example at Physionet's PTB Diagnostic ECG Database[2] [68, 161], one can attain a 3-D model for the heart's electrical activity. Adopting the simplified polar coordinate system (rather than Cartesian) as proposed by Sameni [362], the model can be described as:

$$\dot{d}^p(t)=\sum_{n=1}^{N_k}\delta\frac{\alpha_n^p\lambda}{\left(b_n^p\right)^2}\Delta\theta^p_{n,k-1}exp\left(-\frac{\Delta(\theta^p_{n,k-1})^2}{2(b_n^p)^2}\right)\quad\text{for}\quad p\in\{\hat{i},\hat{j},\hat{k}\}\quad, \tag{5.2}$$

where each component $d^p(t)$ of the dipole $\underline{d}(t)$ is represented by a sum of N_k Gaussian kernels. The variable $\Delta\theta_{n,k}=\theta_k-\phi_n$ denotes the phase of the n^{th} Gaussian at time step k, ϕ_n being the position of the each kernel inside the template. Parameters α_n, b_n and ϕ_n correspond to the amplitude, width, and position of the n^{th} Gaussian kernel, respectively (see Fig. 5.1). The angular frequency (λ) and sampling period (δ) determine the time progression (or pace) of the signal. In McSharry *et al.* [275], realistic HRV changes are introduced by making λ time variant, designed to well-represent the respiratory sinus arrhythmia and the response to Mayer waves [213]. Furthermore, a projection matrix built upon the cardiac dipole model was used to project the VCG waveforms onto the observational points (i.e. electrode positions) on the surface of the volume conductor, thus obtaining propagated ECG signals. The projection matrix contains information about the permittivity of the conductor (assumed constant), dipole origin and relative location between observing electrodes and source. Figure 5.2 shows exemplary fetal and maternal punctual cardiac sources within a cylindric volume conductor. From this Figure, the positive electrodes (numbered from 1-34) and the ground electrode can be seen. The negative potential ($\phi_0(t)$) is calculated as the mean of all available electrodes' signals. The original implementation of McSharry *et al.* [275]'s adult ECG simulation model is available on Physionet[3].

Following the works from McSharry *et al.* [275], Sameni *et al.* [364] suggested the use of this

[1] According to [468], for frequencies below 1000 Hz, the capacitive component of tissue impedance, the inductive and the electromagnetic propagation effect in biological tissues can be neglected.

[2] Available at Physionet under `https://www.physionet.org/physiobank/database/ptbdb/`

[3] ECGSYN toolbox, available at `https://www.physionet.org/physiotools/ecgsyn/`

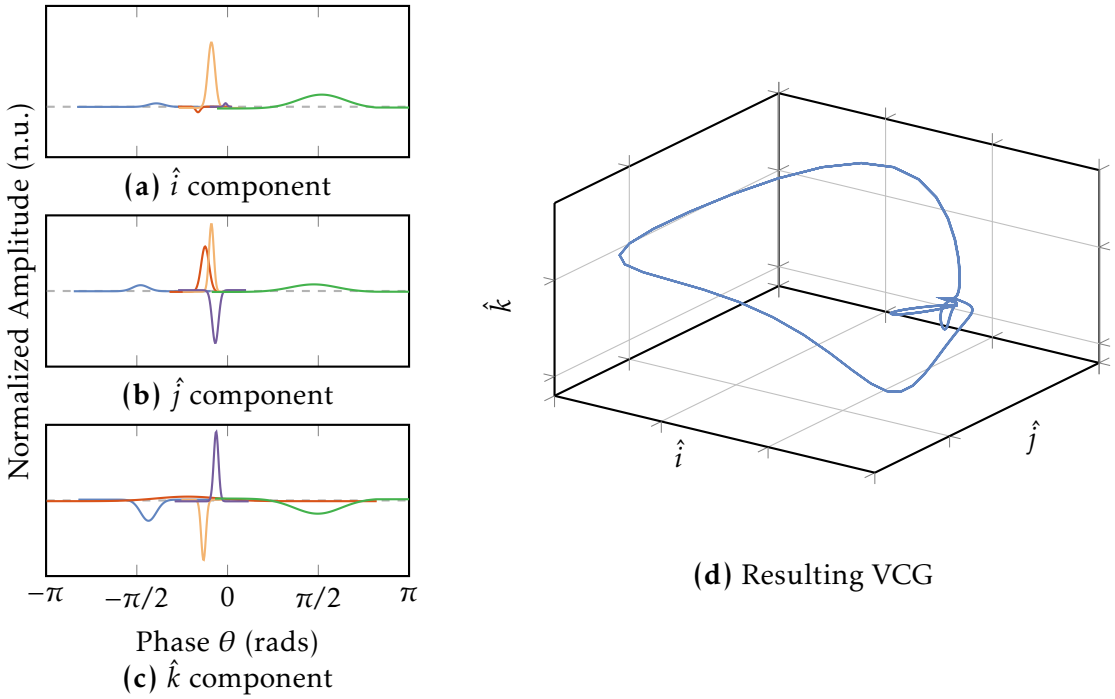

Figure 5.1: Three dipole components (on the left) and resulting VCG (on the right). For illustration purpose, each Gaussian kernel on the dipole model is presented with a different color, the resulting model is obtained by simply summing these kernels. For clarity, the amplitude values were omitted.

framework for NIFECG modelling and included realistic noise. Noise modelling was done using real *muscular artifact (MA)*, *electrode motion (EM)* and *baseline wander (BW)* signals from the Physionet *Normal Stress Test Database (NSTDB)* [161, 287]. Sameni *et al.* [364] proposed the use of AR models to add non-stationarity effects such noise processes while overcoming the restriction of being limited to generating 30 min noise signals (length of NSTDB noise recordings). Thus, the potential measured at an electrode can be described as in Equation 5.3 [50, 364]:

$$\underline{\phi}(t) = \mathbf{H}_m \cdot \mathbf{R}_m \cdot \underline{d}_m(t) + \mathbf{H}_f \cdot \mathbf{R}_f \cdot \underline{d}_f(t) + \underline{\omega}(t), \tag{5.3}$$

where $\underline{\phi}(t) \in \mathbb{R}^M$ corresponds to the signal recorded on the M ECG channels at time t, the dipole vector $\underline{d}(t) \in \mathbb{R}^{1\times 3}$ is given in Equation 5.2, $\mathbf{H} \in \mathbb{R}^M$ corresponds to the projection matrix, $\mathbf{R} \in \mathbb{R}^{3\times 3}$ is the rotation matrix for the dipole vector and $\underline{\omega}(t) \in \mathbb{R}^M$ corresponds to the noise on each ECG channels at time t [50]. The sub-indices m represent maternal and f fetal hearts.

During the development of this thesis, several improvements to the previous simulators were proposed in cooperation with the *Institute of Biomedical Engineering (IBME)* (University of Oxford) (see [18, 50]). Key aspects proposed by Behar *et al.* [50] are listed below:

- Each source, i.e. either cardiac (e.g. mother, fetus) or noise (e.g. MA, EM, BW), was regarded as an individual punctual dipole with different magnitudes and spatial positions, allowing multiple fetuses and any number of noise sources. Moreover, those sources can

be spatially distributed freely within the volume conductor;

- Translatory and rotatory motion of dipole sources were implemented by designing $\mathbf{H}(t)$ and $\mathbf{R}(t)$ to be time variant. This improvement allows the modelling of fetal/maternal respiratory movements and fetal/noise movements inside the volume conductor;
- Different SNRs were assigned to each source, meaning each fetus/noise could have distinct strengths;
- Both HR signal and SNR strength can be modulated, for example, using a hyperbolic tangent function to increase/decrease HR or noises SNR;
- VCG models for ectopic beats derived from the PTB Diagnostic ECG Database[4] [68, 161] were included.

These improvements to the model and encapsulated design enable the production of maternal and fetal signals in both physiological and pathological scenarios as well as a number of non-stationary phenomena. The enhanced simulator, named *Fetal ECG Synthetic Generator (FECGSYN)*, was released[5] under an open-source GNU *General Public License (GPL)* license. Its main purpose is to facilitate stress-testing of NIFECG algorithms under varied conditions. Further, FECGSYN was used to generate a large simulated dataset and benchmark routine described in the following section.

5.1.2 The FECG Synthetic Database (FECGSYNDB)

In this work, the FECGSYNDB was developed and made publicly available on Physionet[6] [18, 161]. The FECGSYNDB is a large database of simulated signals, which enables reproducible research in adult and NIFECG areas. Similarly to the FECGSYN toolbox, the FECGSYNDB was created in partnership with the IBME from the University of Oxford.

The simulated data was generated using the FECGSYN [50] (Section 5.1.1). The modeled volume conductor is presented in Figure 5.2. As observational points, 34 simulated channels (32 abdominal and 2 MECG chest channels) were included (see Fig. 5.2). The ground electrode was positioned on the back of the cylinder at the polar coordinates $\{\pi, 0.5, -0.3\}$. The electrode configuration was designed to span across most of the simulated "maternal abdomen". A total of seven physiological events (i.e. described in table 5.1) was considered. For each case, the heart dipole models (for mother and fetuses) were generated ten times by randomly selecting one of the nine VCGs available in the FECGSYN toolbox. Five different levels of additive noise were included (0, 3, 6, 9, and 12 dB). Simulations were repeated five times, re-generating noise signals on every iteration, to obtain a more representative database. Overall a total of $7 \times 10 \times 5 \times 5 = 1750$ synthetic signals were produced. Each simulation consisted of 5 minutes abdominal mixtures projected onto , totalizing 145.8 hours of multichannel data and 1.1 million fetal peaks. Several

[4] Available at Physionet: https://www.physionet.org/physiobank/database/ptbdb/
[5] Available at: http://www.fecgsyn.com
[6] Available at Physionet: https://physionet.org/physiobank/database/fecgsyndb/

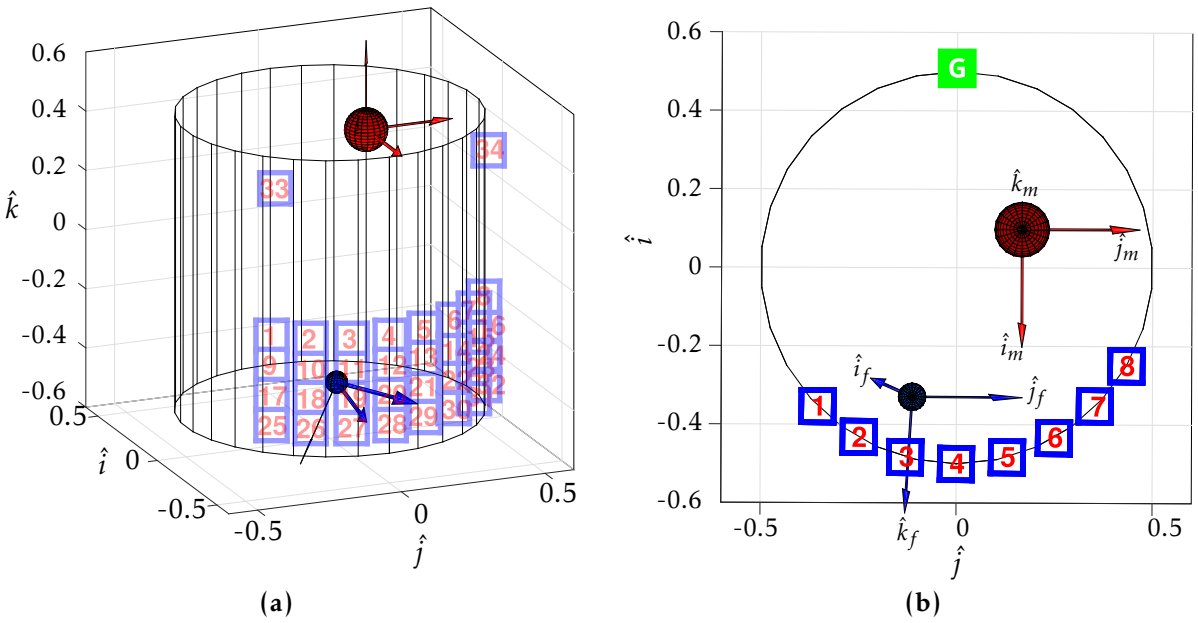

Figure 5.2: Side (a) and upper (b) view the of volume conductor. Positions for fetal (small sphere, blue) and maternal (larger sphere, red) hearts are shown. The square with a "G" represents the position of common mode ground electrode.

Table 5.1: Scenarios used for simulating pregnancy's pathophysiological events. Noise refers to muscular noise added as two independent sources situated on the lower half of the conductor volume. MHR/FHR represent the maternal/fetal heart rates.

Case	Description
Baseline	abdominal mixture (no noise or events)
Case 0	baseline (no events) + noise
Case 1	fetal movement + noise
Case 2	MHR /FHR acceleration / decelerations + noise
Case 3	uterine contraction + noise
Case 4	ectopic beats (for both foetus and mother) + noise
Case 5	additional NIFECG (twin pregnancy) + noise

parameters were required whilst generating these events. The most relevant ones used in this study are summarized in Table 5.2 (for more details the reader may refer to [18, 50]). Some exemplary signals are shown in Figure 5.3.

As the FECGSYNDB provides gold-standards for FQRS detection and unmixed FECG signal morphology, in this work, the FECGSYNDB is used for benchmarking novel signal processing techniques developed in Chapter 4. As in Andreotti *et al.* [18], from the 32 abdominal channels available, eight (i.e. channels 1, 8, 11, 14, 19, 22, 25 and 32 - see Figure 5.2a) were used.

5.2 Clinical Data

5.2.1 Clinical NIFECG recording

Data collection was performed together with our partner from the Department of Obstetrics from the University Hospital of Leipzig. Ambulant and stationary volunteers were asked to

Table 5.2: FECGSYN model parameters used within this work, based on [50]. $\mathcal{N}(\mu, \sigma^2)$ represents a normal distribution with mean μ and variance σ^2 and $\mathcal{U}(a, b)$ a uniform distribution between a and b. *mheart* was allowed to vary its position up to 1% of the conductor's volume in any direction.

Parameters	Definition	Range/type	Unit
fs	sampling frequency	250	Hz
SNR_{fm}	signal to noise ratio of the FECG relative to MECG	$\mathcal{N}(-9, 2)$	dB
SNR_{mn}	signal to noise ratio of the MECG over noise	$\{0, 3, 6, 9, 12\}$	dB
fhr	fetal heart rate	$\mathcal{N}(135, 25)$	bpm
mhr	maternal heart rate	$\mathcal{N}(80, 20)$	bpm
$facc$	fetal heart rate acceleration/deceleration	$\mathcal{N}(30, 10)$	bpm
$macc$	maternal heart rate acceleration/deceleration	$\mathcal{N}(20, 10)$	bpm
$fres$	fetal respiration frequency	$\mathcal{N}(0.90, 0.05)$	Hz
$mres$	maternal respiration frequency	$\mathcal{N}(0.25, 0.05)$	Hz
$mheart$	maternal heart position in polar coordinates	$\{2\pi/3,\ 0.2,\ 0.4\}$	—
$fheart$	fetal heart position in polar coordinates	$\{\mathcal{U}(-\pi/10, \pi/10),$ $\mathcal{U}(0, 0.1)+0.25,$ $\mathcal{U}(-0.4, -0.2)\}$	—

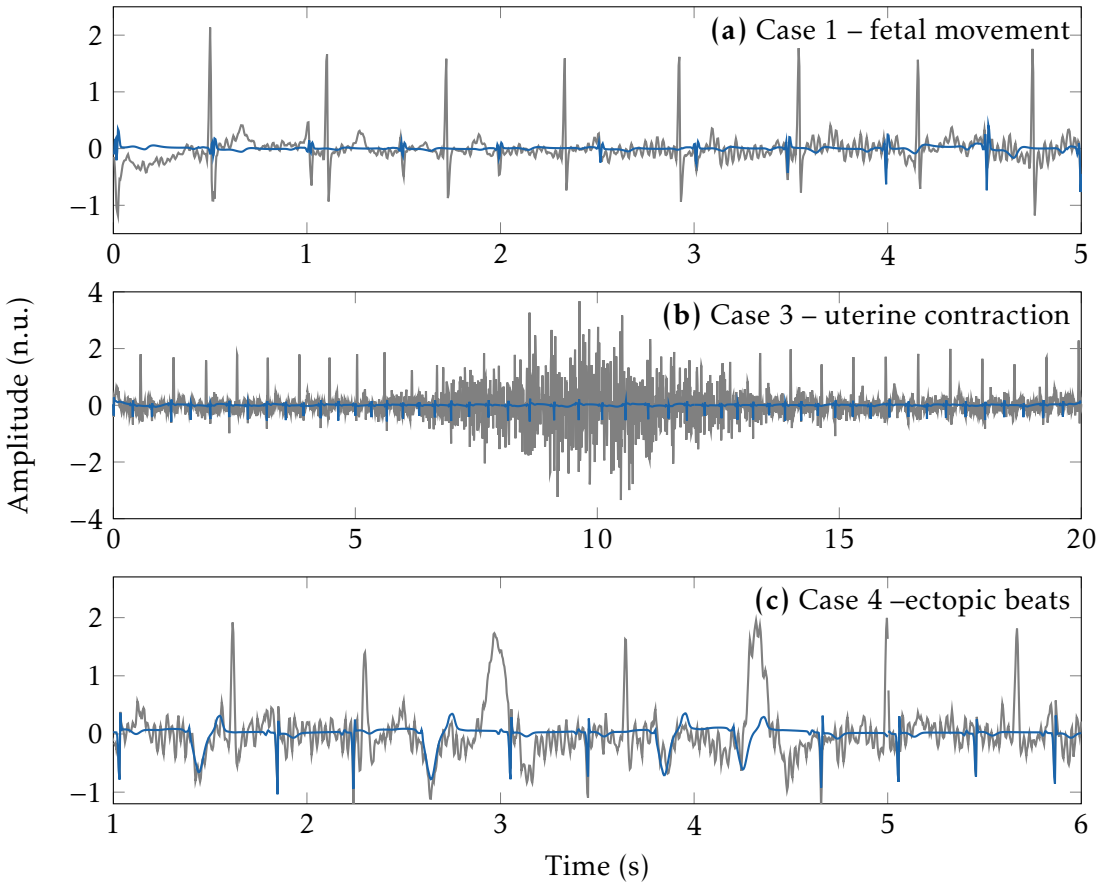

Figure 5.3: Exemplary simulated signals using FECGSYN, with Case 1 (above), Case 3 (middle) and Case 4 (bottom). This figure depicts the abdominal mixture (abdECG - in gray) as well as propagated FECG (blue). See cases description on Table 5.2.

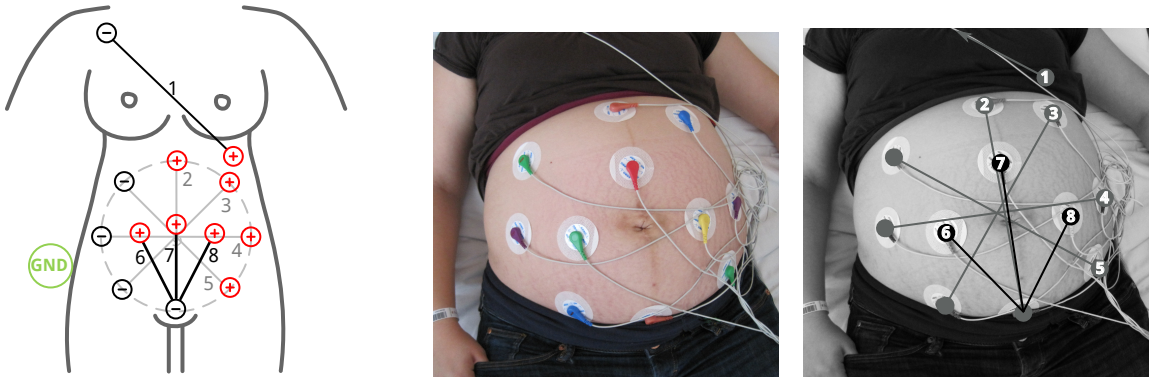

(a) (b) (c)

Figure 5.4: Electrode configuration used in this work (14 electrodes). As demonstrated in (a), the configuration comprises a MECG lead and 7 bipolar abdominal leads; (b) and (c) shows those leads being applied onto a patient (GND electrode not visible).

take part in the study, handled under the supervision of Prof. Holger Stepan and Dr. Alexander Jank by Dr. Claudia Schmieder, Sophia Schröder, and Susanne Löther. This trial was approved by the University Hospital of Leipzig's ethics commission record 348-12-24092012 and written informed consent was obtained from each patient.

Since no lead configuration standard for NIFECG recordings is available, based on the existent configurations (see Figure 3.3) and some own preliminary works [16] a 14-electrode system comprising seven abdominal channels and one MECG channel was proposed (presented in Figure 5.4). This electrode configuration was considered appropriate since it covers a large portion of the maternal abdomen (as many other schemes in literature do - see Figures 3.3d–3.3j), aiming at maximizing the probability of having usable channels containing FECG signals as described in Section 3.2.3. Moreover, the lead configuration includes the same derivations as the first available commercial equipment Monica AN24 (see Figure 3.3a). Regarding this geometry, two different inter-electrode distances were used, namely the diagonal of the external circle and the internal triangular formation of electrodes (see Fig. 5.4).

Recordings were performed at 1000 Hz sampling frequency and 16-bit ADC using the ADInstruments ML138 Octal Bio Amp and ADInstruments PowerLab 16/30 (ADInstruments, Dunedin, NZ). The abdominal channels were filtered in hardware by a mains filter[7] (cutoff frequency at 50 Hz) and a first-order high-pass filter (cutoff at = 1 Hz). The measuring range of the abdominal recordings was ±500 μV. More information on these equipment's specifics can be found in the fabricant's datasheet [1, 2]. Figure 5.5 depicts some examples of recorded data.

Supplementary clinical information

Along with the multichannel data, information about mothers (age, BMI, history of diseases, medications administered), pregnancy (WOG, eventual complications, fetal gender, fetal position, amount of amniotic fluid, placental position, and outcome) and the recording (time, date,

[7] According to the manufacture's manual [1], this adaptive filter tracks the recorded signal for a second and removes both fundamental and harmonic frequencies of the powerline interference.

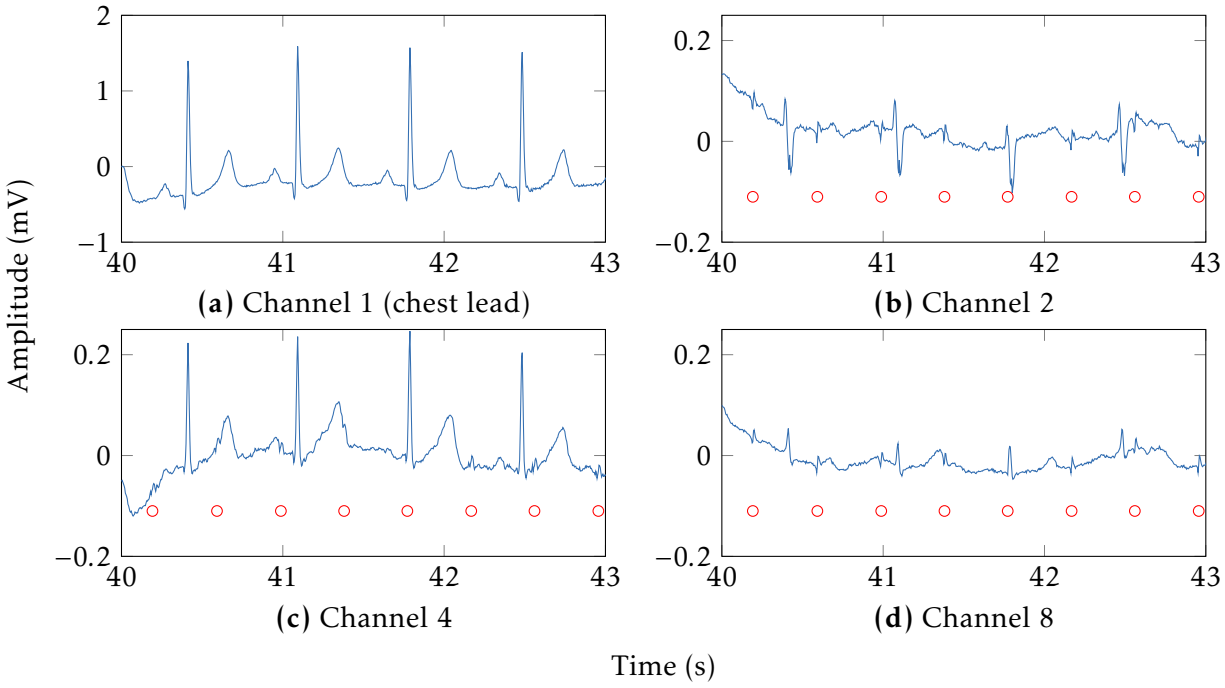

Figure 5.5: Exemplary raw signals collected during this work by our project partners at the University Hospital of Leipzig. The x-axis represents the time (in seconds) and FQRS locations are marked with (○). See electrode configuration on Fig. 5.4 and note the different amplitude scales.

room) were documented. This information was obtained in the form of a questionnaire, based solely on mothers' knowledge. If available, information on the outcome of those pregnancies were also collected, such as: labor date and type of birth (e.g. cesarean or vaginal) as well as newborn's size (i.e. height, weight and head circumference), APGAR scores (for 1, 5 and 10 min after birth), umbilical cord analysis (i.e. pH-level and base excess) and diseases within the few hours after delivery.

5.2.2 Scope and limitations of this study

Between September 2011 and January 2013, a total of $n = 259$ recordings from 107 women were collected. Both individual and longitudinal recordings were performed, on average 2.4 recordings per patient took place (range between 1-12 recordings). The duration of those recordings was on average 20.2 min, ranging from 8.5 to 37.3 min. As mentioned in Section 2.1.4, the period around the end of the second and beginning of third trimester of gestation (i.e. < 28 WOG) is crucial for the fetal development [289, Chap.10]. During this period, a considerable shift in the risk of neonatal death (for premature newborns) occurs. For this reason, the focus of the clinical trial carried out during this doctoral work was on WOG< 28 weeks. Overall statistics on our population are shown in Figure 5.6 and Table 5.1. Regarding the patient categories (see Fig. 5.6), the category "other" entails conditions such as fetal heart failures (5% of total – including e.g. *ventricular septal defect (VSD)*, *double outlet right ventricle (DORV)* and tetralogy of

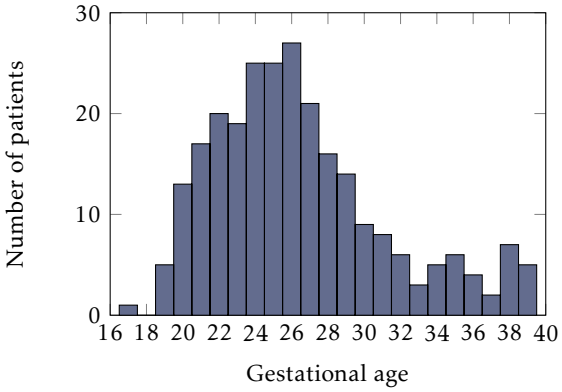

(a) Distribution of recordings' week of gestation

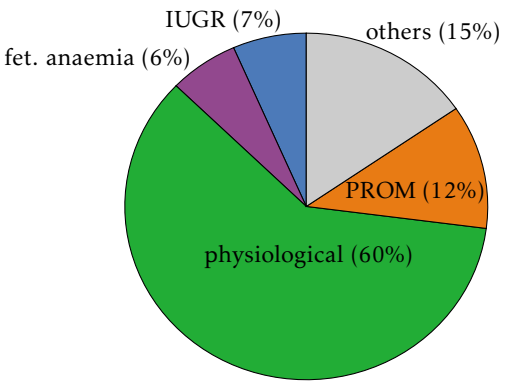

(b) Pie chart with occurrences of different patient conditions

Figure 5.6: Study's population. Abbreviations describe: fet. = fetal; PROM = *premature rupture of membranes (PROM)*; and IUGR = *Intrauterine growth restriction (IUGR)*

Fallot), fetal arrhythmia (2% – e.g. (supra-)ventricular bradycardia/tachycardia and AV block), pre-eclampsia (1%), premature uterine contractions (1%) and less often gestational diabetes and cervical insufficiency.

Several medications were prescribed to this study's population. Between those were antibiotics, anti-arrhytmics, anti-hypertensives, hormonal supplements amongst others. However, due to the absence of test and control groups and the large variety of drugs that were administrated to patients, this information was not regarded in our analysis.

Despite its modest size ($n = 259$) the obtained clinical dataset contains interesting information that is further investigated in an exploratory manner throughout the remaining of this chapter. This analysis is of great relevance since little is known about the quality of NIFECG recordings, particularly during this study's focus period (< 28 WOG). Further, in Chapter 6, this dataset is revisited, aiming at the assessment of developed FECG extraction and FQRS detection algorithms under real circumstances.

To salvage the most information from the clinical data, two different annotation protocols were performed. Those protocols produced reference expert annotations regarding FQRS locations and overall signal quality, as discussed in the following sections.

5.2.3 Data annotation: signal quality and fetal amplitude

In exploratory clinical investigations such as the one performed in this work, it is important to assess the factors that determine the measured FECG signal quality. The motivation for having an annotated dataset is three-fold. First, such quality annotated data enables the characterization of the collected clinical data in terms of FECG-noise content. Such evaluation has the additional benefit of eventually providing some insights about appropriate NIFECG recording conditions. Second, these annotations are a simple manner of determining which recordings have visible/extractable FECG signals, a relevant aspect of the further analysis (presented in Section 5.2.4 and in Chapter 6). Last, such references provide us an interesting

Table 5.3: Descriptive statistics on collected data. Results for numeric variables are presented as "median (IQR)", whereas categorical variables are shown in percent and number of occurrences (n). Left column indicates the pathophysiological categories possible for each patient. Population is divided in the remaining columns according to their clinical assessment.

	physiological ($n = 156$)	**PROM** ($n = 30$)	**IUGR** ($n = 17$)	**fet. anaemia** ($n = 16$)	**others** ($n = 40$)
Maternal age	29.8 (4.7)	27.4 (6.8)	28.8 (10.2)	32.6 (0.2)	28.4 (2.6)
Maternal BMI	25.6 (5.2)	25.9 (15.2)	26.7 (9.2)	28.8 (4.7)	26.1 (7.8)
Gestational week	24.9 (5.4)	26.6 (3.0)	28.0 (3.4)	27.1 (6.7)	29.4 (9.7)
early (< 28)	76.9% ($n = 120$)	76.7% ($n = 23$)	47.1% ($n = 8$)	50.0% ($n = 8$)	35.0% ($n = 14$)
vernix (28 – 36)	19.2% ($n = 30$)	23.3% ($n = 7$)	52.9% ($n = 9$)	50.0% ($n = 8$)	42.5% ($n = 17$)
late (> 36)	3.8% ($n = 6$)	0.0% ($n = 0$)	0.0% ($n = 0$)	0.0% ($n = 0$)	20.0% ($n = 8$)
unknown	0.0% ($n = 0$)	0.0% ($n = 0$)	0.0% ($n = 0$)	0.0% ($n = 0$)	2.5% ($n = 1$)
Fetal gender					
male	50.0% ($n = 78$)	10.0% ($n = 3$)	64.7% ($n = 11$)	12.5% ($n = 2$)	52.5% ($n = 21$)
female	14.7% ($n = 23$)	76.7% ($n = 23$)	11.8% ($n = 2$)	12.5% ($n = 2$)	30.0% ($n = 12$)
unknown	35.3% ($n = 55$)	13.3% ($n = 4$)	23.5% ($n = 4$)	75.0% ($n = 12$)	17.5% ($n = 7$)
Fetal position					
vertex	42.9% ($n = 67$)	50.0% ($n = 15$)	35.3% ($n = 6$)	43.7% ($n = 7$)	57.5% ($n = 23$)
breech	24.4% ($n = 38$)	40.0% ($n = 12$)	23.5% ($n = 4$)	0.0% ($n = 0$)	15.0% ($n = 6$)
shoulder	7.7% ($n = 12$)	0.0% ($n = 0$)	0.0% ($n = 0$)	0.0% ($n = 0$)	5.0% ($n = 2$)
unknown	25.0% ($n = 39$)	10.0% ($n = 3$)	35.3% ($n = 6$)	56.3% ($n = 9$)	22.5% ($n = 9$)
Amniotic fluid					
anhydramnios	0.0% ($n = 0$)	3.3% ($n = 1$)	0.0% ($n = 0$)	0.0% ($n = 0$)	0.0% ($n = 0$)
oligohydramnios	1.3% ($n = 2$)	70.0% ($n = 21$)	29.4% ($n = 5$)	6.2% ($n = 1$)	2.5% ($n = 1$)
under norm	3.8% ($n = 6$)	6.7% ($n = 2$)	5.9% ($n = 1$)	0.0% ($n = 0$)	2.5% ($n = 1$)
normal	91.0% ($n = 142$)	16.7% ($n = 5$)	52.9% ($n = 9$)	43.8% ($n = 7$)	82.5% ($n = 33$)
above norm	3.8% ($n = 6$)	0.0% ($n = 0$)	0.0% ($n = 0$)	25.0% ($n = 4$)	0.0% ($n = 0$)
polyhydramnios	0.0% ($n = 0$)	0.0% ($n = 0$)	0.0% ($n = 0$)	0.0% ($n = 0$)	10.0% ($n = 4$)
unknown	0.0% ($n = 0$)	3.3% ($n = 1$)	11.8% ($n = 2$)	25.0% ($n = 4$)	2.5% ($n = 1$)
Placenta placement					
posterior	28.8% ($n = 45$)	70.0% ($n = 21$)	35.3% ($n = 6$)	87.5% ($n = 14$)	25.0% ($n = 10$)
anterior	28.8% ($n = 45$)	6.7% ($n = 2$)	29.4% ($n = 5$)	6.3% ($n = 1$)	42.5% ($n = 17$)
fundal	1.3% ($n = 2$)	6.7% ($n = 2$)	0.0% ($n = 0$)	0.0% ($n = 0$)	2.5% ($n = 1$)
right lateral	3.8% ($n = 6$)	0.0% ($n = 0$)	11.7% ($n = 2$)	0.0% ($n = 0$)	12.5% ($n = 5$)
left lateral	8.3% ($n = 13$)	10.0% ($n = 3$)	11.7% ($n = 2$)	0.0% ($n = 0$)	0.0% ($n = 0$)
praevia	0.6% ($n = 1$)	0.0% ($n = 0$)	0.0% ($n = 0$)	0.0% ($n = 0$)	5.0% ($n = 2$)
bipartia	0.0% ($n = 0$)	0.0% ($n = 0$)	0.0% ($n = 0$)	0.0% ($n = 0$)	5.0% ($n = 2$)
unknown	28.2% ($n = 44$)	6.7% ($n = 2$)	11.7% ($n = 2$)	6.3% ($n = 1$)	7.5% ($n = 3$)

database for training and evaluating algorithms that attempt to classify the signal quality of both FECG and noise (further discussed in Section 4.3.2).

With regards to the annotation procedure, two aspects are relevant for analyzing the collected NIFECG data, namely the FECG signal amplitude and the power of noise. In this study, segments of every recording of the clinical dataset were annotated including maternal chest lead and 7 abdominal channels (shown in Fig. 5.4). To reduce the amount of noise in those recordings, each channel was preprocessed. Preprocessing was performed using Butterworth filters of 5^{th} or low-pass at 100 Hz and 3^{rd} order high-pass at 3 Hz. A FIR 1000^{th} order notch filter was

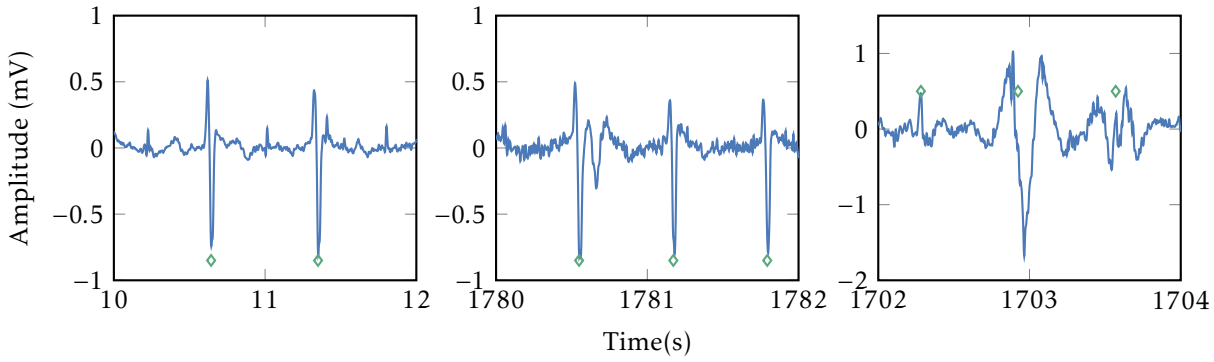

Figure 5.7: Collected signals from own dataset with different signal quality. (a) shows a clean signal with pronounced FECG peaks; (b) exhibits a relatively clean signal with no visible FQRS complexes; (c) depicts a noisy abdominal signal. Please notice the different scaling for the y-axis.

also applied at 50 Hz, to reduce the powerline interference. The first and last minutes of each measurement were disregarded, to avoid that subject's movements on the beginning or end of measurements are considered. The remaining data was divided into five equal intervals from which the first 5 s excerpts were assessed. Therefore, for each channel and each recording, 5 segments (of 5 seconds each) were exported to be annotated producing a total of 10,360 segments (i.e. $259 \times 8 \times 5$). Additionally, a subset of 500 segments was provided twice so that intra-rater variability can be assessed. Annotators were asked to appraise each segment for its FECG signal amplitude (4 classes) and SNR level (5 categories), as specified in Table 5.4. The annotation procedure was carried out using the standalone *graphical user interface (GUI)* shown in Appendix A.

Four experts (here named Annotator $ANN1$, $ANN2$, $ANN3$, and $ANN4$) with both medical and engineering background and different years of experience in the NIFECG field diligently annotated the data. Annotation was performed using a single abdominal 5 s segment (i.e. one channel at a time) and a maternal chest lead for avoiding confusion between maternal and fetal peaks (see Appendix A). Annotators $ANN1$ and $ANN2$ annotated each 100% of the segments. Annotators $ANN3$ and $ANN4$ annotated 72.6% and 37.0% the data, respectively, in a complementary manner so that at least 3 annotations for each segment of the whole data are available. All annotators evaluated the duplicated subset so that intra-observer statistics are available for every annotator.

Intra/Inter-rater agreement and consensus

Several statistics for inter/intra-rater agreement have been proposed in the literature, such as Scott's π [389], Cohen's κ [94, 95] and Fleiss's K [138]. Cohen's κ [94] coefficient is the most commonly used statistic for this purpose [448] and its main advantage is the correction of agreement that is expected to occur by chance alone. The κ values are usually classified into the following categories of agreement [94]: "very good" ($\kappa \in [0.8, 1.0]$), "good" ($\kappa \in [0.6, 0.8)$), "moderate" ($\kappa \in [0.4, 0.6)$), "fair" ($\kappa \in [0.2, 0.4)$), and "poor" ($\kappa \in [0, 0.2)$). Despite its wide use,

Table 5.4: Clinical data annotation classes and definitions.

(a) Recording's annotation criteria for SNR

Classification	Description
unacceptable	no ECG† signal can be spotted on the segment
bad	ECG signal can hardly/intermittently be seen
adequate	ECG signal is clearly visible throughout most of the segment with strong background noise present (or sporadic e.g. artifact)
good	ECG signal is clearly visible through all the segment with moderate background noise
excellent	ECG is clearly visible with low or very low noise content

† ECG was used to generalize the presence of either MECG and/or FECG, indifferently.

(b) Recording's annotation criteria for FECG strength

Classification	Description
not present	FECG is NOT visible
low amplitude	FECG visible with small amplitude
moderate amplitude	FECG visible, its amplitude consists of at most 50% the MECG amplitude
high amplitude	FECG visible and its amplitude is at least 50% as large as the MECG amplitude

Cohen's κ defines expected agreement in terms of contingencies, as the agreement that would be expected if coders were statistically independent of each other [237]. For this reason, κ chance fails to include disagreements between observers' individual predilections for particular categories, punishing raters who agree on their use of categories, and rewards those who do not agree with higher κ values. These drawbacks have been often referred to in the literature as Kappa's paradoxes [133, 168]:

(i) If the percentage of agreement by chance (p_e) is large, the correction process can convert a relatively high value of overall percentage of agreement (p_a) among observers into a relatively low κ. This problem becomes evident from Kappa's formulation $\kappa = p_a - p_e / 1 - p_e$;

(ii) Unbalanced marginal totals may produce higher values of κ than more balanced totals.

These paradoxes make the reproducibility between κ values across different studies difficult and its interpretation counterintuitive. Moreover, κ is a measure of nominal agreement, which cannot be directly applied to ordinal scale as presented in Table 5.4. This because κ penalizes small misclassification (between two adjacent classes, e.g. *adequate* and *good* categories) with the same weight it penalizes e.g. *bad* and *excellent*. To cope with those "less serious" classification errors the Krippendorff's alpha coefficient (α_K) was proposed [174]. Krippendorff's coefficient can be used for any number of raters (not only two), it also is applicable for different kinds of variables (e.g. nominal, ordinal, interval) and can be used for incomplete or missing data [174]. Moreover, unlike Fleiss' K, α_K has no restriction regarding the sample size used.

Krippendorff's α_K can be interpreted as a generalization of several of the previously available metrics. For instance regarding two observers, for nominal data α_K is asymptotically equal to Scott's π, while for ordinal data it is identical to Spearman's rank correlation coefficient ρ (disregarding tied ranks) [174]. As in Cohen's κ, when disagreements are systematic and exceed the expected by chance, α_K can deliver negative values. Since no standard terminology for interpreting α_K values is available[8], in this work the aforementioned scale [94] is used.

Intra-observer agreement is a measure for evaluating each rater's reliability, which is convenient when determining how to build a consensus amongst all raters. In this work, a subset of 500 segments was annotated twice by each annotator. Table 5.5 shows the intra-rater and inter-rate agreement for this study. Overall inter-rater agreement considering both categories (FECG and SNR) was good with 0.65 and 0.68 for FECG strength and SNR criteria, respectively. Similarly, there was a good to very good intra-rater agreement as can be verified in Table 5.5.

Considering the good agreement amongst all observers, majority voting was used to generate a consensus for both FECG and SNR criteria in each segment. In cases of ties amongst observers (i.e. when at least two of the most annotated alternatives have the same number of votes – occurred on 6.3% of SNR and 2.1% FECG annotations), one of the most voted alternatives was randomly chosen to avoid any further bias in our analysis. Figure 5.8 demonstrates these resulting consensus and respective abdominal signal segments. With the consensus annotations for SNR and FECG at hand, one can further define one single measure to describe the visibility of the FECG peaks. This *visibility consensus*[9] was built, following the rules shown in Table 5.6.

Further, using the visibility consensus, one can aim at identifying which recordings have at least one usable channel for every segment. This is relevant when evaluating if a specific pathology or higher BMIs have an overall impact on the quality of our measurements. For this purpose, a *recoding index (RI)* was created in a similar fashion to our consensus for SNR and FECG using the maximum value for the visibility consensus across channels and performing majority voting throughout the segments. This manner, an overall index per recording, which follows the same categories as the visibility index (see Table 5.6), is obtained.

Table 5.5: Intra-observer (on the main diagonal) and inter-observer agreement by means of Krippendorff's α_K statistics for FECG (a) and SNR (b) quality annotation (see Table 5.4).

(a) FECG amplitude

Rater	ANN1	ANN2	ANN3	ANN4
ANN1	0.82	–	–	–
ANN2	0.65	0.72	–	
ANN3	0.63	0.58	0.70	–
ANN4	0.74	0.69	0.68	0.88

(b) SNR

Rater	ANN1	ANN2	ANN3	ANN4
ANN1	0.86	–	–	–
ANN2	0.66	0.82	–	–
ANN3	0.71	0.65	0.84	–
ANN4	0.75	0.65	0.83	0.81

[8] In his book, Krippendorff [238] indeed suggested that a minimum α_K value to confirm a given hypothesis should be chosen according to the importance of the conclusions to be drawn from the available data. For this purpose, the author recommended a threshold of $\alpha_K \geq 0.800$ for conclusive and $0.667 \leq \alpha_K \leq 0.800$ to draw tentative conclusions. This consideration is indeed important and reflect the author's regard with serious empiricism.

[9] Please notice that the experts are only able to annotate what they can identify on the time-domain. However, there may exist a linear/non-linear projection of the available channels, which entails stronger FECG signals. For instance, see Andreotti *et al.* [20] (Figure 5) and Behar *et al.* [54] (Figure 7).

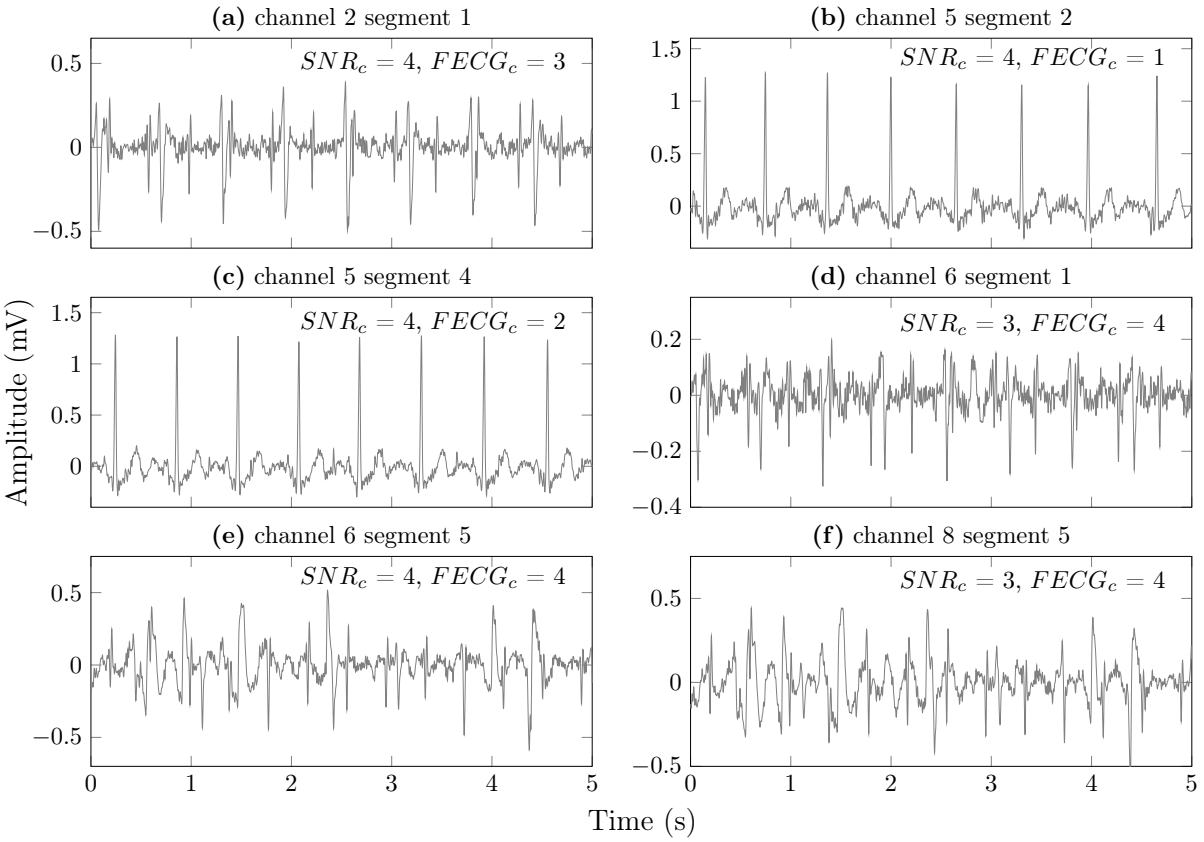

Figure 5.8: Annotated segments of abdominal recordings for NIFECG signal quality. All segments belong to the same recording, the visibility consensus (see Table 5.6) for SNR (SNR_c) and FECG amplitude ($FECG_c$) are described within each subfigure.

Table 5.6: Definition of fetal peak visibility consensus, based on FECG strength and SNR consensus [152]. Scoring is done on a segment basis, one channel at a time.

SNR†	**FECG**‡	**Meaning**	**Visibility consensus**
*§	f1	No FECG visible	1
s1,s2	*§		
s3,s4	f2	FECG visible but low amplitude and SNR	2
s5	f2	FECG visible adequate SNR	3
s3	f3		
s4,s5	f3	FECG very visible adequate SNR	4
s3	f4		
4,5	4	FECG very visible good SNR	5

† $s1$ =unacceptable, $s2$ =bad, $s3$ =adequate,$s4$ =good, $s5$ =excellent
‡ $f1$ =not present, $f2$ =low, $f3$ =moderate and $f4$ =high amplitude
§ The asterisk $*$ represents a don't-care term.

Characterization of collected and annotated dataset

Figure 5.9a and 5.9b demonstrate in a channel-by-channel manner the resulting consensus between experts for FECG and SNR, respectively, as discussed in the previous section. Figure 5.9 (c) shows the results for the visibility consensus on segments regarding fetuses in vertex presentation; similar results were obtained using every presentation. As discussed in Section 3.2.3, the electrode geometry as well as inter-electrode distance plays an important role in the signal SNR and FECG quality. Such effects can be seen in Figure 5.9a and 5.9b, the smaller the distance between electrodes, the higher are FECG peaks but also noise levels. Moreover, channels 2 and 6-8 appear to have proportionally a higher fetal presence. This trend is visually confirmed in Figure 5.9c, where the visibility consensus for FECG and SNR (presented in the previous section) is used.

In order to verify those findings, a statistical analysis was performed under the hypothesis that: if FECG peaks are visible in any channel for a given segment, there is significant difference in quality amongst the individual channels. Since the maternal chest lead does not contain FECG signal, it was excluded from the analysis. Moreover, as it can be seen from Figure 5.9a, there is a great number of segments with no FECG signals visible. Since the goal is assessing channel differences in cases where FECG is present, segments were no FECG could be seen for every channel (i.e. the FECG amplitude is "not present") were excluded from this analysis. Since the data has repetitions (up to 5 segments), a non-parametric variant of the 2-way *Analysis of Variance (ANOVA)* called Skillings-Mack test [260] was applied. This test is a Friedman-type statistic for unbalanced data (due to excluded FECG absent segments). The test indicated highly significant ($p < 0.001$) differences among the different channels with respect to both FECG and SNR consensus. Thus, a post-hoc test was performed using the Sign test for evaluating paired differences between channels, shown in Figure 5.10. From Figure 5.10a it is clear that channel numbers 7, 8, 6 and 2 (in this order), contain highest FECG content. Regarding Figure 5.10b, it is clear that leads in the same groups, i.e. internal (i.e. channels 6-8) or external (i.e. 2-5), have similar SNRs. The internal leads 6, 7 and 8 have worse SNR than the external ones. This confirms the trade-off theory about inter-electrode distance explained in Section 3.2.3.

With regards to the different WOG and the visibility of the fetal signal, Figure 5.11 demonstrates how many of the collected data had observable FECG peaks. From this figure, it is clear that from the 28^{th} WOG onwards, there is a strong decay in FECG quality. The fact is justified by the presence of the vernix caseosa, as described in Section 2.1. Indeed, for WOG < 28, 56.6% the recordings had a $RI \geq 2$, where only 38.1% had a $RI \geq 3$. Meanwhile, for WOG ≥ 28, only 22.3% had $RI \geq 2$ and 20.0% with $RI \geq 3$. Nevertheless, as previously explained, the vernix is expected to slowly dissolve from the 36^{th} week, but only a few recordings are available for these WOGs in this study.

As shown in Table 5.3, in this study every type of independent and dependent variables are present: interval, ordinal and nominal (both dichotomous and polychotomous). Thus, several statistical tests and methods are required to check for dependencies between variables (whether

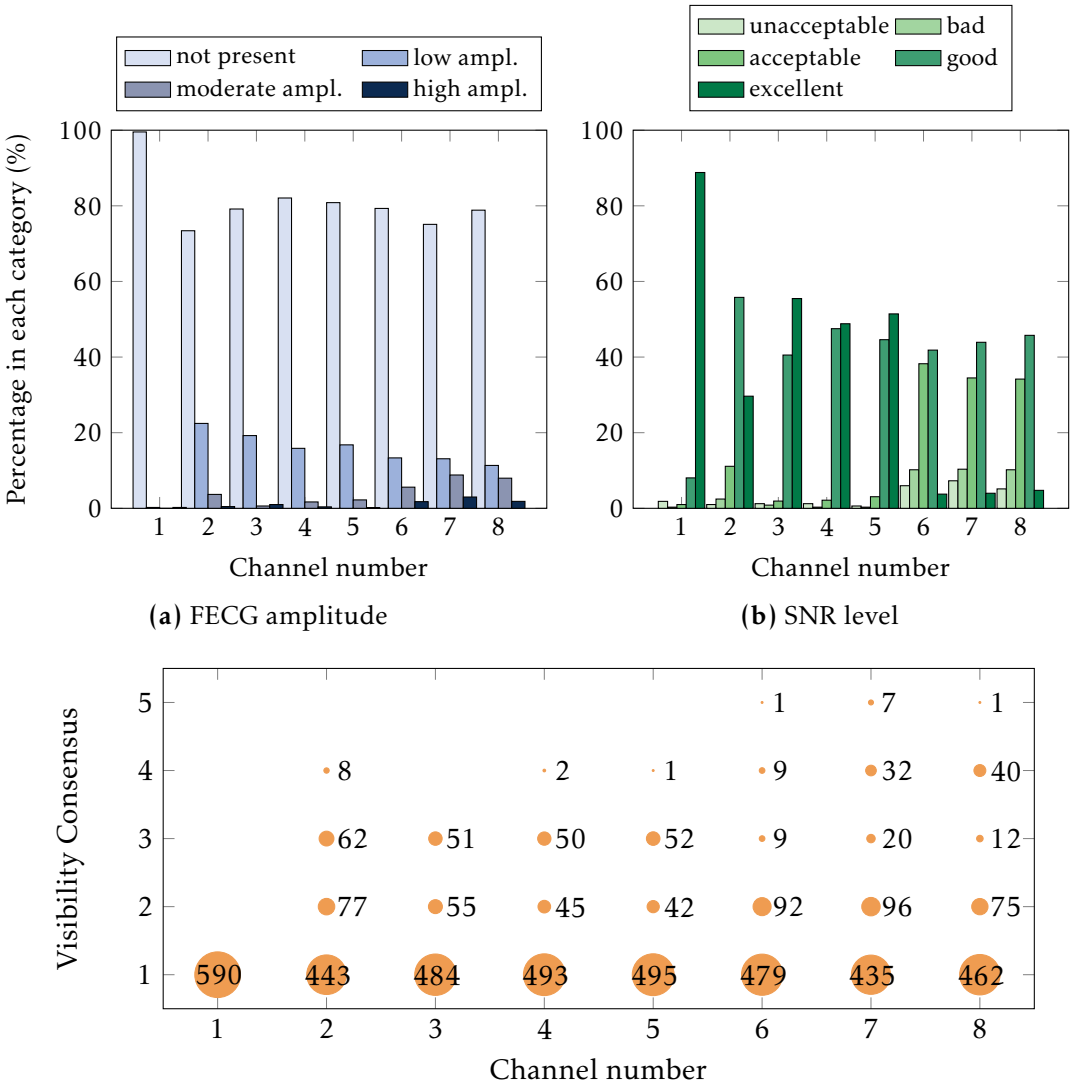

(a) FECG amplitude

(b) SNR level

(c) Occurrences of visibility consensus per channel (fetuses with vertex position only).

Figure 5.9: Channel-by-channel overview of expert's consensus annotations for FECG (top left) and SNR (top right). Below a bubble plot shows the visibility consensus results across different channels, where the number inside the bubbles and their sizes reflect the number of segments which were classified in each category. Please refer to electrode configuration on Fig. 5.4. In Fig. 5.11 the recording index metric regarding multiple channels for this study's population is demonstrated.

dependence is significant[10] or not) and, if so, to assess the strength of association[11] across those variables. Table 5.7 shows the different tests of dependence and bivariate measures for effect size used in this work. Interpreting the strength of a relationship (i.e. if none existing, weak, moderate or strong) is to some extent relative [110]. As suggested by Cohen [96], effect size is defined as according to its absolute value as: 0 – 0.1 (none), 0.1 – 0.3 (weak), 0.3 – 0.5

[10] Each recording in this study is regarded as an independent sample, the author acknowledges that this is a working condition that is not absolutely true for repeated measures of the same subject.

[11] Correlations for nominal variables are usually termed as "association", a term which is used in this work as an umbrella term. In this work the terms "strength of association" and "effect size" are used indiscriminately.

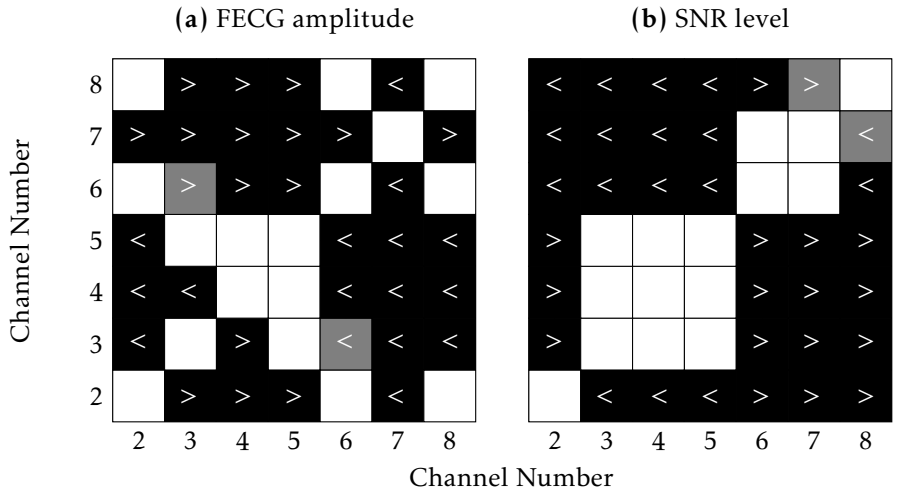

Figure 5.10: Post-hoc analysis using the Signed test for verifying channel quality, i.e. FECG amplitude (on the left) and SNR level (on the right). The channel configuration is presented in Fig. 5.4. The colored boxes indicate the results for the two-tailored sign test, insignificant differences are colored white, significant (i.e. $p < 0.05$) with gray and very significant ($p < 0.01$) with black. Additionally, the test's Z-value sign provide the direction of this difference and are shown with the "<" and ">" symbols. The direction of comparison is from the left to below, e.g. for FECG amplitude channel 7 obtained a very significant higher median than all other channels except channel 2.

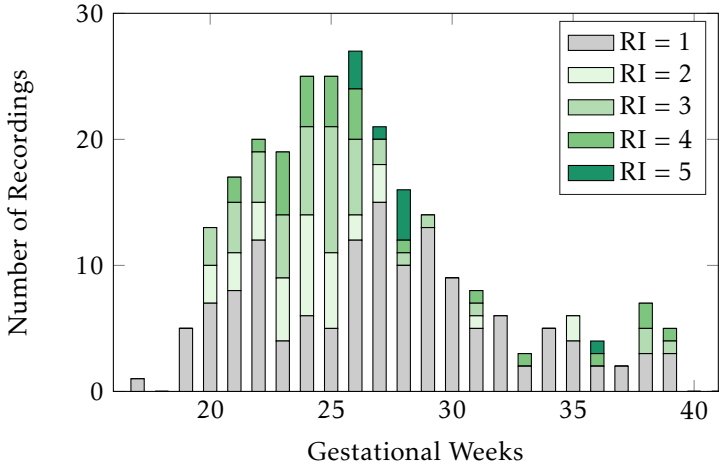

Figure 5.11: Recording's quality across different WOGs for study population. The recording index (RI) is presented in the previous section and ranges from 1 (FECG not visible) to 5 (FECG peaks very distinguishable).

(moderate) and 0.5 – 1.0 (strong). As regards to significance levels, throughout this work thresholds are defined as significant (p-value < 0.05), very significant ($p < 0.01$) and highly significant ($p < 0.001$).

From this point onwards in our analysis, the values for the maternal reference channel are disregarded, since no FECG is present. Moreover, to reduce the number of sub-classes within some of this variables, clustering was applied. Specifically, the level of amniotic fluid

Table 5.7: Measures of dependency and bivariate association used in this study for the different variable types used. Nominal variables are divided into dichotomous (dych. – with two classes) and polychotomous (poly.). On the first line of each cell the test of significance (dependence/independence) is specified, followed by the measure of effect size.

Measures	Interval	Ordinal	Nominal (dych.)	Nominal (poly.)
Interval	Permutation test Spearman's $\rho^{\dagger}$	–	–	–
Ordinal	Permutation test Spearman's ρ	Permutation test Spearman's ρ	–	–
Nominal (dich.)	Kruskal-Wallis test Point-biserial $r_{pb}{}^{\ddagger}$	Permutation test Spearman's ρ	Pearson's χ^2 test Cohen's w [97] §	–
Nominal (poly.)	Kruskal-Wallis test correlation ratio $(\eta)^{\S,\P}$	Kruskal-Wallis test correlation ratio $(\eta)^{\S,\P}$	Pearson's χ^2 test Cohen's w [97]§	Pearson's χ^2 test Cohen's w [97] §

† Pearson's correlation coefficient (r) is an alternative, however it assumes a linear relationship between variables.
‡ This measure is mathematically equivalent to Pearson's r, but specific for dichotomous-interval correlation.
§ Asymmetric coefficient with values ranging between $[0, 1]$, i.e. no direction information.
¶ It is the squared-root of the effect size measure used by ANOVA (η^2), as such it is based on the squared sum of explained/total variance.

was grouped into three categories (low, normal, high) and placental position into 4 (posterior, anterior, sideways, praevia/bipartia), see Table 5.3. Unknown values were disregarded from our analysis. Since some of these relationships are expected to vary throughout the pregnancy, the trends are evaluated by grouping the patients into 4 groups of gestational weeks. Results for these trends are shown in Figure 5.12. From Figure 5.12, a clear decrease and even inversion in the direction of the correlation between FECG and WOG is observable during the formation of the vernix. Aside from that, a moderate association between channel number and SNR consensus is noticeable, the same holds for placental position and FECG grade.

Due to the several classes existing within each variable (described in Table 5.3), overall considerations about the recording quality (i.e. RI) should make use of all recordings (i.e. every WOG available) to avoid miss-conceptions due to small sample-sizes. Given that, associations between RI metric and channel independent variables were evaluated. The estimated effect-sizes for each variable were: BMI ($\rho = -0.10, p = 0.10$); WOG ($\rho = -0.10, p = 0.11$); fetal gender ($\rho = 0.24, p < 0.001$); measuring expert ($\eta = 0.02, p = 0.25$); and patient pathophysiological group ($\eta = 0.21, p = 0.16$). The lack of significant correlations/associations between most of those variables and recording quality comes at no surprise, e.g. some authors [163, 346, 439] have described no decrease of quality with an increase in maternal BMI. Unexpectedly, fetal gender showed a week and highly significant correlation (female fetuses shown on average a slightly better RI); however this results may be attributed to the unbalanced groups or groups having different shape of distribution (e.g. through heteroscedasticity[12]). Particularly regarding fetal gender, data from $n = 115$ male and $n = 62$ female fetuses was collected. Similarly,

[12] Heteroscedasticity denotes when different groups have different standard deviations from each other. In such cases, the probability of obtaining a false positive results even though the null hypothesis is true may be greater than the desired alpha level. Parametric tests assume that data is not heteroscedastic (i.e. homoscedastic) [273].

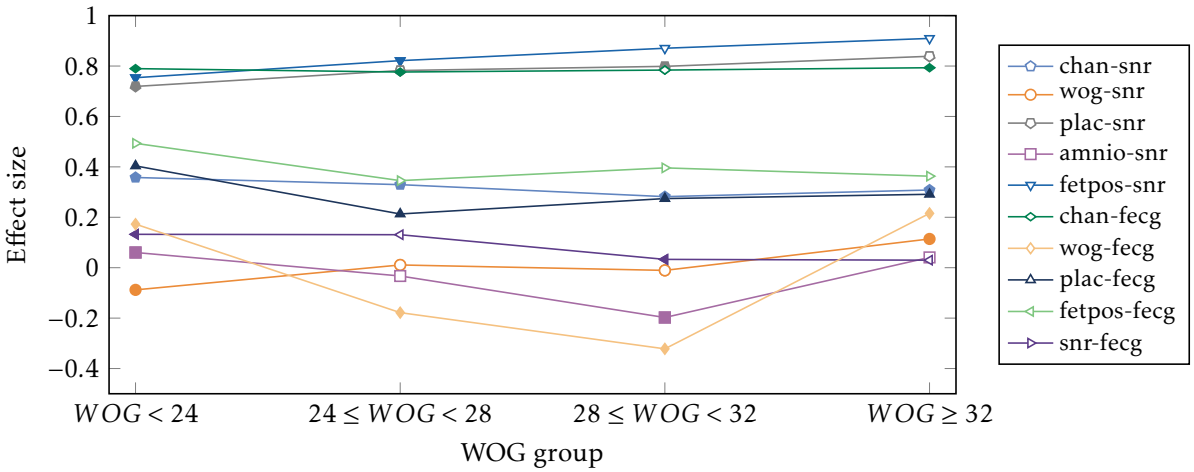

Figure 5.12: Effect sizes across different gestational weeks. Filled markers (e.g. ●) represent significant results, while no significant effect size was obtained otherwise (i.e. ○). Results compare channels (chan), gestational weeks (wog), placental position (plac), amniotic fluid level (amnio), fetal position (fetpos) against both SNR and FECG consensus. The combination amnio-fecg is omitted since no significant dependence was found.

pathological groups have shown a weak not significant association, which can be attributed to Kruskal–Wallis's test sensitivity to the resulting distributions within each group (e.g. the much larger number of physiological pregnancies than some pathologies – see Table 5.3).

The focus of this work is on earlier stages of pregnancy, for this reason, henceforth only recordings where $WOG < 28$ are regarded in our analysis. Before proceeding, the annotated consensus variables (i.e. SNR and FECG), derived in the previous section, are investigated to test if there is a degree of association between those. The intuitive thought behind the idea is that bad SNR signals tend to have no visible FECG peaks at all, meanwhile, strong FECG peaks may influence the observer's classification of SNR values. Aside from this association, the effect sizes across the several variables described in Table 5.3 were evaluated, the results are presented in a correlation matrix (see Table 5.8a and Table 5.8b).

Indeed a highly significant dependency but weak correlation was found between FECG and SNR metrics ($\rho = 0.14$, $p < 0.001$). Nevertheless, the direction of correlation confirms the initial hypothesis that annotators may associate an increase in FECG amplitude with an increase in SNR. Similarly, the visibility consensus was shown to have a weak correlation with SNR and a strong one with FECG consensus. As it can be seen from Table 5.8a, SNR to visibility consensus dependency is highly significant. However, between FECG and the visibility consensus no significant dependency was found. Further investigation using Kendall's τ_b correlation coefficient demonstrated that the FECG–visibility consensus relationship is indeed strong and very significant[13]. The findings are consistent with the expected, i.e. an increase in SNR (and/or FECG amplitude) reflects on better visibility consensus.

[13] The false indication here using ρ is due to the fact that Spearman's ρ does not handle ties well (i.e., both members of the pair have the same ordinal value). Ties often occurred in this analysis, due to the large amount of cases were both FECG and the visibility consensus accuse "1" (i.e., no fetal peak present)

Aside from the assessment metrics, some other effects can be observed in Table 5.8. Some of these effects, such as the reduction of amniotic fluid levels with an increase in WOG, can be physiologically explained. Meanwhile, the cause of other effects such as the association between fetal and placental position are less evident. From Table 5.8 (b) it is noticeable that a strong and significant association was found between channel number and FECG/visibility consensus, which confirms the previous results. Strong associations between placental position and SNR level ($\eta = 0.76$, $p < 0.01$) and moderate association for placental position – FECG ($\eta = 0.30$, $p < 0.001$) were encountered. Further analysis showed slightly inferior SNR results for patients with anterior/fundal placentas, which can be justified by the higher relative permittivity of the placenta compared to muscles/amniotic fluid (shown in [331]). This placental position, thus, could offer resistance on the path between fetal dipole and electrodes. FECG levels were weaker for sideways and praevia/bipartia positions. Different from the results obtained by Graatsma *et al.* [163], fetal position was shown to have a highly significant association for both SNR and FECG parameters, as shown in Table 5.8 (b). Indeed results show higher visibility consensus levels for fetuses in vertex position. Lastly, regarding the levels of amniotic fluid, despite significant dependency no association was found. The counterintuitive results for the interval-scaled variable WOG against nominal variables (fetal and placental position) showing high association with no significance indicate that the dataset is limited in number for providing such analyses. This is because the correlation coefficient (η) for nominal-ordinal/interval variables requires that the frequencies of each class of the categorical variable must be large enough to give statistical stability to the means of these classes. An alternative to obtain more meaningful representation of the real effect-size is to group the different WOGs into ranges. Further tests confirmed a reduction on the effect-size when clustering neighboring WOGs into ranges, nevertheless, the acceptance of the null-hypothesis is not altered.

However, a bivariate analysis does not cover inter-dependencies between multiple variables. For example, the fetal position and channel numbers are both expected to influence the strength of the FECG signal. For assessing how these variables interact, a more elaborate multivariate analysis such as *Factor Analysis with Mixed Data (FAMD)* [124, 207, 318] is further required. Again, due to the limited number of recordings available for this work, such analysis is unfeasible and remains for future works.

5.2.4 Data annotation: fetal QRS annotation

Another feasible analysis using the available clinical dataset is to assess the accuracy of the attained FQRS detections. Exact FQRS are crucial not only for enabling FHR/FHRV analysis but also because morphological analysis of the FECG signal usually relies on FQRS locations to segment the FECG waves. Using a clinical database, one is able to validate the results obtained in a simulated dataset (e.g. FECGSYNDB). Therefore, a conclusive assessment of how these preprocessing, extraction, and detection methods perform is possible.

Table 5.8: Correlation table for clinical data regarding $WOG < 28$. Asterisk notation show the significance level as significant (*), very significant (**) and highly significant (***). Abbreviations used: position (pos.), consensus (cons.) and visibility (vis.).

(a) Effect size for interval-ordinal and ordinal-ordinal variables (both using ρ)

Parameter	WOG†	amniotic fluid	SNR cons.	FECG cons.
amniotic fluid	-0.28^{***}	–	–	–
SNR cons.	×‡	-0.02	–	–
FECG cons.	×‡	-0.03^{*}	0.14^{***}	–
vis. cons.	×‡	-0.03^{**}	0.18^{***}	0.99

† Before calculating the effect size, repeated terms were excluded.
‡ Don't-care term. Since every channel number is contained in every recording, these correlations shall be further investigated using the RI.

(b) Effect size for nominal-nominal (w) and nominal-ordinal/interval (η) variables

Parameter	channel #	WOG†	placenta pos.	amniotic fluid	fetal pos.
WOG	×‡	–	–	–	–
placenta pos.	×‡	0.99	–	–	–
amniotic fluid	×‡	–	0.07^{***}	–	–
fetal pos.	×‡	0.99	0.42^{***}	0.25^{***}	–
SNR cons.	0.34	–	0.76^{**}	–	0.79^{***}
FECG cons.	0.78^{***}	–	0.30^{***}	–	0.23^{***}
vis. cons.	0.76^{**}	–	0.21^{***}	–	0.14^{***}

Hence, a subset[14] of 24 recordings of viable quality were annotated for MQRS and FQRS locations. These recordings were taken from ten women (both healthy and pathological patients were present), aging from 21 to 33 years (27.1 ± 4.3 years), gestational weeks between 20 and 28 weeks (25.0 ± 2.5 weeks) and duration of 19.4 ± 2.4 minutes, where no significant arrhythmia or ectopic beats have been found for neither mother or fetus. Considering the signal quality annotations presented in the previous section, the selected recordings had different RI indices: six recordings with $RI = 2$, eleven with $RI = 3$, two with $RI = 4$ and five with $RI = 5$. Each recording had its MQRS and FQRS annotated by one and corrected by two other trained specialists. Annotators should use four types of annotations for "visible peak", "likely, yet, not visible peak", "begin" and "end of signal loss interval". The annotation procedure was performed using a JAVA GUI developed at the IBMT. Both software and annotation protocol are detailed in Appendix B. The annotated data totalized 465 min, containing over 67,000 fetal complexes, and was used as gold-standard for evaluating the developed FQRS/FHR detection techniques.

[14] The reason behind the choice for a subset was due to the fact that the annotation procedure is very time-costly. The annotation of a single recording by one expert can take a couple hours. The author assumes if the subset is heterogeneous enough, it may nonetheless provide a good reference for further benchmarks.

5.3 Chapter Summary

In this chapter, the two principal sources of data developed throughout this work were presented. First, motivated by the lack of freely available abdECG databases, in cooperation with the IBME (University of Oxford) a NIFECG simulator was developed, i.e. the so-called FECGSYN (see Section 5.1.1). This versatile toolbox provides means for several types of non-stationary abdominal mixtures and several pathophysiological scenarios. By making use of the FECGSYN, a large open-access database was created (i.e. FECGSYNDB – see Section 5.1.2). Second, together with the project partners at the University Hospital of Leipzig, a clinical trial was conducted and resulted in $n = 259$ NIFECG recordings. The obtained clinical data was statistically characterized in Section 5.2. The overall quality of NIFECG at early WOGs (i.e. < 28 weeks) was shown to be fair. Particularly in this analysis, the dependence between WOG and FECG amplitude was demonstrated. Indeed there is a strong attenuation of the FECG around the 28-32 weeks, which is commonly associated with the vernix caseosa. Another important factor discussed was the influence on electrode location and the power of fetal and noise signals, where depending on the NIFECG application, a mixture of more and less distant electrodes may be considered. Other influencing factors were also evaluated using a bivariate analysis, however, the effects are not conclusive due to the modest size of the clinical dataset. Further analysis should focus on multivariate analysis using a much larger dataset (i.e. at least a couple thousand recordings). In the next chapter, the methods proposed in Chapter 4 are comprehensively benchmarked against several other extraction methods available in the literature, using the produced data material here presented.

I only believe in statistics that I doctored myself

– origin unknown, often attributed to Winston S. Churchill

6 Results for Data Analysis

In the previous chapters, several improvements on current extraction and detection techniques for NIFECG analysis as well as valuable data were produced. In this chapter, these suggested approaches are benchmarked in depth. In order to do so, the present chapter is divided into two main sections, based on the type of analysis performed and data material used. In Section 6.1, the simulated data (i.e. the FECGSYNDB - see Section 5.1.1) was used to benchmark several extraction methods, in terms of FQRS detection and morphological fidelity of NIFECG estimates. In Section 6.2, the best performing methods from each algorithmic category (see Figure 3.4) were applied to the own clinical dataset collected throughout this work (see Section 5.2).

6.1 Simulated Data

The application of simulated data for the purpose of characterizing NIFECG is particularly important, since one can evaluate the different algorithms behavior in the presence of different noise levels, non-stationary artefacts and pathophysiological events. In this section, the FECGSYNDB was used to that end in an analog manner as in Andreotti *et al.* [18]. This database comprises several pathophysiological scenarios, shown in Table 5.1.

6.1.1 Fetal QRS detection

This first experiment consisted of comparing different NIFECG extraction techniques in terms of FQRS detection accuracy. As in [18], single-lead extraction methods were applied to simulated leads 1, 8, 11, 14, 19, 22, 25, and 32 (see Fig. 5.2). In order to produce a fair comparison between BSS and the remaining techniques (AM and TS), results are restricted best outcomes amongst all leads/components. Gross statistics were calculated for evaluating agreement (F_1) and distance (MAE) measures (see Section 3.4.2). A case-by-case overview on

Table 6.1: Case-by-case FQRS results for each extraction method (first column) for FECGSYNDB. Presented cases include "baseline" (i.e. no noise source), "case 0" (i.e. noise), "case 1" (i.e. fetal movement), "case 2" (i.e. heart rate accelerations), "case 3" (i.e. uterine contraction), "case 4" (ectopic beats), and "case 5" (twins). For more information see Table 5.1. Results are shown as median (IQR), best performing method is highlighted in each case.

(a) F_1 (%)

Method	Baseline	Case 0	Case 1	Case 2	Case 3	Case 4	Case 5	Overall
$\mathbf{BSS}_{\text{ica}}$	100.0 (0.3)	99.9 (0.7)	98.2 (8.7)	99.9 (0.1)	85.2 (22.9)	85.4 (3.1)	99.5 (10.7)	99.2 (13.0)
$\mathbf{BSS}_{\text{pca}}$	99.3 (6.6)	98.6 (6.8)	95.2 (8.2)	98.7 (6.2)	86.6 (8.9)	84.0 (4.7)	83.9 (21.7)	92.5 (14.8)
$\mathbf{AM}_{\text{lms}}$	99.6 (5.7)	94.3 (20.4)	94.9 (16.1)	96.3 (16.5)	72.9 (13.6)	82.9 (6.7)	79.8 (26.3)	86.8 (23.7)
$\mathbf{AM}_{\text{rls}}$	99.6 (4.2)	94.8 (19.7)	95.5 (14.9)	96.9 (16)	73.2 (14.0)	83.3 (6.4)	79.8 (26.7)	87.6 (23.7)
$\mathbf{AM}_{\text{esn}}$	98.6 (3.6)	97.4 (7.1)	97.5 (6.6)	98.2 (5.3)	77.4 (12.2)	83.1 (5.4)	83.1 (24.9)	92.9 (17.7)
$\mathbf{TS}_{\text{c}}$	99.8 (3.4)	83.5 (35.3)	92.2 (30.7)	90.0 (33.5)	55.2 (17.4)	80.5 (16.5)	73.2 (29.3)	81.8 (35.8)
$\mathbf{TS}_{\text{pca}}$	100.0 (0.1)	85.9 (36.6)	92.7 (32.2)	92.4 (34.3)	55.6 (16.2)	81.3 (16.4)	73.0 (30.9)	83.1 (37.6)
$\mathbf{TS}_{\text{EKF2}}$	99.4 (2.8)	83.0 (34.7)	91.4 (29.8)	89.7 (33.3)	54.8 (17.5)	76.7 (15.5)	72.7 (27.1)	79.8 (35.5)
$\mathbf{TS}_{\text{vEKF2}}$	99.1 (3.9)	83.1 (34.2)	90.7 (30.6)	88.6 (33.0)	54.7 (16.9)	76.5 (16.2)	72.4 (27.7)	79.6 (35.1)
$\mathbf{TS}_{\text{uiEKF2}}$	95.5 (10.2)	75.5 (31.6)	83.0 (30.8)	80.9 (32.2)	53.1 (16.1)	74.8 (21.1)	68.9 (33.6)	74.9 (34.9)
$\mathbf{TS}_{\text{EKF24}}$	99.8 (0.4)	85.5 (36.5)	92.6 (30.7)	92.3 (34.3)	55.2 (17.6)	77.1 (16.4)	72.6 (28.9)	80.8 (37.6)
$\mathbf{TS}_{\text{vEKF24}}$	99.6 (1.4)	82.3 (35.5)	87.7 (34.2)	90.0 (35.3)	54.6 (16.9)	75.6 (16.2)	71.6 (26.5)	78.8 (37.1)

(b) MAE (ms)

Method	Baseline	Case 0	Case 1	Case 2	Case 3	Case 4	Case 5	Overall
$\mathbf{BSS}_{\text{ica}}$	4.0 (1.0)	4.0 (0.9)	4.0 (1.2)	4.0 (0.1)	4.6 (2.7)	4.3 (1.1)	4.0 (0.3)	4.0 (1.0)
$\mathbf{BSS}_{\text{pca}}$	4.1 (1.9)	4.2 (1.8)	4.5 (1.8)	4.0 (1.4)	4.6 (1.7)	4.8 (1.7)	4.2 (2.0)	4.3 (1.6)
$\mathbf{AM}_{\text{lms}}$	3.9 (2.0)	4.1 (1.9)	4.0 (0.7)	3.9 (0.6)	5.9 (1.9)	4.6 (1.5)	4.2 (1.5)	4.2 (1.7)
$\mathbf{AM}_{\text{rls}}$	3.8 (2.3)	4.0 (1.9)	4.0 (0.9)	3.9 (0.7)	6.0 (1.9)	4.6 (1.5)	4.3 (1.5)	4.2 (1.8)
$\mathbf{AM}_{\text{esn}}$	3.9 (1.9)	3.8 (1.6)	3.8 (0.7)	3.7 (0.6)	5.3 (1.6)	4.3 (1.2)	3.9 (1.2)	4.0 (1.4)
$\mathbf{TS}_{\text{c}}$	4.0 (1.9)	4.2 (2.5)	4.2 (0.7)	4.2 (0.7)	8.2 (3.1)	5.1 (2.1)	4.4 (2.3)	4.4 (2.6)
$\mathbf{TS}_{\text{pca}}$	4.1 (2.0)	4.3 (2.5)	4.2 (0.9)	4.2 (0.8)	8.3 (2.9)	5.0 (2.1)	4.4 (2.4)	4.5 (2.8)
$\mathbf{TS}_{\text{EKF2}}$	3.9 (1.9)	4.0 (2.4)	3.9 (0.8)	3.9 (0.7)	8.1 (3.2)	5.1 (1.9)	4.2 (2.4)	4.3 (2.7)
$\mathbf{TS}_{\text{vEKF2}}$	3.9 (1.9)	4.1 (2.3)	4.1 (0.8)	4.0 (0.7)	8.3 (3.1)	5.3 (2.1)	4.3 (2.5)	4.5 (2.8)
$\mathbf{TS}_{\text{uiEKF2}}$	5.1 (4.3)	6.1 (4.7)	4.7 (3.5)	4.8 (3.9)	9.0 (5.2)	5.5 (3.4)	5.6 (6.6)	5.7 (5.0)
$\mathbf{TS}_{\text{EKF24}}$	3.9 (2.0)	4.1 (2.3)	4.0 (0.8)	4.0 (0.7)	8.2 (3.0)	5.3 (1.9)	4.3 (2.3)	4.4 (2.7)
$\mathbf{TS}_{\text{vEKF24}}$	4.0 (1.7)	4.3 (2.4)	4.1 (1.0)	4.2 (0.8)	8.6 (3.2)	5.5 (2.1)	4.5 (2.6)	4.5 (2.8)

each method's performance is shown in Table 6.1. The highest median F_1 for each category of methods was achieved by $\mathbf{BSS}_{\text{ica}}$ (99.2%), $\mathbf{AM}_{\text{esn}}$ (92.9%) and $\mathbf{TS}_{\text{pca}}$ (83.1%). MAE results for most methods were similar. Figure 6.1 provides detailed view considering both metrics (F_1 and MAE) for each technique, cases and SNR levels. Using a Kruskal-Wallis test, a significant effect of the SNR was found for most AM and TS methods, but not for BSS techniques (see Fig. 6.1). Using a two-tailored Friedman test, the effect of the different cases and methods considering each SNR level was separately evaluated. Regarding F_1, low SNRs (i.e. 0 or 3 dB) exhibited extremely significant ($p < 0.001$) differences between cases; highly significant ($p < 0.01$) for intermediate SNRs (6, 9 dB); whereas for a high SNR (12 dB) no significant difference was found ($p > 0.05$). Regarding MAE, extremely significant differences were found in most SNR levels (0, 6, 9, 12 dB) aside from for $SNR = 3$ dB, where it was highly significant. Similarly, the effects of different methods were tested and indicated extremely significant differences on every SNR level for both F_1 and MAE. At last, a post hoc test was performed using the Sign test for evaluating paired differences between methods (shown in Fig. 6.2).

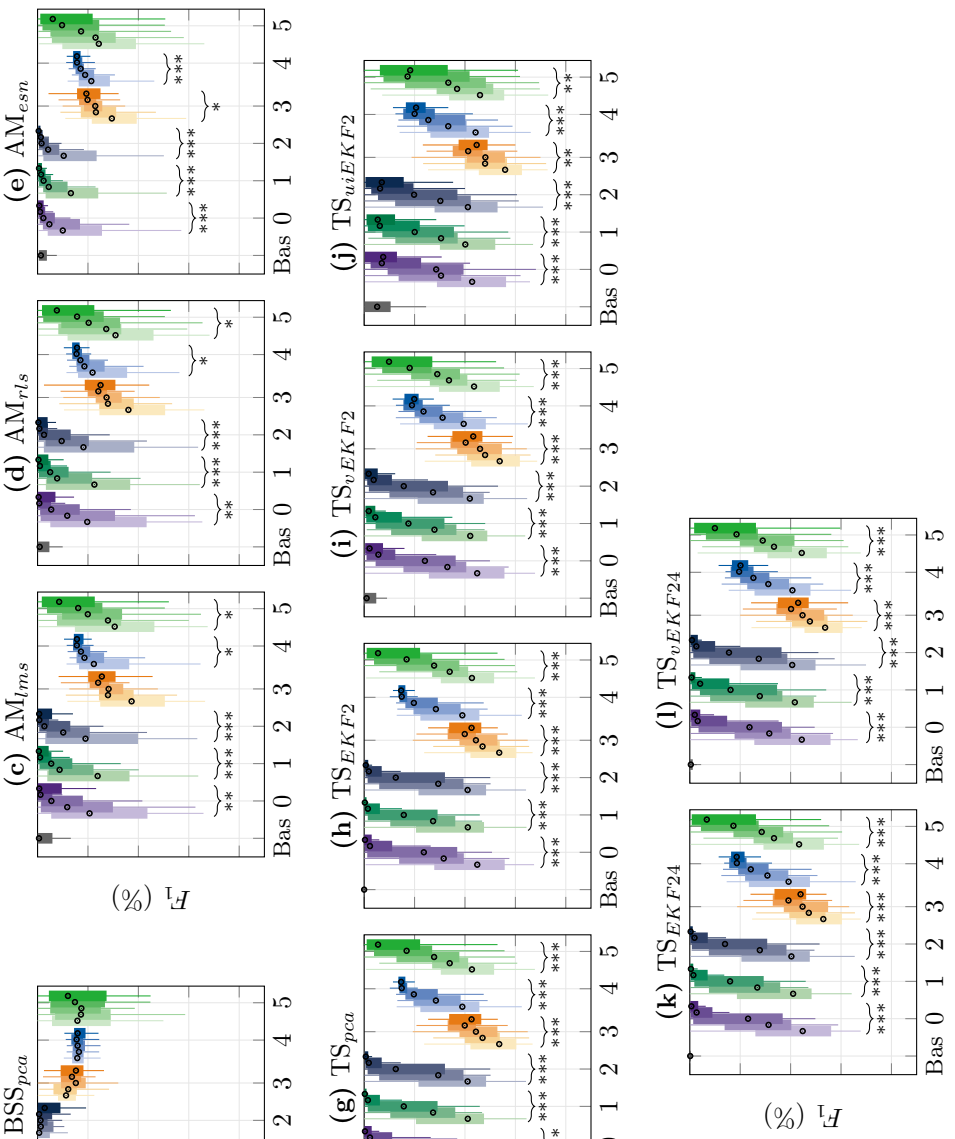

Figure 6.1: Detailed F_1 results for FQRS detection accuracy using different extraction methods. For each case (*x*-axis) there are 5 boxplots, one for each SNR level (improving from left to right), portrayed using different colors contrasts (the darker its contrast, the higher is the SNR). A Kruskal–Wallis test was performed to evaluate statistically significant differences across different SNR levels, where * indicates $p < 0.05$, ** $p < 0.01$ and *** $p < 0.001$. Outliers were omitted for visualization purposes.

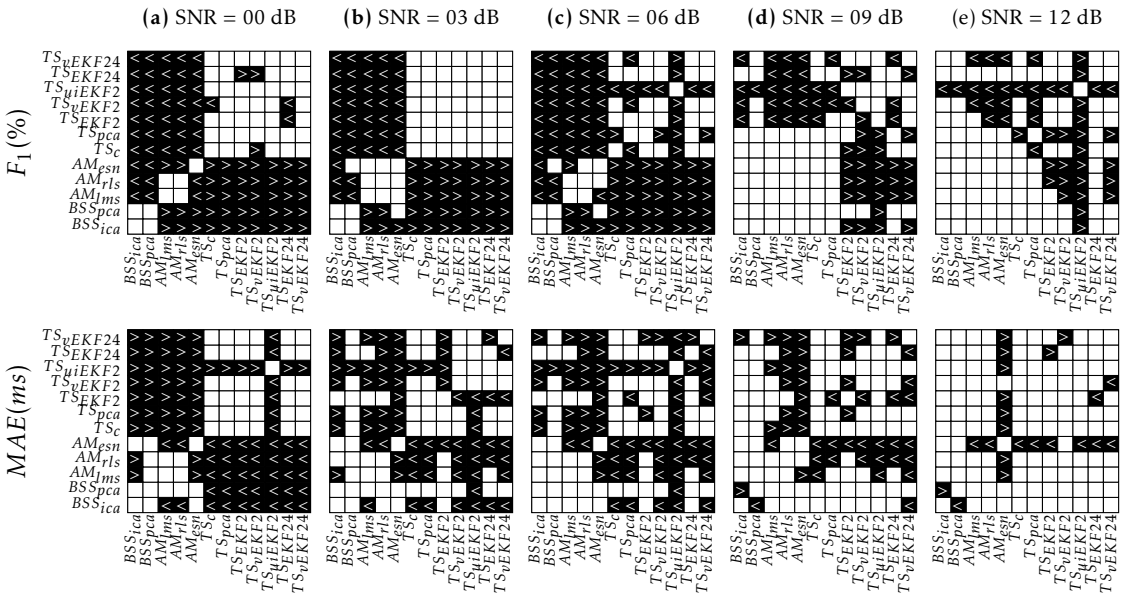

Figure 6.2: Post hoc analysis for FQRS detection accuracy, performed using the Signed test across extraction methods. The first row shows tests regarding F_1, while the second MAE. For this analysis, the Baseline case was excluded due to its independence of the SNR level. Black squares accuse highly significant differences ($p < 0.01$) and white non-significant ($p > 0.5$). Arrows indicate the direction of these significant differences as in Fig. 5.10.

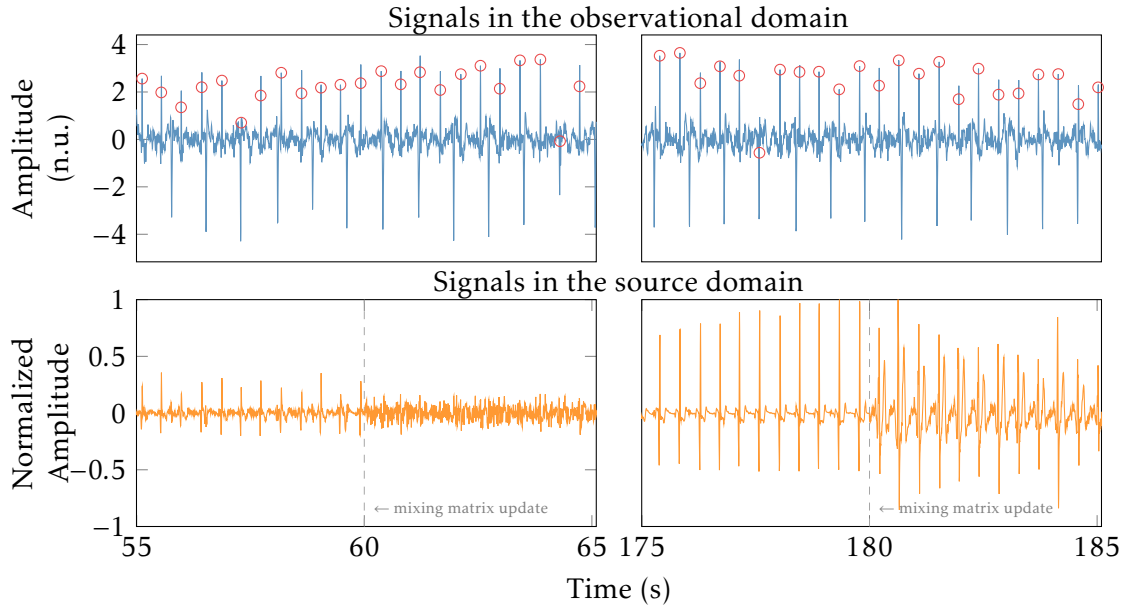

Figure 6.3: Two exemplary segments are portrayed during which **BSS**$_{\text{ica}}$'s mixing matrix is updated (i.e. at 60 s and 180 s - dashed line) for a dataset containing fetal movement. Depicted above are the abdominal mixtures for channel 14, below are the selected components with highest F_1, 8 channels were used as input. The plots on the first row depict abdominal mixture and FQRS locations (marked with ○), the ones in the inferior row show the selected BSS$_{ica}$ components.

6.1.2 Morphological analysis

Morphological analysis aims at assessing how accurate morphological features (described in Section 3.6) can be obtained. As in Andreotti *et al.* [18], the presence of noise and effects of the different NIFECG extraction methods on the estimated morphological measures were assessed. For providing a meaningful pathophysiological analysis and clearer presentation of the results, we concentrate on a subset of the database containing baseline and case 0 (noise only). These cases are similar in the sense that the baseline can be considered as a case 0 with infinite SNR, since no noise is present.

Figure 6.3 displays excerpts of independent components (output from $\mathbf{BSS}_{\text{ica}}$) around segments where the mixing matrix was updated. The dataset presented in this figure includes a highly non-stationary event (case 1 - fetal movement) and demonstrates the expected difficulties of analyzing the morphology in case of non-stationarities. Due to the current state of signal processing techniques to fetal morphological analysis, several beats were excluded either during template generation, segmentation using *ecgpuwave* [203] or due to distortions by the extraction methods. The percentage of excluded beats increased with an decrease in the SNR level ranging from 8 to 78% for TS methods, 19 to 48% for AM, meanwhile it was relatively constant for BSS (14-20%). For performing a fair comparison on the morphological trustworthy, only segments on which template beats could be obtained across all methods were used in our further analysis. Therefore, the number of usable beats monotonically decreased from 69.7% on the baseline case to 11.6% on case 0 (with 0 dB noise) [18].

Figure 6.4 and 6.5 exhibit the correlations between FQT intervals and FTQRS obtained in the FECG reference and extracted channels in the presence and absence of noise. In these figures the methods with best coefficient of determination (r^2) from each class of methods are presented as well as selected Kalman filter variants. The median FQT/FTQRS was taken across all channels and segments which could be obtained for all methods. An overview on the results in terms of $\widetilde{FQT}$ and $\widetilde{FTQRS}$ for different methods, SNR levels and cases (baseline and case 0) is presented in Fig. 6.6. Similarly to the analysis in the previous experiment, the difference between median results was statistically tested (see Fig. 6.6). In this figure, a Kruskal-Wallis test was performed in evaluating if differences in the median $\widetilde{FQT}$ and $\widetilde{FTQRS}$ results for the various SNR levels were significant. It has to be kept in mind that the percentage of missing templates due to failed segmentation or failure in construction is not represented on these plots and increase with a decreasing SNR.

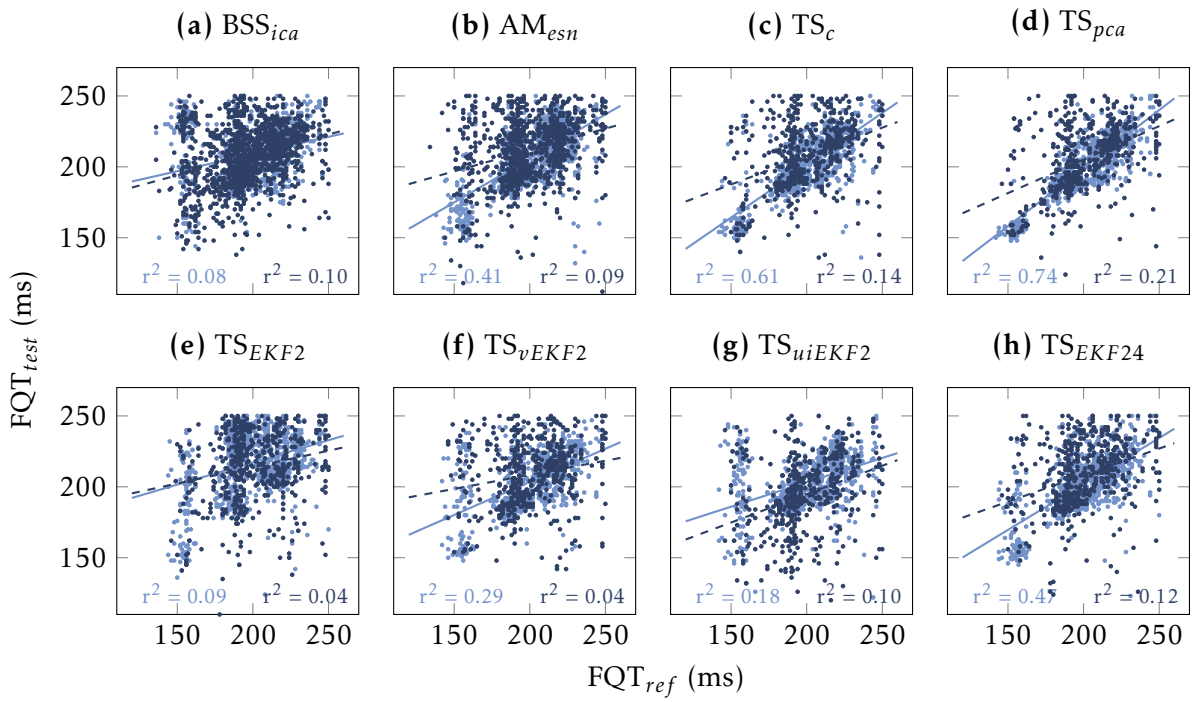

Figure 6.4: Differences in measured FQT intervals between extracted channels/components (FQT$_{test}$) and reference propagated FECG signal (FQT$_{ref}$). Extraction methods with highest coefficient of determination (r^2) for each category are shown as well as selected Kalman filter variants. Results are shown for the baseline (lighter colors, solid lines) and case 0 with SNR = 0 dB (darker colors, dashed lines).

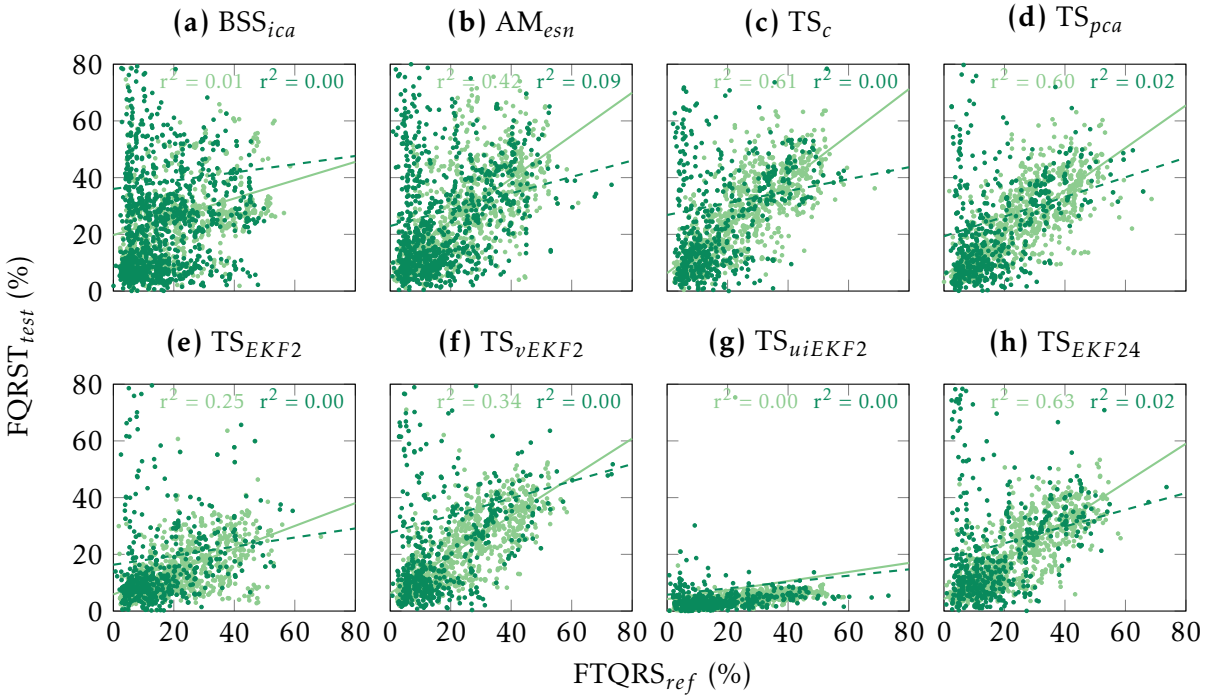

Figure 6.5: Differences in measured FTQRS ratios between extracted channels/components (FTQRS$_{test}$) and reference propagated FECG signal (FTQRS$_{ref}$). Results are presented in an analogous fashion as in Figure 6.4.

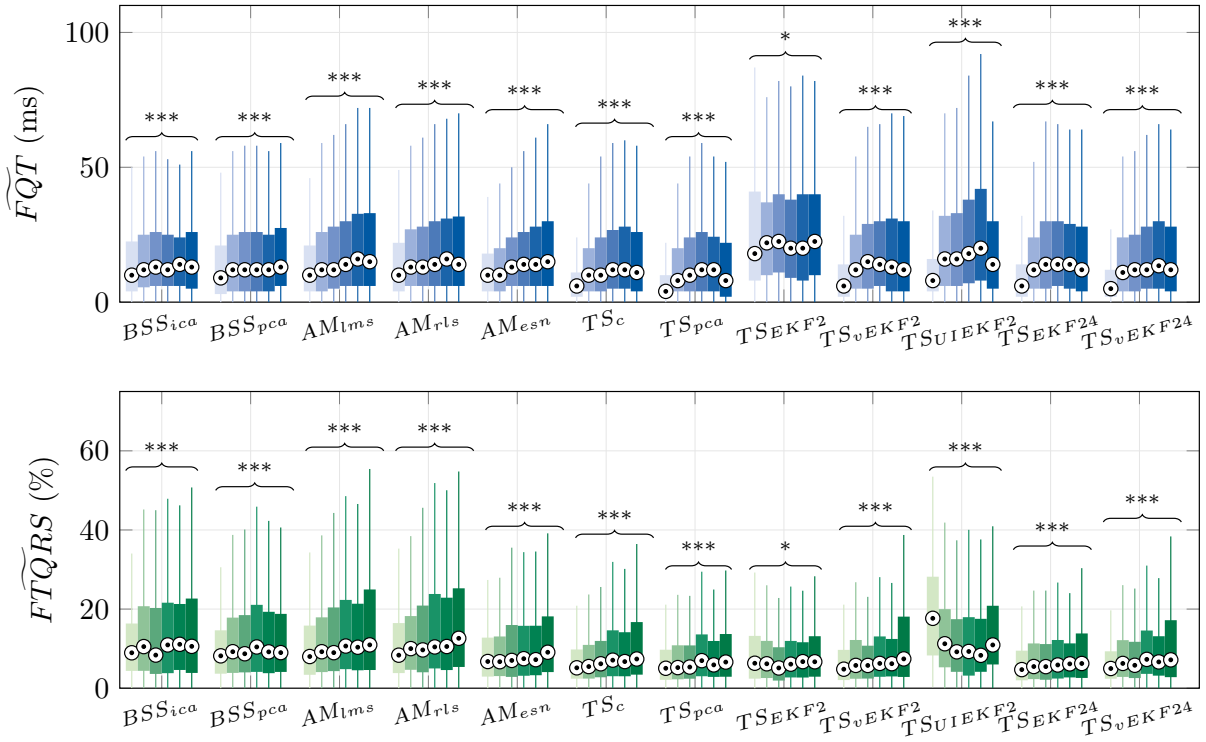

Figure 6.6: Accuracy of FQT and FTQRS extraction for the different methods and when considering different SNR levels (decreasing from left to right, i.e. baseline case furthest to the left). A Kruskal–Wallis test was performed to evaluate significant differences across varying SNR levels. Outliers were omitted for visualization purposes.

6.2 Own Clinical Data

Independent of how realistic the simulations with the FECGSYN are, the use of clinical data enables the assessment of signal processing algorithms under real circumstances. This is necessary, for example when one wishes to evaluate the actual quality of FECG signals. In this section, both FQRS and FHR correction methods, introduced in Section 4.3, are evaluated using the clinical data collected throughout this work, described in Section 5.2.

6.2.1 FQRS correction using the evolutionary algorithm

In order to assess the performance of the eQRS algorithm, the subset containing 24 recordings (see Section 5.2.4) was used. In Table 6.2 the results for SE, PPV, F_1 and MAE (described in Section 3.4.2) are presented. The eQRS was applied to 1, 3, and 7 abdominal channels. The 3-lead scheme comprised the internal leads (see electrode configuration on Fig. 5.4). Figure. 6.7 provides a qualitative example of the resulting corrected FQRS using the proposed eQRS on three channels. Figure 6.8 additionally presents the extraction results for **BSS**$_{ica}$ when 3, 4, and 7 leads from the clinical recording is used as input for ICA.

Table 6.2: Results for FQRS detection accuracy and precision using the eQRS correction algorithm. "Initial" detections denote simple FQRS detections (*maxsearch* algorithm) used to initialize the eQRS routine. "Best" represents the best results considering all available channels (e.g. maximal F_1 or minimal MAE). The best F_1 and MAE results in each category are underlined.

	Method	initial	1 channel	3 channels	7 channels	initial (best)	1 channel (best)
$\mathbf{BSS_{ica}}$	SE (%)	25.7±7.9	21.9±14.7	24.3±13.6	22.6±15.6	31.9±9.3	33.3±20.3
	PPV (%)	28.7±6.5	26.1±14.8	30.5±12.1	30.9±15.6	32.9±19.2	38.5±19.6
	F1 (%)	26.8±7.5	23.7±14.7	26.9±12.9	24.9±15.6	32.0±9.4	35.5±20.0
	MAE (ms)	20.5±2.8	21.4±5.0	20.5±5.2	20.9±5.6	17.5±2.7	17.0±5.9
$\mathbf{AM_{esn}}$	SE (%)	51.6±22.1	79.7±23.8	74.5±22.5	96.5 ±6.3	69.8±19.7	97.2±4.7
	PPV (%)	53.2±21.9	78.9±23.5	83.6±22.2	95.8 ±5.5	70.6±19.2	96.1±5.0
	F1 (%)	53.4±22.0	79.3±23.6	84.0±22.3	96.2 ±5.8	70.1±19.5	96.6±4.8
	MAE (ms)	13.8±5.5	8.2±4.8	7.3±5.5	4.4±2.2	8.5±4.0	4.7±2.0
$\mathbf{TS_{pca}}$	SE (%)	60.6±21.4	81.3±24.9	81.8±26.6	98.3±4.7	79.8±15.0	99.4±0.5
	PPV (%)	60.8±21.3	80.5±24.7	81.0±26.5	97.3±5.0	79.4±15.0	98.4±1.7
	F1 (%)	60.7±21.4	80.9±24.8	81.4±26.5	97.8±4.8	79.6±15.0	98.9±1.0
	MAE (ms)	11.4±5.6	7.4±4.9	7.3±5.5	4.9±1.8	6.3±3.1	4.2±1.6
$\mathbf{TS_{EKF24}}$	SE (%)	56.0±21.4	79.3±24.7	80.2±27.3	98.9±1.9	76.0±16.0	98.9±1.8
	PPV (%)	56.6±21.4	78.5±24.5	79.4±27.0	97.9±2.6	76.4±15.4	97.8±2.4
	F1 (%)	56.3±21.4	78.9±24.6	79.8±27.1	98.4±2.1	76.2±15.7	98.3±2.0
	MAE (ms)	12.9±5.4	7.7±5.0	7.7±5.84	5.1±2.1	7.4±3.2	4.4±1.6

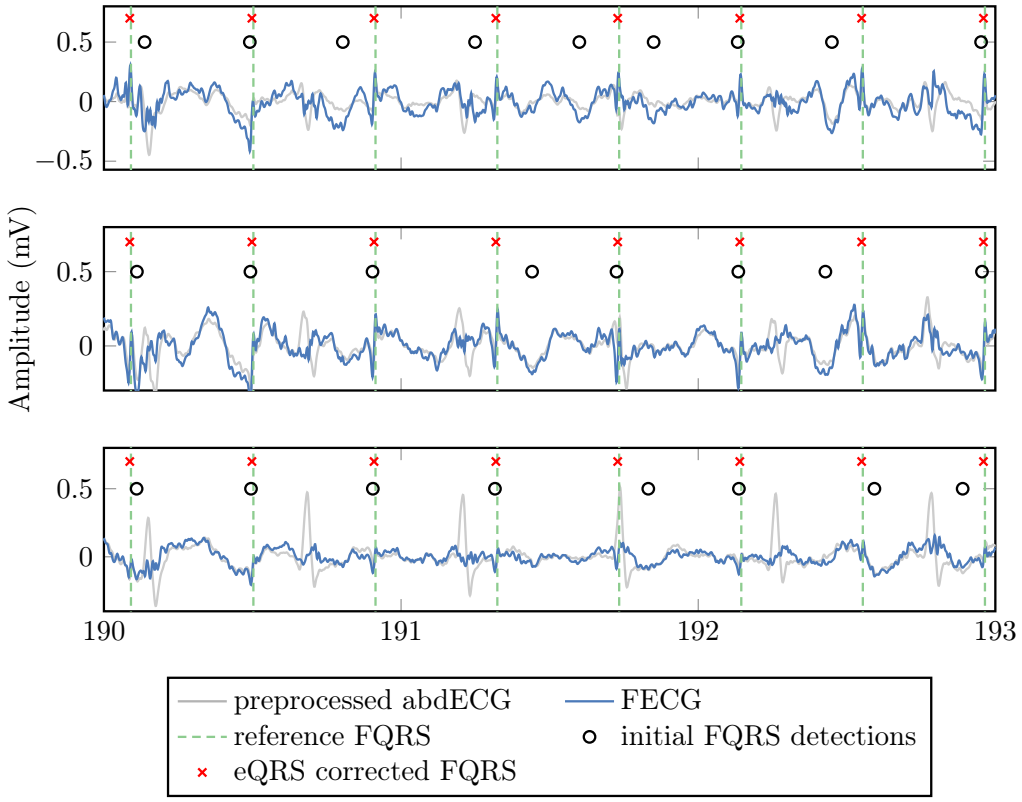

Figure 6.7: Evolutionary QRS correction using three channels and the $\mathbf{AM}_{esn}$ extraction method on three abdominal leads. Each lead presents fairly different signal qualities and initial detections.

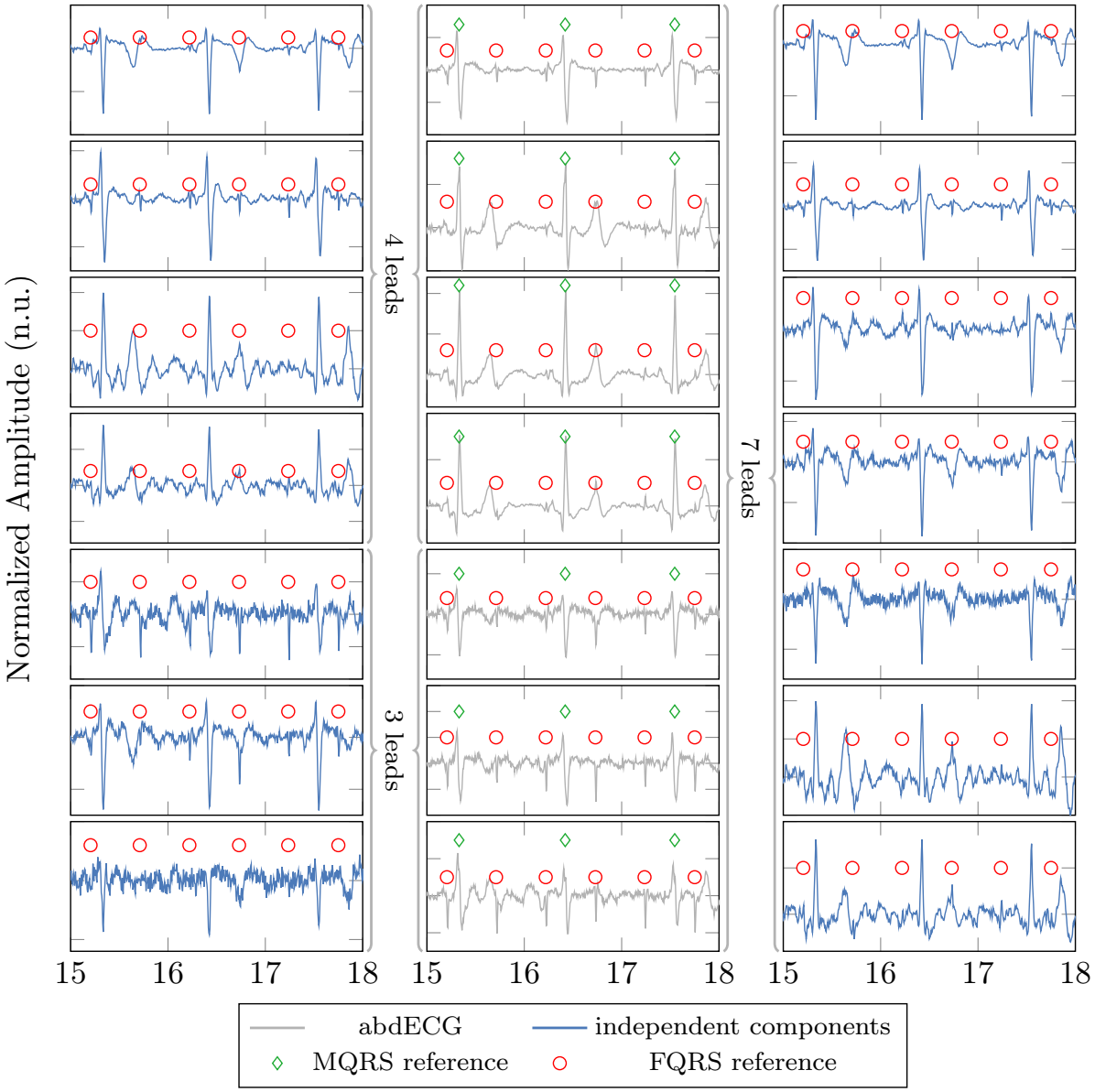

Figure 6.8: Excerpt of clinical signals extracted using $\mathbf{BSS}_{ica}$. Abdominal channels 1 to 7 are presented in the middle column. Extracted signal variants with 4 (external - see Fig. 5.2) and 3 (internal leads are presented on the left, while the 7-lead $\mathbf{BSS}_{ica}$ extracted components on the right column. The braces clarify which abdominal signals lead to which independent components.

6.2.2 FHR correction by means of Kalman filtering

In this section, the results of the methodology for SQI assessment and FHR estimation are presented, as described in Section 4.3.2 and in [19]. The SQI assessment accuracy was performed using the large annotated database containing 9,650 segments (see Section 5.2.3), while FHR accuracy was evaluated on the subset of 24 recordings annotated for FQRS location (see Section 5.2.4).

SQI evaluation

The overall classification accuracy in predicting the 5 classes using the cross validation scheme for the Naive Bayes classifier was $\alpha = 0.65 \pm 0.04$ (i.e. good) and $\kappa = 0.44 \pm 0.03$ (i.e. moderate). The resulting confusion matrix is presented in Table 6.3). Figure 6.9 provides an initial intuition on the behaviour of different types of SQI features during the presence of muscular noise and maternal ectopic beat [19].

Table 6.3: Resulting confusion matrix for the 10-fold cross validation.

		Predicted Class				
		A	**B**	**C**	**D**	**E**
Actual Class	**A**	6434	371	256	78	16
	B	274	378	76	149	33
	C	158	167	139	116	47
	D	18	63	10	101	116
	E	0	3	2	13	47

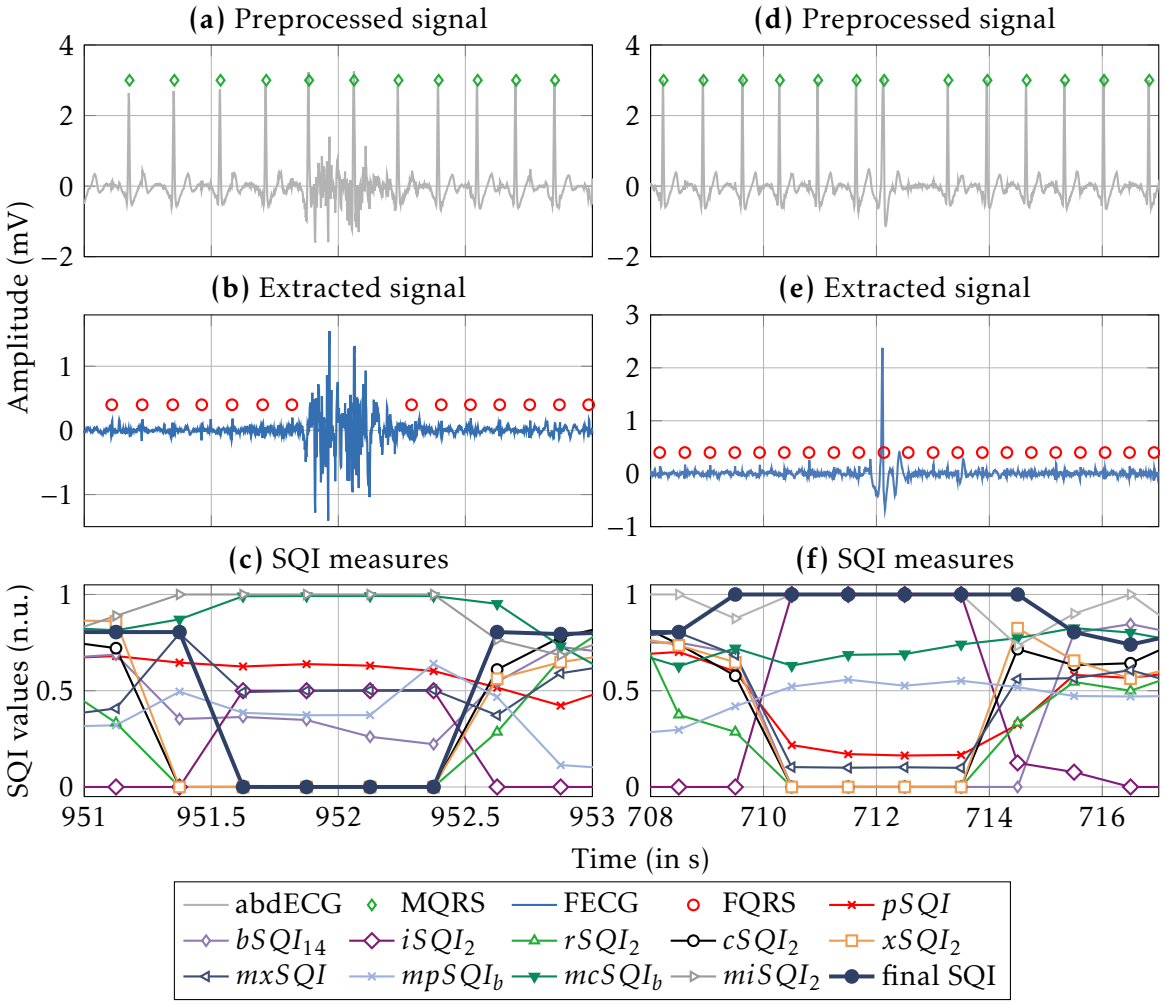

Figure 6.9: Segments of clinical data comprising SQI metrics. On the left column a sudden muscular artefact is portrayed at time 952.5 s. The right column shows the effects of a maternal ectopic beat occurring around 712.0 s.

In order to obtain a further insight into the importance of individual variables independent from the applied classifier, the RELIEFF filter method [234] was applied (see Fig. 6.10). This algorithm, often employed for feature selection, assigns weights to the individual features according to their class separation capabilities. The number of nearest class hits and misses the algorithm considered during weight computation was set to $k = 50$ nearest neighbors of each class (approximately the number of observations on the lowest frequent class) and prior was defined as uniform, so that our analysis does not depend on the presented class distribution (as fetal signal quality may depend on several factors, e.g. gestational week) [19]. For demonstrating the correlations amongst different features, the correlation matrix using the Kendall coefficient is presented in Fig. 6.11.

FHR evaluation

The single channel FHR results before and after applying Kalman filter, as well as multichannel outcomes are presented in Table 6.4. For completeness, the proposed fusion scheme was compared with a weighted average of individual Kalman filtered channels by using their SQI values. For evaluating the information obtained from the different leads, this procedure was divided into a 3-channel (i.e. using the internal leads configuration), 4-channel (i.e. circular lead system around abdomen) and 7-channel (i.e. all leads). An ideal best possible result is shown by always selecting the channel with maximal HDR and minimal RMSE before and after KF processing. An example of the FHR estimation using KF algorithm and classified SQI is shown in Fig. 6.12.

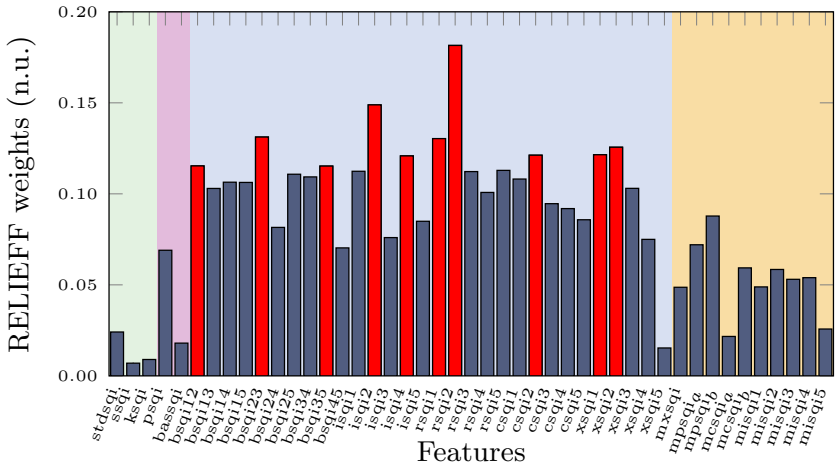

Figure 6.10: Bar graph showing the feature importance using RELIEFF. The different background colors on the graphic denote the different groups of SQI metrics presented in Table 4.2, while the 10 features with highest results are emphasized.

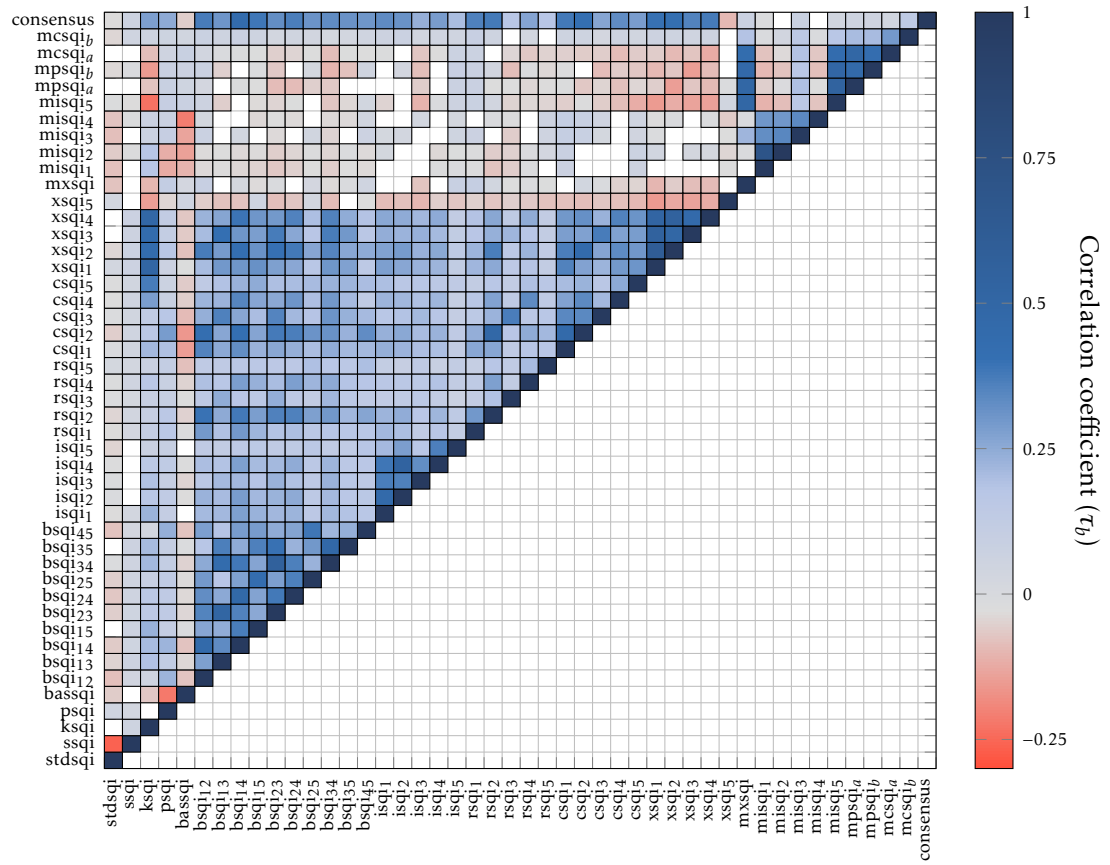

Figure 6.11: Correlations amongst SQI proposed features and annotated consensus ("consensus") using Kendall's τ_b coefficient. Blank spaces represent non-significant correlations (i.e. $p > 0.05$). The matrix is of course symmetric, the repeated occurrences are omitted.

Table 6.4: Performance comparison using proposed KF technique in terms of FHR accuracy ((*a*) HDR) and precision ((*b*) RMSE). Results presented as average ± standard deviation. The best mean results in each category are underlined.

(a) HDR results (in %)

Method	**3 channels**	**4 channels**	**7 channels**
single channel average (without KF)	54.4±16.2	58.5±14.5	56.7±13.5
single channel average (with KF)	59.1±14.4	63.9±12.1	61.8±11.5
multichannel weighted average (using SQI and KF)	61.8±18.0	71.6±16.6	75.0±14.1
proposed multichannel KF	<u>64.2±16.0</u>	<u>73.8±15.0</u>	<u>75.6±13.4</u>
best individual channel (without KF)	59.3±17.4	69.3±17.7	71.2±16.7
best single channel (with KF)	65.0±14.6	75.7±13.0	77.0±12.3

(b) RMSE results (in ms)

Method	**3 channels**	**4 channels**	**7 channels**
single channel average (without KF)	15.5±4.7	14.3±4.2	14.8±4.0
single channel average (with KF)	14.4±4.2	13.1±3.7	13.6±3.6
multichannel weighted average (using SQI and KF)	13.9±5.0	11.4±4.2	10.8±4.0
proposed multichannel KF	<u>13.3±4.6</u>	<u>10.8±4.1</u>	<u>10.5±4.0</u>
best individual channel (without KF)	14.2±5.0	11.5±4.9	11.1±4.7
best single channel (with KF)	13.0±4.5	10.1±4.1	9.8±4.0

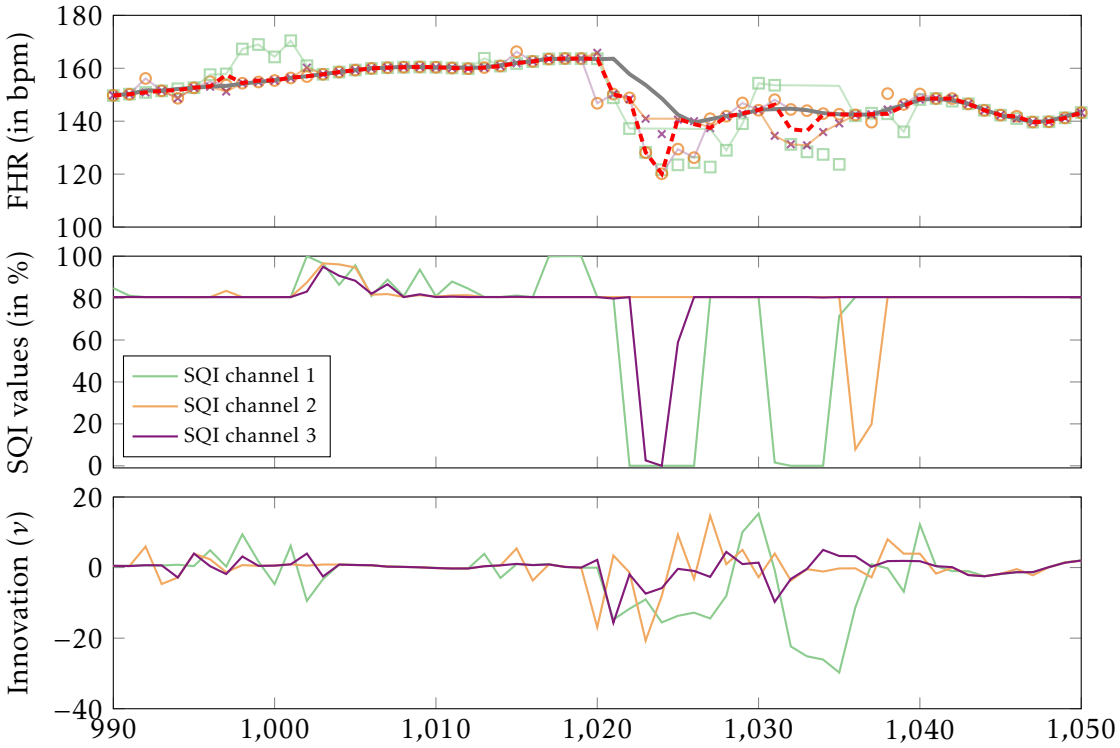

Figure 6.12: Example multichannel FHR estimation by means of Kalman filtering using three channels. Above FHR estimation is shown with the reference FHR (——), estimated multichannel FHR (----), single channel rough FHR estimates (○ , □ and ×) and the respective single channel Kalman filtered estimates (—— , —— and ——). Below are presented the respective SQI values for the 3 channels used.

So, if she weighs the same as a duck, then she's made of wood.
And therefore... A WITCH!

– Monty Python and the Holy Grail (1975)

7 Discussion and Prospective

As demonstrated throughout this work, NIFECG is a topic of ongoing research, whose promising initial results have culminated on the emergence of a first generation of commercial monitors (described in Section 3.2.2). However, there are several important aspects that need to be further investigated before NIFECG becomes a clinical standard in continuous fetal monitoring (see Chapter 2 and Behar *et al.* [51] for details). In the next sections, the main results of this thesis as well as suggestions for future research are discussed.

7.1 Data Availability

The currently available databases for NIFECG analysis were presented in Section 3.2.4. As described in this section, these datasets are very limited in size and spectrum of pathophysiological conditions they contain. With the purpose of making NIFECG analysis more accessible, objective and reproducible, in Chapter 5 the FECGSYN simulator (see Behar *et al.* [50]) and FECGSYNDB (see Andreotti *et al.* [18]) simulated database were developed in this work. This large simulated database can be used to train extraction and detection algorithms with a wide number of non-stationary events (see Section 5.1), which in clinical settings are difficult to collect/quantify. The increasing number of researchers using the developed platforms (and consequent citations to the respective work [18, 50]) are proof of their usefulness.

Still, to demonstrate NIFECG's efficacy, multi-center randomized clinical trials are necessary. With respect to reproducibility, a more comprehensive open access medical database of NIFECG signals is highly desirable (as described in [51]). Similar to the largely available adult QT [98, 239] and arrhythmia databases [286], such dataset would to allow researchers to rapidly discredit unreliable clinical metrics such as the recent case of FTQRS in invasive FECG monitoring (presented in Section 3.1) and allow that automated approaches to analyze FHR/FHRV tracings are compared. This clinical trial/database should comprise different gestational ages (to capture

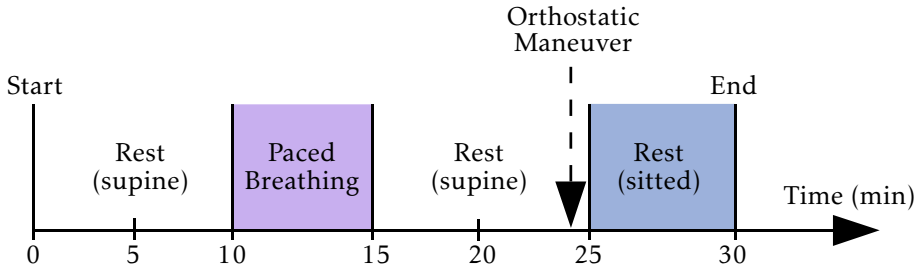

Figure 7.1: Timeline for new measurement protocol.

the physiological changes that take place during pregnancy - see Section 2.1), pathological groups (e.g. IUGR, PROM and fetal anemia - see Section 2.2), physiological events (such as uterine contraction and MHR/FHR accelerations) and fetal behavioral states (see Section 2.1.6). Another aspect to consider when developing such databases, is the use of input signals such as paced breathing and orthostatic maneuvers during part of the recordings. As detailed in Section 2.1.6, several external factors can influence the heart activity, thus, such techniques could be applied to discriminate between pathological or physiological responses (e.g. through FHRV changes as in [443]). The use of these additional arousals would lead to the necessity of a multimodal study comprising e.g. respiratory or BP signals. Reference signals such as CTG or FSE should serve as reference for confirming the validity of NIFECG recordings. Additionally, during intrapartum periods the usability of EHG as a substitute to CTG's pressure transducer should be confirmed by concomitantly measuring both signals. Lastly, medical expert annotations for both FQRS locations and morphological features are of great importance to validate this methodology [51]. Similarly, additional patient background information on the maternal psychological state would further enable studying these states with the fetal development/heart activity e.g. [115, 226, 285, 285]. Lastly, information on the pregnancy outcome such as Apgar scores and umbilical cord blood sampling for pH and base deficit/excess and lactate (see Section 3.1.2) as well as follow up on the newborns first year(s) of life may provide insights on the clinical value of NIFECG.

Considering the lack of available data, in cooperation with the project partners at the University Hospital of Leipzig, an exploratory clinical trial was designed and performed during this work (presented in Section 5.2). Despite its modest size (n = 259 recordings), provided some interesting insights on the nature of the fetal signal, as well as valuable data material for further signal processing analysis. With the obtained experience in collecting NIFECG at hand, an improved protocol was implemented, here presented as future work in the following section.

7.1.1 New measurement protocol

With the goal of producing a more comprehensive dataset, since November 2014 a new measurement protocol was installed at the University Hospital of Leipzig. Whilst the successful abdECG and chest lead configuration (see Fig. 5.4) was maintained as well as the ADC device, several other sensors were added to the setup including:

- **respiration belt:** placed around thorax on the breast area;
- **finger PPG sensor:** applied on the right hand's index finger;
- **continuous blood pressure:** using the Finometer MIDI (Finapres Medical Systems B.V., Amsterdam, Netherlands), applied on the left middle finger as specified by manufacturer. The Finometer was calibrate before each recording and auto-calibration took place on every couple seconds;
- **hand-held Doppler:** model AngelSounds JPD-100S (Jumper Medical, Shenzhen, China), the probe was carefully positioned and hold by recording expert during the whole recording while attempting to minimize movement and contact with the abdominal electrodes, while maximizing the audible FHR sound.

In order to make the recordings more reproducible, a GUI was developed to guide the medical expert throughout the measurement. This GUI was developed in JAVA programming language and is described in Appendix C. In order to observe fetal cardiac response to external arousals, the novel recording protocol consisted of periods of rest and the performance of both paced breathing and orthostatic maneuvers (see Figure 7.1). Based on [443] a breathing rate of 20 cycles/min was chosen, using the aforementioned GUI audible cues were given to "breath in" and "breath out" during a 5 min phase. Obviously, when dealing with pregnant women (often unwell patients) these maneuvers have to be as quotidian as possible. For this reason, as orthostatic maneuver the choice was for natural everyday movement, where the subjects were asked to change their position from supine into sitting position themselves.

On a preliminary study [276] comprising 16 initial recordings, no statistical difference between the mean FHR for spontaneous and pace breathing was found. However, this may be attribute to 1) the choice of breathing rate, which was found to be very similar to the normal rate for pregnant women (generally for adults at rest is around 13 cycles/min, but higher for pregnant women); and 2) the small number and general low quality of the available recordings (ca. 20.5 % had visible FQRS peaks). Another feasibility study [415] using the same dataset has shown a significant change in BP despite the subtleness of the performed maneuver. Similarly, a significance test expressive short-term changes ($\approx$ 1 min after maneuver) and long-term changes ($\approx$ 3 min after maneuver) on the average FHR. An unexpected result was the clear decrease on FECG quality that reduced FQRS visibility from 20.5 % (before maneuver) to 4.4 % (after maneuver). This may be attributed to changes on the position of maternal organs and strong muscular artefact due to movement. However, as in the previous study, due to the limited data available the results have to be considered with care. Nonetheless, this initial knowledge is an important preliminary step before for the actual clinical trial that should follow. With the limitations of current databases in mind, this data should be prospectively made freely available at Physionet [161].

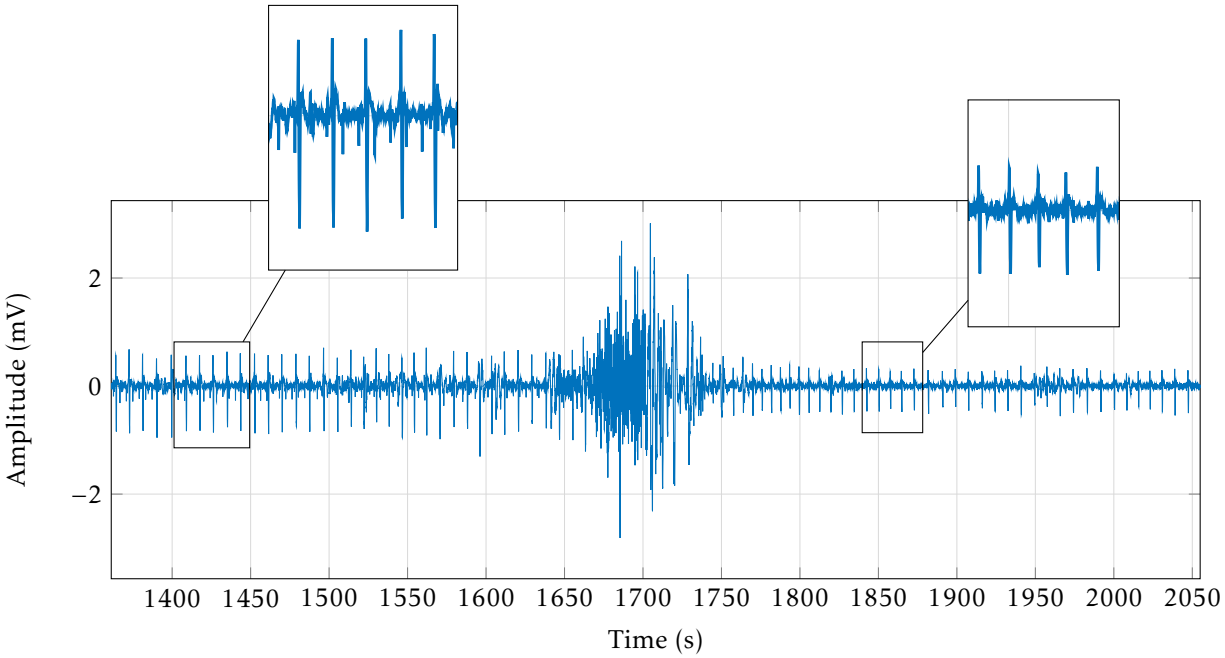

Figure 7.2: Exemplary segment of new measurement protocol. At 1700 s the subject was asked to sit as part of the orthostatic maneuver. FECG complexes are clearly visible prior to maneuver, but less so after it. Moreover, a clear amplitude change is visible.

7.2 Signal Quality

The quality of the NIFECG signal is a matter of great concern. Throughout Section 5.2.3 of this work the collected clinical data was used in assessing the relationships between the signal quality and several pathophysiological variables. The signal quality was shown to widely depend on the gestational age (see Figs. 5.11 and 5.12), channel number (see Figs. 5.9 and 5.10) and other pathophysiological factors such as placental and fetal positions (see Table 5.8). Few works in the literature have addressed this topic in such depth, most of which are limited to high WOG and intrapartum periods. A review on these studies is shown in Section 3.2.5, however most of those make use their own metrics of signal quality or FHR detectability that impede a quantitative comparison. Qualitatively, the trend in FHR success in [333, Fig.9] is consistent with the results obtain in this study (Figs. 5.11 and 5.12), where a much lower FECG quality is present around the 28^{th}-36^{th} WOG period. This decrease in quality is associated with the appearance of the vernix caseosa as explained in Section 2.1.3. Regarding physiological factors that may affect quality, the absence of correlation between BMI and signal quality was also reported by [163, 439], but contradicted by [446].

As described in Section 5.2.2, the partnership with the University Hospital of Leipzig focuses on gestational ages below 28 weeks. During this period, risk pregnancies should be closely monitored due to the higher risk of premature mortality. This is particularly important e.g. when premature PROM occurs, since after the rupture of membranes patients usually remain stationary for a period that may extend to weeks. In these cases, NIFECG continuous monitoring

could significantly improve patient's comfort. However, concerns about the quality of the obtained NIFECG have hampered such approach. In an attempt to better characterize such signals, the analysis presented in Section 5.2.3 is partially direct to this period (shown in Table 5.8). For instance, placental position was found to correlate with both SNR and FECG amplitude, which could be due to its higher relative permittivity. Fetal presentation is also important, since it goes along with electrode configuration, therefore, with signal quality. In this study a strong and highly significant dependency was found between fetal position and SNR ratio and fetuses in vertex position have shown higher FECG amplitude. Despite our dataset being larger than that of most the referred studies, the described statistical results must be considered with care since the population involved in this exploratory study is limited for the broad spectrum of pathophysiological conditions of its patients. The author re-iterates the importance of a large randomized clinical study to verify the true nature of these relationships. Aside from the aforementioned associations, the inter-subject dependency should be regarded [1]. Similarly, a more comprehensive multivariate analysis could provide insights on the associations between multiple variables e.g. the influence fetal position coupled with electrode configuration in the resulting recording quality.

Electrode placement and inter-electrode distance is an important topic that remains virtually unexplored in the literature (addressed in this work's Section 3.2.3). In this thesis, the electrode configuration was shown to have a significant effect on both abdominal signal SNR and FECG content. In Figures. 5.9 and 5.10 it is clear the difference on signal quality for the different leads used in this work. The inter-electrode distance was shown to play a large role on the signal quality, where a trade-off between FECG amplitude and SNR exists. For further works, the combination of shorter and larger leads is recommended (e.g. 2,6-8 – see Fig. 5.4), in order to maximize the chances of obtaining usable NIFECG signals.

With the objective of providing automated means of assessing signal quality in NIFECG recordings, in Section 4.3.2 several SQI metrics were introduced in this work. These metrics, were then applied using a Naive Bayes classifier for estimating the signal quality of 5 s segments of extracted NIFECG data. With respect to the proposed Naive Bayes classifier, good classification results were obtained during cross validation using Krippendorff's α coefficient, i.e. the most suitable metric considering the ordinal dataset used. Meanwhile, Cohen's κ produces moderate results, since it is a nominal agreement measure. Visual inspection of the confusion matrix (Table 6.3) confirms that most false classifications fall within neighboring classes. It is important to mention that the Naive Bayes classifier assumes the features to be normally distributed and conditionally independent given a class, which is a strong assumption that does not hold for our data. Nevertheless, studies have shown [118] that Bayesian classifiers perform quite well in practice even when attribute dependencies are present. Furthermore, its use is justified by the transparent conversion from discrete to continuous-valued classification results, which was necessary for the further processing. The underlying class distribution (see Fig. 4.10) is expected to impact the trained classifier in terms of prior class probability. The assumption

[1] In this work, different measurements from the same subjects were regarded as independent, which may be an erroneous assumption.

of uniform class distribution was relevant for improving the generalization potential of this classifier. Unfortunately, there is no annotated clinical database currently available to serve as a standard for comparing our classification results and provide further insights into the signal quality distribution [19].

As it can be seen from Fig. 6.10, it is evident that time and frequency metrics (see Table 4.2 showed little importance, which can be explained by the well-known similarities and spectral overlap between abdominal ECG/MECG/FECG. Detection-based algorithms such as $bSQI$, $rSQI$, $cSQI$ and $xSQI$ (particularly when using *maxsearch* or $jQRS$ detectors) were relevant. While applying $bSQI$, it is particularly important to use a combination of a more and other less predictive detector, e.g. $jQRS/gqrs$ (similar to the results obtained in [211]). This result goes along with the author's previous works and top scoring entry on the PCINCC 2013 [20], where features like $cSQI$, $xSQI$, and $rSQI$ were responsible for accurate FQRS detections. The proposed FECG-specific features (latter group in Fig. 6.10) showed modest importance. Amongst these, $mpSQI_b$ was deemed as most important by RELIEFF in the latter SQI category (see Fig. 6.10) that can be confirmed its moderate reaction to the presence of noise (on Fig. 6.9). From Fig. 6.11 the correlations amongst some features are made evident, e.g. between $rSQI_1$, $rSQI_2$, and $rSQI_3$. Interestingly, FECG-specific features show a different direction of correlation, compared to the other three groups of SQI approaches. The consensus itself, appears to be uncorrelated with most metrics, except the FECG-specific approaches. This is explained by the fact that RELIEFF weights and Kendall correlation coefficients make different nonlinear transformations to the provided variables. The first evaluates the euclidean distance between available classes for for the nearest-hit/miss in the feature-space, while the second ranks its variables and compares the number of concordant and discordant pairs of variables (features against consensus). Indeed, feature selection is a comprehensive topic which extrapolates the scope of this work. As future work, the author suggests the analysis of these interdependencies for e.g. to reduce the information redundancy from similar SQI metrics.

In Fig. 6.9 (a)-(c) it is visible that most features produce lower values in the presence of muscular noise, while $iSQI_2$ and some FECG-specific indices (i.e. $mpSQI_b$, $mcSQI_b$ and $miSQI_2$) counter-intuitively output higher values. Nevertheless, the resulting continuous-valued SQI showed to be very sensitive to such artefacts. On the other hand, Fig. 6.9 (d)-(f) portrays a drawback of the proposed approach, where the estimated SQI value is larger during a maternal ectopic beat. This is caused by the MECG large amplitude residual left over from a unsatisfactory extraction procedure. In this case, $iSQI_2$ output considerably higher values, since the ectopic maternal complex still present in the residuals is expected to be detected on every lead. For solving this problem, one may for example introduce SQI metrics similar to the fetal $cSQI$ that focus on the morphological consistency of the maternal signal.

Despite being larger than most datasets available in the specific literature, one limitation of our data is the large disparity on the number of observations on each signal quality class, where most data has low signal quality (see Figure 4.10). Another limiting factor is the fact that the quality of the NI-FECG recordings was annotated using abdominal recordings (prior to extraction of the FECG), while most proposed SQI metrics are based on the extracted FECG

signals. Consequently, the training data depends on the extraction method used, which is not ideal. Nevertheless, the method of choice for this analysis, i.e. $\mathbf{TS}_{pca}$, is simple enough and should not produce any major distortion between the annotated and extracted signals. Furthermore, the author recognizes that the defined overall consensus (see Table 5.6) is a subjective concept and may be sub-optimal. However, it was a necessary step for the analysis. Another possibility would be to have two separate sets of SQIs and classifiers, one dealing with the signal SNR and another with the amplitude of the FQRS peaks. Regarding the length of the segments used in this work, although some SQI algorithms may benefit from longer segments (e.g. for building FECG templates or estimating spectral content) the 5 s interval was considered as appropriate for the trade-off between window length and online capability of the proposed algorithm. As described in Section 3.5, Doppler ultrasound approaches currently use a similar 3.75 s interval.

All in all, the proposed SQI metrics are able to reflect changes in signal quality for NIFECG recordings. The developed routines were released as part of the FECGSYN toolbox [50] under a GNU GPL open-source license [19]. As mentioned in Section 4.3.2, such automated estimates for FECG signal quality are indispensable for improving signal processing algorithm's specificity. In this work, these metrics were used in FQRS correction (Section 4.3.1) and FHR estimation (Section 4.3.2). Both these approaches are further discussed in Section 7.4. Future uses for such SQIs are for instance in channel/component selection, e.g. when applying $\mathbf{BSS}_{ica}$ extraction.

7.3 Extraction Methods

Despite the large number of NIFECG extraction methods proposed in the literature (see Section 3.3.1), very few studies have in fact made their code available. The PCINC 2013 promoted a considerable advance in the field by making a dataset and evaluation algorithms freely available, while some participants could voluntarily open-source their own code. In this work, in cooperation with the IBME, the author developed a realistic open-source FECG simulator and toolbox for NIFECG signal processing and analysis (i.e. the FECGSYN Behar *et al.* [50]). The toolbox was further applied in generating a comprehensive simulated dataset, totalizing 145.8 hours of multichannel data and 1.1 million fetal peaks (i.e. the FECGSYNDB [18]). These two well-defined tools, are currently the largest open-source collection of NIFECG extraction algorithms and data known to the author, which allow reproducible research in the field. Throughout this work, these benefits were enjoyed and culminated in a wide-ranging and well-defined benchmark of state-of-the-art (Section 3.3.1) and newly proposed EKF approaches (Section 4.2).

From Fig. 6.1 and Table 6.1, it is clear that under ideal circumstances (i.e. when the best available lead/component is known) BSS techniques (especially $\mathbf{BSS}_{\text{ica}}$) outperforms all other approaches. Meanwhile, $\mathbf{TS}_{\text{pca}}$ and $\mathbf{AM}_{\text{esn}}$ obtained the best results in their respective categories (similar findings for the AM category using real data were presented in [52, 258]). BSS methods have showed to be robust to the presence of noise in any level, while AM and TS techniques are extremely susceptible to noise. *MAE* results were very similar for all methods, notwithstanding,

temporal techniques consistently obtained the best results for baseline to case 2 (c.f. Tab. 6.1). Such results were only possible, since the MAE was used as distance measure and disregarded FP and FN detections (regarded by F_1 measure). It is important to mention that MAE was calculated using a FQRS reference, which was not aligned to each individual channel, therefore, a slight systematic error is expected for all methods as the R-peak location varies slightly from channel to channel. Regarding the proposed EKF techniques, $EKF24$ performed best in terms of F_1 and MAE. This may be due to the absence of intermittent SNR changes in the FECGSYNDB dataset (from which $vEKF2/vEKF24$ could outperform its basic implementation). The $uiEKF2$ variant's under-performance is attributed to its model inability to adapt itself to amplitude changes of the MQRS complexes, which leads to the innovation depicting this "unexpected" peaks. Consequently, the UIEKF estimates MQRS residuals on the unknown input that leads to its lower FQRS detection performance (see Table 6.1). Its further development (e.g. in a $EKF24$ framework) may improve this results. Interestingly, by evaluating Fig. 6.5 (g), it is clear that the UIEKF technique shows a strong bias to an increasing FTQRS ratio (i.e. decreasing difference between fetal T-wave and FQRS amplitudes). That means that the model also depends on the amplitude of the FQRS complexes themselves. The post-hoc tests from Fig. 6.2 indicate that these performance differences amongst EKF variants are only visible at extreme high/low SNRs scenarios for F_1 and MAE, respectively. This sign test also confirms the above average performance of BSS techniques for F_1, but not for MAE. This lower result for the MAE distance metric is explained by Fig. 6.3, which shows the remarkably distinct morphologies of $\mathbf{BSS}_{\text{ica}}$ output components, depending on the calculated mixing matrix [18].

With respect to the individual cases presented in Fig. 6.1, there is a clear decay on $\mathbf{BSS}_{\text{ica}}$'s performance in cases 1 (i.e. fetal movement), 3 (uterine contraction), 4(ectopic beats), and 5 (twin pregnancy). Cases 1 and 4 may be attributed to the highly non-stationarity of the available sources (i.e. the FECG intensity/morphology changes) within the abdominal mixture, which is not foreseen in this implementation. The lower results for cases 3 and 5 may be associated with the model order selection problem [201, 327], i.e. these additional sources may require the presence of more than 8 leads. This latter problem is discussed in depth in [18]. While ectopic beats are problematic for most BSS or TS approaches (see Fig. 6.9 (d)-(f)), it should not impose restrictions for AM methods. This is confirmed by the good results for AM methods regarding case 4 in Fig. 6.1. Specifically to the $\mathbf{TS}_{ekf}$, the approach by Oster *et al.* [314] should overcome this problem by allowing multiple templates (i.e. for different MECG waveforms).

Regarding morphological analysis, the results presented in Section 6.1.2 demonstrate that considerable effort needs to be made in improving currently available techniques, so that clinical relevant information can be obtained from the FECG morphology. The expressive number of excluded beats were either due to problems in the template generation, segmentation or due to the applied methods themselves, therefore further studies should focus on improving these individual steps. Moreover, in order to perform fair morphological comparisons, studies should make sure to use the same segments and report their failure rate, as in [18]. Figure 6.4 and 6.5 demonstrate that BSS techniques are unable to provide satisfactory FQT or FTQRS measures. Meanwhile, TS and AM produced highly correlating FQT/FTQRS measures, if little to no noise

is present. This claim is supported by Fig. 6.3, on which differences in the morphology of the output signals at different time-instants are evident. The suitability of AM and TS techniques is expressed in the FTQRS error in Fig. 6.6. The $\mathbf{TS}_{pca}$ and $\mathbf{TS}_{EKF24}$ techniques delivered the best FQT and FTQRS estimates (see Fig. 6.6). The findings of Figs. 6.4 and 6.5 reiterate the importance of using excluding bad quality ECG segments from the analysis, e.g. using fetal SQI measures. Regarding BSS techniques, an alternative would be to back-propagate specifically selected FECG components from the source domain to the observation domain, in order to perform this analysis. However, as mentioned, component selection is a challenging task, which was not carried out in the present study. The separate analysis of the results for the baseline and case 0 (see Figs. 6.4 and 6.5), enables a clear understanding of each methods performance, and is preferable because ectopic beats and other non-stationarities may cause the algorithm to fail in different routines (e.g. during template construction). This figure suggests rather high FQT errors ($\approx$ 20 ms) for all extraction methods, and technical improvements are therefore required before being tested on more difficult cases. Several explanations are possible for this low performance, e.g. the extraction techniques were optimized for FQRS detection and might therefore distort other segments of the FECG, construction of the template might average out small amplitude components (P or T wave), but also the segmentation was designed for adult ECG and its performance is likely to be sub-optimal for FECG signals. Nevertheless, Fig. 6.5 suggests that TS techniques are more suited for FTQRS analysis.

Despite being a good starting point, the aforementioned results using simulated have to be taken with caution since key algorithmic steps that can cause accuracy to decrease (e.g. channel/component selection) were not accounted for. In this work, the component with highest F_1 was selected, disregarding the component selection step. Moreover, as mentioned in [18], a limitation of the FECGSYN simulator is the linear phase applied to the modelled beats, which leads to a simple stretching of those beats. This simplification has the drawback of disregarding physiological variations, such as T-wave prolongation and ST segments variation. Since the modelled FECG signal was acquired from adult ECG signals, non-physiological FQT intervals are produced. To reliably validate an algorithm's performance (i.e. FQRS detection accuracy and morphological analysis), real clinical data is more suitable. In this study, no morphological analysis using clinical data was possible, due to the absence of clinical goldstandard (i.e. invasive FSE recordings). Nonetheless, data was carefully annotated for FQRS locations (see Section 5.2.4). The results using the proposed eQRS are shown in Table 6.2. This table shows that despite having lower performance on the simulated data, $\mathbf{TS}_{ekf}$ methods have shown to be useful in praxis. In fact, similar F_1 and MAE results were obtain for $\mathbf{AM}_{esn}$, $\mathbf{TS}_{pca}$, and $\mathbf{TS}_{EKF24}$ (see Table 6.2). As previously discussed in Section 7.1, a more substantial amount of annotated data is required to associate the quality of these extraction methods with actual diagnostic value.

Aside the extraction procedure, other aspects of the NIFECG's signal processing should be separately considered, e.g. preprocessing, channel/component selection, smoothing techniques, FQRS detection and FECG enhancement. Preprocessing (mentioned in Section 4.1) is a crucial aspect of morphological analysis. In this work the signal bandwidth was configured as recommended by the American Heart Society for adult electrocardiography [231]. A clinical trial is

required to confirm if such standards can indeed be adopted for FECG analysis. Regarding the template generation, there are no current standards in ECG analysis. For example, signal-averaging is not a consesus among researchers, despite its wide usage in the literature (e.g. [85, 162, 473]). However, for signals with low SNR such as the NIFECG such step is imperative. Template generation played an important role in producing our results, a comprehensive study comparing a number of template construction strategies should be conducted to investigate in which depth its low-pass effect may hinder the morphological analysis. In our preliminary work, the template construction method proposed by [314] obtained better empirical results than simply using mean or medians, even when poorly correlated beats were excluded. It is important to remark that the findings presented here need to be validated using clinical data and expert annotations.

Overall, the EKF is the simplest nonlinear variant of the Kalman filter. The extensive literature available (see Section 3.3.3) indicates that for sharp discontinuities, other algorithms may produce better estimates, e.g. the UKF or Particle Filters. The usage of this latter technique in NIFECG, has been suggested by [365], however, to the author's best knowledge this extension has not yet been applied in the literature. In its current stage, the usage of EKF approaches is linked with a extensive and data-dependent calibration procedure. Depending on the calibration, the filter produces considerably different results. Future works should focus on semi-automating this initialization for improving its applicability and reproducibility. For obtaining morphologic reliable FECG, a promising extension of $\mathbf{TS}_{\text{ekf}}$ model was proposed by [53, 304], which takes into consideration both maternal and fetal heart models. However, accurate FQRS detections are pre-requirements for these techniques. For this reason these methods have not been included in this work. The extraction techniques applied in this work have been often used in the literature, including top-scoring entries during the PCINC 2013. As revealed by Fig. 6.8, the choice of extraction method cannot be dissociated from the recording scheme. For instance, for $\mathbf{BSS}_{ica}$ not only the model order problem (i.e. number of input channels should be reasonable), but these channels should contain relevant information for enabling ICA to properly separate the sources. One of the advantages of using TS techniques, such as the EKF, is that they imply the least restrictions on the recording scheme, being able to operate on a single lead systems. In this section, the advantages and limitations of each of these techniques were demonstrated. In a clinical environment, it is certainly beneficial to use multiple extraction methods in parallel and apply fetal SQI indices to discern successful from unsuccessful extraction results. This manner, the strength of each methodology can be conciliated.

7.4 FQRS and FHR Correction Algorithms

In this work both FQRS detection and FHR estimation were improved based on developed SQI metrics, discussed in Section 7.2. Regarding FQRS detection using the evolutionary computing approach (i.e. eQRS), Table 6.2 shows that the method considerably improves the FQRS detections. The eQRS's performance applied to $\mathbf{BSS}_{\mathbf{ica}}$ output components was understandably poor, due to the lack of features to distinguish between MQRS and FQRS complexes (such as

miSQI - see Table 4.2). As mentioned in [20], permutation indeterminacy denotes a common difficulty which goes along with ICA. The a priori unknown positioning of ICs inside ICA's output imposes the challenging task of automatic selection of the IC of interest (i.e. FECG components) [459]. The eQRS detection using $\mathbf{AM_{esn}}$, $\mathbf{TS}_{pca}$, $\mathbf{TS}_{EKF24}$ was very accurate, with monotonically increasing results with an increase on the number of channels available. These results go along the author's top scoring entry on the PCINC 2013, where TS methods in association with the eQRS were responsible for highly accurate results [20]. Figure 6.7 demonstrates that even in scenarios where the quality of the initial detections or signal SNR are non-ideal, the eQRS is capable of combine/select multichannel detections into a trustworthy consensus. There is a remarkable increase in accuracy between using the 3 internal channels or all available leads, which reiterates the importance of having leads with different inter-electrode distance. As previously mentioned, the eQRS method is a computationally intensive. Future works should focus on reducing its computational load and parallelizing its execution.

Regarding the Kalman filter improved FHR estimation approach (presented in Section 4.3.2), the overall modest FHR accuracy results (see Table 6.4), demonstrates how challenging FHR estimation on real clinical data actually is. Behar *et al.* [52] compared several extraction methods, including TS_{pca}, using 82 min of manually annotated abdominal signals (from PCINC 2013 and a private commercial database). Results for FHR accuracy applying TS_{pca} were 68.7 % and 73.9 % for each dataset (using a ±5 bpm acceptance interval). The multichannel estimation of FHR using Kalman filter showed the best performance both in terms of HDR and RMSE (see Table 6.4). The filter's performance monotonically increased with the growth of available leads, which shows how powerful the method is in incorporating additional information. Meanwhile, the average result from single channel estimation (with or without KF) does not show this trend. Large differences were found between the 3 and 4-lead schemes (i.e. internal or external channels - see Fig. 5.4). The latter performed better, which can be attributed to a lower presence of noise for greater inter-electrode distance between the positive and negative electrodes. After the calibration procedure, the smaller value obtained for the initial observational noise covariance matrix $R_0 = 10^{-3}$ compared to $Q_0 = 1$ shows that the filter tends to "trust" its observations associated with the SQI metrics. Additionally, in Fig. 6.12, a qualitative example demonstrates the filter using 3 channels during a period FHR deceleration and changes of signal quality throughout the available channels. As it can be seen, if the quality is sufficient in some channels, the filter is able to reliably reflect the true FHR. Therefore, it is clear that the KF innovation in association with the proposed SQI metrics is able to improve FHR estimation, as it did in estimating adult heart rates [19, 251].

Differently from many FHR studies that regard periods of "signal loss", in this thesis, segments/recordings with general bad quality were not discarded. In long-term recording scenarios, removing portions of data with bad signal quality from the further the analysis is desirable because FHR estimates during periods of low SQI would disregard the current measurements and follow the filter's dynamic equations (first-order AR process), therefore, delivering unreliable results. The manner with which selection of inadequate segments may be performed is another complex topic, which deserves its own study. Nevertheless, the proposed SQI metrics

and classifier are a favorable starting point for further studies. In Section 3.5 a series of HR preprocessing algorithms were presented that aim at improving such FHR estimates before the multichannel fusion e.g. with the presented KF approach takes place [19].

In this work, multiple KFs running parallel were implemented for estimating each of individual channel FHR. The multichannel fusion was considered as an additional step following this single-channel estimation. Oster and Clifford [315] proposed combining both single-channel FHR estimation and data fusion steps into a single step, rather than implementing multiple KF and fusing those later on. This is performed by considering the consensus amongst those different sensors as an additional Kalman state and allowing the transition and observational matrices ($\mathbf{A}_k$ and $\mathbf{H}_k$) to be time-variant and dynamically include the previously defined weighting factors $\sigma^2_{k,s}$ (see Eq. 4.23) [19].

When comparing the accuracy results for the eQRS and KF FHR algorithms (i.e. Table 6.2) and 6.4), the reader should keep in mind that these algorithms were designed for different applications. The eQRS is a brute force, offline method with high demand for computational power. On the other hand, the KF algorithm for FHR is light weight, online and can be ported to relatively simple hardware structures. Both algorithms were initiated with FQRS detections provided by simple detectors which correspond to the "Initial" column (in Table 6.2) and "single channel average (without KF)" row (in Table 6.4). As it can be noticed, these results are indeed similar for F_1 and HDR (regarding $\mathbf{TS}_{pca}$).

In summary, these results reiterate the importance of having SQI metrics, in order to improve the algorithmic specificity in NIFECG processing. Future works should focus on further developing those correction algorithms as well as further develop and explore SQI metrics and their possible combinations of those. Possible SQI enhancements are, e.g. modifications on $cSQI$ to allow ectopic beats (as preliminary works at the IBMT [472]), or allowing some flexibility on the FQRS regularity metrics (e.g. $rsqi$) so that arrhythmic episodes are better described.

Barba non facit philosophum

– attributed to Herodes Atticus by Aulus Gellius

8 Conclusion

In this work, several relevant aspects regarding the NIFECG research were addressed. For instance, the lack of publicly available databases containing gold standards for FQRS locations and FECG morphology was tackled by further developing an elaborate FECGSYN simulator. This well-defined framework was utilized in creating a large freely available Physionet dataset comprising simulated abdominal signals that model different non-stationary scenarios and pathophysiological conditions.

Aside from the produced simulated data, a large private clinical study was carried out in partnership with the University Hospital of Leipzig. This exploratory study enabled further insights on the nature of the NIFECG signal (particularly at earlier stages of pregnancy, i.e. WOG<28). Moreover, the data supplied important information on the recording technique (e.g. channel selection). Throughout the development of this work, this promising clinical trial evolved into a multimodal study that shall be continued. Future works on the clinical front should aim at generating large randomized trial, to conclusively confirm NIFECG's clinical relevance in prenatal monitoring.

Regarding signal processing methods for NIFECG, this study focused on pushing forward open-source algorithms for enabling direct comparison amongst researchers. For this purpose, the FECGSYN toolbox was furnished with a substantial number of state-of-the-art NIFECG extraction techniques, statistical performance metrics for FQRS detection and morphological analysis. To improve the specificity of current methodologies, novel fetal SQI metrics were proposed, accordingly tested, and included in the FECGSYN toolbox.

A large part of this work dealt with improving the EKF framework. This was performed by enhancing its model to account for the different signal sources contained in abdECG. For this purpose, the $EKF2$ and $EKF24$ models served as base implementations. In order to cope with changes of signal quality, a new time-varying method for updating the observational noise covariance matrix was proposed (i.e. $vEKF2$ and $vEKF24$). A common misconception made

by current models is the assumption that the FECG can be considered as a white Gaussian noise. To deal with this model inaccuracy, the unknown input Kalman model is suggested ($uiEKF2$). Several experiments were conducted to benchmark the performance of those NIFECG extraction methods in their capacity to evaluate the FQRS locations, FQT length and FTQRS ratio. The advantages and limitations of each method were throughly described. Since no extraction algorithm performs systematically better on every experiment, a combination of different extraction techniques should be considered for further applications.

Aside from extraction methods and signal quality estimation, this work focused on improving multichannel FQRS detection and FHR estimation. The first, was performed using a newly developed evolutionary algorithm for offline correction of FQRS locations. The brute force search method showed to be highly accurate and is regarded as main responsible for the author's top scoring entry on the PCINC 2013 challenge. On the other hand, FHR estimation was improved by applying the novel developed SQI metrics on a linear Kalman filter for fusing multichannel information. The algorithm obtained more accurate results than traditional techniques, additionally, its usage is compatible with online applications.

In summary, this dissertation dealt with several steps of the NIFECG signal processing chain. Future works should further fine-tune current extraction methods. Moreover, alternative machine learning approaches to combine the proposed SQI metrics could improve the signal quality estimation for abdominal signals. At last, NIFECG-specific segmentation algorithms are required for improving the reliability of FECG's morphology analysis.

References

[1] ADInstruments. Bio Amp Owner ' s Guide. 2009.

[2] ADInstruments. Powerlab / 30 Series Owner ' s Guide. 2009.

[3] Afonso, V. X., Tompkins, W. J., Nguyen, T. Q., and Luo, S. ECG Beat Detection Using Filter Banks. *IEEE Trans. Biomed. Eng.*, **46**(2):pp. 192–202, 1999.

[4] Agostinelli, A., Grillo, M., Biagini, A., Giuliani, C., Burattini, L., Fioretti, S., Di Nardo, F., Giannubilo, S. R., Ciavattini, A., and Burattini, L. Noninvasive Fetal Electrocardiography: An Overview of the Signal Electrophysiological Meaning, Recording Procedures, and Processing Techniques. *Ann. Noninvasive Electrocardiol.*, **20**(4):pp. 303–313, 2015.

[5] Ahlstrom, M. L. and Tompkins, W. J. Automated High-Speed Analysis of Holter Tapes with Microcomputers. *IEEE Trans. Biomed. Eng.*, **BME-30**(10):pp. 651–657, 1983.

[6] Akhbari, M., Shamsollahi, M., Jutten, C., and Coppa, B. ECG Denoising using Angular Velocity as a State and an Observation in an Extended Kalman Filter Framework. In: *IEEE EMBC*, pp. 2897–2900. IEEE, 2012.

[7] Akhbari, M., Shamsollahi, M. B., Jutten, C., Armoundas, A. A., and Sayadi, O. ECG denoising and fiducial point extraction using an extended Kalman filtering framework with linear and nonlinear phase observations. *Physiol. Meas.*, **37**(2):pp. 203–226, 2016.

[8] Alfirevic, Z., Devane, D., and Gyte, G. M. Continuous cardiotocography (CTG) as a form of electronic fetal monitoring (EFM) for fetal assessment during labour. *Cochrane Database Syst. Rev.*, **5**:p. CD006066, 2013.

[9] Almeida, R., Gonçalves, H., Bernardes, J., and Rocha, A. P. Fetal QRS detection and heart rate estimation: a wavelet-based approach. *Physiol. Meas.*, **35**(8):pp. 1723–35, 2014.

[10] Alspach, D. and Sorenson, H. Nonlinear Bayesian estimation using Gaussian sum approximations. *IEEE Trans. Autom. Control.*, **17**(4):pp. 439–448, 1972.

[11] Amer-Wåhlin, I. and Maršál, K. ST analysis of fetal electrocardiography in labor. *Semin. Fetal Neonatal Med.*, **16**(1):pp. 29–35, 2011.

[12] American College of Obstetricians and Gynecologists. ACOG Practice Bulletin No. 106: Intrapartum fetal heart rate monitoring: nomenclature, interpretation, and general management principles. *Obs. Gynecol*, **114**(1):pp. 192–202, 2009.

[13] American Heart Association. Congenital Heart Defects in Children Fact Sheet. 2016. URL `http://www.americanheart.org/children`.

[14] Anderson, B. D. O. and Moore, J. B. *Optimal Filtering*. Prentice Hall, Inc., 2012. ISBN 0-13-638122-7.

[15] Andersson, S. Acceleration and Deceleration Detection and Baseline Estimation. Technical report, Chalmers University of Technology, Götenborg, Sweden, 2011.

[16] Andreotti, F. Extraction of the Fetal ECG from Electrocardiographic Long-term Recordings. Technical report, TU Dresden, Dresden, 2011.

[17] Andreotti, F., Behar, J., Oster, J., Clifford, G. D., Malberg, H., and Zaunseder, S. Optimized Modelling of Maternal ECG Beats Using the Stationary Wavelet Transform. In: *Comput. Cardiol. (2010)*. Cambridge, USA, 2014.

[18] Andreotti, F., Behar, J., Zaunseder, S., Oster, J., and Clifford, G. D. An Open-Source Framework for Stress-Testing Non-Invasive Foetal ECG Extraction Algorithms. *Physiol. Meas.*, **37**(5):pp. 627–648, 2016.

[19] Andreotti, F., Gräßer, F., Malberg, H., and Zaunseder, S. Non-Invasive Fetal ECG Signal Quality Assessment for Multichannel Heart Rate Estimation. *IEEE Trans. Biomed. Eng.*, (in rev.), 2017.

[20] Andreotti, F., Riedl, M., Himmelsbach, T., Wedekind, D., Wessel, N., Stepan, H., Schmieder, C., Jank, A., Malberg, H., and Zaunseder, S. Robust fetal ECG extraction and detection from abdominal leads. *Physiol. Meas.*, **35**(8):pp. 1551–1567, 2014.

[21] Andreotti, F., Riedl, M., Himmelsbach, T., Wedekind, D., Zaunseder, S., Wessel, N., and Malberg, H. Maternal signal estimation by Kalman Filtering and Template Adaptation for fetal heart rate extraction. In: *Comput. Cardiol. (2010).*, volume 40, pp. 193–196. Zaragoza, Spain, 2013. ISBN 9781479908844.

[22] Andreotti, F., Trumpp, A., Malberg, H., and Zaunseder, S. Improved heart rate detection for camera-based photoplethysmography by means of Kalman filtering. In: *IEEE Conf. Electron. Nanotechnol.*, pp. 428–433. IEEE, Kiev, Ukraine, 2015. ISBN 978-1-4673-6534-5.

[23] Andreotti, F., Zaunseder, S., Schmieder, C., Schröder, S., Löther, S., Malberg, H., Stepan, H., Wessel, N., and Jank, A. Einfluss der mütterlichen EKG-Modellierung auf die fetalen QRS-Detektionen. In: *Automed*, pp. 12–13. Steinbeis-Edition, Dresden, 2013. ISBN 978-3-943356-82-3.

[24] Andreotti, F., Zaunseder, S., Schmieder, C., Wessel, N., Malberg, H., Stepan, H., and Jank, A. Mehrkanalige Extraktion des fetalen EKGs mittels Kalman-Filter. In: *Dresdner Medizintechnik-Symposium*, volume 14, pp. 241—-242. TUD Press, Dresden, 2012. ISBN 978-3-942710-96-1.

[25] Annunziata, M. L., Scala, M., Giuliano, N., Tagliaferri, S., Imperato, O. C. M., Esposito, F. G., Campanile, M., and Di Lieto, A. Fetal vibroacoustic stimulation in computerized cardiotocographic analysis: The role of short-term variability and approximate entropy. *J. Pregnancy*, **2012**, 2012.

[26] ANSI/ AAMI EC57. Testing and reporting performance results of cardiac rhythm and ST-segment measurement algorithms. Technical Report EC57, American National Standards Institute, Inc. / Association for the Advancement of Medical Instrumentation, 1998.

[27] ANSI/AAMI - EC13:2002. Cardiac monitors, heart rate meters, and alarms. Technical report, American National Standard / Association for the Advancement of Medical Instrumentation (ANSI/AAMI), 2002.

[28] Apgar, V. The newborn (Apgar) scoring system. Reflections and advice. *Pediatr. Clin. North Am.*, **13**(3):pp. 645–650, 1966.

[29] Apitz, J., von Brenndorff, C. I., Bruhns, T., and Enders, H. *Pädiatrische Kardiologie*. Springer Berlin / Heidelberg, Heidelberg, 1998. ISBN 978-3-642-53755-4.

[30] Armstrong, L. and Stenson, B. J. Use of umbilical cord blood gas analysis in the Assessment of the Newborn. *Arch. Dis. Child.*, pp. 430–434, 2007.

[31] Arnold, M., Miltner, W. H., Witte, H., Bauer, R., and Braun, C. Adaptive AR modeling of nonstationary time series by means of Kalman filtering. *IEEE Trans. Biomed. Eng.*, **45**(5):pp. 553–562, 1998.

[32] Artal, R., Rutherford, S., Romem, Y., Kammula, R. K., Dorey, F. J., and Wiswell, R. A. Fetal heart rate responses to maternal exercise. *Am. J. Obs. Gynecol.*, **155**(4):pp. 729–733, 1986.

[33] Arulampalam, M., Maskell, S., Gordon, N., and Clapp, T. A tutorial on particle filters for online nonlinear/non-Gaussian Bayesian tracking. *IEEE Trans. Signal Process.*, **50**(2):pp. 174–188, 2002.

[34] Assaleh, K. Extraction of fetal electrocardiogram using adaptive neuro-fuzzy inference systems. *IEEE Trans. Biomed. Eng.*, 2007.

[35] Assaleh, K. and Al-Nashash, H. A novel technique for the extraction of fetal ECG using polynomial networks. *IEEE Trans. Biomed. Eng.*, 2005.

[36] AWMF. 015-029 S1: Empfehlungen zum Vorgehen beim vorzeitigen Blasensprung. Technical report, Deutsche Gesellschaft für Gynäkologie und Geburtshilfe, 2006.

[37] Ayat, M., Assaleh, K., and Al-Nashash, H. A Novel Methodology for Fetal Heart Rate Extraction from the Abdominal Electrocardiogram. In: *Int. Biomed. Eng. Conf.*, pp. 1–5. IEEE, 2008. ISBN 9781424426959.

[38] Ayres-de Campos, D. and Arulkumaran, S. FIGO consensus guidelines on intrapartum fetal monitoring: Physiology of fetal oxygenation and the main goals of intrapartum fetal monitoring. *Int. J. Gynaecol. Obs.*, **131**(1):pp. 5–8, 2015.

[39] Ayres-de Campos, D. and Bernardes, J. Twenty-five years after the FIGO guidelines for the use of fetal monitoring: time for a simplified approach? *Int. J. Gynaecol. Obs.*, **110**(1):pp. 1–6, 2010.

[40] Ayres-de campos, D., Bernardes, J., Garrido, A., Marques-de sá, J., and Pereira-leite, L. SisPorto 2.0: A Program for Automated Analysis of Cardiotocograms. *J. Matern. Fetal Med.*, **9**:pp. 311–318, 2000.

[41] Ayres-de Campos, D., Spong, C. Y., and Chandraharan, E. FIGO consensus guidelines on intrapartum fetal monitoring: Cardiotocography. *Int. J. Gynaecol. Obs.*, **131**(1):pp. 13–24, 2015.

[42] Bacharakis, E., Nandi, A., and Zarzoso, V. Foetal ECG extraction using blind source separation methods. In: *EUSIPCO*. 1996.

[43] Bäck, T. and Schwefel, H.-P. An overview of evolutionary algorithms for parameter optimization. *Evol. Comput.*, **1**(1):pp. 1–23, 1993.

[44] Bailey, R. E. Intrapartum fetal monitoring. *Am. Fam. Physician*, **80**(12):pp. 1388–1396, 2009.

[45] Barnett, S. B., Ter Haar, G. R., Ziskin, M. C., Rott, H. D., Duck, F. A., and Maeda, K. International recommendations and guidelines for the safe use of diagnostic ultrasound in medicine. *Ultrasound Med. Biol.*, **26**(3):pp. 355–366, 2000.

[46] Baumert, M., Porta, A., Vos, M. A., Malik, M., Couderc, J.-P., Laguna, P., Piccirillo, G., Smith, G. L., Tereshchenko, L. G., and Volders, P. G. A. QT interval variability in body surface ECG: measurement, physiological basis, and clinical value: position statement and consensus guidance endorsed by the European Heart Rhythm Association jointly with the ESC Working Group on Cardiac Cellular Electroph. *Europace*, pp. euv405–, 2016.

[47] Becker, J. H., Krikhaar, A., Schuit, E., Mårtendal, A., Maršál, K., Kwee, A., Visser, G. H. A., and Amer-Wåhlin, I. The added predictive value of biphasic events in ST analysis of the fetal electrocardiogram for intrapartum fetal monitoring. *Acta Obs. Gynecol. Scand.*, **94**(2):pp. 175–82, 2015.

[48] Becker, J. H., Westerhuis, M. E. M. H., Sterrenburg, K., van den Akker, E. S. A., van Beek, E., Bolte, A. C., van Dessel, T. J. H. M., Drogtrop, A. P., van Geijn, H. P., Graziosi, G. C. M., van Lith, J. M. M., Mol, B. W. J., Moons, K. G. M., Nijhuis, J. G., Oei, S. G., Oosterbaan, H. P., Porath, M. M., Rijnders, R. J. P., Schuitemaker, N. W. E., Wijnberger, L. D. E., Willekes, C., Visser, G. H. A., and Kwee, A. Fetal blood sampling in addition to intrapartum ST-analysis of the fetal electrocardiogram: evaluation of the recommendations in the Dutch STAN® trial. *BJOG*, **118**(10):pp. 1239–1246, 2011.

[49] Behar, J. *Extraction of Clinical Information from the Non-Invasive Fetal Electrocardiogram*. Ph.d. thesis, University of Oxford, 2014.

[50] Behar, J., Andreotti, F., Zaunseder, S., Li, Q., Oster, J., and Clifford, G. D. An ECG Model for Simulating Maternal-Foetal Activity Mixtures on Abdominal ECG Recordings. *Physiol. Meas.*, **35**(8):pp. 1537–1550, 2014.

[51] Behar, J., Andreotti, F., Zaunseder, S., Oster, J., and Clifford, G. D. A Practical Guide to Non-Invasive Foetal Electrocardiogram Extraction and Analysis. *Physiol. Meas.*, **37**(5):pp. R1–R35, 2016.

[52] Behar, J., Johnson, A. E., Clifford, G. D., and Oster, J. A Comparison of Single Channel Fetal ECG Extraction Methods. *Ann. Biomed. Eng.*, **42**(6):pp. 1340–1353, 2014.

[53] Behar, J., Oster, J., Andreotti, F., and Clifford, G. D. A Bayesian Filtering Framework for Accurate Extracting of the Non Invasive FECG Morphology. In: *Comput. Cardiol. (2010).*, pp. 53–56. IEEE, Cambridge, USA, 2014.

[54] Behar, J., Oster, J., and Clifford, G. D. Combining and Benchmarking Methods of Foetal ECG Extraction Without Maternal or Scalp Electrode Data. *Physiol. Meas.*, **35**(8):pp. 1569–1589, 2014.

[55] Behar, J., Oster, J., Li, Q., Clifford, G. D., and Member, S. ECG Signal Quality During Arrhythmia and Its Application to False Alarm Reduction. *IEEE Trans. Biomed. Eng.*, **60**(6):pp. 1660–1666, 2013.

[56] Behar, J., Zhu, T., Oster, J., Niksch, A., Mah, D., Chun, T., Greenberg, J., Tanner, C., Harrop, J., Esbroeck, A. V., Alexander, A., McCarroll, M., Drake, T., Silber, A., Sameni, R., Ward, J., Wolfberg, A., and Clifford, G. D. Evaluation of the Fetal QT Interval Using Non-Invasive Fetal ECG Technology. In: *SMFM's Annu. Pregnancy Meet.* 2013.

[57] Belfort, M. A., Saade, G. R., Thom, E., Blackwell, S. C., Reddy, U. M., Thorp, J. M., Tita, A. T., Miller, R. S., Peaceman, A. M., McKenna, D. S., Chien, E. K., Rouse, D. J., and Peter, J. A Randomized Trial of Intrapartum Fetal ECG ST-Segment Analysis. *N. Engl. J. Med.*, **373**(7):pp. 632–641, 2015.

[58] Benitez, D. S., Gaydecki, P. a., Zaidi, a., and Fitzpatrick, a. P. A new QRS detection algorithm based on the Hilbert transform. In: *Comput. Cardiol. (2010).*, volume 27, pp. 379–382. 2000. ISBN 0780365577.

[59] Berger, R. D., Kasper, E. K., Baughman, K. L., Marban, E., Calkins, H., and Tomaselli, G. F. Beat-to-Beat QT Interval Variability : Novel Evidence for Repolarization Lability in Ischemic and Nonischemic Dilated Cardiomyopathy. *Circulation*, **96**(5):pp. 1557–1565, 1997.

[60] Bergstra, J. and Bengio, Y. Random search for hyper-parameter optimization. *J. Mach. Learn. Res.*, **13**:pp. 281–305, 2012.

[61] Bergveld, P. and Meijer, W. J. A new technique for the suppression of the MECG. *IEEE Trans. Biomed. Eng.*, **28**(4):pp. 348–54, 1981.

[62] Bernardes, J., Costa-Pereira, A., Ayres-de Campos, D., Geijn, H., and Pereira-Leite, L. Evaluation of interobserver agreement of cardiotocograms. *Int. J. Gynaecol. Obs.*, **57**(1):pp. 33–37, 1997.

[63] Bhide, A., Chandraharan, E., and Acharya, G. Fetal monitoring in labor: Implications of evidence generated by new systematic review. *Acta Obs. Gynecol. Scand.*, **95**(1):pp. 5–8, 2016.

[64] Billman, G. E. Heart rate variability - a historical perspective. *Front. Physiol.*, **2**:p. 86, 2011.

[65] Blackburn, S. *Maternal, Fetal, and Neonatal Physiology: A Clinical Perspective*. Elsevier Saunders, 2014. ISBN 1437716237.

[66] Blix, E., Brurberg, K. G., Reierth, E., Reinar, L. M., and Øian, P. ST waveform analysis vs. cardiotocography alone for intrapartum fetal monitoring: A systematic review and meta-analysis of randomized trials. *Acta Obs. Gynecol. Scand.*, 2015.

[67] Bobrow, C. S. and Soothill, P. W. Causes and consequences of fetal acidosis. *Arch. Dis. Child. Fetal Neonatal Ed.*, **80**:pp. F246–F249, 1999.

[68] Bousseljot, R., Kreiseler, D., and Schnabel, A. Nutzung der EKG-Signaldatenbank CARDIODAT der PTB über das Internet. *Biomed. Tech.*, **40**(s1):pp. 317–318, 1995.

[69] Brodsky, D. and Christou, H. Current concepts in intrauterine growth restriction. *J. Intensive Care Med.*, **19**(6):pp. 307–19, 2004.

[70] Brown, R. G. and Hwang, P. Y. C. *Introduction to Random Signals and Applied Kalman Filtering with Matlab Exercises*. John Wiley & Sons, 1983. ISBN 0470609699.

[71] Bucy, R. and Joseph, P. *Filtering for stochastic processes with applications to guidance*. John Wiley & Sons, 1968. ISBN 470 116528.

[72] Bundesamt für Statistik. Neugeborene in Schweizer Spitälern 2004 : Spitalversorgung von termin- und frühgeborenen Säuglingen. Technical report, Bundesamt für Statistik (BFS) - Swiss Federation, 2007.

[73] Bundesinstitut für Bevölkerungsforschung. Perinatalsterblichkeit. 2016. URL `http://www.bib-demografie.de/DE/Institut/Jahresberichte/jahresberichte{_}node.html`.

[74] Burgers, G., Jan van Leeuwen, P., and Evensen, G. Analysis Scheme in the Ensemble Kalman Filter. *Mon. Weather Rev.*, **126**(6):pp. 1719–1724, 1998.

[75] Callaerts, D., De Moor, B., Vandewalle, J., Sansen, W., Vantrappen, G., Janssens, J., Moor, B. D., Vandewalle, J., Sansen, W., Vantrappen, G., and Janssens, J. Comparison of SVD methods to extract the foetal electrocardiogram from cutaneous electrode signals. *Med. Biol. Eng. Comput.*, **28**(3):pp. 217–224, 1990.

[76] Camps, G., Martinez, M., and Soria, E. Fetal ECG extraction using an FIR neural network. In: *Comput. Cardiol. (2010).*, pp. 249–252. IEEE, 2001. ISBN 0-7803-7266-2.

[77] Caughey, A. B., Robinson, J. N., and Norwitz, E. R. Contemporary diagnosis and management of preterm premature rupture of membranes. *Rev. Obstet. Gynecol.*, **1**(1):pp. 11–22, 2008.

[78] Cerutti, S., Baselli, G., Civardi, S., Ferrazzi, E., Marconi, A. M., Pagani, M., and Pardi, G. Variability analysis of fetal heart rate signals as obtained from abdominal electrocardiographic recordings. *J. Perinat. Med.*, **14**(6):pp. 445–452, 1986.

[79] Cerutti, S., Civardi, S., Bianchi, A., Signorini, M. G., Ferrazzi, E., and Pardi, G. Spectral analysis of antepartum heart rate variability. *Clin. Phys. Physiol. Meas.*, **10**(4B):pp. 27–31, 1989.

[80] Chandraharan, E. Authors' reply: Fetal scalp blood sampling during labour: Is it a useful diagnostic test or a historical test that no longer has a place in modern clinical obstetrics? *BJOG*, **121**(13):pp. 1753–1754, 2014.

[81] Chauhan, S. P., Gupta, L. M., Hendrix, N. W., and Berghella, V. Intrauterine growth restriction: comparison of American College of Obstetricians and Gynecologists practice bulletin with other national guidelines. *Am. J. Obs. Gynecol.*, **200**(4):pp. 409.e1–409.e6, 2009.

[82] Chen, Z. Bayesian filtering: From Kalman filters to particle filters, and beyond. *Statistics (Ber).*, **182**(1):pp. 1–69, 2003.

[83] Chen, Z. and Chan, L. New approaches for solving permutation indeterminacy and scaling ambiguity in frequency domain separation of convolved mixtures. In: *Neural Networks (IJCNN), 2011 Int. Jt. Conf.*, pp. 911–918. 2011.

[84] Chung, D. Y., Sim, Y. B., Park, K. T., Yi, S. H., Shin, J. C., and Kim, S. P. Spectral analysis of fetal heart rate variability as a predictor of intrapartum fetal distress. *Int. J. Gynaecol. Obs.*, **73**(2):pp. 109–16, 2001.

[85] Clifford, G., Sameni, R., Ward, J., Robinson, J., and Wolfberg, A. J. Clinically accurate fetal ECG parameters acquired from maternal abdominal sensors. *Am. J. Obs. Gynecol.*, **205**(1):p. 47, 2011.

[86] Clifford, G. D. *Signal Processing Methods for Heart Rate Variability*. Ph.D. thesis, University of Oxford, 2002.

[87] Clifford, G. D. A novel framework for signal representation and source separation: Applications to filtering and segmentation of biosignals. *J.Biol. Syst.*, **14**(02):pp. 169–183, 2006.

[88] Clifford, G. D., Azuaje, F., and McSharry, P. E. *Advanced methods and tools for ECG data analysis*. Artech House, 2006. ISBN 1580539661.

[89] Clifford, G. D., Behar, J., Li, Q., and Rezek, I. Signal quality indices and data fusion for determining clinical acceptability of electrocardiograms. *Physiol. Meas.*, **33**(9):pp. 1419–1433, 2012.

[90] Clifford, G. D. and McSharry, P. E. Method to filter ECGs and evaluate clinical parameter distortion using realistic ECG model parameter fitting. *Comput. Cardiol.*, **32**:pp. 715–718, 2005.

[91] Clifford, G. D., Shoeb, A., McSharry, P. E., and Janz, B. A. Model-based filtering, compression and classification of the ECG. In: *Proc. Bioelectromagn. 5th Int. Symp. Noninvasive Funct. Source Imaging within Hum. Brain Hear. (BEM NFSI)*, pp. 158–161. Minnesota, USA, 2005.

[92] Clifford, G. D., Silva, I., Behar, J., and Moody, G. B. Non-invasive fetal ECG analysis. *Physiol. Meas.*, **35**(8):p. 1521, 2014.

[93] Clifford, G. D. and Tarassenko, L. Quantifying errors in spectral estimates of HRV due to beat replacement and resampling. *IEEE Trans. Biomed. Eng.*, **52**(4):pp. 630–8, 2005.

[94] Cohen, J. A coefficient of agreement for nominal scales. *Educ. Psychol. Meas.*, **XX**(1):pp. 37–46, 1960.

[95] Cohen, J. Weighted kappa: Nominal scale agreement provision for scaled disagreement or partial credit. *Psychol. Bull.*, 1968.

[96] Cohen, J. *Statistical Power Analysis for the Behavioral Sciences*. L. Erlbaum Associates, 1988. ISBN 0805802835.

[97] Cohen, J. A power primer. *Psychol. Bull.*, **112**(1):pp. 155–159, 1992.

[98] Couderc, J. P. The Telemetric and Holter ECG Warehouse initiative (THEW): A data repository for the design, implementation and validation of ECG-related technologies. In: *IEEE EMBC*, pp. 6252–6255. 2010. ISBN 9781424441235.

[99] Cremer, M. Über die Direkte Ableitung der Aktionstrome des Menschlichen Herzens vom Oesophagus und Über das Elektrokardiogramm des Fetus. *Münchener Medizinische Wochenschrift*, **53**:pp. 811–813, 1906.

[100] Crowe, J. a., Harrison, A., and Hayes-Gill, B. R. The feasibility of long-term fetal heart rate monitoring in the home environment using maternal abdominal electrodes. *Physiol. Meas.*, **16**(3):pp. 195–202, 1995.

[101] Daluwatte, C., Johannesen, L., Galeotti, L., Vicente, J., Strauss, D. G., and Scully, C. G. Assessing ECG signal quality indices to discriminate ECGs with artefacts from pathologically different arrhythmic ECGs. *Physiol. Meas.*, **37**(8):pp. 1370–1382, 2016.

[102] Darouach, M., Zasadzinski, M., and Boutayeb, M. Extension of minimum variance estimation for systems with unknown inputs. *Automatica*, **39**:pp. 867–876, 2003.

[103] Darouach, M., Zasadzinski, M., Onana, a. B., and Nowakowski, S. Kalman filtering with unknown inputs via optimal state estimation of singular systems. *Int. J. Syst. Sci.*, **26**(1995):pp. 2015–2028, 1995.

[104] Darwin, C. *On the Origin of Species by means of Sexual Selection*. D. Appleton and Company, New York, N.Y., 1859.

[105] Dawes, G., Rosevear, S., Pello, L., Moulden, M., and Redman, C. Computerized analysis of episodic changes in fetal heart rate variation in early labor. *Am. J. Obs. Gynecol.*, **165**(3):pp. 618–624, 1991.

[106] Dawes, G. S., Houghton, C. R., Redman, C. W., and Visser, G. H. Pattern of the normal human fetal heart rate. *BJOG*, **89**(4):pp. 276–84, 1982.

[107] Dawes, G. S., Visser, G. H., Goodman, J. D., and Redman, C. W. Numerical analysis of the human fetal heart rate: the quality of ultrasound records. *Am. J. Obs. Gynecol.*, **141**(1):pp. 43–52, 1981.

[108] de Haan, G. and Jeanne, V. Robust pulse-rate from chrominance-based rPPG. *IEEE Trans. Biomed. Eng.*, **60**(10):pp. 1–9, 2013.

[109] De Lathauwer, L., De Moor, B., Vandewalle, J., and Lathauwer, L. {F}etal electrocardiogram extraction by blind source subspace separation. *IEEE Trans. Biomed. Eng.*, **47**(5):pp. 567–572, 2000.

[110] de Vaus, D. *Surveys in Social Research*. Routledge, 2013. ISBN 1136996311.

[111] Deng, Y., Wolf, W., Schnell, R., and Appel, U. New aspects to event-synchronous cancellation of ECG interference: an application of the method in diaphragmatic EMG signals. *IEEE Trans. Biomed. Eng.*, **47**(9):pp. 1177–1184, 2000.

[112] Deutsche Hygiene-Museum Dresden. Mütterliche Fetale Blutkreislauf. 2008.

[113] Di Marco, L., Marzo, A., and Frangi, A. Multichannel Foetal Heartbeat Detection by Combining Source Cancellation with Expectation-weighted Estimation of Fiducial Points. In: *Comput. Cardiol. (2010).*, pp. 329–332. 2013.

[114] Dildy, G., Clark, S., and Loucks, C. Preliminary experience with intrapartum fetal pulse oximetry in humans. *Obs. Gynecol.*, 1993.

[115] DiPietro, J. A., Costigan, K. A., and Gurewitsch, E. D. Fetal response to induced maternal stress. *Early Hum. Dev.*, **74**(2):pp. 125–138, 2003.

[116] DiPietro, J. A., Costigan, K. A., Nelson, P., Gurewitsch, E. D., and Laudenslager, L. Fetal responses to induced maternal relaxation during pregnancy. *Biol. Psychol.*, **77**(1):pp. 11–19, 2008.

[117] DiPietro, J. a., Hilton, S. C., Hawkins, M., Costigan, K. a., and Pressman, E. K. Maternal stress and affect influence fetal neurobehavioral development. *Dev. Psychobiol.*, **38**(5):pp. 659–668, 2002.

[118] Domingos, P. and Pazzani, M. On the Optimality of the Simple Bayesian Classifier under Zero-One Los. *Mach. Learn.*, **29**(2/3):pp. 103–130, 1997.

[119] DuBose, T. J. Embryonic Heart Rate and Age. *J. Diagnostic Med. Sonogr.*, **6**(3):pp. 151–157, 1990.

[120] Duck, F. A. Safety Aspects of the Use of Ultrasound in Pregnancy. *Fetal Matern. Med. Rev.*, **14**(1):p. S0965539502001006, 2003.

[121] Durrant-Whyte, H. Introduction to estimation and the Kalman Filter. Technical report, University of Sidney, 2001.

[122] East, C. E., Begg, L., Colditz, P. B., and Lau, R. Fetal pulse oximetry for fetal assessment in labour. *Cochrane Database Syst. Rev.*, **10**:p. CD004075, 2014.

[123] Ebenezer, D. and Krishnamurthy, V. Wave digital matched filter for electrocardiogram preprocessing. *J. Biomed. Eng.*, **15**(2):pp. 132–4, 1993.

[124] Escofier, B. Traitement simultané de variables qualitatives et quantitatives en analyse factorielle. *Cah. Anal. Donnees*, 1979.

[125] Evensen, G. Sequential data assimilation with a nonlinear quasi-geostrophic model using Monte Carlo methods to forecast error statistics. *J. Geophys. Res.*, **99**(C5):p. 10143, 1994.

[126] Evensen, G. The ensemble Kalman filter: Theoretical formulation and practical implementation. *Ocean Dyn.*, **53**(4):pp. 343–367, 2003.

[127] Evensen, G. Sampling strategies and square root analysis schemes for the EnKF. *Ocean Dyn.*, **54**(6):pp. 539–560, 2004.

[128] Evensen, G. *Data Assimilation: The Ensemble Kalman Filter*. Springer Berlin / Heidelberg, 2007. ISBN 9783540383000.

[129] Fanelli, A. *TeleFetal Care: development of a wearable system for fetal monitoring during pregnancy*. Ph.D. thesis, Politecnico di Milano, 2013.

[130] Fang, H., de Callafon, R. A., and Cortés, J. Simultaneous input and state estimation for nonlinear systems with applications to flow field estimation. *Automatica*, **49**(9):pp. 2805–2812, 2013.

[131] Fang, H., Shi, Y., and Yi, J. On stable simultaneous input and state estimation for discrete-time linear systems. *Int. J. Adapt. Control Signal Process.*, **25**(8):pp. 671–686, 2011.

[132] Farrell, T. G., Bashir, Y., Cripps, T., Malik, M., Poloniecki, J., Bennett, E., Ward, D. E., and Camm, A. Risk stratification for arrhythmic events in postinfarction patients based on heart rate variability, ambulatory electrocardiographic variables and the signal-averaged electrocardiogram. *J. Am. Coll. Cardiol.*, **18**(3):pp. 687–697, 1991.

[133] Feinstein, A. R. and Cicchetti, D. V. High agreement but low kappa: I. The problems of two paradoxes. *J. Clin. Epidemiol.*, **43**(6):pp. 543–9, 1990.

[134] Ferrario, M., Magenes, G., Campanile, M., Carbone, I. F., Di Lieto, A., and Signorini, M. G. Multiparameter analysis of heart rate variability signal for the investigation of high risk fetuses. In: *IEEE EMBC*, pp. 4662–4665. 2009.

[135] Ferrario, M., Signorini, M. G., and Magenes, G. Comparison between fetal heart rate standard parameters and complexity indexes for the identification of severe intrauterine growth restriction. *Methods Inf. Med.*, **46**(2):pp. 295–298, 2007.

[136] Ferrario, M., Signorini, M. G., and Magenes, G. Estimation of long-term correlations from Fetal Heart Rate variability signal for the identification of pathological fetuses. In: *IEEE EMBC*. 2007.

[137] Ferrario, M., Signorini, M. G., Magenes, G., and Cerutti, S. Comparison of entropy-based regularity estimators: application to the fetal heart rate signal for the identification of fetal distress. *IEEE Trans. Biomed. Eng.*, **53**(1):pp. 119–125, 2006.

[138] Fleiss, J. Measuring nominal scale agreement among many raters. *Psychol. Bull.*, 1971.

[139] Frank, B., Pompe, B., Schneider, U., and Hoyer, D. Permutation entropy improves fetal behavioural state classification based on heart rate analysis from biomagnetic recordings in near term fetuses. *Med. Biol. Eng. Comput.*, **44**(3):pp. 179–87, 2006.

[140] Frasch, M. G., Müller, T., Weiss, C., Schwab, K., Schubert, H., and Schwab, M. Heart rate variability analysis allows early asphyxia detection in ovine fetus. *Reprod Sci.*, **16**(5):pp. 509–517, 2009.

[141] Frasch, M. G., Xu, Y., Stampalija, T., Durosier, L. D., Herry, C., Wang, X., Casati, D., Seely, A. J., Alfirevic, Z., Gao, X., and Ferrazzi, E. Correlating multidimensional fetal heart rate variability analysis with acid-base balance at birth. *Physiol. Meas.*, **35**(12):pp. L1–12, 2014.

[142] Frei, M. and Kunsch, H. R. Bridging the ensemble Kalman and particle filters. *Biometrika*, **100**(4):pp. 781–800, 2013.

[143] Fretts, R. C., Schmittdiel, J., McLean, F. H., Usher, R. H., and Goldman, M. B. Increased maternal age and the risk of fetal death. *N. Engl. J. Med.*, **333**(15):pp. 953–957, 1995.

[144] Friesen, G. M., Jannett, T. C., Jadallah, M. A., Yates, S. L., Quint, S. R., and Nagle, H. T. A comparison of the noise sensitivity of nine QRS detection algorithms. *IEEE Trans. Biomed. Eng.*, **37**(1):pp. 85–98, 1990.

[145] Fuchs, T., Pomorski, M., Grobelak, K., Tomiałowicz, M., and Zimmer, M. Signal loss during fetal heart rate monitoring using maternal abdominal surface electrodes between 28 and 42 weeks of pregnancy. *Adv. Clin. Exp. Med.*, **23**(5):pp. 813–9, 2014.

[146] Fukushima, A., Nakai, K., Itoh, M., Horigome, H., Suwabe, A., Tohyama, K., Kobayashi, K., Yoshizawa, M., and Sugiyama, T. Assessment of Fetal Autonomic Nervous System Activity by Fetal Magnetocardiography - ProQuest. *Clin. Med. Cardiol.*, **1**:p. 33, 2008.

[147] Funk, N. A Study of the Kalman Filter applied to Visual Tracking. Technical Report 1, University of Alberta, 2003.

[148] Gacek, A. and Pedrycz, W. *ECG Signal Processing, Classification and Interpretation: A Comprehensive Framework of Computational Intelligence*. Springer Science & Business Media, 2011. ISBN 0857298682.

[149] Gambarotta, N., Aletti, F., Baselli, G., and Ferrario, M. A review of methods for the signal quality assessment to improve reliability of heart rate and blood pressures derived parameters. *Med. Biol. Eng. Comput.*, **54**(7):pp. 1025–35, 2016.

[150] Gardiner, C. W. *Handbook of stochastic methods*. Springer, 1985. ISBN 3540616349.

[151] Gelb, A. *Applied Optimal Estimation*. MIT Press, 1974. ISBN 0262570483.

[152] Gennat, M. Extraktion der fetalen Herzrate unter Berücksichtigung der Signalqualität. Technical report, Technische Universität Dresden, 2016.

[153] Gerstner, T., Sprenger, J., Schaible, T., Weiss, C., and Koenig, S. Reifung des Autonomen Nervensystems: Unterschiede in der Herzfrequenzvariabilität in unterschiedlichen Gestationswochen. *Z .Geburtshilfe Neonatol.*, **214**(01):pp. 11–14, 2009.

[154] Ghaffari, A., Golbayani, H., and Ghasemi, M. A new mathematical based QRS detector using continuous wavelet transform. *Comput. Electr. Eng.*, **34**(2):pp. 81–91, 2008.

[155] Ghaffari, A., Mollakazemi, M. J., Atyabi, S. A., and Niknazar, M. Robust fetal QRS detection from noninvasive abdominal electrocardiogram based on channel selection and simultaneous multichannel processing. *Australas. Phys. Eng. Sci. Med.*, 2015.

[156] Ghahremani, E. and Kamwa, I. Dynamic state estimation in power system by applying the extended kalman filter with unknown inputs to phasor measurements. *IEEE Trans. Power Syst.*, **26**(4):pp. 2556–2566, 2011.

[157] Gierałtowski, J., Hoyer, D., Tetschke, F., Nowack, S., Schneider, U., and Zebrowski, J. Development of multiscale complexity and multifractality of fetal heart rate variability. *Auton. Neurosci.*, **178**(1-2):pp. 29–36, 2013.

[158] Gillijns, S. and De Moor, B. Unbiased minimum-variance input and state estimation for linear discrete-time systems. *Automatica*, **43**(1):pp. 111–116, 2007.

[159] Gillijns, S., Mendoza, O., Chandrasekar, J., De Moor, B., Bernstein, D., and Ridley, A. What is the ensemble Kalman filter and how well does it work? In: *Am. Control Conf.*, p. 6 pp. 2006. ISBN 1-4244-0209-3.

[160] Gillijns, S. and Moor, B. D. Unbiased minimum-variance input and state estimation for linear discrete-time systems with direct feedthrough. *Automatica*, 2007.

[161] Goldberger, A. L., Amaral, L. A., Glass, L., Hausdorff, J. M., Ivanov, P. C., Mark, R. G., Mietus, J. E., Moody, G. B., Peng, C. K., and Stanley, H. E. PhysioBank, PhysioToolkit, and PhysioNet: components of a new research resource for complex physiologic signals. *Circulation*, **101**(23):pp. E215—-E220, 2000.

[162] Gomes, J. A., Cain, M. E., Buxton, A. E. A., Josephson, M. E., Lee, K. L., and Hafley, G. E. Prediction of Long-Term Outcomes by Signal-Averaged Electrocardiography in Patients With Unsustained Ventricular Tachycardia, Coronary Artery Disease, and Left Ventricular Dysfunction. *Circulation*, **104**(4):pp. 436–441, 2001.

[163] Graatsma, E. M., Jacod, B. C., van Egmond, L. A. J., Mulder, E. J. H., and Visser, G. H. A. Fetal electrocardiography: feasibility of long-term fetal heart rate recordings. *BJOG*, **116**(2):pp. 334—-7, discussion 337–8, 2009.

[164] Graczyk, S., Jezewski, J., Wrobel, J., and Gacek, A. Abdominal electrohysterogram data acquisition problems and their source of origin. In: *Proc. First Reg. Conf. IEEE Eng. Med. Biol. Soc. 14th Conf. Biomed. Eng. Soc. India. An Int. Meet*, pp. PS13–PS14. IEEE, 1995. ISBN 0-7803-2711-X.

[165] Greene, K. R., Dawes, G. S., Lilja, H., and Rosén, K. G. Changes in the ST waveform of the fetal lamb electrocardiogram with hypoxemia. *Am. J. Obs. Gynecol.*, **144**(8):pp. 950–8, 1982.

[166] Grewal, M. S., Andrews, A. P., and Grewal Mohinder S. l, A. P. A. *Kalman filtering: Theory and Practice using Matlab*. John Wiley & Sons, Inc., 3rd edition, 2008.

[167] Grunitz, E. Entwicklung von Methoden zur Analyse und Aufbereitung biomedizinischer Messdaten. Technical report, Technische Universität Dresden, 2012.

[168] Gwet, K. *Handbook of inter-rater reliability: The definitive guide to measuring the extent of agreement among raters*. Advanced Analytics, LLC, 2014.

[169] Haghpanahi, M. and Borkholder, D. A. Fetal QRS extraction from abdominal recordings via model-based signal processing and intelligent signal merging. *Physiol. Meas.*, **35**(8):pp. 1591–605, 2014.

[170] Haghpanahi, M., Sameni, R., and Borkholder, D. A. Scoring consensus of multiple ECG annotators by optimal sequence alignment. In: *IEEE EMBC*, volume 2014, pp. 1855–9. 2014.

[171] Hamilton, P. and Tompkins, W. Quantitative investigation of QRS detection rules using the MIT/BIH arrhythmia database. *IEEE Trans. Biomed. Eng.*, 1986.

[172] Harding, R. Fetal pulmonary development: the role of respiratory movements. *Equine Vet. J. Suppl.*, **24**:pp. 32–39, 1997.

[173] Hasan, M. a., Reaz, M. B. I., Ibrahimy, M. I., Hussain, M. S., and Uddin, J. Detection and Processing Techniques of FECG Signal for Fetal Monitoring. *Biol. Proced. Online*, **11**(1):pp. 263–95, 2009.

[174] Hayes, A. F. and Krippendorff, K. Answering the Call for a Standard Reliability Measure for Coding Data. *Commun. Methods Meas.*, **1**(1):pp. 77–89, 2007.

[175] Haykin, S. *Kalman Filtering and Neural Networks*. Wiley-Interscience, 2001. ISBN 0471369985.

[176] Hernando, D., Bailon, R., Almeida, R., and Hernandez, A. Computing in Cardiology Conference (CinC), 2014. In: *Comput. Cardiol. (2010).*, pp. 737–740. 2014.

[177] Herrmann, P. Aufnahme und Verarbeitung des kapazitiven Elektrokardiogramms. Diplomarbeit, TU Dresden, 2014.

[178] Hills, M. Embriology. 2016. URL `https://embryology.med.unsw.edu.au/embryology/`.

[179] Himmelsbach, T. Weiterentwicklung eines Kalman-basierten Algorithmus zur Extraktion des fetalen EKG aus abdominalen Aufnahmen. Technical report, TU Dresden, 2013.

[180] Hoffmann, J. Extraktion von fetalen Elektrokardiogrammen mittels eines zeitvarianten Kalman-Filter Modells. Technical report, Technische Universität Dresden, 2016.

[181] Højgaard, M. V., Holstein-Rathlou, N. H., Agner, E., and Kanters, J. K. Dynamics of spectral components of heart rate variability during changes in autonomic balance. *Am. J. Physiol.*, **275**(1 Pt 2):pp. H213–9, 1998.

[182] Holschneider, M. and Kronland-Martinet, R. A real-time algorithm for signal analysis with the help of the wavelet transform. *Wavelets*, 1989.

[183] Hon, E. H. and Hess, O. W. Instrumentation of Fetal Electrocardiography. *Science (80-.).*, **125**(3247):pp. 553–554, 1957.

[184] Hon, E. H. and Lee, S. T. Electronic evaluation of the fetal heart rate, VIII. Patterns preceding fetal death: Further observations. *Am. J. Obs. Gynecol.*, **87**:pp. 814–26, 1963.

[185] Hopkins, P., Outram, N., Löfgren, N., Ifeachor, E. C., and Rosén, K. G. A comparative study of fetal heart rate variability analysis techniques. In: *IEEE EMBC*, volume 1, pp. 1784–7. 2006.

[186] Hou, M. and Patton, R. Optimal filtering for systems with unknown inputs. *IEEE Trans. Autom. Contr.*, **43**(3):pp. 445–449, 1998.

[187] Houtekamer, P. and Mitchell, H. L. Ensemble Kalman filtering. *Q. J. R. Meteorol. Soc.*, **131**(613):pp. 3269–3289, 2005.

[188] Hoyer, D., Heinicke, E., Jaekel, S., Tetschke, F., Di Pietro Paolo, D., Haueisen, J., Schleusner, E., and Schneider, U. Indices of fetal development derived from heart rate patterns. *Early Hum. Dev.*, **85**(6):pp. 379–86, 2009.

[189] Hoyer, D., Nowack, S., Bauer, S., Tetschke, F., Rudolph, A., Wallwitz, U., Jaenicke, F., Heinicke, E., Götz, T., Huonker, R., Witte, O. W., Schleussner, E., and Schneider, U. Fetal development of complex autonomic control evaluated from multiscale heart rate patterns. *Am. J. Physiol. Regul. Integr. Comp. Physiol.*, **304**(5):pp. R383–92, 2013.

[190] Hoyer, D., Tetschke, F., Jaekel, S., Nowack, S., Witte, O. W., Schleußner, E., and Schneider, U. Fetal functional brain age assessed from universal developmental indices obtained from neuro-vegetative activity patterns. *PLoS One*, **8**(9):p. e74431, 2013.

[191] Hsieh, C.-S. Robust two-stage Kalman filters for systems with unknown inputs. *IEEE Trans. Autom. Contr.*, **45**(12):pp. 2374–2378, 2000.

[192] Hsieh, C.-S. Extension of unbiased minimum-variance input and state estimation for systems with unknown inputs. *Automatica*, **45**(9):pp. 2149–2153, 2009.

[193] Hu, X., Nenov, V., Bergsneider, M., Glenn, T. C., Vespa, P., and Martin, N. Estimation of Hidden State Variables of the Intracranial System Using Constrained Nonlinear Kalman Filters. *IEEE Trans. Biomed. Eng.*, **54**(4):pp. 597–610, 2007.

[194] Huelsbusch, M. and Blazek, V. Contactless mapping of rhythmical phenomena in tissue perfusion using PPGI. In: Clough, A. V. and Chen, C.-T. (editors), *Med. Imaging 2002*, pp. 110–117. International Society for Optics and Photonics, San Diego, USA, 2002.

[195] Hurezeanu, B., Ungureanu, G. M., Taralunga, D. D., Strungaru, R., Gussi, I., and Wolf, W. FECG delineation from abdominal signals using wavelet transform. In: *Int. Conf. Expo. Electr. Power Eng.*, pp. 518–521. IEEE, 2014. ISBN 978-1-4799-5849-8.

[196] Hutter, D., Kingdom, J., and Jaeggi, E. Causes and mechanisms of intrauterine hypoxia and its impact on the fetal cardiovascular system: a review. *Int. J. Pediatr.*, **2010**:p. 401323, 2010.

[197] Hyvärinen, A. Fast and robust fixed-point algorithms for independent component analysis. *IEEE Trans. Neural Netw.*, **10**(3):pp. 626–34, 1999.

[198] Inanlou, M. R., Baguma-Nibasheka, M., and Kablar, B. The role of fetal breathing-like movements in lung organogenesis. *Histol. Histopathol.*, **20**(4):pp. 1261–1266, 2005.

[199] Ivanov, P. C., Ma, Q. D. Y., and Bartsch, R. P. Maternal-fetal heartbeat phase synchronization. *Proc. Natl. Acad. Sci. U. S. A.*, **106**(33):pp. 13641–2, 2009.

[200] Jaeger, H. The "echo state" approach to analysing and training recurrent neural networks. Technical report, German National Research Center for Information Technology, 2001.

[201] James, C. and Hesse, C. Independent component analysis for biomedical signals. *Physiol. Meas.*, 2005.

[202] James, T. N. Cardiac conduction system: Fetal and postnatal development. *Am. J. Cardiol.*, **25**(2):pp. 213–226, 1970.

[203] Jane, R., Blasi, A., Garcia, J., and Laguna, P. Evaluation of an automatic threshold based detector of waveform limits in Holter ECG with the QT database. In: *Comput. Cardiol. (2010).*, pp. 295–298. IEEE, 1997. ISBN 0-7803-4445-6.

[204] Jansen, B. H., Bourne, J. R., and Ward, J. W. Autoregressive estimation of short segment spectra for computerized EEG analysis. *IEEE Trans. Biomed. Eng.*, **28**(9):pp. 630–8, 1981.

[205] Javadi, M., Ebrahimpour, R., Sajedin, A., Faridi, S., and Zakernejad, S. Improving ECG classification accuracy using an ensemble of neural network modules. *PLoS One*, **6**(10):p. e24386, 2011.

[206] Jazwinski, A. H. *Stochastic Processes and Filtering Theory*. Courier Corporation, 1970. ISBN 0080960901.

[207] Jérôme, P. Analyse factorielle de données mixtes. *Rev. Stat. appliquée*, **52**(4):pp. 93—-111, 2002.

[208] Jezewski, J., Matonia, A., Kupka, T., Roj, D., and Czabanski, R. Determination of fetal heart rate from abdominal signals: evaluation of beat-to-beat accuracy in relation to the direct fetal electrocardiogram. *Biomed. Tech.*, **57**(5):pp. 383–94, 2012.

[209] Johnson, A. E. W., Behar, J., Andreotti, F., Clifford, G. D., and Oster, J. R-Peak Estimation using Multimodal Lead Switching. In: *Comput. Cardiol. (2010).*, pp. 281–284. IEEE, Cambridge, USA, 2014.

[210] Johnson, A. E. W., Cholleti, S. R., Buchman, T. G., and Clifford, G. D. Improved respiration rate estimation using a Kalman filter and wavelet cross-coherence. In: *Comput. Cardiol. (2010).*, pp. 791–794. 2013.

[211] Johnson, A. E. W. A., Behar, J., Andreotti, F., Clifford, G. D. G., and Oster, J. Multimodal heart beat detection using signal quality indices. *Physiol. Meas.*, **36**(8):pp. 1665–77, 2015.

[212] Jørgensen, J. S. and Weber, T. Fetal scalp blood sampling in labor–a review. *Acta Obs. Gynecol. Scand.*, **93**(6):pp. 548–55, 2014.

[213] Julien, C. The enigma of Mayer waves: Facts and models. 2006.

[214] Julier, S. J. and Uhlmann, J. K. New extension of the Kalman filter to nonlinear systems. In: *AeroSense*, pp. 182–193. International Society for Optics and Photonics, 1997.

[215] Julier, S. J. and Uhlmann, J. K. Unscented filtering and nonlinear estimation. *Proc. IEEE*, **92**(3):pp. 401–422, 2004.

[216] Kailath, T. An innovations approach to least-squares estimation–Part I: Linear filtering in additive white noise. *IEEE Trans. Autom. Contr.*, **13**(6):pp. 646–655, 1968.

[217] Kalman, R. E. A New Approach to Linear Filtering and Prediction Problems. *J. Basic Eng.*, **82**(1):pp. 35–45, 1960.

[218] Kalman, R. E. and Bucy, R. S. New results in linear filtering and prediction theory. *J. Fluids Eng.*, **83**(1):pp. 95—-108, 1961.

[219] Kanjilal, P. P., Palit, S., and Saha, G. Fetal ECG extraction from single-channel maternal ECG using singular value decomposition. *IEEE Trans. Biomed. Eng.*, **44**(1):pp. 51–9, 1997.

[220] Kaplan, D. T. Simultaneous QRS detection and feature extraction using simple matched filter basis functions. In: *Comput. Cardiol.*, pp. 503–506. 1990. ISBN 0818622253.

[221] Karvounis, E. C. E., Tsipouras, M. M. G., Fotiadis, D. I. D. I., and Naka, K. K. K. An Automated Methodology for Fetal Heart Rate Extraction From the Abdominal Electrocardiogram. *IEEE J. Biomed. Heal. Inform.*, **11**(6):pp. 628–638, 2007.

[222] Kay, S. M. *Fundamentals of Statistical Signal Processing: Estimation Theory*, volume 1. Prentice Hall, 1993. ISBN 0-13-345711-7.

[223] Keller, J. and Darouach, M. Two-stage Kalman estimator with unknown exogenous inputs. *Automatica*, 1999.

[224] Kennedy, R. G. Electronic fetal heart rate monitoring: retrospective reflections on a twentieth-century technology. *J. R. Soc. Med.*, **91**, 1998.

[225] Kiefer-Schmidt, I., Raufer, J., Braendle, J., Muenssinger, J., Abele, H., Wallwiener, D., Eswaran, H., and Preissl, H. Is there a relationship between fetal brain function and the fetal behavioral state? A fetal MEG-study. *J. Perinat. Med.*, **41**(5):pp. 605–612, 2013.

[226] Kinsella, M. T. and Monk, C. Impact of Maternal Stress, Depression & Anxiety on Fetal Neurobehavioral Development. *Clin. Obs. Gynecol.*, **52**(3):pp. 425–440, 2009.

[227] Kirkpatrick, S., Gelatt, C. D., and Vecchi, M. P. Optimization by simulated annealing. *Science (80-.).*, **220**(4598):pp. 671–80, 1983.

[228] Kisilevsky, B. S. and Brown, C. A. Comparison of fetal and maternal heart rate measures using electrocardiographic and cardiotocographic methods. *Infant Behav. Dev.*, **42**:pp. 142–151, 2016.

[229] Kitanidis, P. Unbiased minimum-variance linear state estimation. *Automatica*, 1987.

[230] Kitterman, J. A. Physiological factors in fetal lung growth. *Can. J. Physiol. Pharmacol.*, **66**(8):pp. 1122–8, 1988.

[231] Kligfield, P., Gettes, L. S., Bailey, J. J., Childers, R., Deal, B. J., Hancock, E. W., van Herpen, G., Kors, J. A., Macfarlane, P., Mirvis, D. M., Pahlm, O., Rautaharju, P., Wagner, G. S., Josephson, M., Mason, J. W., Okin, P., Surawicz, B., and Wellens, H. Recommendations for the Standardization and Interpretation of the ElectrocardiogramPart I: The Electrocardiogram and Its Technology A Scientific Statement From the American Heart Association Electrocardiography and Arrhythmias Committee, Council on Clinic. *J. Am. Coll. Cardiol.*, **49**(10):pp. 1109–1127, 2007.

[232] Köhler, B.-U., Hennig, C., and Orglmeister, R. The principles of software QRS detection. *IEEE Eng. Med. Biol. Mag.*, **21**(1):pp. 42–57, 2002.

[233] Kolmogorov, A. N. Stationary sequences in Hilbert space. *Bull. Moscow Univ.*, **2**(6):pp. 1–40, 1941.

[234] Kononenko, I., Šimec, E., and Robnik-Šikonja, M. Overcoming the myopia of inductive learning algorithms with RELIEFF. *Appl. Intell.*, **7**(1):pp. 39–55, 1997.

[235] Kors, J. A., van Herpen, G., and van Bemmel, J. H. QT Dispersion as an Attribute of T-Loop Morphology. *Circulation*, **99**(11):pp. 1458–1463, 1999.

[236] Kotas, M. Nonlinear projective filtering of ECG signals. In: *Biomed. Eng. InTech, Rijeka, Croat.* InTech, 2009.

[237] Krippendorff, K. Reliability of binary attribute data. *Biometrics*, **34**(1):pp. 142–144, 1978.

[238] Krippendorff, K. *Content Analysis: An Introduction to Its Methodology*, volume 79. Sage Publications, 2004. ISBN 0761915451.

[239] Laguna, P. A Database for Evaluation of Algorithms for Measurement of QT and other Waveform Intervals in the ECG. In: *Comput. Cardiol.*, pp. 673–67. 1997.

[240] Lange, S., Van Leeuwen, P., Geue, D., Hatzmann, W., and Grönemeyer, D. Influence of gestational age, heart rate, gender and time of day on fetal heart rate variability. *Med. Biol. Eng. Comput.*, **43**(4):pp. 481–486, 2005.

[241] Lange, S., Van Leeuwen, P., Schneider, U., Frank, B., Hoyer, D., Geue, D., and Grönemeyer, D. Heart rate features in fetal behavioural states. *Early Hum. Dev.*, **85**(2):pp. 131–135, 2009.

[242] Lawn, J. E., Blencowe, H., Pattinson, R., Cousens, S., Kumar, R., Ibiebele, I., Gardosi, J., Day, L. T., and Stanton, C. Stillbirths: Where? When? Why? How to make the data count? *Lancet*, **377**(9775):pp. 1448–1463, 2011.

[243] Lempe, G., Zaunseder, S., and Wirthgen, T. Bildverarbeitung für die Medizin 2013. In: *Bild. für die Medizin 2013*, pp. 99–103. 2013. ISBN 978-3-642-36479-2.

[244] Lewis, D. and Downe, S. FIGO consensus guidelines on intrapartum fetal monitoring: Intermittent auscultation. *Int. J. Gynaecol. Obs.*, 2015.

[245] Lewis, F. L., Xie, L., and Popa, D. *Optimal and Robust Estimation: With an Introduction to Stochastic Control Theory, Second Edition*. CRC Press, 2007. ISBN 1420008293.

[246] Lewis, M. J. Review of electromagnetic source investigations of the fetal heart. *Med. Eng. Phys.*, **25**(10):pp. 801–810, 2003.

[247] Li, C., Zheng, C., and Tai, C. Detection of ECG characteristic points using wavelet transforms. *IEEE Trans. Biomed. Eng.*, **42**(1):pp. 21–8, 1995.

[248] Li, G., Zeng, X., Zhou, X., and Liu, Q. Robust adaptive fetal heart rate estimation for single-channel abdominal ECG recording. In: *Int. Conf. Biomed. Eng. Informatics*, pp. 587–591. IEEE, 2012. ISBN 978-1-4673-1184-7.

[249] Li, H., Kwong, S., Yang, L., Huang, D., and Xiao, D. Hilbert-Huang transform for analysis of heart rate variability in cardiac health. *IEEE/ACM Trans. Comput. Biol. Bioinforma.*, 2011.

[250] Li, Q. and Clifford, G. D. Dynamic time warping and machine learning for signal quality assessment of pulsatile signals. *Physiol. Meas.*, **33**(9):pp. 1491–1501, 2012.

[251] Li, Q., Mark, R. G., and Clifford, G. D. Robust heart rate estimation from multiple asynchronous noisy sources using signal quality indices and a Kalman filter. *Physiol. Meas.*, **29**(1):pp. 15–32, 2008.

[252] Li, Q., Mark, R. G., and Clifford, G. D. Artificial arterial blood pressure artifact models and an evaluation of a robust blood pressure and heart rate estimator. *Biomed. Eng. Online*, **8**:p. 13, 2009.

[253] Lin, C., Bugallo, M., Mailhes, C., and Tourneret, J. ECG denoising using a dynamical model and a marginalized particle filter. In: *Proc. Conf Signals, Syst. Comput.*, pp. 1679–1683. 2011.

[254] Lipponen, J. A. and Tarvainen, M. P. Principal component model for maternal ECG extraction in fetal QRS detection. *Physiol. Meas.*, **35**(8):pp. 1637–48, 2014.

[255] Lukoševičius, M. and Marozas, V. Noninvasive fetal QRS detection using an echo state network and dynamic programming. *Physiol. Meas.*, **35**(8):pp. 1685–97, 2014.

[256] Lunshof, S., Boer, K., Wolf, H., van Hoffen, G., Bayram, N., and Mirmiran, M. Fetal and maternal diurnal rhythms during the third trimester of normal pregnancy: outcomes of computerized analysis of continuous twenty-four-hour fetal heart rate recordings. *Am. J. Obs. Gynecol.*, **178**(2):pp. 247–54, 1998.

[257] Ma, Y., Xiao, Y., Wei, G., and Sun, J. Fetal ECG extraction using adaptive functional link artificial neural network. In: *Signal Inf. Process. Assoc. Annu. Summit Conf. (APSIPA), 2014 Asia-Pacific*, pp. 1–4. IEEE, 2014. ISBN 978-6-1636-1823-8.

[258] Ma, Y., Xiao, Y., Wei, G., and Sun, J. A multichannel nonlinear adaptive noise canceller based on generalized FLANN for fetal ECG extraction. *Meas. Sci. Technol.*, **27**(1):p. 015703, 2016.

[259] Machin, G. A. Differential diagnosis of hydrops fetalis. *Am. J. Med. Genet.*, **9**(4):pp. 341–50, 1981.

[260] Mack, G. A. and Skillings, J. H. A Friedman-type rank test for main effects in a two factor ANOVA. *J. Amer. Stat. Assoc.*, **75**(372):pp. 947–951, 1980.

[261] Maeda, K. History of fetal heart rate monitoring. *Ultrasound Rev. Obs. Gynecol.*, **2**:pp. 129–138, 2002.

[262] Mallat, S. and Zhong, S. Characterization of signals from multiscale edges. *IEEE Trans. Pattern Anal. Mach. Intell.*, 1992.

[263] Mandel, D., Oron, T., Mimouni, G. S., Littner, Y., Dollberg, S., and Mimouni, F. B. The effect of prolonged rupture of membranes on circulating neonatal nucleated red blood cells. *J. Perinatol.*, **25**(11):pp. 690–3, 2005.

[264] Mandel, J. A brief tutorial on the ensemble Kalman filter. *arXiv Prepr. arXiv0901.3725*, 2009.

[265] Marossero, D., Euliano, T. Y., Euliano, N. R., and Principe, J. Maternal-fetal monitoring system. 2005. URL `http://www.google.com.ar/patents/WO2005117692A2?cl=zh`.

[266] Maršál, K. Intrauterine growth restriction. *Curr. Opin. Obs. Gynecol.*, 2002.

[267] Martens, S. Extraction of the fetal ECG and the uterine contraction EMG from simulated abdominal recordings by principal component analysis. Technical report, Technische Universiteit Eindhoven, 2003.

[268] Martens, S. M. M., Rabotti, C., Mischi, M., and Sluijter, R. J. A robust fetal ECG detection method for abdominal recordings. *Physiol. Meas.*, **28**(4):pp. 373–388, 2007.

[269] Martinez, J. P., Almeida, R., Olmos, S., Rocha, A. P., Laguna, P., Martínez, J. P., Almeida, R., Olmos, S., Rocha, A. P., Laguna, P., and Martinez, J. P. A wavelet-based ECG delineator: evaluation on standard databases. *IEEE Trans. Biomed. Eng.*, **51**(4):pp. 570–81, 2004.

[270] Marzbanrad, F. and Kimura, Y. Automated estimation of fetal cardiac timing events from doppler ultrasound signal using hybrid models. *IEEE J. Biomed .Health Inform.*, **18**(4):pp. 1169–1177, 2014.

[271] May, L. E., Glaros, A., Yeh, H.-W., Clapp, J. F., and Gustafson, K. M. Aerobic exercise during pregnancy influences fetal cardiac autonomic control of heart rate and heart rate variability. *Early Hum. Dev.*, **86**(4):pp. 213–7, 2010.

[272] Maybeck, P. S. *Stochastic Models, Estimation, and Control, Volume 1*. Academic Press, Inc. (London) LTD., 1979. ISBN 0-12-480701-1.

[273] McDonald, J. H. Handbook of Biological Statistics. *Sparky House Publ.*, p. 291, 2009.

[274] McDonnell, C., Sameni, R., Ward, J., Robertson, J., Wolfberg, A., and Clifford, G. Evaluation of the Fetal T/R Ratio Using a Fetal Scalp Electrode and Abdominal Sensors. In: *SMFM's Annu. Pregnancy Meet.* 2011.

[275] McSharry, P. E., Clifford, G. D., Tarassenko, L., and Smith, L. A. A dynamical model for generating synthetic electrocardiogram signals. *IEEE Trans. Biomed. Eng.*, **50**(3):pp. 289–294, 2003.

[276] Mehmel, D. Einfluss der maternalen Respiration auf das fetale Elektrokardiogramm. Technical report, Institute of Biomedical Engineering - TU Dresden, 2015.

[277] Mehra, R. On the identification of variances and adaptive Kalman filtering. *IEEE Trans. Autom. Contr.*, **15**(2):pp. 175–184, 1970.

[278] Merwe, R. V. D. *Sigma-point Kalman filters for probabilistic inference in dynamic state-space models*. Ph.D. thesis, Oregon Health & Science University, 2004.

[279] Merwe, R. V. D., Wan, E., and Julier, S. Sigma-point Kalman filters for nonlinear estimation and sensor-fusion: Applications to integrated navigation. In: *Proc. AIAA ...*. 2004.

[280] Merz, E. *Ultrasound in Obstetrics and Gynecology, Volume 1*. Thieme, 2005. ISBN 1588901475.

[281] Mirmiran, M., Maas, Y. G., and Ariagno, R. L. Development of fetal and neonatal sleep and circadian rhythms. *Sleep Med. Rev.*, **7**(4):pp. 321–334, 2003.

[282] Mitchell, H. L. and Houtekamer, P. L. An Adaptive Ensemble Kalman Filter. *Mon. Wea. Rev.*, **128**(2):pp. 416–433, 2010.

[283] Mollakazemi, M. J., Atyabi, S. A., and Ghaffari, A. Heart beat detection using a multimodal data coupling method. *Physiol. Meas.*, **36**(8):pp. 1729–42, 2015.

[284] Monk, C., Fifer, W. P., Myers, M. M., Bagiella, E., Duong, J. K., Chen, I. S., Leotti, L., and Altincatal, A. Effects of maternal breathing rate, psychiatric status, and cortisol on fetal heart rate. *Dev. Psychobiol.*, **53**(3):pp. 221–33, 2011.

[285] Monk, C., Fifer, W. P., Myers, M. M., Sloan, R. P., Trien, L., and Hurtado, a. Maternal stress responses and anxiety during pregnancy: effects on fetal heart rate. *Dev. Psychobiol.*, **36**(1):pp. 67–77, 2000.

[286] Moody, G. B. and Mark, R. G. The impact of the MIT-BIH arrhythmia database. *IEEE Eng. Med. Biol. Mag.*, **20**(3):pp. 45–50, 2001.

[287] Moody, G. B., Muldrow, W. E., and Mark, R. G. A noise stress test for arrhythmia detectors. *Comput. Cardiol.*, **11**:pp. 381–384, 1984.

[288] Moor, B. D., Gersem, P. D., Schutter, B. D., and Favoreel, W. DAISY: A database for identification of systems. Technical Report 3, Department of Electrical Engineering - KU Leuven, 1997.

[289] Moore, K. L. *The developing human*. Elsevier, 10th edition, 2016. ISBN 9788578110796.

[290] Moraes, E. R., Murta, L. O., Baffa, O., Wakai, R. T., and Comani, S. Linear and nonlinear measures of fetal heart rate patterns evaluated on very short fetal magnetocardiograms. *Physiol. Meas.*, **33**(10):pp. 1563–83, 2012.

[291] Moreno, V. M. and Pigazo, A. *Kalman Filter: Recent Advances and Applications*. ISBN 978-953-307-000-1. In-Teh, 2009. ISBN 978-953-307-000-1.

[292] Murabayashi, T., Fetics, B., Kass, D., Nevo, E., Gramatikov, B., and Berger, R. D. Beat-to-beat QT interval variability associated with acute myocardial ischemia. *J. Electrocardiol.*, **35**(1):pp. 19–25, 2002.

[293] Murphy, V. E., Smith, R., Giles, W. B., and Clifton, V. L. Endocrine regulation of human fetal growth: the role of the mother, placenta, and fetus. *Endocr. Rev.*, **27**(2):pp. 141–69, 2006.

[294] Murray, E., Fernandes, M., Fazel, M., Kennedy, S. H., Villar, J., and Stein, A. Differential effect of intrauterine growth restriction on childhood neurodevelopment: A systematic review. 2015.

[295] Nageotte, M. P. Fetal heart rate monitoring. *Semin. Fetal Neonatal Med.*, **20**(3):pp. 144–8, 2015.

[296] National Institute for Clinical Excellence. Inherited Clinical Guideline C - The use of electronic fetal monitoring: The use and interpretation of cardiotocography in intrapartum fetal surveillance. Technical report, National Institute for Clinical Excellence, 2001.

[297] Neilson, J. P. Fetal electrocardiogram (ECG) for fetal monitoring during labour. *Cochrane Database Syst. Rev.*, **3**(4):pp. 1–29, 2006.

[298] Nelson, M. and Gailly, J.-L. *The data compression book*. League For Programming Freedom, 1996.

[299] Nemati, S., Malhotra, A., and Clifford, G. D. G. Data Fusion for Improved Respiration Rate Estimation. *EURASIP J. Adv. Sig. Process.*, **2010**, 2010.

[300] Nijhuis, J. G., Prechtl, H. F. R., Martin, C. B., Bots, R. S., and Jr., C. B. M. Are there behavioural states in the human fetus? *Early Hum. Dev.*, **6**(2):pp. 177–95, 1982.

[301] Niknazar, M. *Extraction and Denoising of Fetal ECG Signals*. Ph.D. thesis, University of Grenoble, 2013.

[302] Niknazar, M., Becker, H., Rivet, B., Jutten, C., and Comon, P. Robust 3-way tensor decomposition and extended state Kalman filtering to extract fetal ECG. In: *EUSIPCO*, pp. 1–5. 2013.

[303] Niknazar, M., Becker, H., Rivet, B., Jutten, C., and Comon, P. Blind source separation of underdetermined mixtures of event-related sources. *Signal Process.*, **101**:pp. 52–64, 2014.

[304] Niknazar, M., Rivet, B., and Jutten, C. Fetal ECG Extraction by Extended State Kalman Filtering Based on Single-Channel Recordings. *IEEE Trans. Biomed. Eng.*, **60**(5):pp. 1345–1352, 2013.

[305] Niknazar, M., Rivet, B., Jutten, C., and Others. Application of Dynamic Time Warping on Kalman Filtering Framework for Abnormal ECG Filtering. In: *ESANN*, pp. 139–144. 2012.

[306] Nybo Andersen, A. M., Wohlfahrt, J., Christens, P., Olsen, J., and Melbye, M. Maternal age and fetal loss: population based register linkage study. *BMJ*, **320**(7251):pp. 1708–12, 2000.

[307] Odelson, B. J., Rajamani, M. R., and Rawlings, J. B. A new autocovariance least-squares method for estimating noise covariances. *Automatica*, **42**(2):pp. 303–308, 2006.

[308] Oikonomou, V. P. and Fotiadis, D. I. A Bayesian PCA Approach for Fetal ECG Extraction. *3rd Eur. Med. Biol. Eng. Conf.*, 2005.

[309] Oikonomou, V. P., Tzallas, A. T., and Fotiadis, D. I. A Kalman filter based methodology for EEG spike enhancement. *Comput. Methods Programs Biomed.*, **85**(2):pp. 101–8, 2007.

[310] Oostendorp, T. F. *Modelling the fetal ECG*. Ph.D. thesis, Katholieke Universiteit te Nijrnegen, 1989.

[311] Oostendorp, T. F., Oosterom, A., and H.W., J. Electrical properties of tissues involved in the conduction of foetal {ECG}. *Med. Biol. Eng. Comput.*, pp. 322–324, 1989.

[312] Orphanidou, C., Bonnici, T., Charlton, P., Clifton, D., Vallance, D., and Tarassenko, L. Signal Quality Indices for the Electrocardiogram and Photoplethysmogram: Derivation and Applications to Wireless Monitoring. *IEEE J. Biomed. Heal. Informatics*, **19**(3):pp. 1–1, 2015.

[313] Ortiz, M. R., Aguilar, S. D., Alvarez-Ramirez, J., Martïnez, A., Vargas-Garcia, C., Gonzalez-Camarena, R., and Echeverria, J. C. Prenatal RR fluctuations dynamics: detecting fetal short-range fractal correlations. *Prenat. Diagn.*, **26**(13):pp. 1241–1247, 2006.

[314] Oster, J., Behar, J., Sayadi, O., Nemati, S., Johnson, A., and Clifford, G. Semi-supervised ECG Ventricular Beat Classification with Novelty Detection Based on Switching Kalman Filters. *IEEE Trans. Biomed. Eng.*, **62**(9):pp. 2125—-2134, 2015.

[315] Oster, J. and Clifford, G. D. Signal quality indices for state space electrophysiological signal processing and vice versa. In: *Adv. State Sp. Methods Neural Clin. Data*, p. 345. Cambridge Univeristy Press, 2015. ISBN 9781139941433.

[316] Oudijk, M. a., Kwee, A., Visser, G. H. a., Blad, S., Meijboom, E. J., and Rosén, K. G. The effects of intrapartum hypoxia on the fetal QT interval. *BJOG*, **111**(7):pp. 656–60, 2004.

[317] Oweis, R. J. and Al-Tabbaa, B. O. QRS Detection and Heart Rate Variability Analysis: A Survey. *J. Biomed. Sci. Eng.*, **2**(1):pp. 13–34, 2014.

[318] Pagès, J. *Multiple Factor Analysis by example using R*. CRC Press, 2014. ISBN 9781482205480.

[319] Palanthandalam-Madapusi, H. and Moor, D. Subsystem identification for nonlinear model updating. In: *Am. Control Conf.*, pp. 3056—-3061. 2006.

[320] Pan, J. and Tompkins, W. J. A Real-Time QRS Detection Algorithm. *IEEE Trans. Biomed. Eng.*, **32**(3):pp. 230–236, 1985.

[321] Pan, S., Xiao, D., Xing, S., Law, S., Du, P., and Li, Y. A general extended Kalman filter for simultaneous estimation of system and unknown inputs. *Eng. Struct.*, **109**:pp. 85–98, 2016.

[322] Panigrahy, D., Rakshit, M., and Sahu, P. An efficient method for fetal ECG extraction from single channel abdominal ECG. In: *Int. Conf. Ind. Instrum. Control*, pp. 1083–1088. IEEE, 2015. ISBN 978-1-4799-7165-7.

[323] Parer, J. T., King, T., Flanders, S., Fox, M., and Kilpatrick, S. J. Fetal acidemia and electronic fetal heart rate patterns: is there evidence of an association? *J. Matern. Fetal Neonatal Med.*, **19**(5):pp. 289–294, 2006.

[324] Pasetto, D., Camporese, M., and Putti, M. Ensemble Kalman filter versus particle filter for a physically-based coupled surface–subsurface model. *Adv. Water Res.*, **47**:pp. 1–13, 2012.

[325] Patrick, J., Campbell, K., Carmichael, L., and Probert, C. Influence of maternal heart rate and gross fetal body movements on the daily pattern of fetal heart rate near term. *Am. J. Obs. Gynecol.*, **144**(5):pp. 533–8, 1982.

[326] Peltola, M. A. Role of editing of R-R intervals in the analysis of heart rate variability. *Front. Physiol.*, **3**:p. 148, 2012.

[327] Penny, W. D., Roberts, S., and Everson, R. M. ICA: Model order selection and dynamic source models. In: *Indep. Compon. Anal. Princ. Pract.*, chapter 12, pp. 299—-314. Cambridge Univeristy Press, 2000.

[328] Peter, K. and Miller, R. K. *Trophoblast Research*, volume 3. Plenum Medical Book Company, 1988. ISBN 9781461278931.

[329] Peters, M., Crowe, J., Piéri, J. F., Quartero, H., Hayes-Gill, B., James, D., Stinstra, J., and Shakespeare, S. Monitoring the fetal heart non-invasively: a review of methods. *J. Perinat. Med.*, **29**(5):pp. 408–16, 2001.

[330] Peters, M., Stinstra, J., Uzunbajakau, S., and Srinivasan, N. *Advances in Electromagnetic Fields in Living Systems*. Springer Science & Business Media, 2005. ISBN 0387239979.

[331] Peyman, A., Gabriel, C., Benedickter, H. R., and Fröhlich, J. Dielectric properties of human placenta, umbilical cord and amniotic fluid. *Phys. Med. Biol.*, **56**(7):pp. N93–8, 2011.

[332] Piccirillo, G., Magri, D., Matera, S., Magnanti, M., Torrini, A., Pasquazzi, E., Schifano, E., Velitti, S., Marigliano, V., Quaglione, R., and Barilla, F. QT variability strongly predicts sudden cardiac death in asymptomatic subjects with mild or moderate left ventricular systolic dysfunction: a prospective study. *Eur. Hear. J.*, **28**(11):pp. 1344–50, 2007.

[333] Pieri, J. F., Crowe, J. A., Hayes-Gill, B. R., Spencer, C. J., Bhogal, K., and James, D. K. Compact long-term recorder for the transabdominal foetal and maternal electrocardiogram. *Med. Biol. Eng. Comput.*, **39**(1):pp. 118–125, 2001.

[334] Pildner von Steinburg, S., Boulesteix, A.-L., Lederer, C., Grunow, S., Schiermeier, S., Hatzmann, W., Schneider, K.-T. M., and Daumer, M. What is the "normal" fetal heart rate? *PeerJ*, **1**:p. e82, 2013.

[335] Pillai, M. and James, D. The development of fetal heart rate patterns during normal pregnancy. *Obs. Gynecol.*, **76**(5 Pt 1):p. 812, 1990.

[336] Pimentel, M. A. F., Santos, M. D., Springer, D. B., and Clifford, G. D. Heart beat detection in multimodal physiological data using a hidden semi-Markov model and signal quality indices. *Physiol. Meas.*, **36**(8):pp. 1717–1727, 2015.

[337] Podziemski, P. and Gieraltowski, J. Fetal Heart Rate Discovery: Algorithm for Detection of Fetal Heart Rate from Noisy, Noninvasive Fetal ECG Recordings. In: *Comput. Cardiol. (2010).*, pp. 333–336. Zaragoza, Spain, 2013.

[338] Pohlheim, H. *Evolutionäre Algorithmen - Verfahren, Operatoren, Hinweise aus der Praxis*. Springer, 1999. ISBN 3-540-66413-0.

[339] Powers, D. Evaluation: from precision, recall and F-measure to ROC, informedness, markedness and correlation. *J. Mach. Learn. Tech.*, **2**(1):pp. 37–63, 2011.

[340] Powers, D. What the F-measure doesn't measure: Features, Flaws, Fallacies and Fixes. *arXiv Prepr. arXiv1503.06410*, 2015.

[341] Rabotti, C., Mischi, M., van Laar, J. O. E. H., Oei, G. S., and Bergmans, J. W. M. Estimation of internal uterine pressure by joint amplitude and frequency analysis of electrohysterographic signals. *Physiol. Meas.*, **29**(7):pp. 829–841, 2008.

[342] Reece, S. and Roberts, S. An introduction to Gaussian processes for the Kalman filter expert. In: *IEEE Conf. Inf. Fusion (FUSION)*,. 2010.

[343] Reid, I. Lecture Notes: B4 Estimation II. Technical report, University of Oxford, 2003.

[344] Reinhard, J., Hayes-Gill, B., Yuan, K., Schiermeier, S., and Louwen, F. Intrapartum ST Segment Analyses (STAN) Using Simultaneous Invasive and Non-Invasive Fetal Electrocardiography: A Report of 6 Cases. *Z .Geburtshilfe Neonatol.*, **218**(3):pp. 122—-127, 2014.

[345] Reinhard, J., Hayes-Gill, B. R., Schiermeier, S., Hatzmann, W., Herrmann, E., Heinrich, T. M., and Louwen, F. Intrapartum signal quality with external fetal heart rate monitoring: a two way trial of external Doppler CTG ultrasound and the abdominal fetal electrocardiogram. *Arch. Gynecol. Obs.*, 2012.

[346] Reinhard, J., Hayes-Gill, B. R., Yi, Q., Hatzmann, H., and Schiermeier, S. Comparison of non-invasive fetal electrocardiogram to Doppler cardiotocogram during the 1st stage of labor. *J. Perinat. Med.*, **38**(2):pp. 179–185, 2010.

[347] Resnik, R. Intrauterine growth restriction. *Obs. Gynecol.*, 2002.

[348] Richter, M., Schreiber, T., and Kaplan, D. T. Fetal ECG extraction with nonlinear state-space projections. *IEEE Trans. Biomed. Eng.*, **45**(1):pp. 133–7, 1998.

[349] Riedl, M., van Leeuwen, P., Suhrbier, A., Malberg, H., Grönemeyer, D., Kurths, J., and Wessel, N. Testing foetal-maternal heart rate synchronization via model-based analyses. *Philos. Trans. R. Soc. Lond. A*, **367**(1892):pp. 1407–21, 2009.

[350] Rivet, B., Niknazar, M., and Jutten, C. Nonparametric modelling of ECG: applications to denoising and to single sensor fetal ECG extraction. In: *Int. Conf. Latent Var. Anal. Signal Sep.* Springer Berlin Heidelberg, 2012.

[351] Roberts, D. and Dalziel, S. R. Antenatal corticosteroids for accelerating fetal lung maturation for women at risk of preterm birth. In: Roberts, D. (editor), *Cochrane Database Syst. Rev.*, 3, p. CD004454. John Wiley & Sons, Ltd, Chichester, UK, 2006.

[352] Rodrigues, R. Fetal beat detection in abdominal ECG recordings: global and time adaptive approaches. *Physiol. Meas.*, **35**(8):pp. 1699–711, 2014.

[353] Rompelman, O. and Ros, H. H. Coherent averaging technique: a tutorial review. Part 1: Noise reduction and the equivalent filter. *J. Biomed. Eng.*, **8**(1):pp. 24–29, 1985.

[354] Rooijakkers, M., Song, S., and Rabotti, C. Influence of electrode placement on signal quality for ambulatory pregnancy monitoring. *Comput. Math. Methods. Med.*, **2014**:p. Article ID 960980, 2014.

[355] Roonizi, E. and Sassi, R. A Signal Decomposition Model-Based Bayesian Framework for ECG Components Separation. *IEEE Trans. Signal Process.*, **PP**(99):pp. 1–1, 2015.

[356] Rooth, G., Huch, A., and Huch, R. Guidelines for the use of Fetal Monitoring. *Int. J. Gynecol. Obs.*, **25**(3):pp. 159–67, 1987.

[357] Roweis, S. and Ghahramani, Z. A Unifying Review of Linear Gaussian Models. *Neural Comput.*, **11**(2):pp. 305–345, 1999.

[358] Royal College of Obstetricians and Gynaecologists. The Use of Electronic Fetal Monitoring - The use and interpretation of cardiotocography in intrapartum fetal surveillance - Evidence-based Clinical Guideline Number 8. Technical report, Royal College of Obstetricians and Gynaecologists, e, 2001.

[359] Ruymgaart, P. A. and Soong, T. T. *Mathematics of Kalman-Bucy Filtering*. Springer Berlin / Heidelberg, 2nd edition, 1988. ISBN 9783540187813.

[360] Saccone, G., Schuit, E., Amer-Wåhlin, I., Xodo, S., and Berghella, V. Electrocardiogram ST Analysis During Labor: A Systematic Review and Meta-analysis of Randomized Controlled Trials. *Obs. Gynecol.*, **127**(1):pp. 127–35, 2016.

[361] Sadler, T. W. *Langman's Medical Embryology*. Lippincott Williams & Wilkins, 12th edition, 2011. ISBN 9788578110796.

[362] Sameni, R. *Extraction of Fetal Cardiac Signals from an Array of Maternal Abdominal Recordings*. Ph.D. thesis, Sharif University of Technology - Institut National Polytechnique de Grenoble, 2008. URL `http://www.sameni.info/Publications/Thesis/PhDThesis.pdf`.

[363] Sameni, R. The Open-Source Electrophysiological Toolbox (OSET). 2010. URL `http://www.oset.ir`.

[364] Sameni, R., Clifford, G. D., Jutten, C., and Shamsollahi, M. B. Multichannel ECG and Noise Modeling: Application to Maternal and Fetal ECG Signals. *EURASIP J. Adv. Sig. Process.*, **2007**(1):p. 043407, 2007.

[365] Sameni, R. and Clifford, G. D. G. A Review of Fetal ECG Signal Processing, Issues and Promising Directions. *Open Pacing Electrophysiol. Ther. J.*, **3**:pp. 4–20, 2010.

[366] Sameni, R., Jutten, C., and Shamsollahi, M. B. Multichannel electrocardiogram decomposition using periodic component analysis. *IEEE Trans. Biomed. Eng.*, **55**(8):pp. 1935–1940, 2008.

[367] Sameni, R., Jutten, C., and Shamsollahi, M. B. A Deflation Procedure for Subspace Decomposition. *IEEE Trans. Signal Process.*, **58**(4):pp. 2363–2374, 2010.

[368] Sameni, R., Shamsollahi, M. B., and Jutten, C. Model-based Bayesian filtering of cardiac contaminants from biomedical recordings. *Physiol. Meas.*, **29**(5):pp. 595–613, 2008.

[369] Sameni, R., Shamsollahi, M.-B., Jutten, C., and Babaie-Zadeh, M. Filtering noisy ECG signals using the extended kalman filter based on a modified dynamic ECG model. In: *Comput. Cardiol. (2010).*, pp. 1017–1020. 2005.

[370] Sameni, R., Shamsollahi, M. B., Jutten, C., and Clifford, G. D. A Nonlinear Bayesian Filtering Framework for ECG Denoising. *IEEE Trans. Biomed. Eng.*, **54**(12):pp. 2172–2185, 2007.

[371] Samueloff, A., Langer, O., Berkus, M., Field, N., Xenakis, E., and Ridgway, L. Is fetal heart rate variability a good predictor of fetal outcome? *Acta Obs. Gynecol. Scand.*, **73**(1):pp. 39–44, 1994.

[372] Sanghavi, M. and Rutherford, J. D. Cardiovascular physiology of pregnancy. *Circulation*, **130**(12):pp. 1003–8, 2014.

[373] Sarkka, S. *Bayesian Filtering and Smoothing*. Cambridge University Press, 2013. ISBN 9781139344203.

[374] Sasaki, Y. The truth of the F-measure. Technical report, University of Manchester, 2007.

[375] Sayadi, O. and Shamsollahi, M. B. ECG Denoising and Compression Using a Modified Extended Kalman Filter Structure. *IEEE Trans. Biomed. Eng.*, **55**(9):pp. 2240–2248, 2008.

[376] Sayadi, O. and Shamsollahi, M. B. A model-based Bayesian framework for ECG beat segmentation. *Physiol. Meas.*, **30**(3):pp. 335–352, 2009.

[377] Sayadi, O., Shamsollahi, M. B., and Clifford, G. D. Synthetic ECG generation and Bayesian filtering using a Gaussian wave-based dynamical model. *Physiol. Meas.*, **31**(10):pp. 1309–1329, 2010.

[378] Sayadi, O., Shamsollahi, M. B., Clifford, G. D., and Member, S. Robust Detection of Premature Ventricular Contractions Using a Wave-Based Bayesian Framework. *IEEE Trans. Biomed. Eng.*, **57**(2):pp. 353–362, 2010.

[379] Sayed, A. L. I. H. *Adaptive Filters*. IEEE Press, 2008. ISBN 9780470253885.

[380] Schmidt, M. Weiterentwicklung und Anwendung Inhomogener Streckungsverfahren zur QT-Intervall-Extraktion in Langzeit-EKG. Technical report, TU Dresden, 2013.

[381] Schmidt, M., Baumert, M., Porta, A., Malberg, H., and Zaunseder, S. Two-Dimensional Warping for One-Dimensional Signals—Conceptual Framework and Application to ECG Processing. *IEEE Trans. Signal Process.*, **62**(21):pp. 5577–5588, 2014.

[382] Schmidt, R. F. and Lang, F. *Physiologie des Menschen - mit Pathophysiologie*. Springer Berlin / Heidelberg, 2007.

[383] Schmidt, S. The Kalman filter-Its recognition and development for aerospace applications. *J. Guid. Control Dyn.*, 1981.

[384] Schmidt, S. F. Computational Techniques in Kalman Filtering. Technical report, NATO Advisory Group for Aerospace Research and Development, AGARDograph 139, 1970.

[385] Schneider, H., Husslein, P.-W., and Schneider, K. T. M. *Die Geburtshilfe*. Springer Berlin Heidelberg, Berlin, Heidelberg, 2011. ISBN 978-3-642-40181-7.

[386] Schneider, U., Frank, B., Fiedler, A., Kaehler, C., Hoyer, D., Liehr, M., Haueisen, J., Schleussner, E., and Jena, D. Human fetal heart rate variability-characteristics of autonomic regulation in the third trimester of gestation. *J. Perinat. Med.*, **36**(5):pp. 433–41, 2008.

[387] Schreiber, T. and Kaplan, D. Signal separation by nonlinear projections: The fetal electrocardiogram. *Phys. Rev. E Stat. Nonlin. Soft. Matter Phys.*, 1996.

[388] Scott, J. M. Anaemia in Pregnancy. *Postgrad. Med. J.*, **38**(438):p. 202, 1962.

[389] Scott, W. Reliability of content analysis: The case of nominal scale coding. *Public Opin. Q.*, 1955.

[390] Shadaydeh, M., Xiao, Y., and Kriedieh Ward, R. Extraction of fetal ECG using adaptive Volterra filters. In: *EUSIPCO*, pp. 1–5. IEEE, 2008.

[391] Shaffer, F., McCraty, R., and Zerr, C. L. A healthy heart is not a metronome: an integrative review of the heart's anatomy and heart rate variability. *Front. Physiol.*, **5**, 2014.

[392] Shyam Mohan, M., Naik, N., Gemson, R. M. O., and Ananthasayanam, M. R. Introduction to the Kalman Filter and Tuning its Statistics for Near Optimal Estimates and Cramer Rao Bound. Technical report, Indian Institute of Technology Kanpur, 2015.

[393] Signorini, M. G., Magenes, G., Cerutti, S., and Arduini, D. Linear and nonlinear parameters for the analysis of fetal heart rate signal from cardiotocographic recordings. *IEEE Trans. Biomed. Eng.*, **50**(3):pp. 365–74, 2003.

[394] Siira, S. M., Ojala, T. H., Vahlberg, T. J., Rosén, K. G., and Ekholm, E. M. Do spectral bands of fetal heart rate variability associate with concomitant fetal scalp pH? *Early Hum. Dev.*, **89**(9):pp. 739–42, 2013.

[395] Silva, I., Behar, J., Sameni, R., Zhu, T., Oster, J., Clifford, G. D., and Moody, G. B. Noninvasive fetal ECG: The PhysioNet/Computing in Cardiology Challenge 2013. In: *Comput. Cardiol. (2010).*, pp. 149–152. 2013.

[396] Silva, I., Moody, B., Behar, J., Johnson, A., Oster, J., Clifford, G. D., and Moody, G. B. Robust detection of heart beats in multimodal data. *Physiol. Meas.*, **36**(8):pp. 1629–44, 2015.

[397] Silva, I., Moody, G., and Celi, L. Improving the quality of ECGs collected using mobile phones: The Physionet/Computing in Cardiology Challenge 2011. In: *Comput. Cardiol. (2010)*. 2011.

[398] Silva, I. and Moody, G. B. An Open-source Toolbox for Analysing and Processing PhysioNet Databases in MATLAB and Octave. *JORS*, **2**(1):p. e27, 2014.

[399] Simon, D. *Optimal State Estimation: Kalman, H Infinity, and Nonlinear Approaches*. Wiley-Interscience, 2006. ISBN 0471708585.

[400] Simon, D. Kalman filtering with state constraints: a survey of linear and nonlinear algorithms. *IET Control Theory Appl.*, **4**(8):pp. 1303–1318, 2010.

[401] Simon, D. and Chia, T. L. Kalman filtering with state equality constraints. *IEEE Trans. Aerosp. Electron. Syst.*, **38**(1):pp. 128–136, 2002.

[402] Sittig, D. F. and Cheung, K. H. A parallel implementation of a multi-state Kalman filtering algorithm to detect ECG arrhythmias. *Int. J. Clin. Monit. Comput.*, **9**(1):pp. 13–22, 1992.

[403] Soernmo, L. and Laguna, P. *Bioelectrical signal processing in cardiac and neurological applications*. Elsevier Academic Press, 2005. ISBN 978-0-12-437552-9.

[404] Sorenson, H. Least-squares estimation: from Gauss to Kalman. *Spectrum, IEEE*, 1970.

[405] Sorenson, H. and Alspach, D. Recursive bayesian estimation using gaussian sums. *Automatica*, **7**(4):pp. 465–479, 1971.

[406] Springer, D. B., Tarassenko, L., and Clifford, G. D. Logistic Regression-HSMM-Based Heart Sound Segmentation. *IEEE Trans. Biomed. Eng.*, **63**(4):pp. 822–32, 2016.

[407] Stampalija, T. and Signaroldi, M. Fetal and maternal heart rate confusion during intra-partum monitoring: comparison of trans-abdominal fetal electrocardiogram and Doppler telemetry. *J. Matern. Fetal Neonatal Med.*, **25**(8):pp. 1517–20, 2012.

[408] Steer, P. J. Has electronic fetal heart rate monitoring made a difference. *Semin. Fetal Neonatal Med.*, **13**(1):pp. 2–7, 2008.

[409] Stinstra, J. G. *The Reliability of the Fetal Magnetocardiogram*. Ph.D. thesis, Universiteit Twente, Enschede, Netherland, 2001.

[410] Stolze, B. Entwicklung von Methoden zur Risikoabschätzung bei Feten anhand der fetalen Herzratenvariabilität. Technical report, Technische Universität Dresden, 2013.

[411] Stratmeyer, M. and Dalecki, D. Fetal ultrasound: mechanical effects. *Curr. Probl. Diagn. Radiol.*, **27**:pp. 597–605, 2008.

[412] Strobach, P., Abraham-Fuchs, K., and Härer, W. Event-synchronous cancellation of the heart interference in biomedical signals. *IEEE Trans. Biomed. Eng.*, **41**(4):pp. 343–50, 1994.

[413] Stroux, L. and Clifford, G. D. The Importance of Biomedical Signal Quality Classification for Successful mHealth Implementation. In: *EPFL-UNESCO*, p. 128. 2014.

[414] Struijk, P. C., Mathews, V. J., Loupas, T., Stewart, P. A., Clark, E. B., Steegers, E. A. P., and Wladimiroff, J. W. Blood pressure estimation in the human fetal descending aorta. *Ultrasound Obstet. Gynecol.*, **32**(5):pp. 673–81, 2008.

[415] Stumpf, A. T. Charakterisierung des fetalen Elektrokardiogramms unter Einfluss von maternalen Blutdruckschwankungen. Technical report, TU Dresden, 2015.

[416] Suhrbier, A., Heringer, R., Walther, T., Malberg, H., Wessel, N., and Benjamin, C. Comparison of three methods for beat-to-beat-interval extraction from continuous blood pressure and electrocardiogram with respect to heart rate variability analysis. *Biomed. Tech.*, **51**(2):pp. 70–76, 2006.

[417] Sykes, G. Do APGAR scores indicate asphyxia? *Lancet*, **319**(8270):pp. 494–496, 1982.

[418] Symonds, E. M., Sahota, D., and Chang, A. *Fetal Electrocardiography*. Cardiopulmonary medicine from Imperial College Press. Imperial College Press, 2001. ISBN 9781860941719.

[419] Tarassenko, L., Mason, L., and Townsend, N. Multi-sensor fusion for robust computation of breathing rate. *Electron. Lett.*, **38**(22):p. 1314, 2002.

[420] Tarvainen, M. P., Georgiadis, S. D., Ranta-Aho, P. O., and Karjalainen, P. a. Time-varying analysis of heart rate variability signals with a Kalman smoother algorithm. *Physiol. Meas.*, **27**(3):pp. 225–39, 2006.

[421] Task Force of The European Society of Cardiology and the North American Society of Pacing and Electrophysiology. Heart Rate Variability : Standards of Measurement, Physiological Interpretation, and Clinical Use. *Circulation*, **93**(5):pp. 1043–1065, 1996.

[422] Taylor, M. J. O., Smith, M. J., Thomas, M., Green, A. R., Cheng, F., Oseku-Afful, S., Wee, L. Y., Fisk, N. M., and Gardiner, H. M. Non-invasive fetal electrocardiography in singleton and multiple pregnancies. *BJOG*, **110**(7):pp. 668–78, 2003.

[423] Taylor, M. J. O., Thomas, M. J., Smith, M. J., Oseku-Afful, S., Fisk, N. M., Green, A. R., Paterson-Brown, S., and Gardiner, H. M. Non-invasive intrapartum fetal ECG: preliminary report. *BJOG*, **112**(8):pp. 1016–1021, 2005.

[424] Teixeira, B. O. S. *Constrained state estimation for linear and nonlinear dynamic systems*. Ph.D. thesis, Universidade Federal de Minas Gerais, 2008.

[425] Teixeira, B. O. S., Chandrasekar, J., Palanthandalam-Madapusi, H. J., Torres, L., Aguirre, L. A., and Bernstein, D. S. Gain-Constrained Kalman Filtering for Linear and Nonlinear Systems. *IEEE Trans. Signal Process.*, **56**(9):pp. 4113–4123, 2008.

[426] Tereshchenko, L. G., Han, L., Cheng, A., Marine, J. E., Spragg, D. D., Sinha, S., Dalal, D., Calkins, H., Tomaselli, G. F., and Berger, R. D. Beat-to-beat three-dimensional ECG variability predicts ventricular arrhythmia in ICD recipients. *Hear. Rhythm*, **7**(11):pp. 1606–13, 2010.

[427] Tetschke, F., Schneider, U., Schleussner, E., Witte, O. W., and Hoyer, D. Assessment of Fetal Maturation Age by Heart Rate Variability Measures using Random Forest Methodology. *Comput. Biol. Med.*, **70**(1):pp. 157—-162, 2016.

[428] Timor-Tritsch, I. E., Dierker, L. J., Zador, I., Hertz, R. H., and Rosen, M. G. Fetal movements associated with fetal heart rate accelerations and decelerations. *Am. J. Obs. Gynecol.*, **131**(3):pp. 276–80, 1978.

[429] Tingting Zhu, Johnson, A., Behar, J., and Clifford, G. Bayesian voting of multiple annotators for improved QT interval estimation. 2013.

[430] Ungureanu, G. M., Bergmans, J. W. M., Oei, S. G., Ungureanu, A., and Wolf, W. The event synchronous canceller algorithm removes maternal ECG from abdominal signals without affecting the fetal ECG. *Comput. Biol .Med.*, **39**(6):pp. 562–567, 2009.

[431] Ungureanu, G. M., Ilincai, A. M., Wolf, W., Gussi, I., Taralunga, D. D., and Strungaru, R. Improved Fetal ECG Extraction by Applying Adaptive Filtering. In: *Int. Symp. Adv. Top. Electr. Eng.*, pp. 3–8. 2011.

[432] Ungureanu, M., Bergmans, J. W. M., Mischi, M., Guid Oei, S., and Strungaru, R. Improved Method for Fetal Heart Rate Monitoring. In: *IEEE EMBC*, pp. 5916–5919. 2005.

[433] Ungureanu, M., Bergmans, J. W. M., Oei, S. G., and Strungaru, R. Fetal ECG extraction during labor using an adaptive maternal beat subtraction technique. *Biomed. Tech.*, **52**(1):pp. 56–60, 2007.

[434] Ungureanu, M. and Wolf, W. M. Basic Aspects Concerning the Event-Synchronous Interference Canceller. *IEEE Trans. Biomed. Eng.*, **53**(11):pp. 2240–2247, 2006.

[435] Unterscheider, J., Daly, S., Geary, M. P., Kennelly, M. M., McAuliffe, F. M., O'Donoghue, K., Hunter, A., Morrison, J. J., Burke, G., Dicker, P., Tully, E. C., and Malone, F. D. Optimizing the definition of intrauterine growth restriction: the multicenter prospective PORTO Study. *Am. J. Obs. Gynecol.*, **208**(4):pp. 290.e1–6, 2013.

[436] Van der Merwe, R. and Wan, E. The square-root unscented Kalman filter for state and parameter-estimation. In: *IEEE Int. Conf. Acoust. Speech, Signal Process.*, volume 6, pp. 3461–3464. IEEE, 2001. ISBN 0-7803-7041-4.

[437] van Laar, J. O. E. H., Peters, C. H. L., Vullings, R., Houterman, S., Bergmans, J. W. M., and Oei, S. G. Fetal autonomic response to severe acidaemia during labour. *BJOG*, **117**(4):pp. 429–437, 2009.

[438] van Laar, J. O. E. H., Peters, C. H. L., Vullings, R., Houterman, S., and Oei, S. G. Power spectrum analysis of fetal heart rate variability at near term and post term gestation during active sleep and quiet sleep. *Early Hum. Dev.*, **85**(12):pp. 795–798, 2009.

[439] Van Laar, J. O. E. H., Warmerdam, G. J. J., Verdurmen, K. M. J., Vullings, R., Peters, C. H. L., Houterman, S., Wijn, P. F. F., Andriessen, P., Van Pul, C., and Guid Oei, S. Fetal heart rate variability during pregnancy, obtained from non-invasive electrocardiogram recordings. *Acta Obs. Gynecol. Scand.*, **93**(1):pp. 93–101, 2014.

[440] Van Leeuwen, P., Cysarz, D., Edelhäuser, F., and Grönemeyer, D. Heart rate variability in the individual fetus. *Auton. Neurosci.*, **178**(1-2):pp. 24–8, 2013.

[441] Van Leeuwen, P., Geue, D., Lange, S., Cysarz, D., Bettermann, H., Grönemeyer, D. H. W., and Leeuwen, P. V. Is there evidence of fetal-maternal heart rate synchronization? *BMC Physiol.*, **3**:p. 2, 2003.

[442] Van Leeuwen, P., Geue, D., Lange, S., and Grönemeyer, D. H. W. Modeling fetal–maternal heart-rate interaction. *IEEE Eng. Med. Biol. Mag.*, **28**(6):pp. 49–53, 2009.

[443] Van Leeuwen, P., Geue, D., Thiel, M., Cysarz, D., Lange, S., Romano, M. C., Wessel, N., Kurths, J., and Grönemeyer, D. H. Influence of paced maternal breathing on fetal-maternal heart rate coordination. *Proc. Natl. Acad. Sci. U S A*, **106**(33):pp. 13661–13666, 2009.

[444] Van Leeuwen, P., Gustafson, K. M., Cysarz, D., Geue, D., May, L. E., and Grönemeyer, D. Aerobic exercise during pregnancy and presence of fetal-maternal heart rate synchronization. *PLoS One*, **9**(8):p. e106036, 2014.

[445] Van Leeuwen, P., Lange, S., Geue, D., Grönemeyer, D., Leeuwen, P. V., Lange, S., Geue, D., and Grönemeyer, D. Heart rate variability in the fetus: a comparison of measures. *Biomed. Tech.*, **52**(1):pp. 61–5, 2007.

[446] Van Leeuwen, P., Werner, L., Hilal, Z., Schiermeier, S., Hatzmann, W., and Grönemeyer, D. Fetal electrocardiographic measurements in the assessment of fetal heart rate variability in the antepartum period. *Physiol. Meas.*, **35**(3):pp. 441–54, 2014.

[447] Varanini, M., Tartarisco, G., Billeci, L., Macerata, A., Pioggia, G., and Balocchi, R. An efficient unsupervised fetal QRS complex detection from abdominal maternal ECG. *Physiol. Meas.*, **35**(8):pp. 1607–19, 2014.

[448] Viera, A. J. and Garrett, J. M. Understanding Interobserver Agreement: The Kappa Statistic. *Fam. Med.*, **37**(5):pp. 360–363, 2005.

[449] Visscher, M. and Narendran, V. Vernix Caseosa: Formation and Functions. *Newborn Infant. Nurs. Rev.*, **14**(4):pp. 142–146, 2014.

[450] Visser, G. and Ayres-de Campos, D. FIGO consensus guidelines on intrapartum fetal monitoring: Adjunctive technologies. *Int. J. Gynaecol. Obs.*, 2015.

[451] Vullings, H. J. L. M., Verhaegen, M. H. G., and Verbruggen, H. B. Automated ECG segmentation with dynamic time warping. In: *IEEE EMBC*, pp. 163–166. IEEE, 1998. ISBN 0-7803-5164-9.

[452] Vullings, R. *Non-invasive fetal electrocardiogram: analysis and interpretation*. Ph.D. thesis, Technische Universiteit Eindhoven, 2010. URL `http://alexandria.tue.nl/extra2/692881.pdf`.

[453] Vullings, R., Peters, C., Mischi, M., Oei, G., and Bergmans, J. Maternal ECG removal from non-invasive fetal ECG recordings. In: *IEEE EMBC*, pp. 1394–1397. 2006.

[454] Vullings, R., Peters, C. H. L., Sluijter, R. J., Mischi, M., Oei, S. G., and Bergmans, J. W. M. Dynamic segmentation and linear prediction for maternal ECG removal in antenatal abdominal recordings. *Physiol. Meas.*, **30**(3):pp. 291–307, 2009.

[455] Wagner, N. and Köninger, A. Fetale Anämie – Diagnostik, Therapie und Management. *Geburtshilfe Frauenheilkd.*, **72**(01):pp. R2–R12, 2012.

[456] Wallwitz, U., Schneider, U., Nowack, S., Feuker, J., Bauer, S., Rudolph, A., and Hoyer, D. Development of integrative autonomic nervous system function: an investigation based on time correlation in fetal heart rate patterns. *J. Perinat. Med.*, **40**(6):pp. 659–67, 2012.

[457] Warrick, P. A., Hamilton, E. F., Precup, D., and Kearney, R. E. Classification of normal and hypoxic fetuses from systems modeling of intrapartum cardiotocography. *IEEE Trans. Biomed. Eng.*, **57**(4):pp. 771–779, 2010.

[458] Wedekind, D. MATLAB Script of the Pan-Tompkins QRS Detector. 2014. URL `https://github.com/danielwedekind/qrsdetector`.

[459] Wedekind, D., Malberg, H., and Zaunseder, S. Cascaded output selection for processing of capacitive electrocardiograms by means of independent component analysis. In: *Sens. Data Fusion Trends, Solut. Appl. (SDF), 2013 Work.*, pp. 1–6. IEEE, 2013. ISBN 978-1-4799-0778-6.

[460] Wedekind, D., Malberg, H., Zaunseder, S., Gaetjen, F., Matschke, K., and Rasche, S. Automated identification of cardiac signals after blind source separation for camera-based photoplethysmography. In: *IEEE Int. Conf. Electron. Nanotechnol.*, pp. 422–427. IEEE, 2015. ISBN 978-1-4673-6534-5.

[461] Welch and Bishop. An Introduction to the Kalman Filter. Technical report, University of North Carolina at Chapel Hill, Department of Computer Science, 2006.

[462] Whitley, D. An overview of evolutionary algorithms: practical issues and common pitfalls. *Inf. Softw. Technol.*, **43**(14):pp. 817–831, 2001.

[463] Widrow, B., Glover J.R., J., McCool, J. M., Kaunitz, J., Williams, C. S., Hearn, R. H., Zeidler, J. R., Eugene Dong, J., and Goodlin, R. C. Adaptive noise cancelling: Principles and applications. *Proc. IEEE*, **63**(12):pp. 1692–1716, 1975.

[464] Wiener, N. *Extrapolation, interpolation, and smoothing of stationary time series*, volume 2. MIT Press, 1949.

[465] Wladimiroff, J. and Seelen, J. Fetal heart action in early pregnancy. Development of fetal vagal function. *Eur. J. Obs. Gynec.*, **2**(2):pp. 55–63, 1972.

[466] Wolfberg, A. J. The future of fetal monitoring. *Rev. Obstet. Gynecol.*, **5**(3-4):pp. e132–6, 2012.

[467] Wolfberg, A. J., G.D., C., and Ward, J. Fetal ECG Monitoring. 2011. URL `http://www.google.ch/patents/US7949389`.

[468] Wolters, C. and de Munck, J. C. Volume conduction. *Scholarpedia*, **2**(3):p. 1738, 2007.

[469] Xodo, S., Saccone, G., Schuit, E., Amer-Wåhlin, I., and Berghella, V. Why STAN might not be dead. *J. Matern. Fetal Neonatal Med.*, **(accepted)**:pp. 1–10, 2016.

[470] Yang, J. N., Pan, S., and Huang, H. An adaptive extended Kalman filter for structural damage identifications II: Unknown inputs. *Struct. Control Hlth.*, **14**(3):pp. 497–521, 2007.

[471] Yong, S. Z., Zhu, M., and Frazzoli, E. A unified filter for simultaneous input and state estimation of linear discrete-time stochastic systems. *Automatica*, **63**:pp. 321–329, 2016.

[472] Yu, J. QRS detection using evolutionary algorithm. Technical Report April 2015, TU Dresden, Dresden, 2015.

[473] Zaman, A. G. A., Archbold, R. A., Helft, G., Paul, E. A., Curzen, N. P., and Mills, P. G. Atrial fibrillation after coronary artery bypass surgery a model for preoperative risk stratification. *Circulation*, **101**(12):pp. 1403–1408, 2000.

[474] Zarzoso, V., Nandi, A., and Bacharakis, E. Maternal and foetal ECG separation using blind source separation methods. *Math. Med. Biol..*, **14**:pp. 207–225, 1997.

[475] Zarzoso, V. and Nandi, A. K. Noninvasive fetal electrocardiogram extraction: blind separation versus adaptive noise cancellation. *IEEE Trans. Biomed. Eng.*, **48**(1):pp. 12–18, 2001.

[476] Zaunseder, S., Andreotti, F., Cruz, M., Stepan, H., Schmieder, C., Malberg, H., and Jank, A. Fetal QRS detection by means of Kalman filtering and using the Event Synchronous Canceller. In: *Int. Work. Biosignal Interpret.* Como, Italy, 2012.

[477] Zaunseder, S., Andreotti, F., Cruz, M., Stepan, H., Schmieder, C., Malberg, H., Jank, A., Wessel, N., Jank, A., and Malberg, H. Fetal QRS Detection by means of Kalman Filtering and using the Event Synchronous Canceller. *Int. J. Bioelectromagn.*, **15**(1):pp. 83–89, 2013.

[478] Zaunseder, S., Heinke, A., Trumpp, A., and Malberg, H. Heart Beat Detection and Analysis from Videos. In: *IEEE Conf. Electron. Nanotechnol.*, pp. 286–290. Kiev, Ukraine, 2014. ISBN 978-1-4799-4580-1.

[479] Zhu, T., Johnson, A. E. W., Behar, J., and Clifford, G. D. Crowd-sourced annotation of ecg signals using contextual information. *Ann. Biomed. Eng.*, **42**(4):pp. 871–84, 2014.

[480] Zong, W., Moody, G., and Jiang, D. A robust open-source algorithm to detect onset and duration of QRS complexes. In: *Comput. Cardiol. (2010).*, pp. 737–740. IEEE, 2003. ISBN 0-7803-8170-X.

A

Appendix A - Signal Quality Annotation

As described in Section 5.2.3, in order to allow clinicians to annotate the NIFECG signal quality, a stand-alone Matlab® GUI was implemented. The interface (presented in Fig. A.1) was made available under a GNU GPL license at `https://github.com/fernandoandreotti/sqi_annotation`. The GUI enables the annotation of abdECG segments using two criteria, namely the SNR (electrocardiographic signals versus other sources – in 5 levels) and FECG amplitude (4 levels). The procedure may also be performed with the keyboard shortcuts alpha-numeric "1"-"5" (for SNR classes) and "a" to "f" (for FECG amplitude). The output provided by the software is a text file with extension ".dat", located at a pre-determined folder. Given a set of pre-selected segments in graphical format (e.g. ".jpg"), the annotation procedure can be initiated. The software displays segments in a random order to avoid rater's bias. The annotation procedure can be stopped at any time and continued using the generated annotation file.

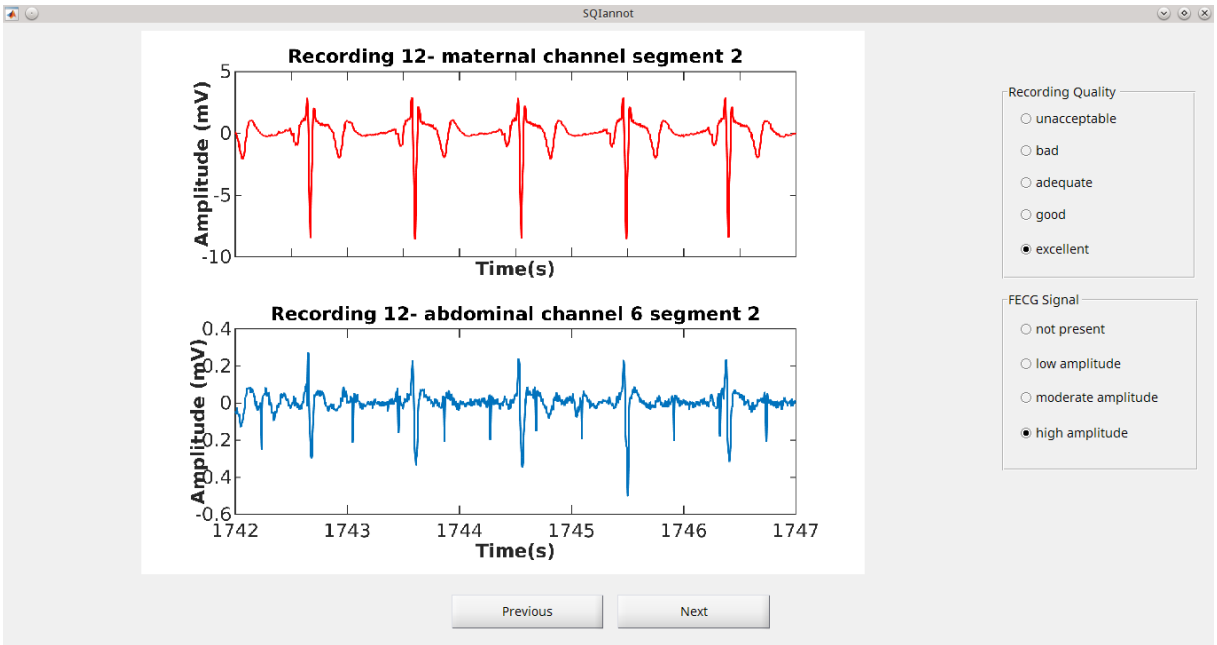

Figure A.1: Signal quality annotation interface.

B

Appendix B - Fetal QRS Annotation

For the purpose of performing FHR/FHRV analyses, preferably exact annotations on the FQRS locations are necessary. Throughout this work, one of the objectives is to enable semi-automated methods that allow accurate FQRS detection and FHR estimation. In order to evaluate those methods, an expert-annotated gold-standard is necessary. With that in mind, a straightforward annotation scheme with four possible annotation markers (see Table B.1) was introduced as described below [410]:

1. The annotation procedure should (if possible) be performed by using simultaneously at least two different leads (preferably with different FECG polarities). That means, recognizing a fetal peak in one channel and comparing with the other if it is really a QRS complex or an artifact;

2. Real-time RR generation function should be enabled at all times in providing a simple method for auto-assessment;

3. The chosen channels should be the ones on which the FECG appear to have the best signal quality (according to visual inspection). The used data can be either the raw signal channels, pre-processed or processed leads. Other two channels for the annotating procedure may be chosen at any time due to quality fluctuation throughout the different leads;

4. A peak is annotated (as normal peak 'N') as long as it is visible in at least one of the two abdominal channels. That, of course, if the form of the peak, QRS duration or heart rate is in accordance with FECG properties;

5. Peaks which are buried into noise or fetal peaks overlapped with maternal QRS complexes should be annotated (as invisible peaks, or 'V'), as long as the number omitted beats in a row is not greater than two;

6. If the signal does not present a fetal R-peak due to signal quality issues, according to rules 3 and 4, the annotation "loss of FECG signal" in this area should be started ('B' marker should be placed). This condition may be reversed (with an end marker 'E') as soon as two fetal peaks in a row are once again visible. The stop for the annotation "FECG signal loss" should be placed before these peaks;

7. Otherwise, no annotation is made.

Table B.1: Fetal QRS annotation markers used in this work [410].

Marker	Meaning
N	normal, clearly recognizable fetal peak
V	probable, yet invisible peak. This marker applies e.g. when the fetal complex is not visible due to an overlapping MQRS complex
B	beginning of bad signal quality segment, where no fetal peak is discernible
E	end of bad signal quality segment

For the purpose of annotating FQRS data, the JAVA GUI developed by Grunitz [167] was used. This GUI (shown in Fig. B.1) requires data to be in the Unisens format[1] and allows the simultaneous display of signals (e.g. MECG leads, raw, preprocessed or extracted abdECGs) and annotations (e.g. MQRS and FQRS). This versatile interface enables stretching and compression on both X and Y axes, modification, deletion and inclusion of signals at all times, to facilitate the GUI's usage. Moreover, the GUI enables the presentation of live RR-intervals (see Fig. B.1), by taking the first derivative of "N" and "V" annotations, which enables specialists to quickly detect and correct mistakes. The resulting annotated files are simple comma-separated files (".csv") containing markers and potential commentaries.

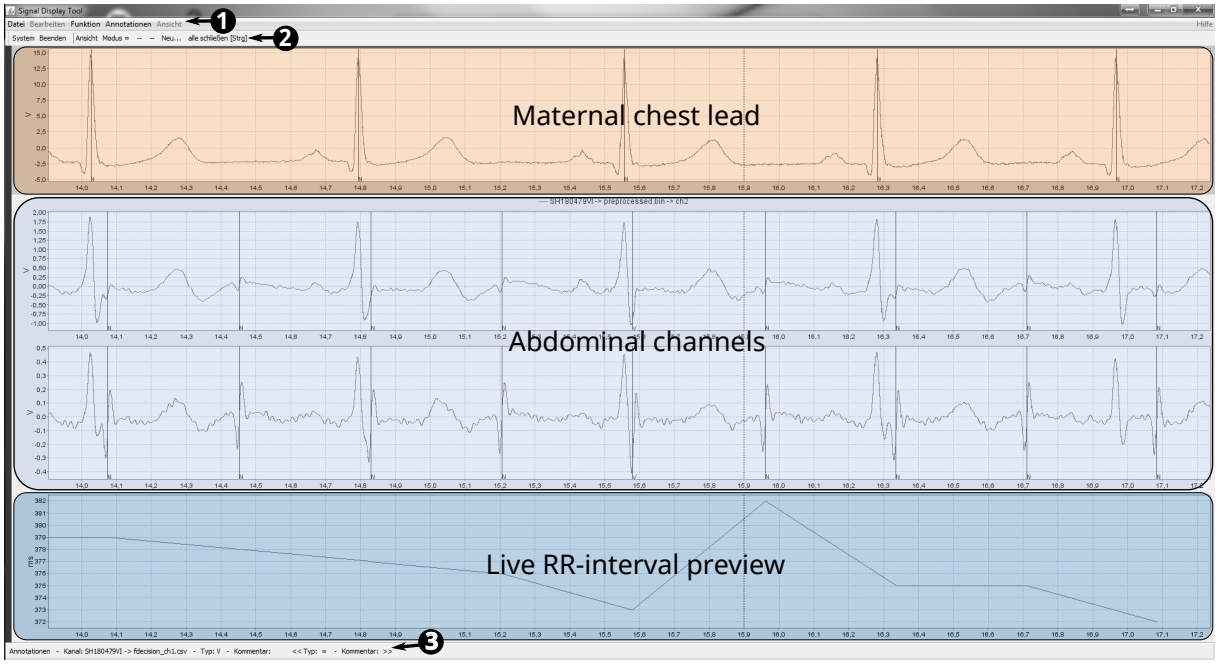

Figure B.1: Java GUI used for FQRS annotation. In the screenshot are depicted (1) main menu with open, close and save functions; (2) secondary menu with information to displayed plots; and (3) quick view of current file, annotation types and commentaries. In the screen are portrayed a MECG chest lead, two abdominal leads (with FQRS annotations as vertical bars) and the live RR viewer.

[1] Unisens was developed at the FZI Research Center for Information Technology and the Institute for Information Processing Technology (ITIV) at the University of Karlsruhe. It is an open-source format available at: `http://www.unisens.org/`.

C

Appendix C - Data Recording GUI

Recording NIFECG data in a clinical setup as the one described in this work is an arduous task. The author's first-hand experience with such problem lead to the development of a user interface with the following goals:

- facilitate the recording procedure with an intuitive and simple interface, which is extremely necessary when the medical expert is responsible for positioning a Doppler ultrasound probe and be in charge of performing maneuvers (e.g. using the novel measurement protocol described in Section 7.1.1);
- increase reproducibility of the recorded data regarding time duration and expert annotations relevant to further analysis. This is particularly important on the newly proposed recording protocol (Section 7.1.1), during events such as paced breathing or blood pressure impulse;
- improve consistency on the medical collection of patients' information, such as limiting the possible inputs for pathological conditions or placenta locations. This is important for the posterior analysis on how this clinical conditions may influence the NIFECG analysis, as performed in Section 5.2.3.

For this purpose, a JAVA GUI (see Fig. C.1) was developed. The GUI was personalized to the measurement system used in Leipzig and, after its opening, LabChart (ADInstruments' recording interface) is automatically started with a preset configuration file (".adiset" extension) included in the GUI. The responsible expert is then prompted with the patient information collection form showed in Fig. C.1a. This form was developed through direct interaction with the project partners from Leipzig and includes all the information usually collected by them. After the completion of this form and checking by the specialist, the recording may be initiated and the user is prompted with the screen presented in Fig. C.1b. On the course of the recording, the expert is asked if the respiratory and blood pressure maneuvers (see Section 7.1.1) should be performed by alerts (in case the step should be skipped), depicted in Fig. C.2a. The color of the interface is changed to indicate that a maneuver is being performed as detailed in Fig. C.2b. When the recording is finished, the expert is required to provide additional information on the measurement that may be relevant for further analysis (e.g. interruptions or problems - see Fig. C.1c). Finally, the interface produces the following output data:

- collected patient information on tabular format (".csv" extension), incrementally;

(a) Initial screen with Labchart recording on the background and patient form.

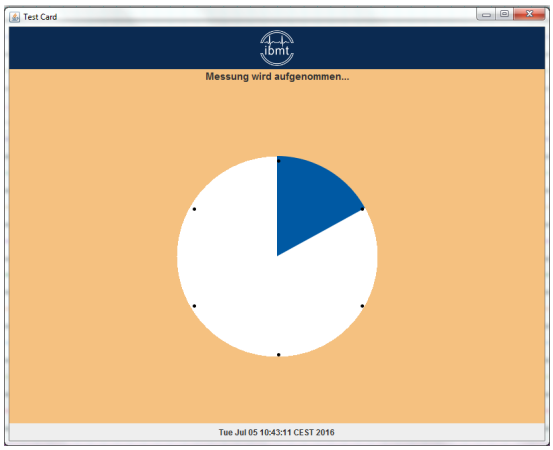

(b) Screen demonstrating recording stage.

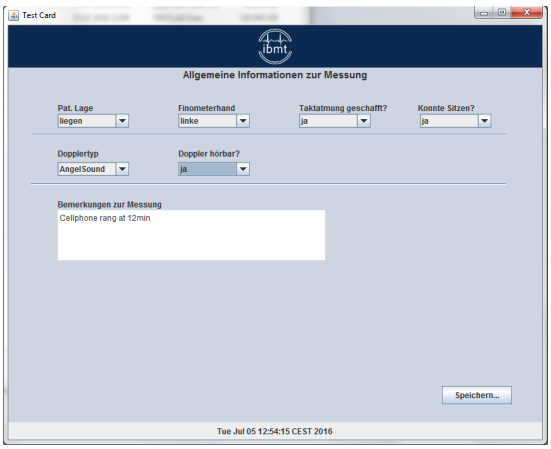

(c) Final form containing recording remarks.

Figure C.1: Screenshots of recording GUI.

- for backup reasons each patient has a metadata file (as ".info");
- time stamps respective to measurement start and begin of maneuvers is contained in an additional text file (".time")
- the resulting recording is automatically saved in LabChart's (".adicht") and Matlab's (".mat") formats;
- a ".log" file showing any problems the interface may have encountered.

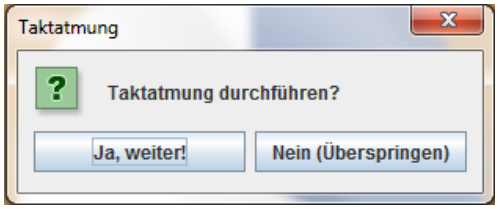

(a) Alert

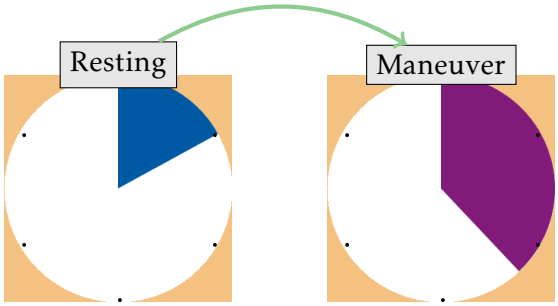

(b) Color states during different recording phases

Figure C.2: Chages to the GUI during physiological maneuvers.